Automation and Control Architecture for Hybrid Pipeline Robots

BECCI, GRACIELA,MONICA

Durham University

Automation and Control Architecture for Hybrid Pipeline Robots

Graciela Mónica Becci

School of Engineering and Computing Science
Durham University

A thesis submitted for the degree of
Doctor of Philosophy

April 2010

Abstract

The aim of this research project, towards the automation of the Hybrid Pipeline Robot (HPR), is the development of a control architecture and strategy, based on reconfiguration of the control strategy for speed-controlled pipeline operations and self-recovering action, while performing energy and time management.

The HPR is a turbine powered pipeline device where the flow energy is converted to mechanical energy for traction of the crawler vehicle. Thus, the device is flow dependent, compromising the autonomy, and the range of tasks it can perform.

The control strategy proposes pipeline operations supervised by a speed control, while optimizing the energy, solved as a multi-objective optimization problem. The states of robot cruising and self recovering, are controlled by solving a neuro-dynamic programming algorithm for energy and time optimization, The robust operation of the robot includes a self-recovering state either after completion of the mission, or as a result of failures leading to the loss of the robot inside the pipeline, and to guaranteeing the HPR autonomy and operations even under adverse pipeline conditions

Two of the proposed models, system identification and tracking system, based on Artificial Neural Networks, have been simulated with trial data. Despite the satisfactory results, it is necessary to measure a full set of robot's parameters for simulating the complete control strategy. To solve the problem, an instrumentation system, consisting on a set of probes and a signal conditioning board, was designed and developed, customized for the HPR's mechanical and environmental constraints.

As a result, the contribution of this research project to the Hybrid Pipeline Robot is to add the capabilities of energy management, for improving the vehicle autonomy, increasing the distances the device can travel inside the pipelines; the speed control for broadening the range of operations; and the self-recovery capability for improving the reliability of the device in pipeline operations, lowering the risk of potential loss of the robot inside the pipeline, causing the degradation of pipeline performance. All that means the pipeline robot can target new market sectors that before were prohibitive.

Declaration

I herewith certify that all material in this dissertation which is not my own work has been properly acknowledged.

Statement of Copyright

Graciela Mónica Becci

I would like to dedicate this thesis
to my loving mother Maria Elena
and to my mother-in-the-heart,
my aunt Celeste.

“We who lived in concentration camps can remember the men who walked through the huts comforting others, giving away their last piece of bread. They may have been few in number, but they offer sufficient proof that everything can be taken from a man but one thing: the last of the human freedoms -- to choose one's attitude in any given set of circumstances, to choose one's own way.”

Viktor Frankl

This thesis is a humble tribute to those people all over the world that for any circumstances couldn’t accomplish with their dreams.

Acknowledgements

This research project is funded by the Alban Programme, from the European Community research grant E03D20854AR; it is also supported by Durham University and Durham Pipeline Technology Ltd.

I am profoundly grateful to Professor Ernest Appleton, who provided the initial concept of this research project; his constant help, advice, and encouragement allowed me to accomplish a childhood dream of doing research in robotics. He also gave me the possibility of experiencing the great freedom and pleasure of independent research.

I had the good fortune of getting to know Professor Valentin Vitanov at the critical moment when my thesis most needed him. He exercised his usual diplomacy while shepherding my PhD through the final stage of writing up and viva.

Professor Peter Tavner generously gave part of his precious time, as head of Engineering Department, to discuss about my writings. My gratitude goes especially to Dr Dagou Zeze for his assertive guidance at different stages of my PhD, particularly the time before the viva voce exam. Professor Jon Trevelyan and Dr Richard Scott gave kindly suggestions related to strain measurement for the pipeline robot.

I am deeply indebted to Dr Oscar Nasisi, Dean of the School of Engineering of the National University of San Juan, Argentina, and Dr Ricardo Carelli, Head of the Institute of Automatic of the same University for their unconditional support of my project and helpful comments about my thesis.

Many people gave their time and knowledge generously discussing the many aspects of my thesis. I am grateful to Dr Jim Bumby, Professor Roger Crouch, Mr Peter Baxendale, Dr Grant Ingram, Dr Sherri Johnstone, Professor Alan Purvis, Professor Sana Salous, Dr David Sims-Williams, Professor Philip Taylor, Professor Tony Unsworth. From each of them I received extraordinarily thoughtful advice.

I wish to record my deep gratitude to the group of technicians for untiring effort to build the hardware and to make the experiments of my thesis all the more efficient. Mr Tony Collinson did a stellar job in making real the probes I designed for the robot's measurement system; Mr Roger Little amazingly assembled the frictional model of the pipeline robot; and Mr Neil Clarey skilfully fabricated the 4-layered data acquisition board in a constrained space. I really appreciate the collaboration of technicians and

supporting staff that make easier the life of PhD students. Thanks to Mr Adam Bent, Mr Ian Hutchinson, Mr Colin Dart, Mr Ian Garrett, Mr John Gibson, Mr Paul Jarvis, Mr David Jones, Mr Kevan Longley, Mr Lee McAlpine, Mr Bernie McEleavey, Mr. Tony McFarlane, Ms Julie Morgan Dodds, Mr Trevor Nancarrow, Mr Arthur Newman, Mr Gary Parker, Mr Steve Richardson, Mr Stuart Watson, Mr Mike Wilson, Mr Colin Wintrip. Special thanks go the Janice Smith and Leslie Stokoe for their timely support. Whenever I needed a solution they got it!

Many friends gave their loving support and shepherded me through the clouds of the life as PhD student. Big thanks go to Cindy, Jane, Elizabeth, Eulalia, Stecy and the guardian angels Peter and Chong. Especial thanks go to Dr Xu Qi for her encouraging words and support at earlier stage of my PhD.

My deep gratitude goes especially to Jo, Brian and Edward Cheesman for reading and patiently correcting various drafts of my thesis. They gave me extraordinarily helpful advice and also lightened and brightened my days as student, in particular before the viva voce exam.

And last but not least I am deeply indebted to my mother Maria Elena, and to my mother-in-the-heart, my aunt Celeste; God sent them to guide my way as guardian angels.

I thank you all.

Contents

Table of Figures

Table of Boxes

List of Tables

Symbols and Abbreviations

Symbol	Description
c	Damper constant
c_E , c_t	energy cost, time cost
D	Turbine diameter
E	Energy
E{.}	Expectation of the set
F	Force
f(.)	Function operator
G(s)	Transfer function
g	Gravity force
g(.)	Cost function
I	Identity matrix
k_i	variable
k	Spring constant
L, l	Length Units, length
M, m	Mass Units, mass
m	variable
N	Rotational speed
N_i *for I = 1, 2…,n*	Horizon upper limit
n	variable
P	Pressure
Q	Flow rate
Qdot	Volumetric flow rate
q^{-1}	Backwards operator
s	Laplace Transform operator
T	Torque
T, t	Time Units, time
U	Flow linear speed
U(s)	Input matrix frequency domain
u(.)	Vector input of the system

Symbol	Description
v(.)	Noise vector
W	Work
w(.)	Noise vector
x(.)	Vector states of the system
x	Displacement
Y(s)	Output matrix frequency domain
y(.)	Vector output of the system
ANN	Artificial Neural Networks
ANOVA	Analysis of Variance
ARMAX	Auto Regressive Moving Average with eXogenous variable
AUV	autonomous underwater vehicle
CARIMA	Controlled Auto Regressive Moving Average w/eXogenous variable
CC	Cruise Control System
DOE	Design of Experiments
dof	Degree of freedom
EMS	Energy Management System
FSM	Finite State Machine
FMEA	Failure Mode and Effects Analysis
HEV	Hybrid Electric Vehicles
HPR	Hybrid Pipeline Robot
MLD	Mixed Logical Dynamical system
MPC	Model Predictive Control
MRC	Model Reference Control
NDP	Neuro-dynamic Programming
NMPC	Neuro-Model Predictive Control
PCA	Principal Component Analysis
PIG	Pipeline Inspection Gauge
PMC	Pressure Measurement Chamber
PWA	Piecewise affine function
RHPC	Receding Horizon Predictive Control
RPN	Risk priority number
TD	Temporal Difference

Symbol	Description
α	Variable/weighting factor
a_i	System parameters
β_i	Parameters vector
Δ, Δx	Difference operator
ε	Slack variable
γ	Slack variable
η	Efficiency
φ	Nonlinear regression vector/matrix (System Identification)
	Energy Transfer Coefficient (Turbine Efficiency)
λ	Slack variable
μ	Kinematic viscosity
$\mu\{\}$	Set of policies (dynamic programming)
$\pi\{\}$	Policy space
θ	Parameters vector
ρ	density
Σ	Sum
$J(.)$	Cost function/Performance Index
z	Head of the fluid

Chapter 1 Introduction

The University of Durham has been researching into traction devices for pipeline robots for more than ten years. The university holds eight patents in this area. One patent relates to a robot tractor that can crawl long distances along oil pipelines moving against the flow or with the direction of the oil product. This research is being transferred into industry through involvement with major oil companies and industry contractors. The first machines that will be applied will be relatively simple machines used for wax removal of relatively clean pipes. The aim is to develop an advanced hybrid machine that uses the on-board turbine to generate electrical power which it can store or use directly for traction. The exploitation of such a machine requires some research in a number of areas including intelligent control. For example, if the robot was to be used to recover heavily waxed up pipes and bring them back to full production flow the robot would have to machine away heavy wax coating deposits.

This would require the use of auxiliary tooling and the concept is that this tooling would be electrically powered using some form of electrical energy storage. As the wax was removed the stored energy would decrease and eventually run out. However, the robot would be equipped with a turbine driven generator and could recharge the electrical storage system. This system would have to operate autonomously and therefore needs its own intelligent energy management system.

In a similar manner the robot would also be used for remote pipeline inspection, looking for pipe-wall defects. In the remote mode the robot would survey the pipe storing the data it collects. Such a survey may take several days so a repeat journey to check out date would be very expensive Real time monitoring is not possible so it would be desirable that the robot would have the ability to recognize a defect and pass over the defect point several times to verify the data. This obviously requires the device to have the intelligence to analyze the data and take the appropriate action.

Finally, these machines will travel into demanding environments in terms of temperature, pressure and contamination or blockages. It will be imperative that the machine be able to self-recover whatever the condition. This then leads onto intelligent use of sensor information and its use to formulate a recovery strategy.

The intelligence aspects are central to the potential in this important area of technological development. Therefore, the aim of this research project is the automation and development of the control architecture for a Hybrid Pipeline Robot (HPR), based on reconfiguration of the control strategy for speed-controlled pipeline operations and self-recovery action while performing energy and time management.

The literature review, Chapter 2, is organized in two sections to support the control architecture design. The first section, HPR Controllability and Context Overview is divided according to the classes of vehicles to which the HPR belongs, such as hybrid, autonomous, and pipeline vehicles, and antecedents for the HPR. This review is the theoretical framework for the HPR models developed in Chapter 3.

The second section, HPR Control Strategy Framework, is a review of the main areas involved in the development of control architecture and controller strategy, presented in Chapter 4; the four categories are: Reconfigurable Systems, Hybrid Control, Model Predictive Control, and Artificial Neural Networks.

These four areas of control development are followed by a survey on the main topics of Model Predictive Control and HPR controllability. The selection of the bibliographic material refers to publications from leading groups working in these research areas, with the aim of seeking quality and trends in the research area.

The control architecture and the control strategy are based on the HPR models. Therefore, in order to explore the models, a taxonomy of hybrid pipeline machines is used in this project. The Hybrid Pipeline Robot (HPR) is a class of self-powered device that converts the energy from the pipeline flow into mechanical energy for traction, in turbine-driven mode, and into electrical energy for charging batteries, in motor-driven mode. Therefore the energy generation and dissipation in the HPR system are fundamental factors for the development of the energy management and control strategy. For that reason, the objective in Chapter 3 is to derive models for analyzing the HPR turbine and crawler vehicle in order to give the HPR specifications.

A model based on mass and energy conservation is derived for the turbine and tractor. As a result, the minimum set of variables is extracted from this model with the purpose of defining the system identification parameters.

A force analysis is performed for the driving system of the tractor and for the bristle-based locomotion system with the purpose of identifying driving patterns and predicting ways of failure of the HPR that need to be considered in the controller

architecture to perform a self-recovery action. Additionally, A State space model for the HPR is derived considering the flow as a source of energy.

Finally, a system identification model for the HPR is proposed in Chapter 3, which is the base for the neuro-system identification model developed and tested in Chapter 4. The development of the control architecture and control strategy for the Hybrid Pipeline Robot is presented in Chapter 4.

Reconfigurable control architecture is designed for controlling pipeline operations, guidance and recovery stages. Multi-objective optimization is the strategy proposed for solving the objective function of the speed control state; and objective prioritization for guidance and recovery stage.

The development of models based on Neuro-Model Predictive Control and Neuro-Dynamic Programming are presented for speed control, energy and time management control, respectively. The development and test of a Model Reference Control for the HPR is presented as benchmarking for the speed control. The chapter finalizes with data analysis and conclusions of simple inspection of data from the rig; and concludes with the test and results of the system identification and tracking system based on neural networks.

The development of the instrumentation system is presented in Chapter 5, and consists on the novel design of probes, and development of a signal conditioning board. The instrumentation is customized to the HPR environment for measuring the HPR parameters required for system identification and control.

The order of presentation of the probes is related with the measurement of the parameters necessary for calculating the turbine efficiency, which is the input of the HPR system. The probes are: Kiel-reverse, Pitot-Gracey and Pressure Measurement Chamber (PMC) for pressure measurement, leading to the calculation of the flow rate and pressure drop across the turbine. The hollow universal joint is customized as torque transducer. A standard magnetic sensor is used for calculation of the rotational speed. The output of the HPR system, tractor speed, is sensed by an on-board accelerometer. It is also presented the design and development of the on-board signal conditioning and data acquisition board, which is designed for the particular use in the harsh HPR environment and to acquire the data in a stand-alone way.

Chapter 2 Literature Review

2.1. INTRODUCTION

The literature survey is selected to support the aim of this research project, which is the automation and development of control architecture for the HPR. Therefore, the literature review chapter is organized in two major sections: the HPR Controllability, Context Overview, and HPR Control Strategy. Figure 2.1-1 presents the main topics of the chapter.

The first section of the literature review, HPR Controllability and Context Overview, is divided into sections according to the classes to which the HPR belongs, to review controllability antecedents of each class: hybrid vehicles, autonomous vehicles, pipeline vehicles and research antecedents on the HPR itself. This review is the theoretical framework for the HPR system models presented in Chapter 3.

The second section, HPR Control Strategy Framework, is a review of the main areas involved in the development of control architecture and controller strategy, presented in Chapter 4; the four categories are: Reconfigurable Systems, Hybrid Control Systems, Model Predictive Control and Artificial Neural Networks, and Model Predictive Control.

These four areas of control development are followed by a survey on the main topics of Model Predictive Control and HPR controllability, which are: Models for the HPR, System Identification, Receding Horizon Strategy, Tracking System, Model Predictive Control (MPC) Objective Function, System Constraints, Objective Function Optimization, HPR Neuro-Dynamic Programming Model, System Performance Evaluation, System Stability and Constraints and Robustness and Uncertainty.

The selection of the bibliographic material refers to fundamental publications for each section in addition with reports from leading groups working in these research areas, with the aim of seeking quality and trends in the research area.

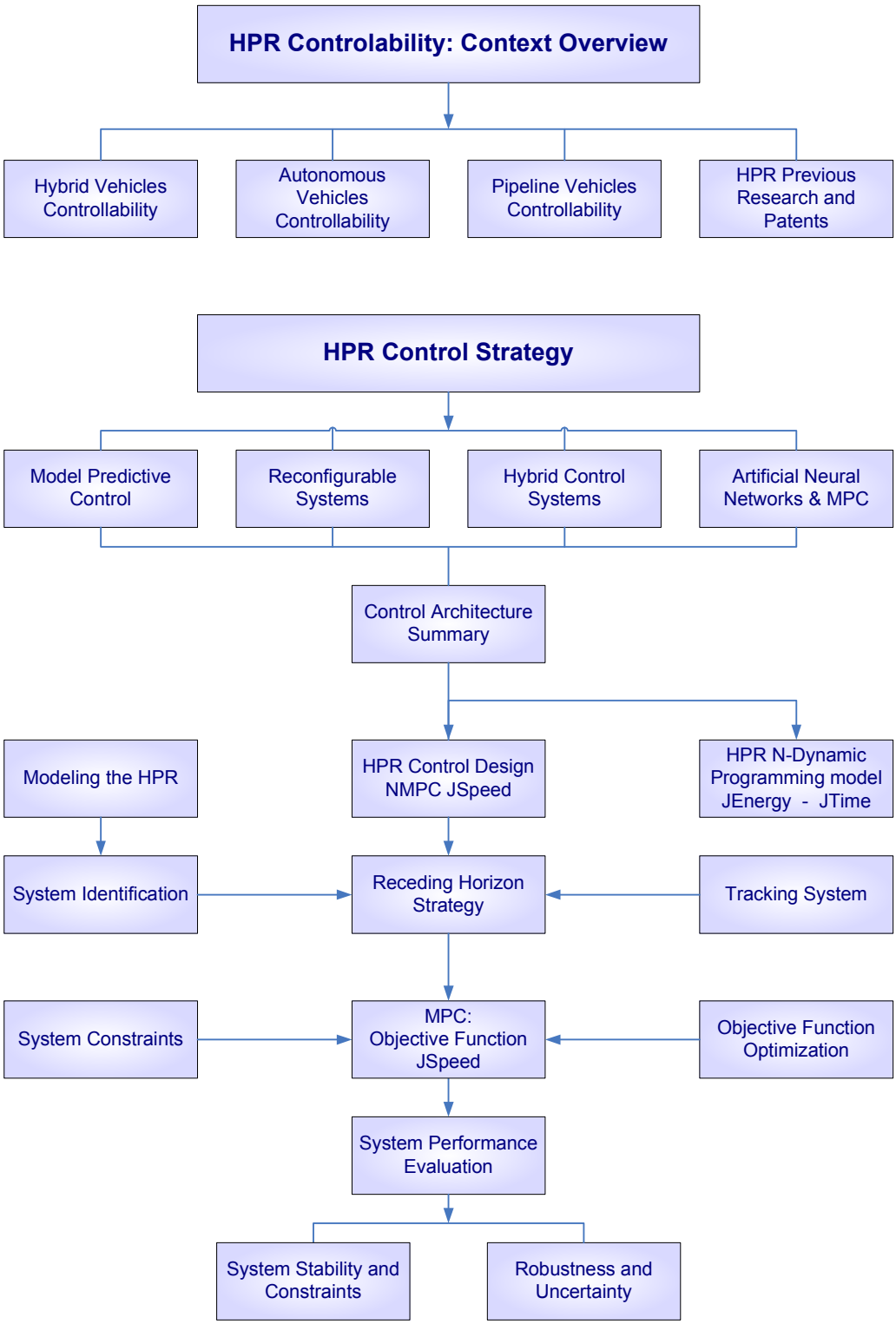

Figure 2.1-1 Chapter 2 contents: literature survey

Controllability of a family of vehicles and control strategies applied in the HPR control development

2.2. Hybrid Pipeline Robot Controllability and Context Overview

The first part of this overview explores the controllability antecedents for the Hybrid Pipeline Robot (HPR) as a pipeline device, belonging to a taxonomy of vehicles: hybrid vehicles, autonomous vehicles, pipeline vehicles and hybrid pipeline vehicles, which are described in the following paragraphs.

2.2.1. Hybrid Vehicles Controllability

Publications in the area of hybrid electric vehicles (HEV) show a tendency to solve the energy management of such vehicles using dynamic programming (Sciarretta and Guzzella 2007). The stepwise dynamic programming approach is applicable to problems where the energy optimization does not need to be minimal all the time. Instead, a good solution is to keep the consumption at the lowest rate through the overall mission. Apart from the dynamic programming approach, the solution of the energy optimization of hybrid vehicles is combined with a predictor method and it is an inherently constrained problem: battery depleted boundaries and engine output torque limits define the hard and soft constraints upon the controller design. Results of the dynamic programming solution are a base comparison for other different optimization approaches such as real-time simulation with Quasi Static Simulation Toolbox (QSS) (Lyshevski 2000; Pérez, Bossio *et al.* 2006; Loenhout 2007; Guzzella 2009; Pérez and Pilotta 2009).

These energy management constraints may present high gradients of the cost-to-go, in the boundaries of the feasible state region (Sundström, Ambühl *et al.* 2009). High gradients may represent instability, so a way to stabilize the system is to impose final state constraints in some cases or the stability in a Lyapunov sense in other cases (Lyshevski 2000).

An energy management system based on consumption minimization is combined with a regenerative braking system for energy optimization of a hybrid electric vehicle (Hui and Junqing; Xu, Li *et al.* 2009) . Results show the greater part of the fuel economy is due to regenerative braking rather than the energy optimization in itself. A different way of optimizing the energy is through the addition of a bank of super capacitors, to reduce the hydrogen consumption (Feroldi, Serra *et al.* 2009).

Energy optimization of a series-parallel electric hybrid vehicle (Johannesson, Pettersson *et al.* 2009) is developed through the simulation of all possible states of

future speed and torque of the vehicle and through the application of a dynamic programming optimal path with prediction of the propulsion load. Another approach is to use a hierarchical model predictive control for optimizing simultaneously the power consumption and the oxygen cycle for the hybrid electric vehicle (Rodatz, Paganelli *et al.* 2005; Chen, Gao *et al.* 2009). A journey prediction for hybrid passenger vehicles is presented in (Quigley, Ball *et al.* 2000). The methodology is based on pattern recognition from measured data and fuzzy logic heuristic classification. The purpose is to optimize the energy consumption when the journey is known in advance.

2.2.2. Autonomous Vehicles Controllability

The research is vast in relation to **autonomous vehicle navigation**, for example the **autonomous underwater vehicle (AUV)** for under ice-exploration is a GPS navigated unit (Pebody 2008). The velocity is monitored by an Acoustic Doppler Current Profiler (ADCP) for the rudder control. An example of navigation control is the **hybrid controller** for highway navigation. The term hybrid is because the finite state automaton uses continuous and discrete signals. The controller is intended to avoid collisions and congestions of unmanned terrestrial vehicles (Girault 2004).

The report refers to the system identification of a linear system of two DoF and multiple input multiple outputs of a twin-rotor hover vehicle (Ahmad, Chipperfield *et al.* 2001). However the main challenge is the **correlation and cross correlation** between the different input output channels.

A project based on the **optimization of components configuration** is in the field of design optimization. The optimization is based on **Genetic Algorithm** for operations of mutation and cross over for the different configuration of all the parts in order to achieve the optimized design (Ng and Leng 2007). However different application field, the **HPR** may share the concept of optimization of components configuration. In particular different **energy components combinations** may be optimized so as to improve the energy performance.

A rather different control approach is the **launch vehicle** modeled by a nonlinear and six degrees of freedom analytical model (Roshanian, Saleh *et al.* 2007). The controller developed has three different approaches: the gain scheduling, gain scheduling with decoupling of the vehicle dynamics and adaptive controller based on the Model Reference Control.

A **trajectory tracking** system, based on a PID controller, is the example of an unmanned excavator vehicle, modeled upon its kinematics and dynamic characteristic (Zweiri, Seneviratne *et al.* 2003).

2.2.3. Pipeline Vehicles Controllability

PIGs and pipeline environment overview

PIGs are devices that carry on several tasks in pipelines. The **PIG's name** has unknown origins, some claims are related to the shape, the kind of tasks it performs, the noise it produces inside the pipe and the sophisticated version of the name is that it stands for **Pipeline Inspection Gauge**.

PIGs are used in activities such as **commissioning, decommissioning** and **maintenance** of the line as well as **inspection**. PIGs are doing their job in places where the human activity is dangerous or impossible such as in oil or gas pipelines, deep water, toxic environment and extreme temperatures, just for citing a few. As a consequence PIGs contribute to reducing operating costs, increase the efficiency of the line and play a role in environmental friendly installations (Lyons 2000).

However, when problems arise such as a **stalled PIG** inside a pipeline, it implies **high costs** due to the degradation of the line performance and even higher when it is required special **rescue procedures**. Main causes for **PIG's stall** in the pipeline may deal with environmental conditions or mechanical failure (O'Donoghue 2007). Therefore, the design stage of a PIG is fundamental to avoid operational failures.

There are several considerations about **PIG and pigging** of particular interest when designing the PIG and PIG related devices. In particular, the **material flowing** in the line (food, oil, gas, water) and the pipeline **environmental factors**, which are originating the **deposits in the line**. All these factors affect the type of deposits, the way and the rate at which these deposits are built up in the wall of the pipe, and therefore the means by which they are removed (Gray 2007). Some of the activities in relation to pipe maintenance are cleaning and dewatering, scale and paraffin control, inhibitor application and biocide treatments, just to give the most common (Cameron 2007).

Crude oil, for example, leaves deposits of gypsum, paraffin, hydrogen sulphide, sulphur etc; these materials build up in a different manner and define the type of PIG and the way of pigging. In comparison, **natural gas** leaves lighter materials though they are also restrictive deposits that are the case of condensates, which may leak to the

lower pipe loop with the risk of freezing or leaving salt sediments dangerous for the PIG.

The main variables that condition the PIG behaviour are **flow rate and pressure**. Steady velocities of PIGs are desirable in particular for inspection tasks. However steady regimes are rather difficult to find particularly in gas lines due to the compressible characteristic of the flow, which behaves like a spring-mass-damper model, causing velocity excursion of PIGs (Cameron 2007; Matthews, Kennard *et al.* 2007). This model produces highly unsteady flow and uneven velocity profile or **velocity excursion** with sudden acceleration and stops followed by high velocity. This makes the inspection task rather difficult, not to mention the risk of a PIG carried by a flow with such erratic characteristics.

The natural unsteadiness of compressible flows is augmented by occasional **blockages of the pipe,** for instance by the PIG itself due to effective inner diameter reduction or changes in cross-sectional symmetry at bends, tees etc. The blockage produces a sudden increase in the pressure difference across the PIG. This pressure can reach values high enough to exert sufficient force on the PIG to unblock the line, reaching approximately 50 meters per second of sudden speed (in the order of the peak velocity of an urban train (Wikipedia 2009)). The high acceleration and velocity compromise the line efficiency, the PIG effectiveness and safety conditions. The solutions are in the range of PIG design changes and in the operating conditions of the pipe. Changes to the PIG may include redesign of the traction and braking system, mass reduction, and an on-board control system for variable by-pass mechanism that alleviates the high pressure that builds across the PIG.

Another important variable affecting the PIG activity is the **temperature profile.** It is an important factor in oil pipelines because it indicates the wax deposits and therefore the sector to inspect for wax removal (Cordell 2007).

Physical factors affecting the PIG activity are the **line topology,** for example valves, pump, bends' radius, T junctions, pipe diameter, and even fibre optic cable laid inside the pipe. All these pipe features may hinder the PIG activity if the PIG design is not appropriate (Quarini and Shire 2007). Some articulated PIGs may "jack-knife" and therefore stall the PIG. In less severe cases the PIG's seal may cause the PIG to lose drive and to deteriorate over time (Cordell 2007).

The **type of valves** determines the piggability: full-port valves and regular opening valves are piggable, compared with the butterfly valve which cannot be pigged through (Gray 2007).

Conditions causing an **unpiggable line** are for example corrosion, which is directly related to the pipeline ageing, compromising the line integrity (Cameron 2007). In addition, the pressure range and pipe wall thickness may endanger the pigging activities in corroded lines; these characteristics are ranked as **maximum allowable working pressure MAWP** and **minimum allowable wall thickness MAWT respectively**.

Inspection of **offshore loading and offloading lines** with confined spaces is a challenge for pigging activities (van Agthoven 2007). To add more difficulties, these lines end in auxiliary vessels close to the shore where shallow waters imply high turbulence. All these factors, combined with the presence of manifolds, make the area in unpiggable. The solution to this problem is to use **cable operated PIGs** with ultrasonic inspection tools.

PIGs for **in-line inspection (ILI)** perform activities such as inspection for wall thickness and cracks. The most complex faults to be detected are geometry fault, crack, leakage and metal loss. Inspection technologies reported are electronic calliper, electromagnetic flux leakage MFL, ultrasonic tools, inertia tools and transverse magnetic flux leakage TMFL. (Beller and Reber 2007).

PIGs Alternatives

A review of **fluid-driven pipeline PIGs** lists different categories such as tethered and self-powered, according to variants of crawler and swimming PIG's (Quarini and Shire 2007). They are selected upon the appropriate activity to accomplish such as displacement and cleaning, batching and separation, survey and inspection and maintenance in general.

New trends in PIGs are the **non-solid PIGs,** for example ice PIGs, gel and thixotropic gel PIGs find application in unpiggable lines and in other industrial sectors than Oil&Gas, such as food, paint and general process industry. These kinds of PIGs are preferred for hygienic reasons; the launching and catching process is simple and they can be disposed without risk of contamination.

The field of robots for inspection is vast. **Snake-like robots**, for example, are efficient devices for in-line-inspection; depending on the size they can negotiate

constrained sectors, bends and diameter-constrained line topology (Transeth, Ytterstad Pettersen *et al.* 2009).

A **self-actuated tether** is powered by hydraulic transients by holding and releasing the flow through a hose (Perrin, Kwon *et al.* 2004). The design allows a small device that can carry its own load and is capable of negotiating bends.

PIGs Characterization Models

There are several approaches to model in the literature based upon different elements that constitute the PIG, even modelling the environment. A **model for by-pass PIG** that accounts for transients in the PIG behaviour is based on **mass-conservation**, **linear-momentum** and **energy equations of the fluid** in addition to the **momentum equation** for the PIG (Azevedo, Braga *et al.* 2007). The models are for compressible and uncompressible flow and are embedded in a program for transient simulation. The models are also combined with finite-element analysis of different friction conditions of deposits built up in the pipe wall and the buckling effect on the discs of the PIG.

A rather different model approach is in the field of **Tribology**, of the steady state of a seal PIG including also the model for the friction and lubricants for the PIG's seal (O'Donoghue 1996). On the other hand, the characterization for the self-drive tractor, consists of a **first-order model** of the PIG's dynamics, which includes changes of parameters following changes of the motion stages (Zheng and Appleton 2005).

Snake-like robots present a complex motion pattern. Unlike crawler tractors, they do not require active wheels or legs; the movement is based on active joints under the effect of side forces. The mathematical model usually has a high DoF. Mathematical models as a function of the motion patterns give a wide range of **dynamic and kinematic models** for this kind of robot (Date, Hoshi *et al.* 2000; Brunete 2006; Transeth, Ytterstad Pettersen *et al.* 2009). An **object oriented simulator** for a multiphase flow evaluates the behaviour of a slug PIG inside the oil pipeline (Klebert and Nydal 2003).

Pipe robot control

A robot for small-size pipes of the order of 10-20mm controlled by an electromagnetic motor and driven by anisotropic stops, which are directional dependent with respect to the friction drag (Chashchukhin 2008). The reversibility of the robot motion is a challenge for this kind of driven system controlled by **PWM** signals. Another type of

control of in-pipe inspection micro-modular robot is by **PIC with I2C** connection and PWM control signal for a 2 DoF servomotor (Brunete 2006). The author has developed control programs for a range of tethered bristle-based tractors based on **ladder logic** on a programmable logic controller (**PLC**).

A semi-autonomous control for a gas pipeline robot is based on **PID controller and fuzzy logic** for interpreting the signal of propioceptive sensors (Ong, Kerr *et al.* 2003). Infrared and tilt sensor indicate the position and tilt of the robot in the pipe. The controller has three modes: speed control, climbing angle recognition and pipe fittings recognition.

An example of controller for a pipeline robot is the vehicle able to adapt itself to the pipe shape by a **selective clutch** operated driving system (Roh, Kim *et al.* 2009).

2.2.4. HPR Previous Research and Patents

The **Hybrid Pipeline Robot** holds several **patents** as a conduit traversing, bi-directional conduit traversing and surface traversing vehicles (Appleton and Stutchbury 2002; Appleton 2003; Appleton and Stutchbury 2004).

Original research presents a novel **brush drive robotic tractor** for inspection and maintenance of sewers and water pipes (E. Appleton 2000). The study includes the bristle behaviour analysis and test of the bristles units in challenging pigging pipes such as collapsed pipes with successful results. The flexible joint tractor is capable of negotiating bends and obstructions without the jack-knife effect in straight sectors of the pipe.

The characterization for the **bristle-based traction pipeline robot** is given in (Wang and Hong 2008). The study also calculates the approximate bristle forces based on the Euler buckling theory and demonstrates the results with several experiments. Tests of **the unidirectional bristle-based tractor** are performed for straight and curved pipes, with steel and plastic bristles (Han 1999).

A **reconfigurable shape of the bristle based robot** is a variation of the bristle based robot (Wang 2003 (a)). Experiments in relation to the load and displacement have been done for wooden pipes of different shapes and bristle units of several bristles arrangements. An example of an instrument for inspection is the strain gauge based sensor **for detecting the void of collapsed pipes,** modelled by a spline-interpolation algorithm for determining the void shape (Wang and Appleton 2003 (c)).

The **HPR scroll cam** is a crucial component of the tractor and it is at the core of friction losses. Studies of different factors affecting the losses suggest improving the driving system, such as modifying the design of the screw of the scroll cam, so as to reduce the friction drag losses (Bygate 2005; Zheng and Appleton 2005). Research into utility PIGs and **wax removal** is presented in a PhD thesis (Southgate 2004). The twisted blade is a modification of the blade design introduced to improve turbine efficiency (Pulker 2005).

The present research project is a continuation related HPR's studies, though in the different field of automation. The author gained insight in pipeline tractors through developing programmes for a range of bristle based tractors and through invaluable discussion with many of the authors of the HPR related projects.

2.2.5. HPR Control Strategy Framework

The development of the HPR controller is based on several theoretical grounds. The purpose of this survey is to give the background for such development. The following classification of controller theories is an attempt to frame the main control streams on which the HPR controller is based. These categories are four, namely: Model Predictive Control, Reconfigurable Systems, Hybrid Control Systems and Artificial Neural Networks for Control. The survey is far from being exhaustive due to the extent and depth of each of these areas. Instead, the leading idea is to find a suitable knowledge background for the Hybrid Pipeline Robot.

2.2.6. Reconfigurable Systems

Why reconfigurable Systems?

Reconfigurable systems have their main development in the appealing area of spacecraft; yet it is applied successfully in different fields. In the design of the HPR controller, several ideas have been tried during this research project. Finally the controller is composed mainly of the three leading characteristics: energy management, cruise control and recovery system. The evolution was toward a reconfigurable system, which gives a structure with more freedom to design independent systems upon the situation under control. However, the approaches proposed here are far from being exhaustive in the field of control structures. The following paragraphs refer to examples

of reconfigurable control approaches, which is in itself a broad field with such current interest and development.

An example of reconfigurable control based on the GPC approach is given in (Soloway, Shi *et al.* 2004 (b)). This work gives the stability proof for the reconfigurable MIMO system for actuator saturation. The system model is based on the Controlled Auto regressive Integrated Moving Average (CARIMA) model and input/output complete information. Reconfigurable control with state augmentation is presented in (Soloway and Haley 2004 (a)). Reconfiguration based on multi-model of uncertainties is given in (Rauch 1995). Examples of fault diagnosis detection and isolation (FDI) are given in (Rauch 1994).

Multi-model based predictive control is represented in the state space structure for the simplicity of constraints computation. The multi-model approach represents a starting point for **reconfigurable control** for different control scenarios such as failures (Huzmezan and Maciejowski 1996). Rauch presents a similar approach to multi-model compared with a unitary model adaptive control (Rauch 1995).

Reconfigurable control has evolved from several approaches in particular for aircraft applications. The traditional method of **hardware redundancy** has been replaced progressively by **software reconfiguration** such as failure detection and isolation (FDI) with included estimator, the generalized predictive control (GPC) based on receding horizon for output prediction combined with constraints (Steinberg 2005).

A different approach is the reconfiguration of an aircraft based on **augmentation** of the controller structure with error correction, so as to reduce the position error in the stationary state (Soloway and Haley 2004 (a)).

Example of software reconfiguration is the anti-windup strategy, which prevents the actuator signals to grow beyond bonds and it is commanded through cumulative values flagged by software (Soloway, Shi *et al.* 2004 (b)). Recalling that windup is the undesirable oscillating effect of the controller due to actuator saturation in combination with an integrator in the control structure such as CARIMA model. The integrator helps to reduce the steady state error, although the undesirable associated oscillations.

Therefore, reconfigurable systems strategy combined with MPC offer an efficient structure for the HPR controller development.

2.2.7. Hybrid Control Systems

Why Hybrid Systems?

MPC has successful results in industrial plant and particularly in slow processes. This sustainable and solid success encouraged researchers to go further so as to include fast switching signals, logic states, heuristics inferences and prioritization of constraints just to cite a few. All these components are found in actual systems either playing a role at different levels of the controller hierarchy or interacting at the same level. As a result, the traditional successful MPC is adapted to a broader range of plant/system, apart from the traditional chemical industry, of typical slow processes; hybrid control finds application in the field of fast control. Hybrid control is the new trend of the traditional MPC and has a promissory future open to new and creative approaches with a solid theoretical background stemming from optimization theory such as multiparametric programming.

A summary of hybrid control systems evolution and trends is given in (Antsaklis 2000). The stability of a **supervisory hybrid system** is guaranteed through the subdivision of the state space in stable subspaces (Koutsoukos and Antsaklis 2001). The stabilizing strategy is to derive a global piecewise Lyapunov function to steer the whole switching space to a stable final state. The subdivision in subspaces depends upon the different objectives and constraints to be fulfilled. This controller design has the functionality of coordinating individual subspace controllers upon the related specifications.

A control of **Hybrid System** based on a supervisory system is presented by (Koutsoukos and Antsaklis 1999). Hybrid systems consist in continuous processes and discrete control laws that can be subdivided into a number of subspaces. The supervisory control system, based on Petri Nets, coordinates the transition from one subspace to the next one toward the optimal state.

Another branch to consider in the evolution of the standard GPC is **hybrid systems** with switching input and output signals and decision logic in the states and constraints such as heuristic decision and prioritizing constraints (Dechter, Cohen *et al.* 2003; Borrelli, Baotic *et al.* 2005). An alternative to the hybrid system model is the **Mixed Logical Dynamical (MLD)** model approach for cases where the hierarchy of control levels is not clearly defined, containing interrelated logic states and dynamic characteristics (Bemporad and Morari 1999 (b)).

Hybrid control theory offers the HPR a broad approach to accommodate the real problem and real constraints so as not to bog down the control problem with oversimplification.

2.2.8. Model Predictive Control

Why Model Predictive Control?

Among several control theories with different applications and variable performance, the **Model Predictive Control (MPC)** offers a complete and open structure for controlling linear and nonlinear systems. It is complete because it relies on a **system model** and a **control law** obtained from the optimization index in a **receding horizon** time span. Also it is complete because it considers the **tracking system** and a powerful **objective function**, which includes **constraints** of varied categories from physical constraints related to sensors and actuators limits, to process performance, even economic or quality constraints. Apart from the completeness of the **MPC** it is open because each of the above mentioned components can be customized upon several theoretical approaches, for example the model of the system may be based on first principles, a predefined model structure, system identification or any model that science can conceive. Another example of the "openness" or flexibility of the **MPC** is the objective function, which in itself belongs to the broad area of optimization, with a solid past and promising future. So, **MPC** offers a wide range of options to explore in order to develop the appropriate controller for the **Hybrid Pipeline Robot**. In the following paragraphs are some ideas of researchers who pioneered the MPC field.

The bases and strategy of the Generalized Predictive Control (GPC) is presented in (Clarke, Mohtadi *et al.* 1987 (a); Gawthrop 1996 (a)). The second part analyzes the solution to the problem of stabilizing a non-minimum phase plant with unknown or variable dead time (Clarke, Mohtadi *et al.* 1987 (b)). Properties of the GPC and choices of different parameters of the controller such as predictor model, horizons for prediction and control and weighting factors are presented. Criteria for robustness and stability are also studied. so as to get a controller stable, robust to the plant/model mismatch and of real applicability (Clarke and Mohtadi 1989).

The **GPC** offers characteristics that solve common drawbacks of the standard self tuners such as minimum variance and pole placement (Clarke, Mohtadi *et al.* 1987 (a)). In the case of the Minimum Variance self tuner, the plant model is not so exigent.

However the output might show high dispersion from the desired value when unknown or variable dead-time is present in the input of the system. The opposite situation occurs with the pole placement approach. The model of the system is demanding in terms of the order of the plant, which needs to be known with close precision, otherwise the response of the system might be unexpected. However, this kind of controller is robust to dead time changes. The GPC solve these drawbacks through the identification of the plant, so it is not required to know the order of the plant. In addition, the receding horizon approach solves the offset of the plant output in particular when variable or unknown dead-time is present in the input of the system.

The GPC is an efficient control strategy for unstable open-loop systems. Theses cases are difficult to model with conventional self tuners; however, the receding horizon approach combined with the cost function optimization makes feasible the unstable open-loop control. Stable systems but not necessarily minimum phase can be stabilized through the GPC approach. As a result, systems with zeros outside the unit circle, produced by high sample rates, may be difficult to stabilize with standard controllers. Therefore, the integrative approach for the GPC offers a solution to this kind of problems by stabilizing the plant dynamics.

Gawthrop presents a review of different PID structures and presents the PID controller as an antecedent for the internal model control developed by Morari et al (Gawthrop 1996 (a); Garcia and Morari 2002). Neural Networks combined with **GPC** are applied for solving nonlinear system. In particular, ANN are structured as a network of local model networks constituting an array of PIDs for the control of nonlinear systems (Gawthrop 1996 (a)).

The variations in the GPC models are intended to cover differences in performance, for example the report of two particular cases of MPC: the **Emulator-based Control (EMC)** and the **Internal Model Control (IMC)** (Gawthrop, Jones *et al.* 1996; Gawthrop, Virden *et al.* 2008). Both control strategies are based on the algebraic solution of the transfer function of the system; even more, both are robust to unmodeled system dynamics. The main difference is the system model structure. The **IMC** is based on a parallel identification model, which may lead to instability; and the **EMC**, similar to a series-parallel system identification structure, which is a variation of the Generalized Minimum Variance.

To conclude, from this short review, the MPC evolves from adaptive control combined with a receding horizon approach to optimize an objective function that gives

the suitable control law. The combination and variations of these ingredients generates a myriad of MPC offspring. This proliferation of approaches is not irrational; it has a solid background with the aim of stabilizing the system with a robust controller.

2.2.9. Artificial Neural Networks and Model Predictive Control

Why ANN and MPC?

Artificial Neural Networks (ANN) are ubiquitous learning systems for several applications such as modelling, pattern recognition, filtering and any application that requires a learning stage capable of characterizing nonlinear systems. Artificial Neural Networks are an efficient tool for nonlinear system identification and prediction. ANN also has the flexibility of different learning approaches based on optimization algorithms. ANN are an open approach: it may be combined with several theoretical backgrounds such as fuzzy logic, Genetic algorithm etc.

The HPR is a nonlinear system; thus ANN are a useful tool for representing the HPR nonlinearities, particularly for system identification and tracking system. These approaches applied to the HPR will be developed in chapter 4.

There are several approaches to the **ANN**-based **Model Predictive Control** (Hecht-Nielsen 1990; Miller III 1990; Hecht-Nielsen 1992; Kosko 1992; Warwick, Irwin *et al.* 1992; Cichocki and Unbehauen 1993; Haykin 1994; Pham and Xing 1995; Chong and Parlos 1997; Dingankar and Sandberg 1998; Lazar and Pastravanu 2002; Ławry Nczuk 2007). Antecedents of an inferential data estimator and a nonlinear predictive control based on Artificial Neural Network is presented in (Willis, Montague *et al.* 1992). The objective is to provide an augmented set of measurements of quality variables, which are complex to be measured (Willis, Montague *et al.* 1992; Herrmann 2007). The new set of measurements is obtained by the application of the real reduced set to an appropriate Artificial Neural Network. The objective function is a standard quadratic function with a neural predictive term. The control values are obtained through the numerical optimization of the cost function. The optimization method is a gradient free approach such as hill climbing.

Camacho et al. present several approaches to the ANN based Generalized Predictive Control. One interesting approach is the use of Hopfield network for the optimization stage of the GPC (Quero, Camacho *et al.* 1993). Hopfield networks are of particular interest due to the characteristic of parameters space optimization.

In the context of MPC, **ANN** can be used with a different approach for example as system linearization. Gawthrop presents a piecewise-linear model for the approximation and control of nonlinear systems (Gawthrop 1996 (a)). The strategy consists in an arrangement of local linear models based on ANN controlled by respective PID regulators, creating therefore a linear-piecewise grid representation of the system.

A different approach is presented by (Haley, Soloway *et al.* 1999) for modelling a magnetic levitation device (MAGLEV), which is an open-loop unstable system. The controller strategy is based on the GPC and the minimization of the objective function. The model of the plant based on **ANN** consists of a combination of a fixed linear network structure and a variable network structure so as to identify the unmodeled dynamics of the MAGLEV. The result is a stabilized plant with low computational cost due to few iterations of the Newton-Raphson optimization method.

Another approach is the reconfigurable controller based on **ANN;** a comparison between the Neural GPC and Neural Dynamic-Inverse controller for aircraft is given in the literature (Soloway and Haley 2004 (a)). The reconfiguration consists in the augmentation of the controller structure so as to account for surfaces and engine failure. The Neural GPC controller gave better results than the Neural Dynamic-Inverse approach due to the inclusion of constraints and the receding horizon approach.

2.2.10. Controller Architecture Summary

The field of controller architecture has been extensively researched by the scientific community. So, in order to narrow the choices, the author decided to explore two leading ideas: **simplicity** and **effectiveness** for the HPR controller structure.

The **simplicity** of the model is supported by hints in the field of system identification, coarse granularity, adaptive control and model predictive control, apart from common sense (Ljung 1987; Narendra 1989; Camacho and Bordons 1999; Israeli and Goldenfeld 2006).

The **effectiveness** of the HPR controller structure is based on ideas of Brooks about the importance given to the whole process with respect to individual requirements of the HPR (Brooks 1987; Brooks 1991). For example, this idea is applied by giving high priority to the energy management compared to other scheduled activities because of the crucial role of the energy optimization for the HPR journey.

Finally, the HPR controller model incorporates useful characteristics from Meystel's and Albus' Multiresolutional Hierarchical Planning Model, such as the architecture operators and the structure evaluation by a performance index (Meystel and Albus 2000).

An example of **heterarchy** is the control architecture for flexible control based on a bus communication for sensors/actuators with redundancy (Kim and Yuh 2004). The heterarchical architecture is a combination of the traditional **hierarchical and the subsumption architecture** approach in a sense of input/output devices shared by different controller activities. The purpose of this structure is controllability, stability and time response, at the same time lowering the communication load.

A different point of view is the biological mimic architecture for instance the **artificial immune system (AIS)** for collaborative autonomous guided vehicles in a warehousing environment (Lau, Wong *et al.* 2007). The control approach is composed of **self-organized distributed multi-agents,** opposed to centralized control in a hierarchical architecture; this allows vehicles to accomplish the task whilst communicated with each other and sensing the environment.

2.2.11. Modelling the HPR system

What kind of model is suitable for the HPR?

System identification relates to modelling. The basic question in modelling a system is: **what kind of model is the most suitable for the problem under research?**

Narrowing the spectrum, **what is the model for?** Here is a list of options for model applications (Ljung 1987; Nelles 2001):

1. Model for Prediction, relates inputs-states vs. output
2. Model for Simulation, relates input vs. output disregarding the states
3. Model for Optimization for performance evaluation
4. Model for System Analysis based on input/output measurements
5. Model for Control, to be included in a more general structure
6. Model for Fault detection for a benchmarking of plant vs. nominal model and plant vs. fault model. Any discrepancy triggers the unbalance among the models.

The function of the **HPR model is for prediction** of future states of the output. The obvious reason is because the HPR model is inserted in a class of predictive controller, Model Predictive Control (MPC). The less obvious one is because predictive

models depict the system in their overall characteristics including dynamics rather than exploring a particular feature of interest, which is the case of simulation models for testing a range of dynamic behaviour.

What experts say about models?

Camacho argues that almost any industrial plant/process can be modeled with first order differential equations. In most complicated processes, the modelling can be a **chain of first order differential equations** (Camacho and Bordons 1999).

The theory of cellular automata demonstrates that coarse-grained models are efficient for describing large scale dynamics without the need of small-scale information (Israeli and Goldenfeld 2006). This proved theory calls for efficiency combined with simplicity.

In relation to the function approximation of a system, two theorems, Weierstrass and Stone-Weierstrass theorems, refer to the system description; in short: a system can be accurately approximated by a large number of functions (provided a dense space of approximating polynomials) (Åström and Wittenmark 1995).

A different point of view (common sense) but, to some extent with equivalent result, is presented by Ljung, who says that *"a model doesn't need to be perfect; it needs to be good enough for the purpose of the model"* (Ljung 1987). Furthermore, any modelling mismatch needs to be addressed specially, in particular because the model uncertainties affect the behaviour of model-based controllers(Ljung 1987).

Following the line of thought of Ljung of finding a suitable model for the purpose of the study, there are three main characteristics conveying useful information of the system however with high mathematical and computational cost. These characteristics are **accuracy, nonlinearities and disturbances**. Thus, the question is: **how important are these characteristics for the HPR model?**

Accuracy and granularity of the HPR model relates to have perfect knowledge about the HPR energy conversion and energy dissipation. Such a model is efficient because it includes the turbine, tractor and environment.

Nonlinearities are inherent in every single component of the Hybrid Pipeline Robot, e.g. turbine, tractor, environment and subcomponents. Therefore, the nonlinearities contain distinctive information that cannot be neglected.

Disturbances, specifically random disturbances, are the core of the HPR controller challenge because they affect the availability of energy, energy dissipation and therefore energy optimization (Bolkvadze 2002).

In conclusion, these three characteristics, **accuracy, nonlinearities and disturbances**, in spite of the modelling cost, are fundamental components to be considered in the HPR model and define the "goodness" of the model in Ljung's words.

Now, how to match the HPR model with the controller?

It is important to outline the controllability requirements for the HPR system: the purpose of the controller is to drive the HPR to the target point, to perform scheduled tasks and to return to the starting point. Additionally, in case of failure, it is required that the HPR performs a self-recovery action. Based upon these requirements, the **HPR predictor model** needs to include information related to flow rate characteristics, turbine efficiency, tractor efficiency and HPR Environment, referred mainly to pipeline wall conditions

The system identification of the HPR is a Simple Input Simple Output (**SISO)** plant: **flow rate** as the input and the **tractor speed** as the output. Therefore, tractor efficiency and environment characteristics are modeled through drag forces affecting the behaviour of the bristle units and measured through the tractor speed.

The controller output is the control signal, which drives the system to the desired state. The control signal is the result of observing future predicted states of the system and future moves or control actions. The system predictor is based on the system model and the control actions are the input of the system model. Hence the importance of the system model for control purpose.

Therefore, the next step after finding the system model is to design the system predictor. The classical approach is to characterize the system through **state observers** and **predictors**.

The standard approach for the **state observer** is based on the Kalman filter, where the estimated values of the output are obtained through a recursive state estimation. However, when constraints are considered, the Kalman filter is of no applicability. Therefore, the concept of moving horizon has a fundamental role in limiting the dimensionality of the problem as it is proposed in the literature (Rao, Rawlings *et al.* 2001). However in cases where the state information is unavailable, the literature proposes the design of a state observer based on the concept of set-membership. The set-membership is defined by the division of the state space in

regions through a minimum volume of a parallelotopic approximation (Bemporad and Garulli 2000). The model also has added disturbances to account for model uncertainties and noise in the output.

There are several approaches to the prediction of system output but the most popular are the use of a state observer like the **Smith predictor**, recursion **of Diophantine equations** and **system identification**.

One of the most popular observers is the **Smith predictor** for the prediction of the system output, which can be used in different ways so as to improve the system performance. For instance, errors in the dead-time estimation can be reduced with the application of a filtered Smith predictor; thus making the system robust to the variations of the dead-time (Torrico and Normey-Rico 2007). Another application, for example, is a MPC combined with a Smith predictor used for controlling a solar air conditioning plant. The predictor produces a feed-forward signal so as to compensate the system for variations due to clouds or temporary disturbances (Núñez-Reyes, Normey-Rico *et al.* 2005). The result is a controller robust to disturbances model.

2.2.12. HPR model: System Identification approach

Another approach for building the system model is the **system identification.** One of the many approaches of system identification is the **black box model** that is appropriate for systems that are difficult to characterize through parametric or analytical models, yet where it is feasible to perform measurements of the main system variables. Thus, the characterization is through the measured values of input and output of the system. This approach is applied to the HPR modelling and it presents the advantage of modelling system characteristics, which are otherwise rather difficult to include in the model such as drag forces or friction losses (Ljung 1987; Söderström and Stoica 1989; Nelles 2001; Chadeev 2004).

The concepts of Narendra summarize fundamental considerations for system identification and control in particular structures based on Artificial Neural Networks (ANN) (Narendra 1990 (b)). Narendra proposes basically two models for system identification based on ANN: **parallel and series-parallel models**. This reasoning can be extended to nonlinear systems, although it is originally conceived for linear systems (Narendra 1990 (b)).

The literature about **ANN and control systems** is vast and the research area is mature with continuously successful applications. Merely citing some referential work,

the survey of (Hunt, Sbarbaro *et al.* 1992; Pham and Xing 1995; Chong and Parlos 1997; Bernd, Kleutges *et al.* 1999; Lazar and Pastravanu 2002; M'Sahli and Matlaya 2005; Ławry Nczuk 2007) contributes with several "seminal" work, and gives solid theoretical background for applying consistently connectionist theory to real world problems.

Despite these identification structures are expressed as linear systems, they represent nonlinear systems when the neural networks are applied in the feed-forward and feedback path.

The main feature of neural networks in approximating nonlinear functions is that they are composed of a large number of layers, each performing a nonlinear transformation (Narendra 1990 (a)). Therefore, ANN can be a dense set of arrays of parameters capable of approximating or mapping any arbitrary dynamic system. This fact is supported by the theorems of Weierstrass and the Stone-Weierstrass, which in a few words state that the space of function approximation is dense (Narendra 1990 (b))

Combination of ANN with different control approaches also has steadily received attention over years. A variation of MPC, the Dynamic Network Control (DNC) uses a plant identification, which is denominated here "inferential control", combined with a PI controller (Willis, Montague *et al.* 1992). The ANN are used for output prediction and the cost function is computed in an explicit way.

An example of **system identification** for linear systems with complex correlation and cross correlation patterns for the input and output variables is presented in (Ahmad, Chipperfield *et al.* 2001). A twin-rotor hover vehicle system model has two degrees of freedom and multiple input multiple outputs. The main difficulty or challenge is the correlation and cross correlation between the different input and output channels as well. The model was tested for prediction with good results.

2.2.13. Receding Horizon Strategy: Prediction and Control Horizons

The **model predictive control** (**MPC**) is based on the **receding horizon** strategy. Receding or moving horizon means the control action is obtained upon the optimization of the objective function and then it is applied to the plant; this process repeats at every sample state. But, what does the receding horizon mean? Receding horizon is the time span during which tracking errors and the control increments are considered. As a consequence, the information contained in the horizons is affecting the control signal to be applied to the plant. There are several combinations of horizons for tracking error

and control steps, as many as there are different control problems. However, the leading thought behind the horizons is to stabilize the system under control whilst tracking the reference with a minimum error in a predefined time span. Several studies offer different receding horizons approaches (Shreve and Bertsekas 1977; Clarke, Mohtadi *et al.* 1987 (a); Clarke, Mohtadi *et al.* 1987 (b); Alamir and Bornard 1994; De Nicolao and Scattolini 1994; Yoon and Clarke 1995; Primbs, Nevisti *et al.* 1999; Bemporad and Morari 1999 (a); Rao, Rawlings *et al.* 2001; Lee, Kouvaritakis *et al.* 2002; Torrico and Normey-Rico 2007; Grune and Rantzer 2008)

2.2.14. Tracking System

Why tracking system for the HPR?

The definition of tracking in the dictionary is *"to follow … to record the progress or development of something over a period"* (Cambridge Dictionary 2009). In the context of control system tracking means to manipulate the system to produce the output of the system to follow a target value.

In its simple conception, tracking means to follow only one desired target at a time. However, most of the real systems need further specifications such as the time required to reach the target, defined as the **reachability**, and the tracking error, which is the difference of the output of the system and the desired value. The tracking error is the **stationary state error** for invariant systems, otherwise the **stability analysis** for dynamic systems.

Hence, from the simple definition of tracking, the theory about tracking starts to expand in order to represent cases in the real world, and due to the complexity of the tracking problem, it is better defined as tracking system rather than tracking. The following paragraphs are examples of the core aspects of tracking systems that bear relation to HPR tracking characteristics to define and develop the tracking system for the Hybrid Pipeline Robot.

In relation to the **reference model**, two basic categories can be distinguished: tracking of a constant and tracking of an arbitrary reference. The idea behind the constant tracking system is to match the tracking point with the equilibrium point of the system output (Mayne, Rawlings *et al.* 2000). In the last option the literature makes reference to **tracking governors** that modulate the tracking signal through integration

of the set point trajectory. The main goals in relation to the reference modelling are to achieve an **offset-free** and **stable** controlled system when tracking the reference.

Tracking errors are affected by the model of the system. An example from the literature on Receding Horizon Control, where the observer output is a piecewise linearized function at each point in a seed trajectory. In this case the error due to the linearization of the function is included in the tracking error so as to define realistic **bounds of the error** (Lee, Kouvaritakis *et al.* 2002). Therefore, in the design of consistent optimization policies it is important also to specify the tracking error and its bounds.

Different approaches to modelling **nonlinear tracking systems** are: the State-Dependent Riccati Equation (SDRE), the Sontag's formula, which include the Lyapunov Function, the geometric approach and the Input-to-State approach with uncertainties (Wei 2007).

Several strategies can be found in the literature in order to pursue these goals. A particular case of GPC, the **Long-Range Predictive Control (LRPC)** applies an algorithm for **reference smoothing**. The smooth transition of the output to the desired set point is achieved through the use of a transition set point defined in the literature (Clarke and Mohtadi 1989).

A class of **reference smoothing** is given by the inclusion of **constraints** in the tracking system (Bemporad 2006). In this report, the constraint is the time elapsed during which the tracking error is tolerated, apart from the tracking error in itself

An **offset-free** response is proposed by Soloway through an augmented controller in a reconfigurable approach. The reconfiguration of the controller consists in the inclusion of the position error, the controller becomes redundant in the tracking sense (Soloway and Haley 2004 (a)). This redundancy becomes of particular interest when controlling unstable open loop plants such as aircraft or MAGLEV devices.

Another way of offset-free response when tracking the reference, is achieved with the inclusion of a disturbance model to the state observer, as it was reported in (Pannocchia and Bemporad 2007) and (Maeder, Borrelli *et al.* 2009). In the particular case of the first paper it was an integrating disturbance model. This approach is interesting when dealing with non stationary disturbances as in the case of the Hybrid Pipeline Robot.

A similar approach for differences to the **tracking schedule** is presented in the dual mode approach for tracking system of a formation of UAV (Wang, Yadav *et al.*

2007). This dual approach refers to the safe and danger modes, which relate to the **obstacle-free and obstacle-constraint** respectively. The tracking path generation for the safe mode, without obstacles, is accomplished through a global optimization algorithm, which is based on the individual and combined dynamics of the vehicles. The danger mode, with inclusion of obstacles, is based on the vision system for generating optimal/suboptimal trajectories. These trajectories are generated through Grossberg Neural Networks. The control architecture, a two layered approach, consists of a route generation in the upper layer, and a model predictive control in the lower layer for tracking control based on constraints.

Another example of a multimode tracking system is the **multi-objective** independent controllers to give **stable** sub-controllers for conic sub partitions of the total reference space, provided each conic subdivision is stable (Koutsoukos and Antsaklis 2001).

2.2.15. MPC: Objective Function J_{Speed}

Why objective function for the HPR?

The objective function is the representation of the optimization problem. It is open to include any term the designer considers useful to optimize. In spite of this freedom, the Model Predictive Control has its basic objective function, which includes the tracking error and the control steps. Apart from this basic function, the optimization problem can grow freely based upon the designer criteria.

In the HPR case there are three objective functions: objective function for speed control, objective function for travelling action and objective function for recovery action. To give more details, the first objective function refers to the tracking process and it is strictly the objective function of the GPC problem that involves the error of tracking and the control increments. It is a constrained optimization problem with energy and stability constraints. The second and third objective functions are similar in terms of the energy optimization equation and belong to a dynamic programming approach because it is a problem of energy optimization through the whole trip. The difference between both objective functions is the set of constraints and the constraints prioritization. The next paragraphs give some foundations for objective function optimization, the constrained problem and the way of solving the optimization problem, which gives as a result the control action to be sent to the plant.

As mentioned earlier, the control law is derived from the optimization of a cost function (Clarke, Mohtadi *et al.* 1987 (a)). The control law gives a sequence of control actions u(t), from which only the first term is applied to the system and the others are discarded. The solution implies to finding the inverse matrix of the system. The matrix inversion is an impediment for many real systems, which are nonlinear (Camacho and Bordons 1999).

This cost function is the successor of the **generalized minimum variance (GMV)** control approach, with the improvement of the cost horizons, which allows the algorithm to converge inherently to a **stable** system, provided a suitable stabilizing constraint is included in the control law. The predictive characteristic and the receding horizon strategy of the GPC make the controller **robust** to variable or unknown dead time (Clarke, Mohtadi *et al.* 1987 (a)).

The **prediction horizons** are selected so as to observe the output signal and its meaningful changes e.g., dead-time and rise time. Therefore, the lower output horizon needs to be greater or equal to the dead-time (it would be meaningless to observe the output during a time before the dead-time). The upper output horizon needs to include the rise time. For non-minimum phase system, with zeros in the unstable region, it is recommended to choose the upper horizon in a sufficient span to observe at least the first oscillations (Clarke, Mohtadi *et al.* 1987 (b)).

In relation to the **control horizon**, choosing a horizon of only one step performs very well for a stable minimum phase system. If the system is non-minimum phase, the value of the control horizon needs to be approximately equal to the number of poles close to the boundary of equilibrium (Clarke, Mohtadi *et al.* 1987 (a)). Therefore, the control horizons need to account for future unstable states of the system. The idea of predicting future moves is to lead the system output to the target value in a smooth way. This feature gives the characteristic of **offset-free** to the Generalized Predictive Control (Clarke and Mohtadi 1989).

The importance of considering **the increments of the control actions** instead of the actual value in the objective function, leads to a terminal state minimization of the objective function even for non-zero control signals. As a result, a zero control signal is not required in order to get the optimization of the objective function. This approach for increments of control moves reduces the number of parameters included in the control action compared with the full-valued control signal approach. Hence, one practical

approach in choosing the control horizon is to set the increments of the control signals to zero after the predefined control horizon (Clarke and Mohtadi 1989).

A variation **of Receding Horizon Predictive Control (RHPC**) includes a time varying **weighting factor** (Yoon and Clarke 1995). The weight increases in time so as to compensate for future errors. The weighting effect produces an increase in both the objective function and the control signal. This approach is applied in the Constrained Receding Horizon Predictive Control (CRHPC) and the Stabilizing Generalized Predictive Control (SGPC). The time variability and the increase of the weights have an effect of time averaging of the errors. As a consequence the control signal is smooth, preventing overshooting and therefore dynamic instability.

The on-line solution of the control law is computationally expensive because it implies the solution of a quadratic programming problem at every sampling stage; yet it is suitable for processes with long time constant. For fast systems faster solutions are required; therefore, off-line computation is preferred. In this case, the state space is converted into a **multiparametric vector** and the solution is a piecewise linear function. The state space can be visualized as a set of polyhedral sub-partitions. The optimization algorithm is reduced to a function evaluation at each polyhedral region. This is a case of **multiparametric programming**. This method is exhaustively studied by the research group of Professor Morari and includes the development of free software for the solution of multiparametric programming (Bemporad and Mosca 1998 (a); Bemporad and Morari 1999 (a); Munoz de la Pena, Alamo *et al.* 2004; Borrelli, Baotic *et al.* 2005; Munoz de la Pena, Alamo *et al.* 2005; Bemporad 2006; Björnberg and Diehl 2006; Baotic, Borelli *et al.* 2008).

The evolution of the MPC has a close relation with the algorithm evolution or the way in which the cost function is calculated. The traditional objective function calculates implicitly the control law; this way is suitable for on-line computation. New solutions are based on the explicit expression of the state variable to get the vector of control or manipulated variable; this approach requires off-line computation. The last method is based on **multi-parametric quadratic programming (MPQP)** instead of the linear quadratic programming for the original MPC (Bemporad 2006). A complete survey of Model Predictive Control (MPC) and the main features is provided in (Bemporad and Morari 1999 (a)). Fundamental topics such as robustness and conditions of stability for the MPC and in general Receding Horizon Controllers (RHC) are addressed.

Therefore, the solution of the objective function is an optimization problem; and it can be unconstrained or constrained. The simplest version, the unconstrained, requires only the solution of the objective function so as to get the control signal. However, in real life, constraints are everywhere defining systems and designs. So, the next section gives an overview of the rationale of constraints.

2.2.16. System Constraints

The control law of the MPC is the solution of an optimization problem: the objective function is minimized with respect to some criterion such as the control moves and tracking error. The model of the control law may include some constraints so as to shape not only the system response but also the control moves, in particular with the objective of **stabilizing** the system. For instance, the control law may include a constraint that set the control steps to zero after a determined horizon, this is the case of the Dynamic Matrix Control approach (Clarke, Mohtadi *et al.* 1987 (a)). One variation of this scheme is to include a constraint that **attenuates** unbounded control signals (Alamir and Bornard 1994).

Constraints affect different components of the control system: constraints in the input or manipulated variable, constraints in the tracking process, constraints on the states, which lead to bounded output, apart from other functional or economical constraints (De Nicolao and Scattolini 1994; Torrico and Normey-Rico 2007). The constraint space leads to a complex representation of the cost function.

There are several variations of **stability constraint** but the most common are terminal state constraint, invariant terminal set-membership constraint, constraint of a terminal weighting matrix, which require the solution of a Riccati inequality and contraction constraint, which is the convex hull of a constraint of the terminal state in some norm (Bemporad and Morari 1999 (a)). System stability and constraints are developed in more detail in the System Performance section.

Hard **constraints** can be relaxed through the inequality relationship of the variable and the bound region. This alternative is to make feasible the region of the variable through the **soft constraint**. Some approaches include a **penalizing factor** so as to qualify the constraint violation. Other approaches include the **time factor** and relate the constraint violation with the time around which the constraint transgression is admissible. The last approach relates to multi-objective control, mentioned in the literature (Mayne, Rawlings *et al.* 2000).

One interesting example of objective function with **constraints** is given in the literature for **reconfigurable control** (Soloway and Haley 2004 (a)). The reconfigurable control law consists of four terms: one trajectory error, and three constraints. Two of those constraints are for actuators of position and speed, and the third constraint is for symmetrical use of actuators, for example to prevent conflicting operation of ailerons and elevators or surfaces, spoilers and flaps (Soloway and Haley 2004 (a)). The quadratic function is solved through the application of the Newton-Raphson recursion method. The applicability of the Newton-Raphson method is subject to the definition of the constraints as a convex set; this condition implies that all constraints are derivable. Despite the fact that Newton-Raphson method needs the solution of the Jacobian and the Hessian of the system, the expensive computation is reduced to fewer iterations due to the selection of a short run horizon (Soloway, Shi *et al.* 2004 (b)).

The state transition in a finite time or finite number of steps for discrete signals is considered in the **reachability analysis.** A particular problem is posed by the reachability for **hybrid control systems** with mixed signals constraints in the input and output variables, which can be solved through a piece wise affine function (PWA) with constraints defined as polygons (Rakovic, Kerrigan *et al.* 2006). The solution is through **Polyhedral Algebra** and **computational geometry** (Bemporad, Heemels *et al.* 2001).

2.2.17. Objective Function Optimization

As it was expressed before, the **constrained control law** results from the **optimization of the objective function** subject to system constraints such as input/output, stability, robustness, performance, and even economical constraints (Bemporad 2006). **Optimization** algorithms can be **classified** as for linear or nonlinear systems. The structure of the cost function and constraints determine the **method of solving the optimization problem**: if the cost function is quadratic, **L_2-norm**, and the constraints are linear so the method for solving the problem is quadratic programming (QP); in the case of cost function structures of **L1-L∞-norm** the method is linear programming (LP); **nonlinear objective function** and nonlinear constraints are solved through nonlinear programming (NLP); if the cost function solution relates to a stepwise decision process, then dynamic programming is the natural solution for optimizing the cost function (Rao 1996). A comprehensive optimization survey is in (Roy, Hinduja *et al.* 2008).

In the case of quadratic optimization function and linear constraints, solved by quadratic programming, the solution space can be visualized as a Polytopic hull with inner approximation in a convex space (Mayne, Rawlings *et al.* 2000). If the optimization problem is nonlinear the space is not convex and it calls for sub-optimal optimization with local rather than global optimization.

A survey of trends in optimization in three of the main optimization areas: design, operations and control is given in (Biegler and Grossmann 2004). In particular the paper focuses on the new developing areas of nonlinear programming NLP in the case of nonlinear objective function and **mixed integer linear and nonlinear programming MINLP** for cases of decision making and scheduling. The paper summarizes the methods and the convergence conditions.

One approach to the solution of the objective function optimization is through the application of **interior point method** and the solution of the Riccati recursion as a quadratic programming QP problem (Rao, Wright *et al.* 1998).

In the literature an approximation of the solution of the **min-max problem** through the application of quadratic programming is found. This approximation consists in modification of the original objective function, where the new objective function is the upper bound of the original one plus an appropriate matrix, which satisfies the equality $\overline{M} = M + F$ (Alamo, Ramirez *et al.* 2007). This boundary approach in the solution of the objective function is an alternative to Linear Matrix Inequality method, multiparametric programming and feedback MPC, which enforces the state to converge to a trajectory tube membership (Alamo, de la Pena *et al.* 2005).

When the objective function is no longer a single objective, but the constraints represent side objective functions, the optimization problem is a **multi-objective optimization**. The solution of multiple objective functions is not unique and constitutes a **set of Pareto optimal solutions.** These solutions are selected because they optimize the related objective function without affecting the optimization of the other objective functions. The selection of optimal solutions, taken from a set of **Pareto optimal solutions**, is facilitated by the even distribution of solutions. There are several methods to achieve this desirable characteristic, one is the inference method of search in the feasible space, finding global Pareto solutions rather than local ones (Utyuzhnikov, Fantini *et al.* 2009).

Some constraints in the inference process can be thought of as tasks in a scheduler with their own **constraints**, for example, **time-window** and **precedence constraints** (Sciomachen 1994). In that way, constraints are arranged in a hierarchy of inference rules for the optimization function to select the optimal region among a set of **optimal Pareto values** (Rao 1996).

Ruzika et al. present a survey of the approximate methods for selecting the meaningful points in a set of **Pareto optimal solutions**, so as to simplify the final decision stage (Ruzika and Wiecek 2005). The paper also provides a quality approach for the measurements and the classification of the approximation measurements.

A survey of **trends in optimization** in three main areas: design, operations and control is given in (Biegler and Grossmann 2004). The survey particularly focuses on the new developing areas of **nonlinear programming (NLP)** in the case of nonlinear objective function; **and mixed integer linear-nonlinear programming (MINLP)** for cases of decision making and scheduling. The paper summarizes the methods and the convergence conditions.

A different approach considers the **multi-objective optimal problem** equivalent to a single-objective problem composed of the addition of **weighted constraints** (Rangan and Poolla 1997). The paper presents a theorem, which demonstrates the equivalence of the single and multi-objective problem, provided it is possible to find a controller for the different combinations of weighted constraints.

Evolutionary algorithms are used for improving the solution of **multi-objective optimization**, for example the optimization of a poly reactor process with several decision variables using a n**on-dominated sorting genetic algorithm** for the generation of Pareto optimal solutions (Tarafder, Rangaiah *et al.* 2007). The problem is solved by considering the decision variables separately, identifying and increasing the **multimodal solutions**, which are Pareto optimal solutions capable of optimizing simultaneously different objective function (Tarafder, Rangaiah *et al.* 2007). However, the algorithm turns out to be expensive in terms of the amount of time.

The area of **design optimization,** although different from control optimization, has interesting approaches. For instance, the design optimization of Unmanned Aerial Vehicles, based on Genetic Algorithms (Ng and Leng 2007). Although a different application field, the common objective with the **HPR** is the **optimization of the components configuration**. The common point with the HPR may be the consideration of the energy components: turbine and battery; the components structure

can be optimized so as to give optimal performance. The method presented is the performance optimization after operations of mutation and cross over of the configuration options.

Another consideration about optimization are the solution of systems greater than second order; this solution embodies the concept of **global optimization** for finding global minima-maxima for constrained problems and characterizing the set of neighbour points (Floudas, Akrotirianakis *et al.* 2005) . A rather different approach is **Multiparametric programming (MP**), which offers the solution of multi parameter objective function. The algorithm solves the convergence to a stable point of a piecewise affine function (PWA) in a sub-partitioned state space (Baotić 2005; Borrelli, Baotic *et al.* 2005; Baotic, Borelli *et al.* 2008).

The optimization approaches overviewed so far bear comparison with the optimization of one of the objective functions of the HPR controller: the one related to Model Predictive Control in order to find the optimal control law for speed control. The next paragraphs give a different approach, optimization through time, which is dynamic programming and is used in the HPR controller for defining the algorithmic solution of the other two objective functions related to energy optimization.

2.2.18. Energy optimization: a Neuro-dynamic programming approach

Why DP?

The HPR energy management system needs to optimize the energy at every stage of the process. In particular the stored energy can be seen as a **final cost optimization**, a problem composed of several stages with their own decision. The general problem can be thought of as an **optimization problem over time**. A classical and efficient method to solve optimization over time is **dynamic programming (DP)** (Barto and Dietterich 2004). The following paragraphs give the dynamic programming background that supports the **HPR energy optimization** solving two of the three objective functions of the HPR controller.

A system can be described as a function of the process, and evaluated through the cost function. The **cost function** is the relation of the present and future states of the system, weighted by cost factors or penalties on future actions. The idea behind it is to minimize the cost function so as to minimize the overall penalties. Besides the

minimization it is a problem of function optimization because it is rather difficult to know in advance and with certainty the future costs to be incurred (Bertsekas 2005 (b)).

Where decision taking is concerned, **DP** considers two approaches: **open and closed loop**. In the open loop algorithm all the decisions are taken at the same time, while in the closed loop decisions are taken in several successive steps. Therefore, the closed loop has the advantage of making a decision based on the knowledge of previous steps (Bertsekas 2005 (b)).

One advantage of the closed loop approach is that decisions can be delayed until k-period, to collect more information to support decisions, provided there is no future cost in the delay. The final cost, for stocks problems, depends on the penalties of having stock in excess or in shortage when the period finishes (Bertsekas 2005 (b)).

In the **HPR** case the energy optimization has a final cost to be optimized, e.g. to return to the starting point with a certain level of energy. The objective function has a final energy cost to be optimized and additional terms of penalty for a shortage in energy.

Dynamic Programming and **Hybrid Systems**: Borelli et al. provide a solution for hybrid systems in particular a discrete time hybrid system (Borrelli, Baotic *et al.* 2005). The solution of the problem has three parts. The first part is the **design of the system** through a **piecewise affine (PWA)** model for discrete time systems. The second stage is the **design of the control law** or the optimal control solution and the third is the method **to solve the optimal control function**. The contribution of the paper is a novel algorithm to solve the **Hamilton-Jacobi-Bellman equation** through **multiparametric programming**.

Forward dynamic programming and arrival cost is applied for the smoothing effect of the arrival cost, which has an integrating effect so that fixing the dimensionality of the problem becomes feasible (Rao, Rawlings *et al.* 2001).

The **min-max control** approach is a frame for stochastic variables which are defined by their bounds. So the stochastic variables are bounded by above by the maximum, which is the smallest greatest value and bounded by below by the infimum, which is the greatest minimum value (Bertsekas and Rhodes 1971 (d)). The min-max control is a feasible alternative to stochastic control, which needs information about the probabilities of occurrence of the phenomena that is sometimes difficult to know in advance.

The **neuro-dynamic programming** approach bases its principle on **reinforcement learning**: a concept of the cost associated with each decision of an overall stepwise optimization problem in a sense of reward and punishment (Barto and Dietterich 2004). Neuro-dynamic programming structure consists of an artificial neural networks for the system model and a cost function for evaluating the overall cost of dynamic programming (Bertsekas and Tsitsiklis 1996 (a)). Neuro-dynamic programming optimization has its solution in the policy space based on a vector of optimal policies. It is an alternative to numerical optimization and vector optimization (Bertsekas and Tsitsiklis 1996 (a)). In that sense, neuro-dynamic programming offers a solution to problems with the course of dimensionality mentioned by Bellman (Bellman 1965). By making feasible many of the dynamic programming problems, ANN offers an advantage over HPR energy optimization in particular because the final stage is unknown a priori and it is only determined in the course of action of the tractor. Therefore, the energy optimization problem is of variable dimensionality and the ANN are a ubiquitous solution for this kind of problem.

Another useful notion of dynamic programming for **HPR energy optimization** is the **separable dynamic programming** approach to deal with the state space decomposition when there are stages of different natures. These sub-dynamic programming problems can be approximated by sub-structures of neural networks, which perform the space approximation of the problem (Bertsekas 2007). One important concept in the separable dynamic approach is the r**eachability of the state**, which is equivalent to the transformation of one state to the next state through the control action in a finite time (Åström and Wittenmark 1990). This concept of reachability has been embedded in the constraints of the MPC for the control speed of the tractor. To conclude, the constraint of positive speed assures the transition of one stage to the next one in a finite time, avoiding the forbidden state of energy optimization at the cost of zero speed or stalled tractor.

2.2.19. System Performance Evaluation

The performance of the system is determined by the specifications combined with three fundamental concepts: **stability**, **robustness** and **feasibility**. The next sections explore briefly antecedents of these concepts for their applicability to the HPR system.

System Stability and Constraints

The bases for discrete and optimal control and fundamental concepts for stability and robustness are presented in (Åström and Wittenmark 1990), the foundations for adaptive control, stability and robust control (Narendra 1989; Åström and Wittenmark 1995).

The s**tability of the system can be modelled mainly in two ways:** implicit in a Lyapunov sense or explicit by the enforcement of some norm criterion of the terminal state. In the implicit way, the control law includes a Lyapunov candidate function with the structure of a value function and equality constraint approaching infinity. In the explicit way for stability modelling, the terminal state constraint is a single-valued function or a set-membership in the constraint space, which can be assumed to be an invariant set. This approach for invariant set membership constraint has a shape of convex hull and is represented by a L_2-norm, with quadratic programming solution (Bemporad and Morari 1999 (a)). Another approach to stability enforcing is the contraction constraint where a normed final state shrinks or contracts toward infinity.

One of the ways of **Model Predictive Control** is to include additional terms as **constraints** to guarantee system stability. Another way is to enforce the stability through a **receding horizon strategy**, which can be classified mainly in two classes: **classical receding horizon** where only the present value of the control law is applied to the system and interval-wise or **periodic receding horizon** where the control law for several steps ahead is calculated and applied to the system. In the last approach, the control law is not recalculated at every sample time but only at defined periodic steps; it helps to smooth the control action improving the system stability. This approach is valid for plants where the sample rate is high (De Nicolao and Scattolini 1994). This paper gives also the proof that the inclusion of terminal constraints in the objective function is a valid strategy for stabilizing the system. Additionally, weighting of the error and control terms are applied to improve further the stability of the system.

The stabilizing characteristic of the **Constrained Receding Horizon Predictive Control** through the application of the Predictive Control and Dynamic Programming approach are given in (Chisci and Mosca 1994). A comparison of the receding horizon control algorithm and the infinite horizon control from the point of view of stability is presented in (De Nicolao and Bitmead 1997). The study point out the application of the

truncated or Fake Riccati Equation for analysis of stability in the two different modes: monotonic and cyclic-monotonic.

Model Predictive Control and optimal feedback control is based on the Hamilton-Jacobi-Bellman sufficient condition for optimality and the principle of optimality of Bellman, which presents the basis for step-wise calculation of the optimal open-loop control (Bellman 1965). This approach leaves the feedback control loop for cases with uncertainty. Another important remark is related to Kalman's observation that optimality does not necessarily represent stability for the infinite horizon case. But stability can be reached at infinity defining the **stability in a Lyapunov sense** or asymptotic stability, finding a Lyapunov candidate function associated with the control law. In this way the process of the calculation of the control law starts to increase the complexity, yet also increases effectiveness because not only is the control signal calculated at every step but also stability is guaranteed at least asymptotically (Mayne, Rawlings *et al.* 2000). Rao, Rawlings et al. give an example of stability in the observer sense, based on a **Lyapunov candidate function** (Rao, Rawlings *et al.* 2001). The stability conditions of the state observer are based on the constrained measurements and receding horizon forgetting effect.

The open-loop optimal control approach for the MPC with terminal equality constraints can stabilize plants that cannot be stabilized with continuous feedback control (Mayne, Rawlings *et al.* 2000). In general the stabilizing methodology can be categorized **as terminal state constraint** and **terminal cost constraint**. Terminal state constraint is a set-membership constraint X_f (.) and the terminal cost function is a weighting function F_f(.).The stability of a piecewise linearized system at points of a seed trajectory is guaranteed through the inclusion of a terminal cost as a terminal inequality constraint (Lee, Kouvaritakis *et al.* 2002).

The stability analysis for the GPC-based reconfigurable system has two stability approaches: stability of the system without reconfiguration based on the monotonicity of the Riccati recursion and stability under reconfiguration so as to ensure the state after reconfiguration and the transition states are stable (Soloway, Shi *et al.* 2004 (b)). Stability is guaranteed through the final state equality constraint approach.

MPC is stable by design through the inclusion of terminal state constraints in the objective function. However, in practice, sometimes these constraints are removed so as to provide the system with good performance, in particular for a short run prediction horizon. Consequently, once the stability constraint is removed it is necessary to use

alternative stability tools to keep ensuring the stability of the system. One alternative solution to stability assurance is to apply approaches from **hybrid control systems** (Bemporad, Heemels *et al.* 2001). This paper proves that the MPC is a sub class of a set-membership Hybrid Control System.

A particular case of MPC is presented by Bemporad where stability of a linear system with state and input constraints is guaranteed (Bemporad 1998 (b)). To reach stability, two options are mentioned in the publication: the first is stability guaranteed by a zero-terminal state constraint and the second alternative is stability under an infinite horizon. The first option, the zero terminal constraint produces tracking errors in particular for short prediction horizons. Thus, the infinite horizon option presents a viable alternative. However, as the horizon recedes to infinity the constraints also increase asymptotically to infinity. To solve this problem, instead of zero terminal constraint, the idea is to increase the region in which the state can be found at infinity. So, an ellipsoid space is defined by the quadratic terms of a Lyapunov candidate function. The terms are considered as a L2-norm so the solution is a quadratic programming approach and the geometry is a convex polytope. Therefore, stability improves when the volume of the ellipsoidal solutions is increased, in order to contain the majority of the feasible states. To conclude, the stability problem of a linear constrained system is solved in the range of a finite horizon, through the inclusion of a terminal constraint, which converges to an ellipsoidal region with a high probability of finding feasible states.

System Robustness and Uncertainties

A general definition of robustness relates to the response of the system to the variability of the parameters, more specifically a robust system keeps good performance even in the presence of parameters change. Bemporad and Morari cite several types of robustness (Bemporad and Morari 1999 (a)). For example, robustness to model uncertainties, robustness to disturbances, robustness to uncertainty of the variable, robustness to some performance or constraint criteria, and so forth.

A complementary point of view is to consider three approaches to the system robustness: **inherently robustness of the closed loop**, and the **open-loop robustness** assured through the exploration of all possible uncertainties through a min-max concept of model predictive control and the third approach is a **combination of both**, which is the closed-loop of a min-max model predictive control (Mayne, Rawlings *et al.* 2000).

Robust performance has a different approach depending on whether the control is open or closed loop (Bemporad and Morari 1999 (a)). The control signal or input to the system is inherently bounded in closed loop, yet it requires a bounded approach in open loop so as to guarantee system performance. A detailed analysis of robust stability and stability of the nominal model compared with stability of the robust model for constrained receding horizon control is presented by (Primbs and Nevistic 2000)

Another important concept that affects the performance is **uncertainty**, which is defined from different point of view: uncertainty of input coefficients, uncertainty of disturbances of states, uncertainty regarding the feedback loop or a combination of uncertainties forming a convex hull or Polytopic uncertainty.

A model for **robustness to disturbances** is proposed by Bemporad and Morari, which includes modelled disturbances in the input and output, similar to the proposed model of Ljung for system identification (Ljung 1987; Bemporad and Morari 1999 (a)). The difference is that the robust model is defined as a set of state-space models with disturbances rather than a single state-space model.

Robustness to errors of dead time is analyzed by Camacho in the dead-time controller combined with the Smith predictor (Camacho 2002). This work is an antecedent to the paper of (Torrico and Normey-Rico 2007), where they present a reformulation of the Constrained Receding Horizon Predictive Control (CRHPC) of Clarke et al (Yoon and Clarke 1995). In addition to the final state constraint and constraint of the input, the new approach enforces the control action to zero after the horizon control. This is to improve the stability of the system after the period of interest. The state observer, based on a Smith predictor, is robust to variations of dead time of the system, when it is under norm-bounded uncertainties.

Finally, robust performance needs to guarantee the system feasibility by assuring the feasibility of next instant signal, not necessarily for the whole time span of the HPR journey (Bemporad and Morari 1999 (a)).

To conclude, system **stability**, **robustness** and **feasibility** are interlaced concepts; thus an appropriate control design needs to provide a model for the three aspects together with the system specifications.

System Uncertainties

Another aspect to be considered is the information about the states: **imperfect** vs. **perfect state information**. Perfect state information is when the measurements are

available all the time or at the period of interest with complete certainty. Conversely, imperfect state information is when the measurements are not available or they are corrupted by noise. In this case the **probability of occurrence** is considered, leading to a stochastic control. Sometimes it is impossible to count on even with the probability of the measurements but it is possible to define boundaries of probability. In this aspect the state can be considered as belonging to a set-membership (Bertsekas and Tsitsiklis 1996 (a)).

Bertsekas proposes an alternative of state definition for systems with state uncertainties (Bertsekas 1972). This approach is applicable in cases where it is difficult or impossible to know with a degree of certainty the state variables. The method solves the uncertainty problem by the definition of an ellipsoidal region of the state space, where the state can be confined through feedback control. The control effort is therefore concentrated on study of the behaviour of the variable in the elliptical regions and through time, as the time tends towards infinity in the denominated n-steps of reachability. Extrapolating this approach, the iterative computation of the control law is the basis for the HPR controller.

Theory of global stability of the Receding Horizon Controller are described by Alamir, Bornard (Clarke 1994). Convergence to the desired state of the state variable is analyzed for cases of finite and infinite horizon under a constrained state variable. The paper concludes with the postulation of sufficient conditions causing global stability.

Disturbances in the input and output require particular considerations. From the **model point of view**, the Wiener and Hammerstein models are designed for disturbances of the output and input respectively (Ljung 1987; Åström and Wittenmark 1995). From the **hardware point of view**, Clarke proposes plant and loop validation in order to account for sensor and actuator effects in the open and closed loop (Clarke 1999 (a); Clarke 1999 (b)). From the **measurement point of view**, the data conditioning and analysis is a key factor to get a meaningful data set for the next steps of system identification and controller design. Such analyses include uncertainty analysis (Kline 1965; Holman 1968; Kurowicka and Cooke 2006), principal component analysis (Jolliffe 2002), dimensional analysis (Taylor 1974; Japikse and Baines 1994) and parametric and non-parametric statistics (Efron 1993; Davison and Hinkley 1997; Conover 1999; Keller and Warrack 2000; Anderson, Sweeney *et al.* 2003; Montgomery, Runger *et al.* 2004).

2.3. CONCLUSIONS

The literature survey of this chapter gives a structured knowledge base for the development of the control architecture and control strategy.

In particular, the literature survey of the HPR controllability and Context Overview, based on the classes of vehicles to which the HPR belongs, gives a framework to understand the controllability aspects of pipeline robots and is the base for the development of system models, presented in Chapter 3.

The second section survey, HPR Control Strategy, gives theoretical background, tools and techniques in developing control architecture and the controller strategy, which is presented in Chapter 4.

Further work related to simulation and tests of Neuro-Dynamic Programming and multi-objective optimization and objective prioritization, may require more specialized literature survey in these areas. However, these topics are out of the scope of this thesis.

Chapter 3 Analyses towards Specifications for the Hybrid Pipeline Robot

3.1. INTRODUCTION

The Hybrid Pipeline Robot (HPR) is a class of self powered device that converts the energy from the pipeline flow into mechanical energy for traction, in the turbine-driven mode. Additionally, it is expected to have a surplus of energy for charging batteries for energy supplying in the motor-driven mode. Therefore the energy generation and dissipation in the HPR system are fundamental factors for the development of **the energy management and control system**.

For that reason, the aim of this chapter is to **derive models** for representing and analyzing the main components of the HPR system, which are turbine and pipeline vehicle. Refer to chapter structure in Figure 3.1-1

A model based on **mass and energy conservation** is derived for the turbine and pipeline vehicle. As a result, the minimum set of variables is extracted from this model with the purpose of defining the **system identification parameters**.

A **force analysis** is performed for the driving system of the pipeline vehicle and for the bristle-based locomotion system with the purpose of identifying driving patterns and predicting ways of failure of the HPR that need to be considered in the controller architecture to perform a **self-recovery action.** A State space model for the HPR is derived considering the flow as a source of energy.

Finally a system identification model for the HPR is proposed in this chapter, which is the base for the neuro-system identification model developed and tested in Chapter 4 as part of the Model Predictive Control.

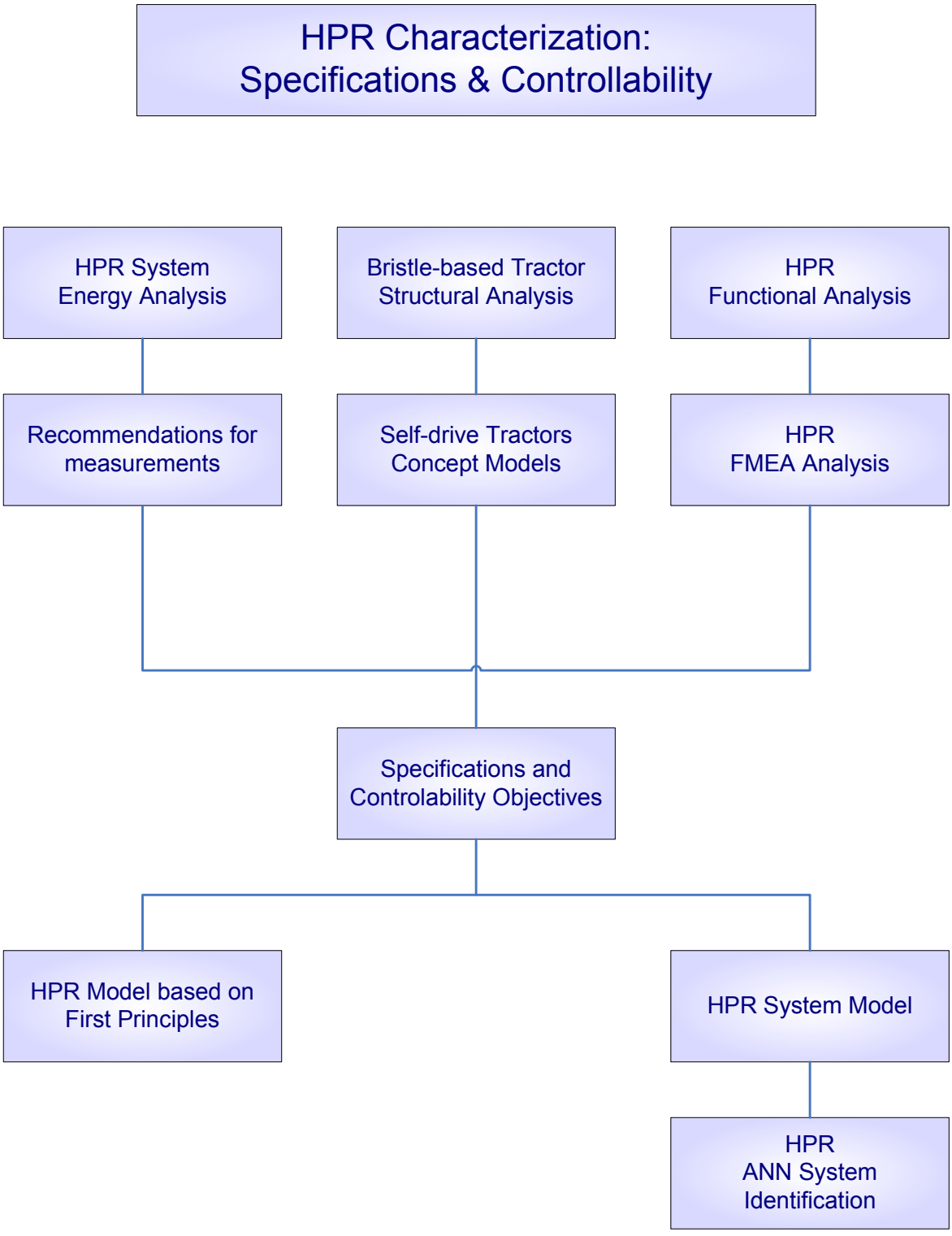

Figure 3.1-1 Chapter 3 contents: HPR characterization
Scheme of the HPR analyses and the controllability aspects

3.2. HPR System Energy Analysis

The purpose of this writing is to frame the Hybrid Pipeline Robot, HPR, in a context of an energy system. This approach is based on four interrelated principles: the *principle of energy conservation* and its main derivation, the *mass conservation principle*, the *first law of thermodynamics* and the *Bernoulli's equation*. These three principles are combined in the *general energy equation for steady flow applied to any fluid* (Massey 2006), in order to determine the suitable parameters carrying useful information about the turbine performance. It is important to determine the key parameters because they define the test to be done.

The HPR can be thought of as composed of the turbine and the bristle-based vehicle immersed in the environment of a pipe rig with any uncompressible flow, such as water. The notion of using an energy frame for the HPR is because the turbine is an energy converter unit.

In order to facilitate the energy analysis, the HPR is considered inside boundaries of flowing energy, described in Figure 3.2-1. The imaginary boundaries of the control volume are represented by some point upstream, another point downstream and the pipe walls. These boundaries represent the inlet and outlet of the control volume and they are identified by points *1* and *2* respectively.

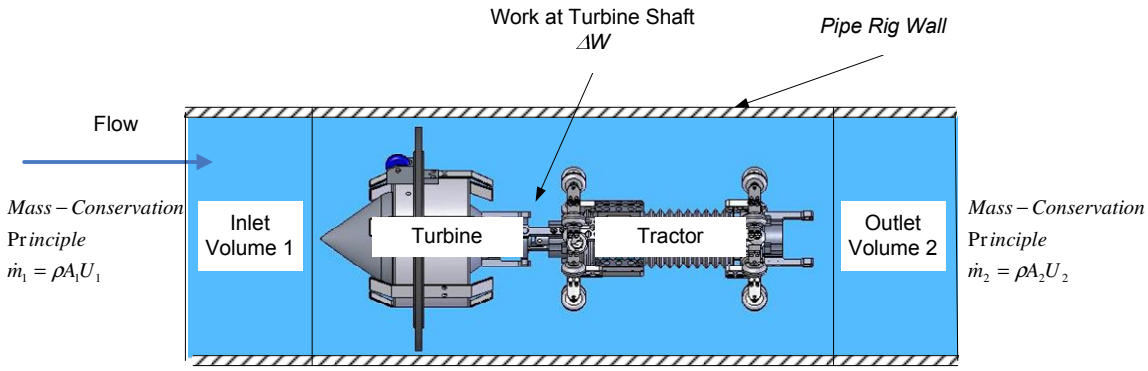

Figure 3.2-1 HPR - System Energy Boundaries
Mass-Energy conservation principle is the base to derive the HPR study

Although the HPR is crawling inside the pipe, for the purpose of this energy analysis, the control volume will be considered as stationary.

The HPR, as a unit of conversion of energy, is under the law of conservation of energy: no energy is created nor destroyed; only a transformation of energy exists. This principle can be viewed as a conservation of mass; the rate of mass entering a system or control volume equals the rate of mass leaving the same control volume, expressed as,

$$\dot{m}_1 = \dot{m}_2 \qquad \textbf{3-1}$$

In the HPR's case, the mass is the water flow and, in accordance with the mass conservation principle, the flow rate entering control *volume*$_1$ is the same as the flow rate leaving control *volume*$_2$. Considering the mass as the product of the volume and fluid density, ρV, and applying the rate of change through time, the *mass conservation principle* can be expressed as,

$$\rho \frac{Vol_1}{dt} = \rho \frac{Vol_2}{dt} \qquad \textbf{3-2}$$

Therefore the *mass conservation principle*, or *continuity equation*, can be described as a function of the cross sectional area of the control volume, A, and considering a displacement of a volume of water through a distance, ds/dt. This displacement of the fluid volume equals the flow passing through the section under study, or flow rate U, expressed as follows:

$$\rho_1 A_1 \frac{ds_1}{dt} = \rho_2 A_2 \frac{ds_2}{dt}$$
$$\rho_1 A_1 U_1 = \rho_2 A_2 U_2 \qquad \textbf{3-3}$$

The same principle can be expressed as a function of the discharge, Q.

$$\rho_1 \dot{Q} = \rho_2 \dot{Q} \qquad \textbf{3-4}$$

Two important conclusions can be derived from the mass *conservation principle*. Firstly, the energy is constant inside the control volume. It can be restated as the mass flow rate upstream of the HPR is the same as the mass flow rate downstream. Secondly, the flow velocity and the cross-sectional area are inversely proportional: the narrower the cross sectional area of the pipe the higher the speed of the flow. However, the cross-section of the pipe loop is constant so, the effect of the pipeline vehicle inside the pipe can be thought of as a reduction in the cross-section of the pipe; it is a constraint inside the pipe. This reduction means higher speed in the surroundings of the turbine-pipeline vehicle assembly.

Now, a close look inside the control volume can show the transformation of energies performed by the turbine: from hydraulic energy, or the energy of the flow, into mechanical energy at the shaft of the turbine immersed in the fluid.

The *first law of thermodynamics* helps us to analyze this energy transformation. It states that when the energy, as a form of heat, is added to a mass of fluid, then the total energy of the system is increased. The supplied energy can be converted into useful work at the shaft of the machine and it is also used to overcome losses in the system. This law is expressed in the next formula,

$$\Delta Q = \Delta E + \Delta W \qquad \textbf{3-5}$$

where ΔQ is the provided energy as a heat rate; it yields an increase of the total energy, ΔE and energy as work, ΔW, is performed.

The total energy of the system can be classified in two categories, the overall level of energy and the molecular level of energy. The overall level of energy relates to all physical components such as turbine, pipeline vehicle and fluid, and forces correlating them. These forces represent different forms of energy; kinetic energy, when speed is involved, and potential energy related to the position of the system and a reference level. Also these forces are the result of electrical, mechanical and magnetic energy. The molecular energy depends on the temperature and viscosity of the fluid.

The following are the assumptions for this particular case. The energies considered in the HPR system are the kinetic and flow energies. As the rig under test is horizontal, there is no hydraulic jump; therefore the potential energy has no effect in this particular case because all points are at the same datum. Assuming, temperature and viscosity are kept constant, thus other forms of energy are considered of insignificant or null effect for this environment.

Also for this particular case, no heat is supplied. Instead, the external energy is provided by a pump, which determines the mass flow rate inside the pipe. But for simplicity, the control volume is considered as a closed system without interchange of energy with the exterior. Then the left hand side of the equation is zero. This assumption is not a limitation as the flow is still doing work, and the energy is represented by the displacement of fluid volume or mass flow rate. Then the equation of the *first law of thermodynamics* applied to the HPR can be rewritten as follows:

$$0 = \Delta E + \Delta W \qquad \textbf{3-6}$$

Now it will be interesting to get a further close approach inside the control volume to find out how the turbine transforms the energy from the flow into mechanical energy, which is the useful form of work. This approach is based on the *general energy equation for steady flow applied to any fluid* (Massey 2006). This analysis includes the effective work at the turbine shaft and the system losses incurred during the energy transformation. It gives us the key parameters to be measured and required in order to obtain the performance of the system.

The overall energy, E, enclosed in the control volume is considered constant. The displacement of a small inlet volume, $A_1 ds_1$, produces a general displacement of $E+A_2 ds_2$ at the outlet.

Throughout this displacement of the small volume of water, two forms of energy can be distinguished. Figure 3.2-2 shows the energy due to the displacement of the volume, and the work done by the fluid. shows the control volume and the energy distribution.

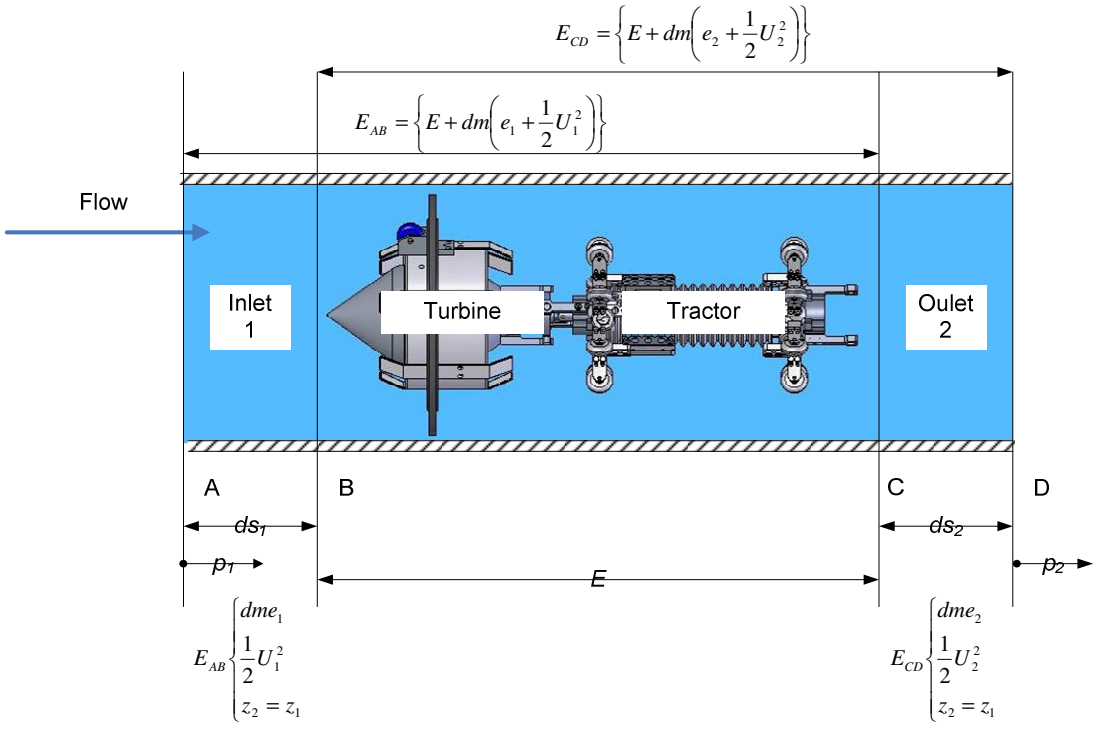

Figure 3.2-2 HPR System Energy Balance

Illustrate the equation 3-7

The energy contained in each small volume is the internal energy, e, and the kinematic energy, $1/2U_2$. Considering the total energy supplied by the displacement, ds, and the equation is expressed as follows:

$$E_{CD} - E_{AB} = \left\{ E + dm\left(e_2 + \frac{1}{2}U_2^2 \right) \right\} - \left\{ E + dm\left(e_1 + \frac{1}{2}U_1^2 \right) \right\} \quad \textbf{3-8}$$

As the overall energy, E, is constant, the term is cancelled and the equation resulting is the following:

$$E_{ds} = dm\left\{ (e_2 - e_1) + \frac{1}{2}\left(U_2^2 - U_1^2\right) \right\} \quad \textbf{3-9}$$

The work done by the fluid consists of the work done by the small volume, p_2Ads, thus it is work done by the turbine, W_{SHAFT}, as the pipeline vehicle is connected to its shaft. The following equation summarizes the overall excerpted work carried out by the fluid.

$$W_{FLUID} = W_{SHAFT} + W_{SmallVolume} = W_{SHAFT} + p_2A_2ds_2 - p_1A_1ds_1 \quad \textbf{3-10}$$

In order to express the work per unit mass and following the *mass conservation principle*, the displacement of flow mass is the same at the inlet and outlet, $dm=\rho_1A_1ds_1=\rho_2A_2ds_2$. Thus the equation for work can be rearranged in the next equation.

$$W_{FLUID} = \frac{\Delta W}{dm} + \frac{p_2A_2ds_2}{\rho A_2ds_2} - \frac{p_1A_1ds_1}{\rho A_1ds_1} \quad \textbf{3-11}$$

The terms related to volume, Ads, are cancelled. The sum of energy, ΔE, and work, ΔW yield the *general energy equation* for steady flow, based on the *first law of thermodynamics*. It is expressed as follows:

$$\frac{E_{ds}}{dm} = \left\{ (e_2 - e_1) + \frac{1}{2}\left(U_2^2 - U_1^2\right) \right\} + \left\{ \frac{W_{SHAFT}}{dm} + \frac{p_2}{\rho_2} - \frac{p_1}{\rho_1} \right\} \quad \textbf{3-12}$$

The terms of the *general energy equation* can be rearranged giving a similar result to that of *Bernoulli's equation.* This representation as energy per unit volume or M/LT^2, gives a clear description of the energy in terms of the different pressures along the pipe rig, expressed in the next equation.

$$p_{TOTAL} = p_{STATIC-1} + \frac{1}{2}\rho U_1^2 + e_1 = p_{STATIC-2} + \frac{1}{2}\rho U_2^2 + e_2 \quad \textbf{3-13}$$

The internal energy, e, is used to overcome the viscous forces of the fluid. This work done represents a release of energy in a form of heat that cannot be converted into any other form of useful energy. However, the increase in temperature is insignificant; the work done is considered as a loss of energy. These losses can be represented in the

equation as $-q$ and the internal energy at *point 1* is diminished at *point 2* by the $-q$ loss factor, giving e_1-e_2-q.

The following assumptions need to be considered. The flow is water, at ambient temperature so the density, ρ, is considered constant. The pipe rig is horizontal of constant diameter so, based on the mass conservation principle, the speed upstream, U_1, is the same as the speed downstream, U_2. Thus the kinetic term of the *general energy equation* can be dropped.

$$0 = (e_2 - e_1 - q) + \frac{W_{SHAFT}}{dm} + \frac{p_2 - p_1}{\rho} \qquad \textbf{3-14}$$

This interchange of energy and losses makes useful the measurement of the pressure at two different points, inlet and outlet, of the control volume.

$$\frac{p_2 - p_1}{\rho} = q + \frac{W_{SHAFT}}{dm} \qquad \textbf{3-15}$$

This equation shows that the difference of pressures, upstream and downstream of the turbine gives the amount of energy available at the shaft of the turbine for doing work and for overcoming losses of the fluid due to viscosity.

This conclusion from the *general energy equation* gives the bases for measuring the pressure at these two points in order to obtain the energy efficiency of the system. From *Bernoulli's equation,* the pressure to be measured is the static pressure at two points, upstream and downstream of the turbine.

3.3. Energy Analysis and recommendations for measurement

The HPR is composed of the turbine and a crawler pipeline vehicle. The aim of this research project is to automate the self driven pipeline vehicle. It is called self driven or free flow machine because the pipeline vehicle is attached to the turbine, which is operated by the flow inside the pipeline. In addition, the bristle based traction gives the crawling pipeline vehicle the bidirectional characteristic.

The autonomy is achieved by the **Energy Management System, EMS**, and a supervisory system, capable of evaluating the available energy generated by the turbine and stored in the batteries. The available energy is compared with the power consumption and the environment characteristics affecting it. Upon this information, the EMS acts as a decision maker based on artificial intelligence algorithms in order to optimize the energy levels required for cruising, operations and self-recovering. If the

energy is not enough, or its tendency indicates a shortcoming in energy, then the EMS defines the course of action that could include a self-recovery stage.

An autonomous pipeline vehicle is able to travel longer distances and the self-recovery characteristic solves the problem in the event that the pipeline vehicle is trapped inside the pipe due to environmental adverse conditions or mechanical failures, thus eliminating the need of an external emergency rescue with the high costs associated. Therefore efficient usage of energy, autonomy and self recovery characteristic are remarkable improvements for this kind of crawler pipeline vehicles.

Therefore, from the total available energy must be always considered the energy required for the recovery phase. As soon as the turbine starts to operate, it starts to generate energy and the HPR starts to travel. As a consequence the overall energy level starts to increase. But, at the same time, starts to increase the energy required for the recovery stage; that's why the further the distance travelled by the pipeline vehicle, the higher the energy required for returning to the starting point. As a result the available energy is discounted by a factor that increases with the distance travelled.

The demanded overall energy increases with the distance travelled, schematized in Figure 3.3-1. The available energy includes the energy generated by the turbine and the energy stored in the batteries. The fuzzy region is the energy surplus required for self-recovering, as it is a critical requirement that the pipeline robot returns to the starting point in case of failure or after completing the predefined tasks. The denomination of "fuzzy region" is because the value of the generated energy is unknown a priori; it has random variations depending on the flow inside the pipe.

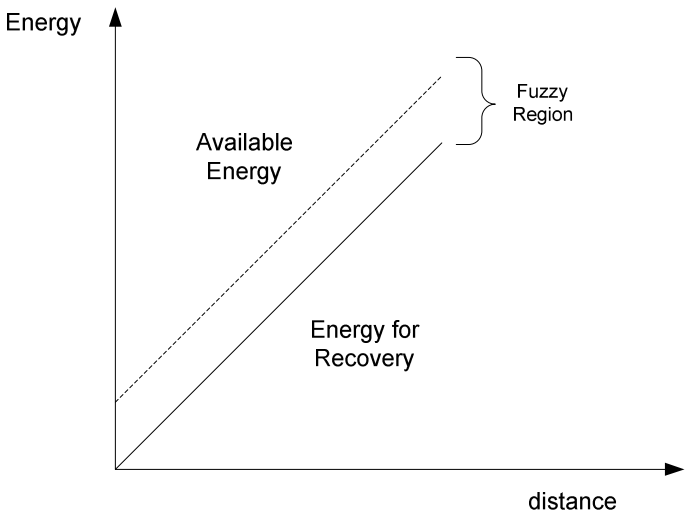

Figure 3.3-1 HPR Energy distribution
Surplus of energy required as the mission develops

The turbine can be regarded as an energy converter; the hydraulic energy from the flow is transformed into mechanical energy at the coupling shaft of the turbine. The performance of the turbine is reflected in its efficiency curve and the EMS bases its decisions on this result.

The efficiency of the turbine is analyzed in conjunction with the battery efficiency, in order to get the overall existence of energy for the HPR. The efficiency graph shows the region of optimal energy availability. The analysis of energy also includes the evaluation of the tendencies of energy usage and flow rate, as it is the flow the principal source of energy inside the pipe. If the HPR starts to operate outside of this optimal working region then the EMS defines the course of actions, upon the application of a control law. These actions consist of a range of options from continuing with the planned schedule to returning to the starting point.

The information about the available energy is useful not only for the EMS but also for the **Cruise Control system, CC**. The amount of energy is crucial information and, if fact, it is a constraint for the regulation of the pipeline vehicle speed. Therefore the available energy is included in the optimization function of the controller. This concept will be explored in detail in the section dedicated to the controller algorithm.

To conclude, the physical variables required for the two controllers of the HPR are the pipeline vehicle speed for the Cruise Control and the power output and efficiency of the turbine for the Energy Management System.

Turbine Efficiency

In this context, the definition of efficiency, η, is the relation of the mechanical energy at the turbine shaft to the energy of the fluid; it is expressed in the next formula. This is the definition for the overall efficiency and, among any other definitions; it has been selected because the interest of this research project is the power delivered by the turbine.

$$\eta_{overall} = \frac{E_{mechanic@shaft}}{E_{fluid}} \qquad \textbf{3-16}$$

For simplicity in the measurements it is used power as equivalent of energy. So, the mechanical output *power at the shaft* P_{shaft} is obtained through the measurement of *torque, T*, and *rotational speed of the shaft, N*. And the fluid energy is obtained through the measurement of the *volumetric flow rate Q* and *pressure drop across the turbine,* ΔP. This relation is showed in the following formula.

$$\eta_{overall} = \frac{P_{shaft}}{P_{rotor}} = \frac{TN}{Q\Delta P} \quad \textbf{3-17}$$

To conclude, the minimum necessary variables for the calculus of the turbine efficiency are the pressure drop across the turbine, torque, rotational speed and flow rate. The independent variables of the system are the flow rate, Q, and the diameter of the turbine, D. The diameter is considered here as the main design parameter of the turbine affecting its efficiency. The other variables are all dependent on these two.

Dimensional Analysis applied to the HPR

Although the efficiency is a dimensionless expression, the parameters included in its definition do have dimension. This fact represents a limitation at the time of evaluating the HPR tests. For example, if several parameters are of interest for the experiment, a collection of curves need to be examined in conjunction. This kind of analysis becomes cumbersome as the number of variables increases. This problem is solved efficiently through the use of Dimensional Analysis, which expresses the parameters through dimensionless coefficients, a set of variables, instead of single variables.

Dimensional Analysis represents considerable advantages in order to simplify the representation of results, to devise experiments and eventually to apply a scale factor.

The simplicity is because Dimensional Analysis converts each variable in dimensionless coefficients through a mathematical procedure. Each coefficient inter-relates a group of key variables involved in the behaviour of the turbine. So, one single curve can represent simultaneously the variations of several parameters, as long they are included in the dimensionless coefficients. Therefore, it is simpler to analyze the tendency of only one curve compared with the analysis over a set of curves that should be done otherwise.

Another advantage of Dimensional Analysis relates with experiment design, as the dimensionless coefficients include several variables, it is clear to recognize which parameter to change in order to explore a particular performance of the turbine (Taylor 1974; Palmer 2008).

Once obtained the basic results from tests, the dimensionless coefficients also help to apply the same results to a similar device or similar test conditions, without the need of new experiments, only applying a scale factor. This is the principle of similitude (White 2008). For example, when it is required to know the behaviour of the HPR under different fluids, say changing air by water. Thus, the new result is 1000

times greater compared with the test for air; this is the scale factor that relates the density of water to air, and no further experiment is required.

Dimensionless coefficients for the HPR

The main interest for the EMS is the efficiency and it can be expressed as a function of the flow coefficient, Reynolds numbers and general design characteristics of the turbine (Japikse and Baines 1994; Dixon and Knovel 1998). This dependency is expressed in the following formula.

$$\eta = f\ (\frac{Q}{ND^3}, \frac{\rho ND^2}{\mu}, \frac{L_1}{D}, ...) \qquad \textbf{3-18}$$

In the particular case of the HPR, the Reynolds number and design parameters of the turbine are considered constant. Therefore the efficiency is a function only of the *volumetric flow coefficient*.

$$\eta = \frac{TN}{Q\Delta P} = f\ (\frac{Q}{ND^3}) \qquad \textbf{3-19}$$

The same assumptions are applied to the *Energy Transfer Coefficient,* φ, and it is represented in the following formula.

$$\varphi = \frac{gH}{N^2D^2} = f\ (\frac{Q}{ND^3}) \qquad \textbf{3-20}$$

The expression gH, gravity times the height of fluid involved in the hydraulic energy, can be replaced by its equivalent, the difference of pressure, ΔP. The resulting equation is more applicable for the Hybrid Pipeline Robot. Due to the horizontal pipe loop, the energy from the fluid is produced by the pressure drop across the turbine instead of the height of the column of fluid. Therefore the expression for the HPR is:

$$\varphi = \frac{\Delta P}{N^2D^2} = f\ (\frac{Q}{ND^3}) \qquad \textbf{3-21}$$

The net hydraulic power supplied, $P_{N,}$ is converted in useful power at the turbine shaft and power dissipated to overcome friction losses.

$$PN = P_{shaft} + losses \qquad \textbf{3-22}$$

The expression of the power in a form of dimensionless coefficient, $\hat{P}$, is as follows:

$$\hat{P} = \frac{P}{\rho N^3D^5} = f(\frac{Q}{ND^3}) \qquad \textbf{3-23}$$

As a conclusion, from the above dimensionless coefficients, it can be seen the simplicity of the final graphic representation. For example, in the case of efficiency, the result is only one curve expressed not only as a function of the flow rate, *Q,* but also as a function of the rotational speed, *N*, and turbine diameter, *D*. at the same time. Otherwise, it is required one efficiency curve for the variation of each of the other parameters.

Dimensional Analysis also helps in this case in designing the test. Continuing with the example of the efficiency, it can be seen from the formula that the parameters to be varied and of significant effect in the efficiency are those included in the flow coefficient, *Q, N, D*. Furthermore, if the interest is on the output power of the turbine then the dimensionless coefficients indicate that, apart from the parameters mentioned earlier, it is required to vary the flow density if an impact is required in the output power.

HPR and the Energy loss

The previous section (paper handed in before and not her(e) gave the context of energy for the HPR inside a virtual control volume of its environment. The main conclusion was the relation of the drop of pressure across the turbine to the losses in the system. This section investigates what kind of pressure and how to measure the pressure that gives the information of the mentioned energy losses.

The general expression of Bernoulli's equation relates the different pressures inside a control volume: static pressure, dynamic pressure, proportional to the speed of the flow U^2, and pressure due to the head of the fluid, z. If the flow is frictionless, there are no losses and then the result of the addition of all these pressures is a constant value that is the total or stagnation pressure (Massey 2006).

$$p_{STATIC} + \frac{1}{2}\rho U^2 + \rho g z = p_{TOTAL} = \text{constant} \qquad \textbf{3-24}$$

For a particular case of a horizontal rig the term of the pressure due to head is dropped. So, considering the Bernoulli's expressions at two different points, 1 and 2, the expression is:

$$p_{TOTAL} = p_{STATIC-1} + \frac{1}{2}\rho U_1^2 = p_{STATIC-2} + \frac{1}{2}\rho U_2^2 \qquad \textbf{3-25}$$

However, for real systems the total pressure is not constant and there exist a reduction in pressure due to friction losses; it is represented in the following expression.

$$\Delta p_{total} = p_{total1} - p_{total2} \neq 0 \quad \textbf{3-26}$$

Therefore, rearranging the terms of Bernoulli's equation, the total pressure is,

$$p_{TOTAL} = p_{STATIC-1} - p_{STATIC-2} + \frac{1}{2}\rho(U_1^2 - U_2^2) \quad \textbf{3-27}$$

Applying the conservation of mass or continuity principle, the velocities at two different points of the pipe are equal as long as the density and the area are kept constant, thus $U_1 = U_2$. So, the loss of total pressure can be represented as the drop of static pressure across the turbine.

$$p_{TOTAL} = \Delta p = p_{STATIC-1} - p_{STATIC-2} \quad \textbf{3-28}$$

Summarizing, the loss of energy due to friction in the system can be obtained through the measurement of the static pressure at two points, upstream and downstream the turbine.

The flow rate, Q, is derived from Bernoulli's equation and it is based on the measurement of the difference of total and static pressure. It is represented in the following equation:

$$Q = U_1 = \sqrt{\frac{2(p_{TOTAL} - p_{STATIC-1})}{\rho}} \quad \textbf{3-29}$$

To conclude, the expression $Q\Delta P$, the power from the fluid in the efficiency equation, contains the information of the energy of the fluid, Q, and the information about the losses due to friction, ΔP.

Recalling from previous section, the necessary variables for the calculus of the turbine efficiency are the pressure drop across the turbine, ΔP, torque, T, rotational speed, N, and flow rate, Q. Although these variables constitute the minimum necessary set to be measured there are a couple of questions to be considered in order to optimize the measurement procedure. For example, are all these variable necessary to be measured or could be considered a reduction in the number of variables?. Another important question relates to the use of data of previous test. These questions, intended to economize time and costs related to the experiments, are explored in the next section.

Recommendations for measurements

There are several reasons for recommending new experiments for the HPR but the most important is the need of the measurements of the full set of parameters involved in the calculations of the turbine efficiency and pipeline vehicle speed. In addition, these data need to be updated values containing the dynamic information of the HPR system.

It is through the measured data that it is possible to represent, in a suitable model, the complex dynamics of the turbine and pipeline vehicle. Applying system identification techniques based on Artificial Neural Networks and considering the turbine-pipeline vehicle unit as a black box, it is possible to build models representing all the complexities of the actual system. Otherwise it is rather difficult to build such models without making several assumptions and keeping the mathematical model as simple as possible. Thus, both control systems, Energy Management System and Cruise Control, are developed upon the full set of measured parameters. Apart from that, the controller needs the updated measurement of energy levels as the pipeline vehicle travels down the pipe. This data carries the dynamic behaviour of the HPR working in a particular environment.

Under the assumptions of Dimensional Analysis, mentioned earlier, it would be convenient to use the data from a previous test for the twisted blade turbine carried out at the time it was designed (Pulker 2005). Even though the differences, the density of the media and turbine diameter, between the prototype and the actual turbine, the scaling principle of Dimensional Analysis makes it feasible to use the results of the prototype only applying a scaling factor. However, due to the assumptions that have been made in the mentioned test, in particular those referred to the averaging of pressure and flow rate, it makes this kind of data unsuitable for the purpose of this research project. Therefore, in the design of the controller for the HPR it is required the full range of dynamic information rather than the average in order to make an accurate representation of the HPR and its environment.

This recommendation also considers the downside of setting up tests in particular for the turbine-pipeline vehicle working under water, as it is time consuming without the certainty of successful results. Furthermore, the wet media has several constraints in particular related to electronics that implies to deal with fewer and more expensive options compared with dry media. In order to cope with unpredictable it has been considered the experience and recommendations found in tests from other fields like

aeronautics and turbo-machinery using similar probes or sensors. So, on the light of careful considerations in devising the experiments for the HPR it is expected to get useful information about the turbine and pipeline vehicle in order to feed the models for the Energy Management System and Cruise Control systems.

3.4. Bristle-based Pipeline vehicle Structural Analysis and Concept Models

HPR as a class of self drive pipeline vehicle

The characterization of the HPR has a close relation with the characterization of the bidirectional bristle based pipeline vehicle. In order to understand the particularities of the pipeline vehicle locomotion,

The denomination of reciprocating and stationary cycles is with respect to the scroll cam: reciprocating unit because this group is displaced through the groove of the cam, while the two stationary units are fixed to the cam. So while the stationary bristle units offer a support to the pipeline vehicle, the reciprocating unit is displaced forward along the scroll cam.

The scroll cam is a double threaded helical worm gear and belong to the class of rotating cam and translating follower. The scroll cam is covered by a cowling, which has a guide channel for allowing the follower associated to the reciprocating unit to move along the shaft following the cam thread.

Pipeline vehicle displacement: pigging vs. crawling

The bristle based pipeline vehicle is a class of crawler pipeline vehicle. It is important to note the difference between crawling and pigging (Wang and Hong 2008). Pigging is when the flow produces the displacement of the pig basically due to the difference of pressure created across the pig; so the higher the pressure difference the fastest the velocity the pig develops. This is the mechanism of displacement for standard pigs like foam pigs or seal pigs. The disadvantage of this method is that it relies on the pressure drop; therefore, the pig cannot develop an independent velocity rather than the velocity created by the pressure difference. So the crawler pipeline vehicles offer a solution through the development of a range of velocities independent of the flow rate and dependent on the crawling mechanism, which is subject to be controllable.

The common characteristic of all crawlers is the “gripping” effect of the crawler to the wall surface. This gripping effect can be achieved using several principles such as vacuum, magnetic fields, friction forces, just for citing a few. However the interest

of this project is on the bristle-based crawler vehicle, which belongs to the frictional forces category of crawler vehicles (Stutchbury 1999; Appleton and Stutchbury 2000; Appleton and Stutchbury 2002; Appleton 2003; Appleton and Stutchbury 2004).

Self-drive pipeline vehicle Concept Models

The traction mechanism of the bristle-based self drive pipeline vehicle is based on the principle of functioning of a standard brush with radial arrangement of bristles, when it is inserted in a pipe of diameter slightly smaller than the brush cross section.

When the brush is inserted in the pipe, the bristles flip back due to the reduced diameter of the pipe compared with the brush diameter. Therefore, the friction forces between the pipe wall and the bristles generate two different magnitudes of the friction forces: a lower force required for pushing the brush further compared with a higher force required for pull the brush back.

The main reason for the existence of theses two magnitudes of friction forces is because when the bristle bends, the effective diameter of the brush is reduced and adapts to the pipe surface producing a rather smooth displacement of the brush inside the pipe. Conversely, when the bristles are pulled back, they pass through a transition of the bristle length, which at the maximum point, develops the full brush diameter, imposing a tight contact of the bristles against the pipe wall, and therefore increasing the friction forces.

These two magnitudes of friction forces are used as a principle for the pipeline vehicle to crawl in a similar way as the human gait: the high friction gives support to the leg that rests on the floor, which helps the other leg, to move forward. In an equivalent sequence, the bristle based pipeline vehicle, composed of two types of displacement bristle units, alternate the movements: whilst one unit gives support with high friction, the other unit moves forward at low friction. High friction forces, apart from support for crawling displacement, help to maintain the crawler centred in the pipe.

Bristle-based pipeline vehicle locomotion

Apart from the bristles-based principle, the locomotion of the pipeline vehicle is composed of a turbine, which produces the rotation of the cam shaft through the gearbox. The cam shaft has a pair of stationary bristle units attached on it, and the other unit, the reciprocating bristle unit, is driven along the cam groove by the cam thrust,

originating the crawling or reciprocating cycle. The reciprocating cycle is divided into driving and recovery cycle. Driving cycle because it is the only one that produces the actual displacement of the pipeline vehicle; whilst recovery is a cycle for alignment and although the reciprocating bristles unit displaces along the cam groove, no actual pipeline vehicle displacement is produced.

So, the reciprocating bristle unit is the pivot point for driving the cam with the stationary bristle units or for be driven by the cam shaft, provided the bristles give a support through the "gripping" effect on the pipe wall. Details of the locomotion sequence and of the reciprocating cycles are given in Figure 3.4-1 and the description is as follows:

(a) Initial Conditions: HPR launching

The pipeline robot is setup inside the pipe line, with no flow and therefore no thrust produced by the turbine. The bristles are flexed back and take the proper alignment for driving forward; by convention, the positive direction of the movement is to the left.

The forces acting on the pipeline vehicle are in equilibrium, and they are the shear stress of the three bristle units produced by the tension of the bristles against the pipe wall. The total shear stress over the vehicle equals the friction exerted by the pipe wall over the bristles units, when trying to revert to the original alignment. The summary of forces in the initial conditions is as follows:

$$\text{Initial Conditions} \quad \begin{cases} \text{Flow Drag} = 0 \\ \text{Cam Thrust} = 0 \\ \Delta x = 0 \end{cases} \quad \begin{cases} \sum F = 0 \\ 2F_{ShearStressSBS} + F_{ShearStressRBS} + 2F_{FrictionSBS} + F_{FrictionRBS} = 0 \end{cases} \tag{3-30}$$

(b) Recovery Cycle Start

The onset of the flow produces the turbine rotation and therefore the rotation of the cam shaft, inducing a thrust of the scroll cam over the bearing of the reciprocating bristle set.

As a consequence the reciprocating unit moves forward guided by the cam thread, which serves as a pivot. The principal forces are the cam thrust and the shear stress over the reciprocating unit opposed to the friction of the two stationary bristle sets. The friction of the reciprocating unit and the shear stress of the two stationary bristle units are smaller than the forces in the opposite direction and are denoted by the

small slack variable ε in the following equation. The cycle is called recovery because it is an alignment process of the vehicle rather than an actual displacement inside the pipe. The summary of forces for this stage is as follows:

$$\text{Recovery Stage}\begin{cases}\text{Flow Drag} > 0\\ \text{Cam Thrust} > 0\\ \Delta x = 0\\ \sum F > 0\end{cases}\quad\begin{cases}F_{FrictionRBS} < \varepsilon\\ 2F_{ShearStressSBS} < \varepsilon\end{cases}\quad Pivot\quad\begin{cases}Thrust + 2F_{FrictionSBS} = 0\\ Thrust + 2F_{FrictionSBS} - F_{ShearStressRBS} > 0\\ Thrust + 2F_{FrictionSBS} > F_{ShearStressRBS}\end{cases}\qquad \textbf{3-31}$$

(c) Recovery Cycle Final

At the end of the **recovery cycle**, the scroll cam exerts a thrust toward the far front of the reciprocating bristle unit. Due to the double helix cam, the reciprocating unit is free to move backwards and forwards; however, in the backward direction, the reciprocating unit needs to overcome the high friction required to flex back its own bristles. The low friction is presented instead by the stationary bristle units, which are previously aligned, setting up the conditions for the next stage, the driving cycle.

The forces are in equilibrium during the transient state**,** and they are the shear stress and friction of the three bristle units in addition to the scroll cam thrust.

(d) Driving Cycle Start

The reciprocating bristle unit serves as a pivot for the cam shaft, which moves forward with the stationary bristle units attached on it. The principal forces are the cam thrust and the shear stress over the stationary bristle units opposed to the friction of the reciprocating bristle set. The summary of forces for this stage is as follows:

$$\text{Driving Stage}\begin{cases}\text{Flow Drag} > 0\\ \text{Cam Thrust} > 0\\ \Delta x > 0\\ \sum F > 0\end{cases}\quad\begin{cases}F_{ShearStressRBS} < \varepsilon\\ 2F_{FrictionSBS} < \varepsilon\\ Thrust + F_{FrictionRBS} - 2F_{ShearStressSBS} > 0\\ Thrust + F_{FrictionRBS} > 2F_{ShearStressSBS}\end{cases}\qquad \textbf{3-32}$$

(e) Driving Cycle Final

The reciprocating bristle unit, serving as a pivot, exert a thrust over the cam shaft, producing the forward displacement of the cam and the two attached stationary bristles

sets. From this position, the low resistance is posed by the reciprocating unit, which is free to move forward along the cam thread. And the cycle starts again. The forces are in equilibrium during the transient state, and they are the shear stress of the three bristle units, the friction of the three and the cam thrust.

These recovery and driving stages repeat, cycling between a high friction condition imposed by the alignment of he reciprocating bristle unit; and a low friction condition, presented by the actual displacement of the two stationary bristle sets. However, it is important to note that the reciprocating unit serves only as a pivot for the actual displacement of the stationary bristles units, and do not contribute at all to the robot displacement. From an external reference point, the robot displacement is regarded as cycling between driving and idle stages. The dead time of each cycle last approximately 30 seconds and is due to the time required for the turbine torque to overcome the inertia of the vehicle structure and mechanical friction mainly in the cam shaft.

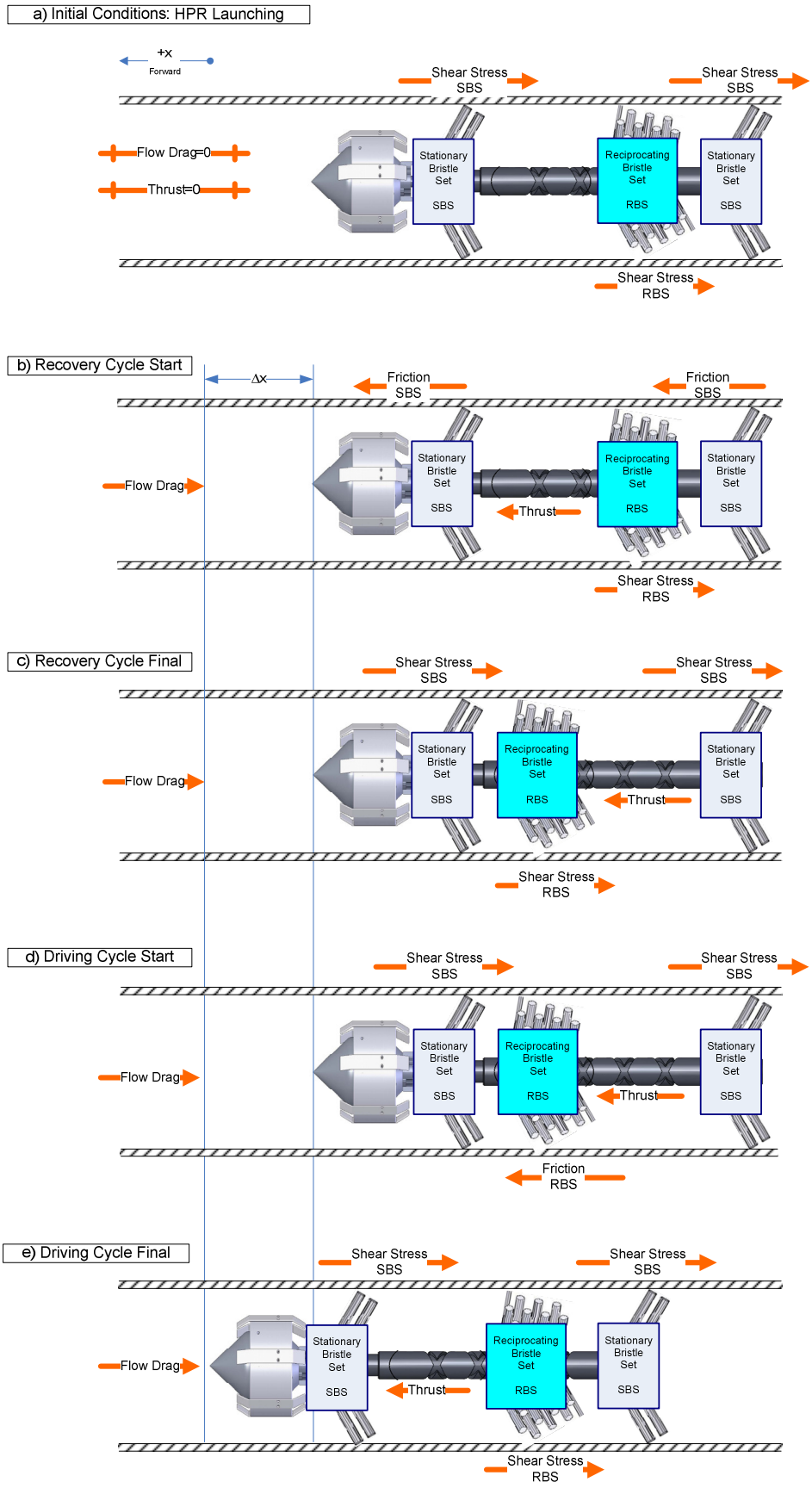

Figure 3.4-1 HPR: locomotion cycles

The effective robot forward displacement is marked by the blue lines across the stages

Forces at camshaft level

A close look to the cam shaft and the follower, allows us to visualize the forces acting upon the ball bearing of the follower (Wang and Appleton 2003 (d)). Figure 3.4-2 shows an augmented view of the cam shaft with the double helix thread, which is the support for the stationary bristle units (not in the schem(e). The figure also shows a section of the cowling, which is the guide for the reciprocating bristle unit. The cowling has a guide orifice for the ball bearing, at Figure 3.4-2 (a).

The Figure 3.4-2 (b) shows the forces as the cam shaft starts to rotate. The forces of the cam shaft acting on the ball bearing are the friction and the normal force of the groove wall. The resultant force of the cam groove, which is the thrust, opposes to the follower resultant force (Maxwell 1960).

The follower resultant force is the result of the shear stress of the bristles in contact with the pipe wall and any other external forces (not in the schem(e), which may impede the displacement of the reciprocating unit along the camshaft, such as debris or any of the other bristle units.

The direction and magnitude of the resultant of the cam thrust and follower force, determines the path the ball bearing follows (b). If the follower force is smaller than the thrust, then the ball bearing follows the forward path of the cam groove, at Figure 3.4-2 (c).

Otherwise if the follower force is bigger compared with the thrust; as a result, the follower forces the bearing to follow the backward thread of the cam groove, producing the reversing movement and flexing even more the bristles in the opposite direction, as in Figure 3.4-2 (d).

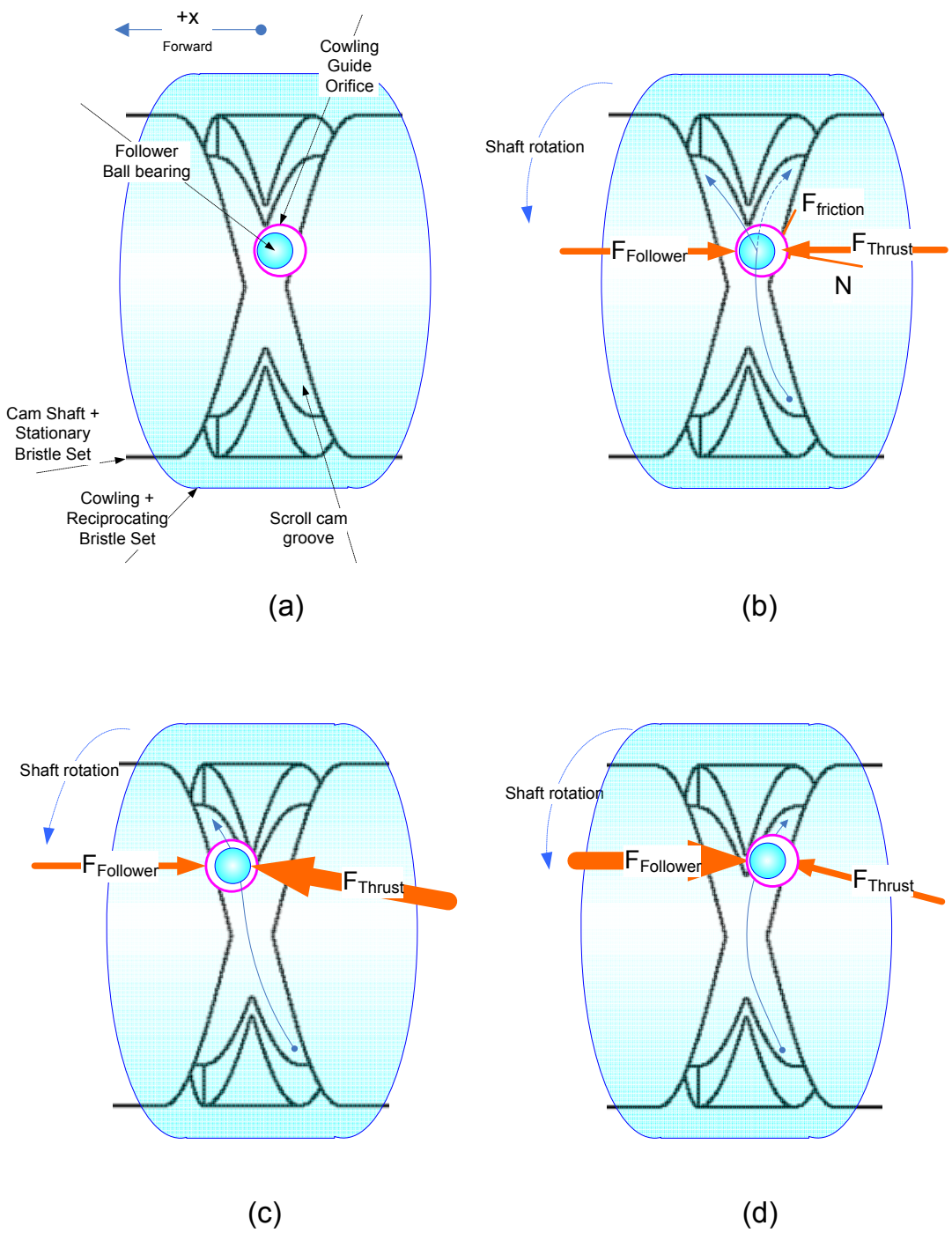

Figure 3.4-2 HPR camshaft forces

Reverse Sequence

The pipeline vehicle sequence described so far is the forward movement. However, one of the remarkable capabilities of the pipeline vehicle is its bidirectional movement. The reverse sequence is showed in the Figure 3.4-3Figure 3.4-3 HPR reversing cycles and is described as follows.

Reversing Cycles

The reversed direction starts when the robot finds unsolvable constraints on its way, which imposes a high resistance enough to flex back the bristles, and overcome the internal tension of the aligned bristles, denoted in the equations by the Greek letter γ. Figure 3.4-3 shows the scheme of the pipeline vehicle reversing, in its recovery and driving stages. Therefore, the external force of the constraint lead the bristles to yield and flex back, following the thread of the cam, depicted in Figure 3.4-3 (a) and (b) for the recovery stage.

The reversing driving stage is produced by the flexion of the stationary bristles sets. And the cycle continues in the same way driving the robot in the opposite direction, as depicted in Figure 3.4-3 (c) and (d) for the reversing driving stage. Reversing models of forces is summarized in Box 3-1.

Box 3-1 HPR reversing concept models

Main cycles for driving and recovery phase

Recovery Reversing	Driving Reversing
$FlowDrag > 0$ $CamThrust > 0$ $F_{Obstacle} > F_{FrictionRBS}$ $\Delta x = 0$ $\sum F > 0$	$FlowDrag > 0$ $CamThrust > 0$ $F_{Obstacle} > F_{FrictionRBS}$ $\Delta x > 0$ $\sum F > 0$
Reverting bristles alignment	
$F_{FrictionRBS} > \gamma F_{FrictionRBS}$ $2F_{ShearStressSBS} < \varepsilon$ $F_{ShearStressRBS} < \varepsilon$	$2F_{FrictionSBS} > \gamma 2F_{FrictionSBS}$ $2F_{ShearStressSBS} < \varepsilon$ $F_{ShearStressRBS} < \varepsilon$
Pivot	
$Thrust - 2F_{FrictionSBS} = 0$	$Thrust + F_{FrictionRBS} = 0$
Displacement	
$Thrust > F_{FrictionRBS}$	$Thrust > 2F_{FrictionSBS}$

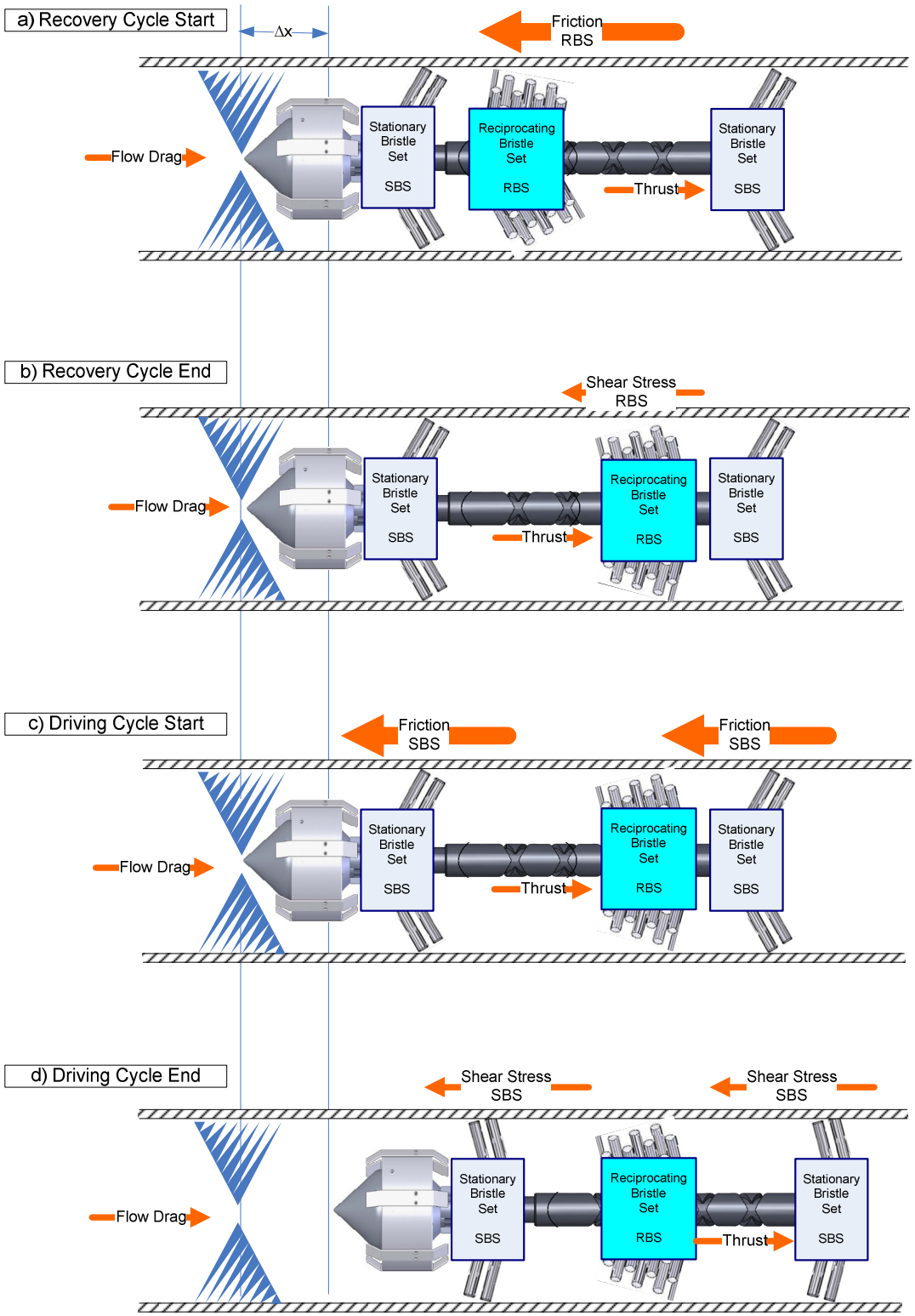

Figure 3.4-3 HPR reversing cycles

The effective robot backward displacement is marked by the blue lines across the stages

Rule of exemption

The locomotion regime described above is based on ideal bristle behaviour. However, in the practice, bristles are not exempt of wear, corrosion and material yielding that produces the bristles to bend instead of flex, even beyond the limit of elasticity. As a result of the bristles bending, the pipeline vehicle starts to slip instead of crawling ending with the vehicle excursion with the flow, which is an undesirable condition.
The idle condition can be temporarily tolerated; it can be even useful and an idle stage induced purposely for charging the batteries. However, if the idle conditions persist over time without particular function, it is considered as an undesirable stage as well. The following equations represent the forces involved in slipping and idle stages.

Undesirable States

Slipping conditions	Idle conditions
$\sum F_{Friction} - F_{Flow} < 0$	$\sum F_{Friction} + F_{Thrust} - F_{Flow} < 0$
$\sum F_{Friction} < F_{FlowDrag}$	$\sum F_{Friction} < F_{FlowDrag}$
$\Rightarrow \Delta x < 0$	$\Rightarrow \Delta x = 0$
	$F_{Thrust} < \varepsilon$

So, the stiffness of the bristles material and an adequate design are fundamental requisites for the crawling locomotion. The difference, at a bristle level, between the crawling and slipping behaviour is depicted in Figure 3.4-4 and described in the next paragraphs.

How is the behaviour of a single bristle?

One way of characterizing the bristle behaviour is by the changes of the angle between the longitudinal axis of the bristle and the plane of the pipe wall. We name it bending angle of the bristle (Wang 2003 (a); Wang and Appleton 2003 (b)).

This angle is a parameter for measuring the bristle deformation and together with the stiffness of the material, the dimensions, and bristle design, determines whether the bristle recovers the original characteristics after applying a flexing momentum.

Therefore the difference between a flexed or bent bristle relates with the maximum angle deviation the bristle can reach when compressed in the insertion to the pipe, and if the angle is in the limit of elasticity permanent deformation.

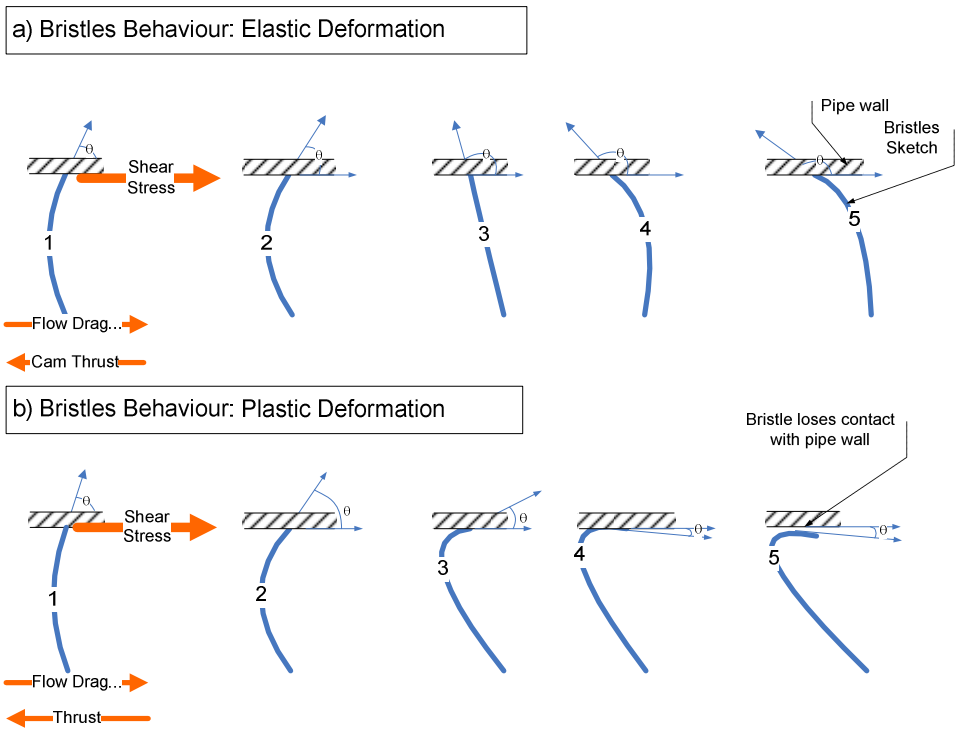

Figure 3.4-4 Bristle deformation due to shear stress

Elastic deformation is the ideal behaviour, while plastic deformation indicates material wear.

The shear stress is the result of the cam shaft thrust and the flow drag (Hibbeler 2007). This shear stress exerted by the pipe wall over the bristle, force the bristle to flex. If the bristle flexion is such that the bending angle is close to the 90 degrees on either side, the bristle remains inside the elasticity boundaries of the bristle material. As a result the bristle can recover the original shape after the force is released. This situation is depicted in the Figure 3.4-4 (a). Consequently, the effective diameter of the bristles units remains close to the original one, showing a tight attachment to the pipe wall, so the pipeline vehicle is still able to crawl in one of either direction.

Conversely, if the bristle flexion is such that the bristle is forced to bend to smaller angles further than the elasticity limit for the bristle material, the deformation of the bristle is permanent. This situation is depicted in the figure b. As a result the effective diameter of the bristle units is reduced producing the vehicle to slip instead of crawl and furthermore, the effect renders the bristle useless as a supporting unit for the complementary bristle sets. This situation is augmented by the flow rate that may produce the vehicle to pig instead of crawling. The bristles that surpass the elasticity limit can not recover the shape, so a solution is to gang the bristles together so as to make them stronger and account for individual failures.

3.5. HPR Functional Analysis

One of the fundamental requisites for the **controllability** of the HPR is a **robust operation** particularly to avoid the unit lost in the pipeline. In order to accomplish with such robust operation, the control strategy includes a **self-recovery stage** as a standard completion of any mission, based on the bidirectional characteristics of the vehicle. However, it is necessary to determine the ways in which the unit can **fail** leading to the unit lost inside the pipeline; and the ways in which these failures can be predicted and/or avoided by a **self-recovery strategy**.

Therefore, a functional analysis was performed following the method of the **FMEA** (Failure Mode and Effects Analysis), in order to determine the modes in which the HPR and its components can fail. This analysis was performed for the turbine and the traction unit considering the components included in the interaction between them, in addition to the interaction with the pipeline environment. These components are analyzed as **individual and as a chain of components,** because they can fail as a group, or as a single component affecting the whole group.

The **causes of failure** are classified as independent or interactive causes. An example of **independent causes** of failure is the wear or corrosion of the bristles units, with immediate effect on the units, but slow incidence on other components, such as bristles hub or the robot itself. This slow incidence may lead, in the long run, to the loss of gripping forces and eventually the excursion of the vehicle with the flow. An example of **interactive causes** is the fatigue or buckling of the clutch, leading to an immediate malfunction of the chain of components, in this case turbine, gearbox, drive shaft and vehicle camshaft; resulting in the stalling of the robot inside the pipeline.

The interaction of the robot with the environment was also of particular interest for the design of the control strategy, because it gives the modes in which the environment affects the robot, the resultant behaviours of the robot, and the ways in which these behaviours can be identified.

Following the FMEA method, these modes of failure are scored and ranked, in order to **prioritize the components with high risk of failure. The general score is** the risk priority number RPN, which is the result of determining the severity of the failure, the frequency of occurrence and the detection methods. The most critical score has a value of 10 and relates to the negative consequence of losing the robot inside the

pipeline. The hard scoring is due to the degradation of the pipeline performance and potential environment damage, incurring in high expenditures and sanctions.

In order to determining the **severity of a failure**, they are classified in both partial or total failure; and gradual or sudden failure. The most critical severity is considered for the robot lost with no possibility of being rescued by tethers. The **occurrence of a failure** is based on the experience and the estimation of the occurrence by extrapolating the mode of failure to a similar context. For example, the mode and frequency of failure of the bristle units can be considered for the class of vehicle to which the HPR belongs, not only for the hybrid robot in itself. The most critical score is for a failure occurring more than once. Finally, the high score for **detection of the failure** is for the absence of control, or lack of detection in tests or in post-operation inspection.

Figure shows the ranked risk priority number RPN and the accumulative scores. As a result, the evaluation by the Pareto rule indicates that the 75% of the causes of failure are targeted by addressing the first four modes of failure.

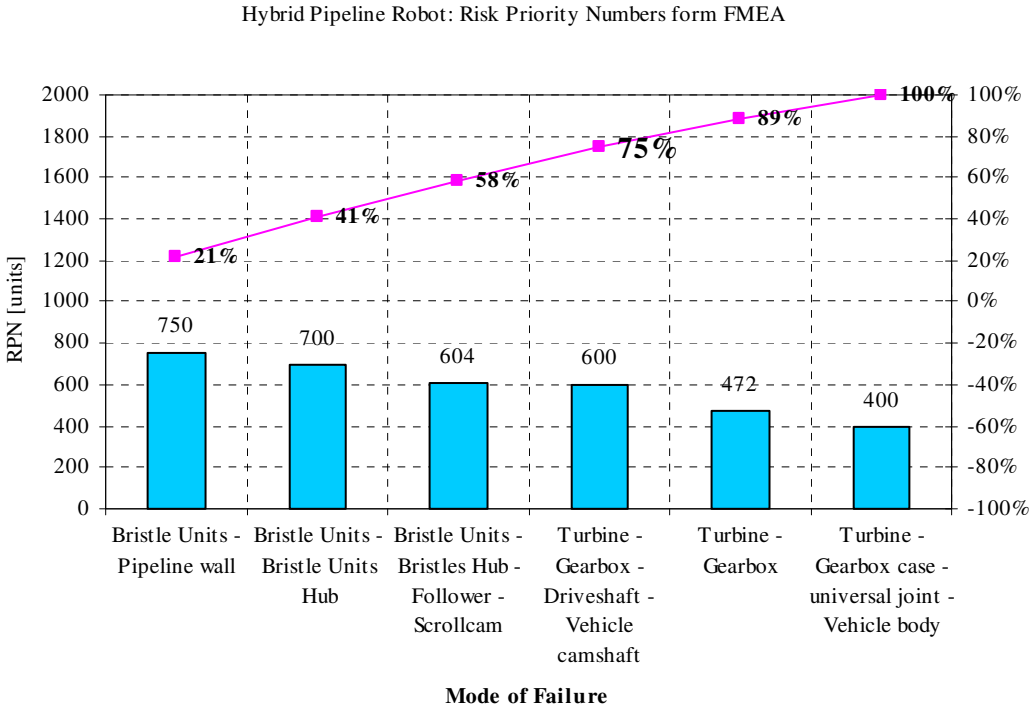

Figure 3.5-1 HPR Failure Mode and Effects Analysis FMEA
The 75% of the causes of failure are solved by targeting the first four mode of failure

Concluding, the control strategy needs to identify the behaviour of the bristle-based vehicle and the performance of the turbine in order to assure a robust robot operation, targeting the 75% of the causes of failure. This fact suggests that including

an additional strategy of fault detection and isolation at component level, would contribute to solve no more than the 25% of the causes of failure, which is of no relevance at this stage of the HPR control development in terms of cost/benefits.

3.6. HPR model based on first principles

The theory of **mass-spring-damper model** is used to explain mainly the oscillation or vibration of bodies, the conservation and transfer of energy and the dissipation factors. Furthermore complex systems can be described as a set of different mass-spring-damper units. The model for the mass-spring-damper can be expressed as follows:

$$Energy = M\ddot{x} + c\dot{x} + kx \quad \textbf{3-33}$$

The value of energy will be given depending upon the conservation of energy frame; if the conservation of energy can be applied then the value of energy is zero. But if the system is under forced vibration the total value for the energy will have a positive value.

For the particular case of the hybrid pipeline vehicle this kind of model can be applied to the oscillation that appears in the bristles and cam shaft as it was explained before in the stroke dynamic analysis. But explaining the energy dynamics of the system as a whole using a mass-spring-damper model might be challenging task. The mass-spring-damper model can be assumed as conservation of energy system, a closed system where the energy transformation is modelled by the spring-mass relation and the dissipation through the damper. When thinking about the crawling pipeline vehicle the energy supplied by the flow is converted into useful work through the set turbine-camshaft that through the axial thrust and the bristle gripping forces react giving as a result a displacement inside the pipe.

This idea is considering the flow as an abstract source of energy that can be simulated by an electric motor. But when considering actual system the flow as a source of energy is a complex system that can be described by the Bernoulli's equation (Massey 2006):

$$Energy = \rho gz + p_{static} + \frac{1}{2}\rho U^2 \quad \textbf{3-34}$$

Considering the energy due to the elevation, ρgz where ρ is the flow density, g is the gravity acceleration, and z is the elevation from the datum point and represents the potential energy of the flow. The second term is the static pressure and relates to the transmission of energy from one point to another point of the pipe. The third term

relates to the dynamic pressure and the energy due to the velocity. All these terms represent a complex interrelation of energy of the flow. Therefore for the model of the crawling vehicle would be an approximation to the actual system considering not just the mass-spring-damper model but also to include the energy model provided by the flow, then the equation that represents such model will be:

$$Energy = \rho gz + p_{static} + \frac{1}{2}\rho U^2 = M\ddot{y} + c\dot{y} + ky \quad \textbf{3-35}$$

Analyzing the general equation one can make a relation between the terms at both sides. Then fluid dynamic that refers to the pressure head relates to the mass acceleration term in the mass-spring damper system. In the same way can be referred the velocity term of the Bernoulli's equation to the damper term in the mechanical formula. The term that relates the displacement of the mass can be associated with the static pressure, recalling fluid mechanics theory the static pressure relates to the force displacement from one point to another in the pipe (Massey 2006). It is worthy to point out that although I have considered the Bernoulli's equation in order to represent the energy model for the pipeline vehicle, this equation is not valid for turbulent flow and it is precisely in the back of the turbine when appear turbulence and the flow can not be recovered until well after passing through the turbine. Although this non applicability of Bernoulli's term this equation can be assumed as a good approximation in order to describe the system. These relations can be expressed in the following equations

$$\rho gz \propto M\ddot{y} \quad \textbf{3-36}$$

$$\frac{1}{2}\rho U^2 \propto c\dot{y} \quad \textbf{3-37}$$

$$p_{static} \propto ky \quad \textbf{3-38}$$

The described equation represents the physical system but it is required to represent the system in terms of input/output variables to be analyzed from the control point of view.

The general state space structure can be represented in the following equation where x(t) is the matrix of the states, u(t) represents the input to the system and y(t) is the output (Ogata 1970). The term w(t) represents the disturbance or noise in the output or in the states. The terms F, G, K, H, D are matrices of coefficients that can be constant or time dependent.

$$\dot{x}(t) = Fx(t) + Gu(t) + Kw(t)$$
$$y(t) = Hx(t) + Du(t) + w(t) \quad \textbf{3-39}$$

In order to express the above relation in the form of state space equations I need to make the following assumptions.

$$x_1(t) = y(t) \quad \textbf{3-40}$$

$$\dot{x}_1(t) = \dot{y}(t) = x_2(t) \quad \textbf{3-41}$$

$$\dot{x}_2 = \ddot{y} = -\frac{1}{M}c\dot{y} - \frac{1}{M}ky + \frac{1}{M}(\rho gz + p_{static} + \frac{1}{2}\rho U^2) \quad \textbf{3-42}$$

$$\dot{x}_2 = \ddot{y} = -\frac{1}{M}cx_2(t) - \frac{1}{M}kx_1(t) + \frac{1}{M}(\rho gz + p_{static} + \frac{1}{2}\rho U^2) \quad \textbf{3-43}$$

$$\begin{bmatrix}\dot{x}_1 \\ \dot{x}_2\end{bmatrix} = \begin{bmatrix}0 & 1 \\ -\frac{k}{M} & -\frac{c}{M}\end{bmatrix} \times \begin{bmatrix}x_1 \\ x_2\end{bmatrix} + \begin{bmatrix}0 \\ \frac{1}{M}(\rho gz + p_{static} + \frac{1}{2}\rho U^2)\end{bmatrix} \times u \quad \textbf{3-44}$$

The above equation relates the states and their derivatives. The importance of such structure is that allows analyzing the states of the system based on the past values of the states and the input as well. In order to build the system description will be required to find the parameters of the system represented by the matrices this could be a cumbersome task without any granted successful result.

An alternative option is to find the transfer function of the system expressed in terms of the input/output as in the following equation in the frequency domain applying Laplace transformation:

$$\frac{Y(s)}{U(s)} = G(s) \quad \textbf{3-45}$$

The relationship between the state space and transfer function can be expressed as it follows:

$$sX(s) - X(0) = AX(s) + BU(s)$$
$$Y(s) = CX(s) + DU(s) \quad \textbf{3-46}$$

Considering the initial conditions as zero X(0)=0 and rearranging terms:

$$sX(s) - AX(s) = BU(s)$$
$$(sI - A)X(s) = BU(s)$$
$$X(s) = (sI - A)^{-1}BU(s)$$
$$Y(s) = [C(sI - A)^{-1}B + D]U(s) \quad \textbf{3-47}$$

Rearranging this equation and expressing it in the form of transfer function:

$$\frac{Y(s)}{U(s)} = G(s) = C(sI - A)^{-1}B + D$$

$$G(s) = \frac{Q(s)}{(sI - A)^{-1}}$$

The term $(sI - A)^{-1}$ is the polynomial characteristic of the transfer function and the Eigen values of the matrix A are the poles of the system. This expression is based on the inverted matrix that may represent a constraint due to the matrix A should be singular.

3.7. HPR system model

The HPR system model is based on system identification, considering the hybrid machine as a black box where the input is the turbine efficiency and the output is the vehicle speed. Figure 3.7-1 shows the relation between the input/output variables in the robot context.

Compared with models based on first principles described in Chapter 3, the system identification approach based on measurements of the input/output variables has the advantage of characterize the nonlinearities of the hybrid pipeline robot and the dynamics of the pipeline environment.

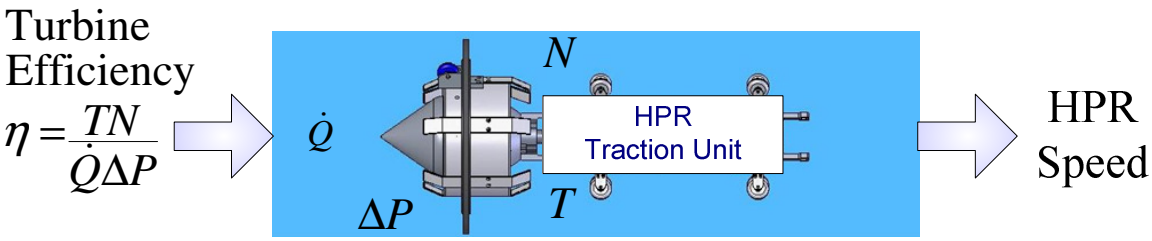

Figure 3.7-1 HPR model variables

Ljung says that, in many cases, the nonlinearities can be treated as a function transformation and included in standards models. This approach is using physical insight of the system to be identified. In terms of equations, the nonlinear system can be described as follows

$$y(t \mid \theta) = \varphi(t, Z^t; \theta)$$
$$Z^t = f(u, y)$$

where

φ is the vector/matrix of nonlinear Regressors

θ is the vector of Parameters

Z is the nonlinear function transformation of the system

Some nonlinear systems are because sensors/actuators introduce nonlinearities, although the system itself is linear. These cases are modelled by the structures of Wiener-Hammerstein models (Åström and Wittenmark 1990; Bolkvadze 2002). In the equation of the state space model the input/output disturbances are modelled by *r(.)* and *m(.)* nonlinear functions, and it is expressed as follows:

$$x(t \mid \theta) = f(u, x; \theta) + r(u, v; \theta)$$
$$y(t \mid \theta) = h(x; \theta) + m(w; \theta) \qquad \textbf{3-49}$$

where

f is is the nonlinear transformation of the input and states

h is the nonlinear transer function of the system

r and m are nonlinear functions of the disturbances

in the input and output respectively

For the HPR case, apart from the nonlinearities of the sensors, the turbine and pipeline vehicle are nonlinear in themselves, as it has been proven by the mathematical model. So as to account for the sensors nonlinearities, the approach in this research project is to characterize the probes/sensors in the calibration process and compensate by software at the data acquisition process.

Therefore, the output of a nonlinear system can be modelled by a finite length of the function expansion of the regressors or basis functions. This concept is expressed as follows:

$$\hat{y}(t \mid \theta) = \varphi_1 + ... + \varphi_d \qquad 3\text{-}50$$

So, the regressors are the shape of the nonlinear transformation of the nonlinear system. The most famous series expansions for function approximation are Taylor and Volterra series. And the most largely applicable is Taylor's series in particular in the search algorithm. Several researches have been done in relation to Volterra series. Soloway presents a design of dynamic systems based on ANN system identification through the application of Volterra series with very good results (Soloway and Bialasiewicz 1992 (b)). However good results for Volterra series, this method is rather computational cumbersome (Narendra 1990 (b)). Some simplification approaches,

based on industrial experience, support the idea of modelling a complex system as a chain of first order polynomials (Camacho and Bordons 1999).

As a general rule in this research project, it is applied the theory of coarse-grained that means to find out the minimum largest granularity or resolution to describe the HPR control system (Israeli and Goldenfeld 2006).

From the previous discussion, the central question now is: how to find the nonlinear regressor capable of representing the HPR system?

Answer 1: using physical insight

Answer 2: using black-box methods (based upon input/output measurements)

Answer 3: using a set of basis function expansions

Ljung presents a different approach: the transformation of the mother basis function $\Phi(\bullet)$ such as scaling or dilation, translation and coordinates location (Ljung 1987). The analytical expression for the mother basis function is:

$$\Phi(\cdot) = \sum_{k=1}^{n} \alpha_k k[\beta_k(\varphi - \gamma)] \qquad \textbf{3-51}$$

α : coordinates location

β : scaling/dilation

γ : translation

The different transformations of the mother basis function, give rise to three different approaches, mentioned in the literature, of basis function models for nonlinear system identification: 1) tensor (product), 2) radial construction (distance of the regressor to a point) and 3) ridge construction (regressor distance to an hyper plan(e). This is the principle of neural networks, which are structures of the basis function

Emulating the series expansion, it can be constructed a network of basis functions or mother basis functions of which linear, hard limit, sigmoid mother basis functions are some ubiquitous examples (Hagan, Demuth *et al.* 1996).

So, the answer in this research project, to the question of finding a suitable regressor capable of explaining the nonlinear HPR system is a combination of all the proposed answers: the regressor is a network expansion of basis (regressors) function. The transformation of location, scaling and translation are performed by the arrangement of weights and bias of the network. The black-box approach is the way of training the network through the presentation to the network the input and output values of the variables. The physical insight or heuristic of the system is applied not only for

the selection of the activation function but also for the way of arranging different network structures similar to the blocks of the block diagram of control system.

Smith predictor and state observers in general are well known in fields of system identification (Bemporad and Garulli 2000; Rao, Rawlings *et al.* 2001; Núñez-Reyes, Normey-Rico *et al.* 2005; Torrico and Normey-Rico 2007).

The classical output predictor is solved through the recursion of the Diophantine polynomials with the purpose of obtaining a set of predictors for the different horizons (Clarke, Mohtadi *et al.* 1987 (a); Camacho and Bordons 1999). However the recursion of the Diophantine equations is cumbersome and calls for an oversimplified system model. Some alternative approaches are proposed in the literature to solve the continuous time polynomial recursion (Demircioglu 1994). The optimum predictor has the form of (Clarke, Mohtadi *et al.* 1987 (a)):

$$\begin{aligned} y(t+j\,|\,t) &= G_j(z^{-1})\Delta u(t+j\,|\,t) + F_j(z^{-1})\,y(t) \\ G_J(z^{-1}) &= E_j(z^{-1})B(z^{-1}) \end{aligned} \qquad \textbf{3-52}$$

E_j and F_J polynomials result from the solution of the Diophantine equation :

$1 = \mathrm{E_j} A\Delta + z^{-1}F_j$

The set of future steps ahead are expressed as follows:

$$\mathrm{y} = \mathrm{Gu} + \mathrm{f} \qquad \text{3-53}$$

where G is a function of the past values of the output and input.

So, the minimization of the main equation can be rearranged as a function of the tracking terms,

$$\mathrm{J} = (\mathrm{Gu} + \mathrm{f} - \mathrm{w})^{\mathrm{T}}(\mathrm{Gu} + \mathrm{f} - \mathrm{w}) + \lambda \mathrm{u}^{\mathrm{T}} u = \frac{1}{2} u^T Hu + bu + c \qquad \text{3-54}$$

The last expression is the standard equation methods of quadratic programming approach (Fletcher 1987).

3.8. HPR ANN System Identification

The HPR model is based on the system identification approach. The turbine-pipeline vehicle and environment are considered as a black box and the measured input/output are the efficiency and pipeline vehicle speed respectively. So, through system identification, it is possible to include in the model the environmental nonlinearities, the pipeline vehicle-turbine characteristic and the dynamic changes. These features are

rather difficult to express with analytical or parametric models (Ljung 1987; Söderström and Stoica 1989; Nelles 2001; Chadeev 2004).

Narendra discuss the performance of the parallel vs. series-parallel model structure for system identification (Narendra 1990 (b)), in this book also offers the general structures for system identification and control based on neural networks (Narendra 1990 (a))

The expression of the model is the output of the system as a linear combination of the inputs, the past values of the inputs and the past values of the output (or states) and it is represented in the following expression.

Output of a Linear System

$$y_p(k+1) = \sum_{i=0}^{n-1} \alpha_i y(k-i) + \sum_{j=0}^{m-1} \beta_j u(k-j) \qquad \textbf{3-55}$$

where

$y_p(\cdot)$ is the output of the system

$u(\cdot)$ is the input of the system or control signal

α, β predefined weighting factors

n, m are the prediction and control horizons

This simple representation of the system output can be expressed in an equivalent way in terms of system identification or the expression of the estimated value of the system output $\hat{y}(\bullet)$. The main difference between series-parallel and parallel structure is that for the series-parallel structure, the output of the model is a function of the actual input and output of the plant and in the case of the parallel model, it is a function of its own past values and the input of the plant (Narendra 1989). The difference is represented in the following diagrams.

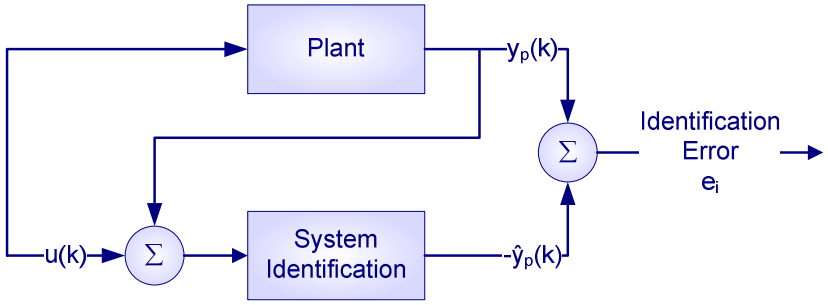

a) System Identification: Series-Parallel Model

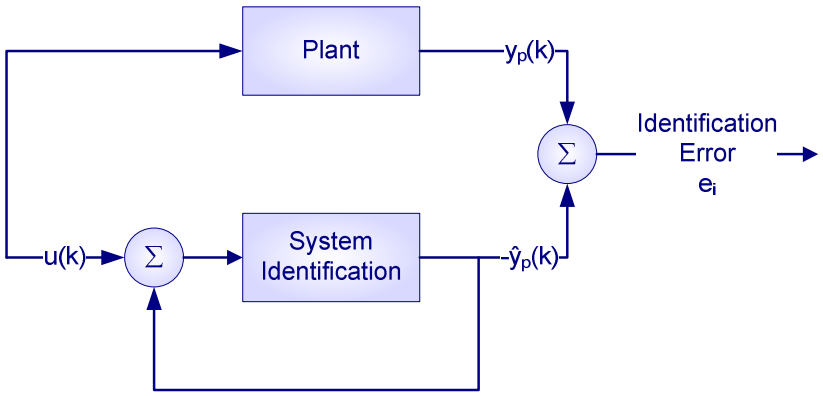

b) System Identification: Parallel Model

Figure 3.8-1 System Identification: Series-parallel and parallel structures

The HPR system model is based on the series-parallel structure.

The mathematical expression for series-parallel and parallel model structure are:

Estimated ouput of a Series - Parallel model

$$\hat{y}_p(k+1) = \sum_{i=0}^{n-1} \hat{\alpha}(k)\, y(k-i) + \sum_{j=0}^{m-1} \hat{\beta}(k) u(k-j) \qquad 3\text{-}56$$

Estimated ouput of a Parallel model

$$\hat{y}_p(k+1) = \sum_{i=0}^{n-1} \hat{\alpha}(k)\, \hat{y}(k-i) + \sum_{j=0}^{m-1} \hat{\beta}(k) u(k-j) \qquad 3\text{-}57$$

Although the subtle difference, the series parallel model offers some advantages in relation to the parallel model: the series-parallel model is based on the true values of the plant instead of the estimated outputs. That means the series-parallel model represents more accurately the observed plant. So the estimator of the series-parallel structure is more likely to accomplish with the desired characteristics of the estimators, say unbiased, consistent and efficient (Eykhoff 1974). These properties indicate the system is stable and the recursion of the equation makes the model adaptive.

An interesting point is the mathematical expression given in the literature for the recursion of the weights $\alpha(k)$ and $\beta(k)$: this expression represents an optimization

problem, where η is the step size of the adaptation algorithm. This fact opens the field to several algorithm for parameters optimization of the identification problem (Narendra 1990 (b))

$$\hat{\alpha}_i(k+1) = \hat{\alpha}_i(k) - \eta \frac{e(k+1)\, y_p(k-i)}{1 + \sum_{i=0}^{n-1} y_p^2(k-i) + \sum_{j=0}^{m-1} u^2(k-j)} \qquad 3\text{-}58$$

Therefore, the application of neural networks for system identification can be thought as the network parameters optimization so as to find the best fit to the real plant. The evaluation of the optimization performance is given by the objective function, which is expressed as a function of the network parameters vector θ (Narendra 1990 (b)), and its representations for static and dynamic systems are as follows:

Performance Index for System Identification

Static system **3-59**

$$J(\theta, k) = \sum_{Set} \left\| e(k) \right\|^2$$

Dynamic system

$$J(\theta, k) = \frac{1}{T} \sum_{k=1}^{T} \left\| e(k) \right\|^2 \qquad \textbf{3-60}$$

One of the methods to solve this optimization model is the general linear search, which expression is,

$$\theta = \theta_{nom} \pm \eta s \qquad \textbf{3-61}$$

θ_{nom} is the point at which θ is evaluated

η is the search step

The +/- sign indicates the ascent/descent gradient direction of search (Fletcher 1987).

For the particular case of the neural networks, the objective is to minimize the objective function; therefore a negative gradient is selected for the linear search. The parameter vector at each iteration time is computed as follows:

$$\theta = \theta_{nom} - \eta \nabla_\theta J \mid_{\theta = \theta_{nom}} \qquad \textbf{3-62}$$

where

$$\nabla_\theta = \frac{\partial J}{\partial \theta}$$

The last expression is the sensibility of the performance index to the variations of the parameter and it is the search gradient. The importance of the sensibility of the network performance is because it is at the core of one of the most famous algorithms in training neural networks, which is the back propagation algorithm.

The good performance of ANN for nonlinear system identification combined with the flexibility and open potential of the networks for solving complex learning problems makes the connectionist approach an efficient approach for solving the HPR controller modules (Hunt, Sbarbaro *et al.* 1992; Willis, Montague *et al.* 1992; Pham and Xing 1995; Chong and Parlos 1997; Bernd, Kleutges *et al.* 1999; Ahmad, Chipperfield *et al.* 2001; Lazar and Pastravanu 2002; M'Sahli and Matlaya 2005; Ławry Nczuk 2007). In particular ANN are applied in the system identification and tacking system as it will be developed later in this chapter. However the networks approximation can be extended to another part of the controller solution such as the optimization and the dynamic programming approach for solving the objective function of the on-schedule system. However this is out of the scope of this project and it is a proposal for further project, here will be only proposed the algorithmic solution.

3.9. CONCLUSIONS

Analyses towards Specifications for the HPR: Mass-energy conservation analysis for determining the minimum set of variables for system identification

As the controllability of the HPR is a **problem of energy generation**, thus a mass-energy conservation model for the turbine-vehicle is applied. First law of thermodynamics incorporates the energy at a shaft of a machine to produce work and to overcome losses

Models based on **mass-energy conservation, and linear momentum** have been mentioned in Chapter 2, for determining the friction effect on discs buckling, for disc pipeline devices, under different pipeline scenarios. However, for HPR bristle-based locomotion, a different analysis is required. A HPR model needs to consider the robot behaviour, affected by several factors such as pipeline environment, and its own internal mechanism, particularly the cam shaft, and the behaviour of the bristles units.

The **mathematical expression for the turbine efficiency** is an alternative for characterizing the turbine, in order to determine the basic variables of interest. However, the energy-mass conservation analysis gives the insight of the transformation of the energy in a conservative system and the losses of the HPR, mainly mechanical losses.

The **energy analysis if based on a conservative system** for inviscid flow and therefore without losses due to friction. However, any real system possesses losses indeed; but for the purpose of determining the minimum set of variables to be observed the energy-mass conservation analysis is a consistent frame. However, this analysis is valid only for uncompressible flow, such as water, which is the given medium for this test rig.

Recommendation from mass-energy conservation analysis are towards the measurement of the turbine efficiency as input variable, and the vehicle speed as output variable, which are the basis for designing the energy management system.

Structural analysis for determining robot behaviours

The main HPR behaviours has been characterised from the structural analyses, these states are **crawling, reversing, cycling and idle and excursioning**. However, other extraneous behaviours have been observed such as temporarily excursions with the flow or irregular dead-time. Apparently these patterns have no clear explanation

and may affect the overall performance. These behaviours deserve a dedicated characterization further than direct observations reported in this project. So, the measurement system described **in Chapter 5** is designed to perform such observations in order to get a suitable insight.

Therefore, the proposed states namely, **operating, cruising and self recovering for the on-schedule states; and cycling and idle for the off-schedule** states, intend to capture the expected and most of the unexpected robot behaviours.

Functional analysis (FME(A) for determining the modes of failure of the HPR

One of the fundamental requisites for the **controllability** of the HPR is a **robust operation** particularly to avoid the unit lost in the pipeline. In order to accomplish with such robust operation, the control strategy includes a **self-recovery stage** as a standard completion of any mission, based on the bidirectional characteristics of the vehicle. However, it is necessary to determine the ways in which the unit can **fail** leading to the unit lost inside the pipeline; and the ways in which these failures can be predicted and/or avoided by a **self-recovery strategy**.

Results of the **FMEA** (Failure Mode and Effects Analysis), suggest that the control strategy needs to identify the behaviour of the bristle-based vehicle and the performance of the turbine in order to assure a robust robot operation, targeting the 75% of the causes of failure. This fact suggests that including an additional strategy of fault detection and isolation at component level, would contribute with no more than the 25% to solve the causes of failure. Therefore, the self-recovery strategy is the most significant to be implemented at this stage of the HPR control development.

System Model: data driven vs. model driven system identification

The two leading options for modelling a system are the model driven vs. data driven approaches. Models based on first principles has been suggested in the literature such as the one for a class of bristle-based pipeline vehicle, based on studies of the buckling effect of the bristles, or including analyses in the tribology field. However, these models the more accurate the more cumbersome for control purposes.

Therefore, the decision was to use a data driven system identification based on ANN, embedded in the series-parallel structure suggested by Narendra (Narendra 1990 (b)). The network structure design, simulation and results are developed in Chapter 4.

Chapter 4 HPR Controller Development

4.1. INTRODUCTION

The hybrid pipeline robot, as a flow-powered vehicle calls for a **robust energy management** for coordinating the power generated and stored, in order to accomplish with the whole mission. Note that the energy management strategy is to lead a fully autonomous mission without external communication. This is because the pipe walls and the fluid inside the pipeline are serious impediment to the data transmission, in the wired or wireless version, requiring a special research in the field of communications.

The whole mission of the bidirectional pipeline robot calls for a **robust operation** including **self-recovering state** either after completion of the mission, or as a result of failures leading to the loss of the robot inside the pipeline. However, no other fault detection and isolation strategy is performed such as component failures.

Reconfigurable control architecture is designed for controlling pipeline operations, cruising and self-recovering states. Multi-objective optimization is the strategy proposed for solving the objective function of the speed control state; and objective prioritization for cruising and self-recovering state. Therefore, a control architecture is based on a reconfigurable control law, for energy management, speed control and self-recovering system, schematized in Figure 4.1-1.

Figure 4.1-2 shows the HPR control strategy design, based on model predictive control MPC, reconfigurable system, hybrid control system, and neural-networks.

The development of models based on Neuro-Model Predictive Control and Neuro-Dynamic Programming are presented for the speed control, and energy and time management control, respectively.

The chapter finalizes with data analysis and conclusions of simple inspection of data from the rig; and concludes with the test and results of the system identification and tracking system based on neural networks. Figure 4.1-3 shows the scheme of the trial models approach.

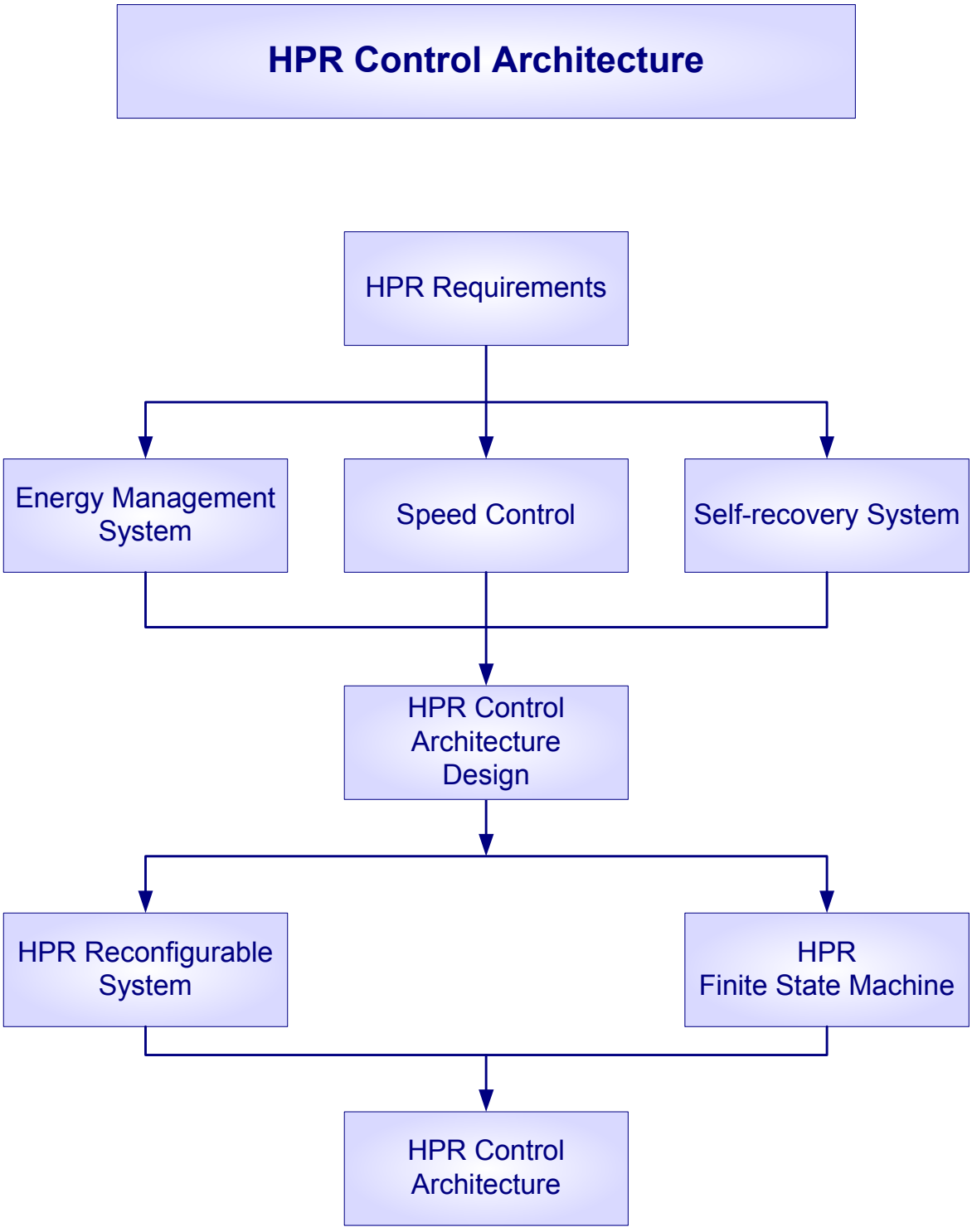

Figure 4.1-1 Chapter 4 contents: HPR Control Architecture

The control architecture is based on the core requirements of the HPR, energy management, speed control and self recovering system. The architecture is proposed as a reconfigurable system with control strategy reconfiguration, and it is presented as a Finite State Machine.

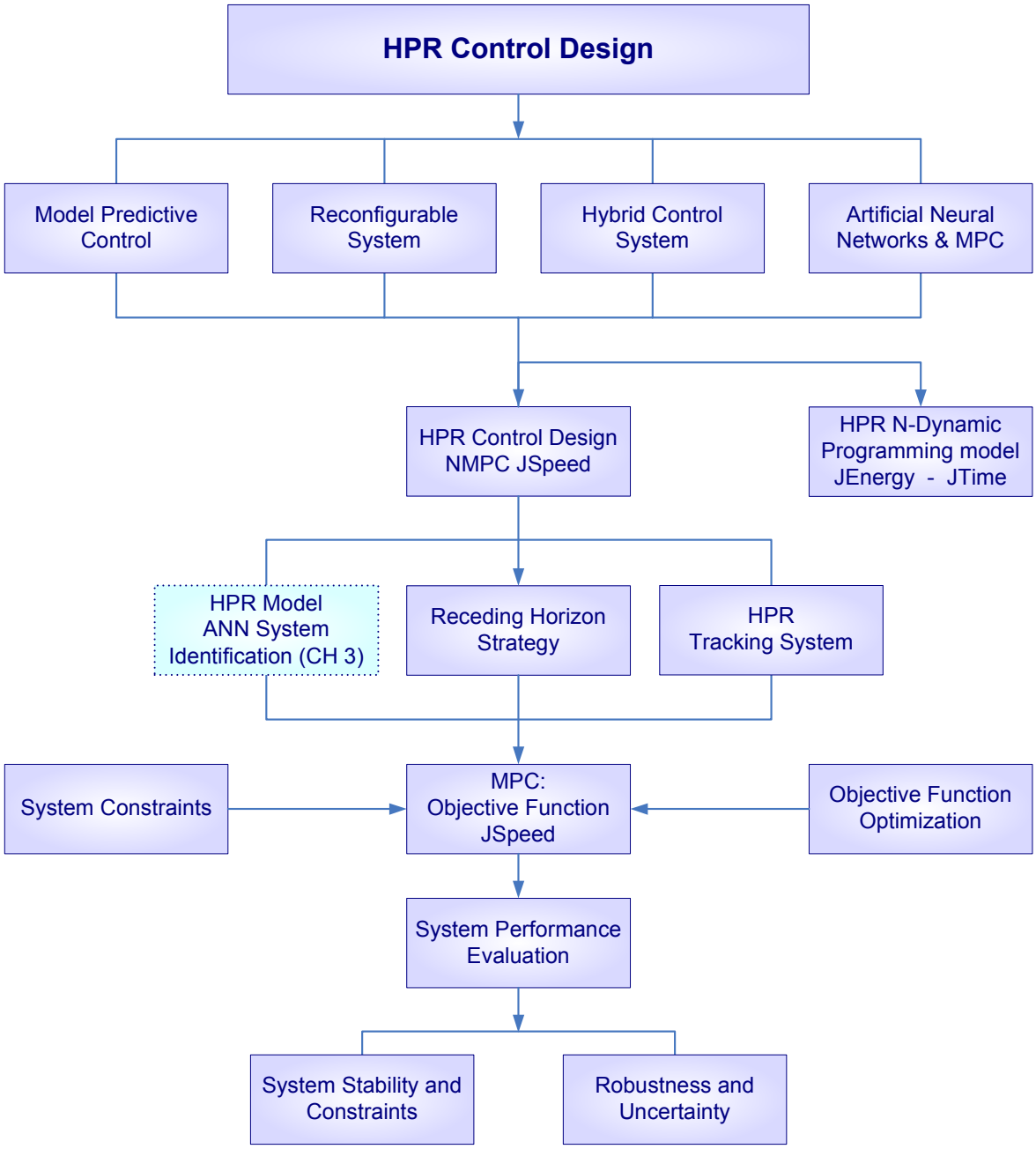

Figure 4.1-2 Chapter 4 contents: HPR Control design

The control strategy for each of the states of the reconfiguration is developed. A Model Predictive Control MPC is designed for speed control while optimizing the energy and time, for operating state. Energy and time optimization is designed based on a neuro-dynamic programming approach, for cruising and self-recovering states.

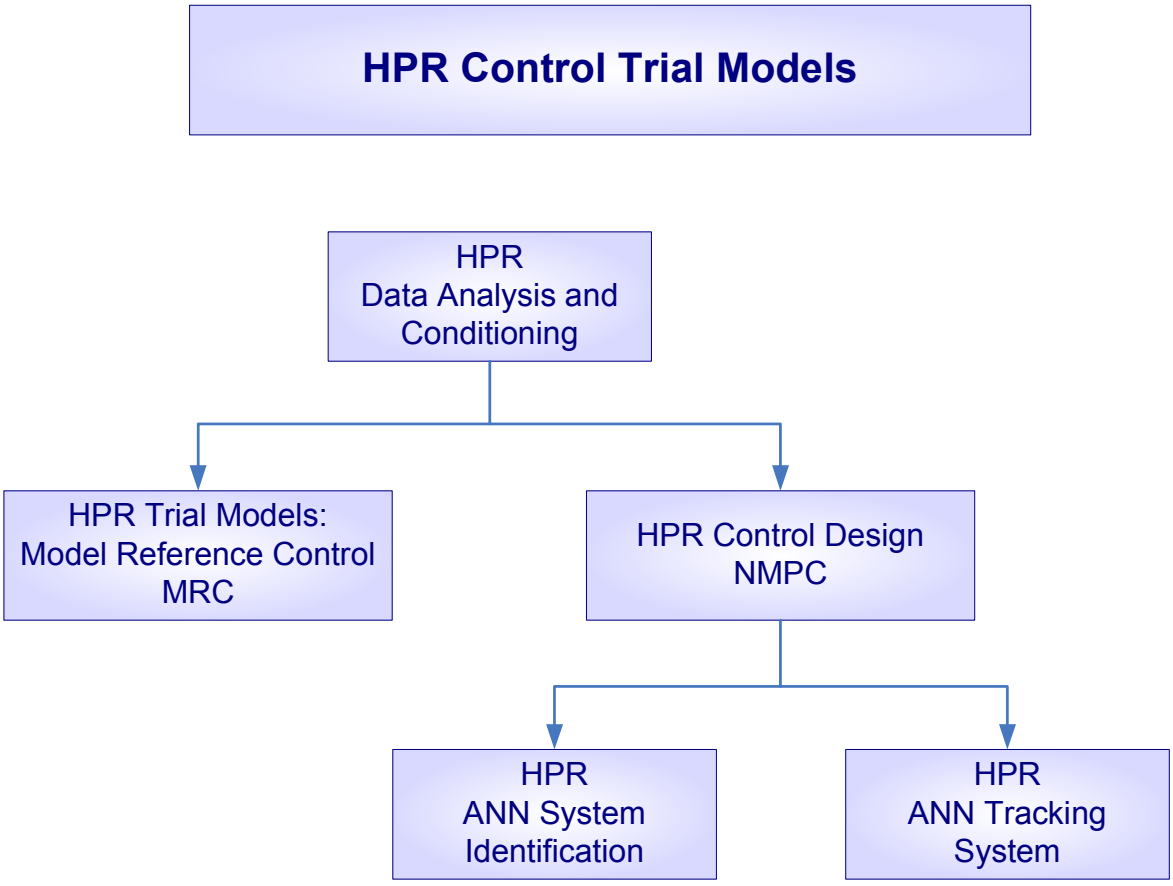

Figure 4.1-3 Chapter 4 contents: HPR Control trial models

Trial control models are simulated based on measured data. Two models are compared, the model reference control MRC to emulate a linear system while tracking the reference; and model predictive control MPC based on artificial neural networks for system identification and tracking.

4.2. HPR Control Requirements

4.2.1. Energy Management System (EMS)

The energy management system is an energy observer in charge of evaluating the available energy, stored and generated, and predicts the future availability in a predefined prediction horizon. The generated energy is based on the efficiency of the turbine and the payload the crawler vehicle exerts at the turbine shaft. In this sense, the turbine efficiency reflects environmental conditions, and therefore the crawler speed is also hindered. So, the environment features are represented by the counter torque of the turbine shaft and the crawler speed. The information of the energy levels is the basic information for the on-schedule states, which are controlled upon the energy optimization algorithms. Details of the signal flow may be seen on the Finite State Machine for the Hybrid Pipeline vehicle Figure 4.1-5.

4.2.2. Speed Control

The speed control has the purpose of regulating the operations speed for tasks such as inspection, cleaning or any other specified pipeline services. The speed controller need to be able to follow a non-stationary reference, which may be a single constant speed or a periodic sequence of different speeds upon the task requirement; for example to inspect a pipeline sector, it may be required several loops of forward and backward crawler vehicle cycles of not necessarily the same speed. The HPR controller proposed in this research project is based on a Model Predictive Control, which is developed later in this chapter.

4.2.3. Self-recovering System

The self-recovering system has a two-fold function: one is to perform the scheduled self-recovering journey after completion of the predefined task; the other function is the emergency self-recovering in case of failure or adverse conditions inside the pipe. The self-recovering system is based on the information from the energy management system that allows the planning of the self-recovering state in a predictive way even before the adverse conditions are fully developed. However, the self-recovering event is fired after an inference and counter algorithm are executed rather than immediately; this is to prevent faux self-recovering actions. The counter algorithms are intended to

provide the HPR with the necessary time for generating energy so as to continue with the scheduled state.

4.3. HPR Control Architecture Design

The HPR controller architecture, as it was mentioned in the literature review, stems from two ideas: simplicity and effectiveness. In the context of knowledge representation of an event, simplicity is defined as the minimal explanation of the event so as to meet the required purpose. Even more, the measurement of the simplicity is expressed as the number of changes in the reasoning chain of the causal explanation for this particular event (Long and Garigliano 1994).

Extrapolating these concepts to the HPR controller architecture, simplicity means to find the representation of the minimum necessary number of events that produce the change of states of the system. This definition has a close relation with the granularity of the system in terms of number of states that are required to be the minimum number so as to meet the robustness requirement for the HPR controller. Therefore, simplicity in the controller design means to find the minimum number of events and states that define the efficient controller.

The effectiveness of the proposed HPR controller structure is based on Brooks' ideas. He presents a control architecture based on intelligence in a process of building up the intelligence rather than constructing intelligence based on the perception of sensors or "world representation" (Brooks 1991). The architecture is based on cooperative concept of sharing sensors/actuators between behaviours at different level in the hierarchy. This architecture approach is called **subsumption** with the purpose of giving the idea of each layer performing a "subsume" of the layer below in the hierarchy; in that sense it is a bottom-up approach. The role of finite state machine is of implementing the minimum resolution in the architecture yet the question is if higher levels of inference may still be represented by finite state machines.

As a result, Brooks' knowledge building has a close relation with the engineering approach of analyzing and solving problems: decompose the whole system in **functions and activities** to build up the whole automaton, rather than a human mimic of the knowledge representation. In the same line of thought, Brooks prioritize the whole process rather than fixed structures inside a global planning. Planner is an "abstraction barrier" as Brooks quotes, and the planner may be obsolete if they do not represent the

total objective of the robot. The summarizing idea is in Brooks' words: *planning is just a way of avoiding figuring out what to do next* (Brooks 1987).

Although the **HPR** has a standard scheduler of tasks, the schedule may be superseded by a change of the state upon the needs of the crawler vehicle. This is in line with Brooks' thoughts: priority to the process rather than subordinate structures. The basic information is given by sensors and predictor. So, based on this information, the controller takes the next action; in Brooks' words: sensor and predictor help *to figure out what to do next*.

Meystel and Albus mention that system architecture is a structure of artificial agents; and every agent is an architecture in itself (Meystel and Albus 2000). In that sense the **HPR** proposed architecture is able of prioritizing critical scheduled tasks such as operations or self-recovering states and supervise transitory states such as idle and cycling states.

The algorithm of **Multi-resolutional Hierarchical Planning** is a behaviour-generation structure, defined by the interaction of different layers of information, goal specification, and decision maker (Meystel and Albus 2000). The **multi-resolutional** denomination refers to the granularity of the specification to be controlled. In this context, three management operators for the controller structure are defined: job assignment, schedule concatenation and focusing attention. The improvement of the structure performance is valued by the objective function of a multi-resolutional optimization problem.

Among several controller architecture, the approach of Meystel and Albus is utilized here as a frame to point out some similarities and differences with the HPR structure. For example, the HPR controller structure, although different from the one proposed by (Meystel and Albus 2000) they share some practical approaches. The HPR control strategy is based on three systems: Energy Management System, Speed Control and the self-recovering System. Thus the objective function and its constraints are modelled by the three main systems, which may be seen as virtual systems rather than actual separated structures. So, in this aspect the HPR structure is similar to the Multi-resolutional operator of job assignment and schedule concatenation of the model of Meystel and Albus. The HPR controller approach of the schedule of tasks of on-schedule and off-schedule states is similar to the approach of Meystel and Albus of focus attention: the resolution or granularity of the controlled characteristic may be managed by defining hard and soft constraints: hard constraint for operations

conditions (high resolution) and soft constraints by relaxing the speed requirement (less resolution) for cruising and self-recovering states.

Two main strategies are at the core of the HPR controller architecture: Model Predictive Control (MP(C) and Dynamic Programming (DP). Both are based on the optimization of an objective function; however, the MPC, for speed control, optimizes the objective function in a receding horizon approach and the dynamic programming, for energy and time management, optimizes a cost function through the time, which is the time the robot's journey lasts.

However, instead of only one controller structure with a multi-resolutional objective function, the proposed architecture for the HPR is a reconfigurable controller, with reconfiguration of the objective function and its constraints. This approach is selected because of its flexibility and adaptability: the objective functions are designed for the particular state so as to act in accordance with the random characteristics of the pipeline environment. So, the architecture structure is a multi-objective reconfigurable system for each of the scheduled states, each of these states controlled by a multi-resolutional controller. Therefore, the HPR structure makes use of the architecture operators mentioned by Meystel and Albus, job assignment, schedule concatenation and focusing attention, yet in a reconfigurable and adaptable approach.

4.3.1. HPR reconfigurable system

The strategy of the **HPR reconfigurable controller** is to change the objective function upon the states of the two main system conditions**: on-schedule** and **off-schedule conditions**. There are three main **on-schedule states**: **operations, cruising** and **self-recovering conditions**. The first state, operations, is based on the controller for the scheduled speed, energy and time optimization and it is solved as a **multi-objective optimization**. The second and third states, cruising and self-recovering, are similar in the sense that they share the **objective prioritization** strategy for the energy and time optimization; however, the solely difference between cruising and self-recovering performance is the additional energy provided by a second pack of batteries for self-recovering state. This extra energy is not available when the robot is crawling to the target point because these batteries are in reserve for operation condition.

The **off-schedule** states, cycling and idle, are temporary; they have an OR state decomposition in the finite state machine. The cycling stage is characterized by a resultant zero displacement although the speed is positive. This is because although the

flow rate is enough to produce the turbine shaft rotation, obstacles inside the pipe are impeding the actual HPR displacement. In this case the accelerometer, for speed measurement, detects spurious back and forward displacement with no effective displacement of the robot. Similar conditions characterize the idle stage yet it differs in the zero displacement due to zero velocity. In this case the accelerometer detects only spurious signals produced by the turbine thrust, originated by controlled or uncontrolled actions. In the case of controlled idle state, it is for recharging batteries otherwise it is produced by external causes such as low flow rate or severe impediments inside the pipeline. The flow chart summarizes the HPR control architecture.

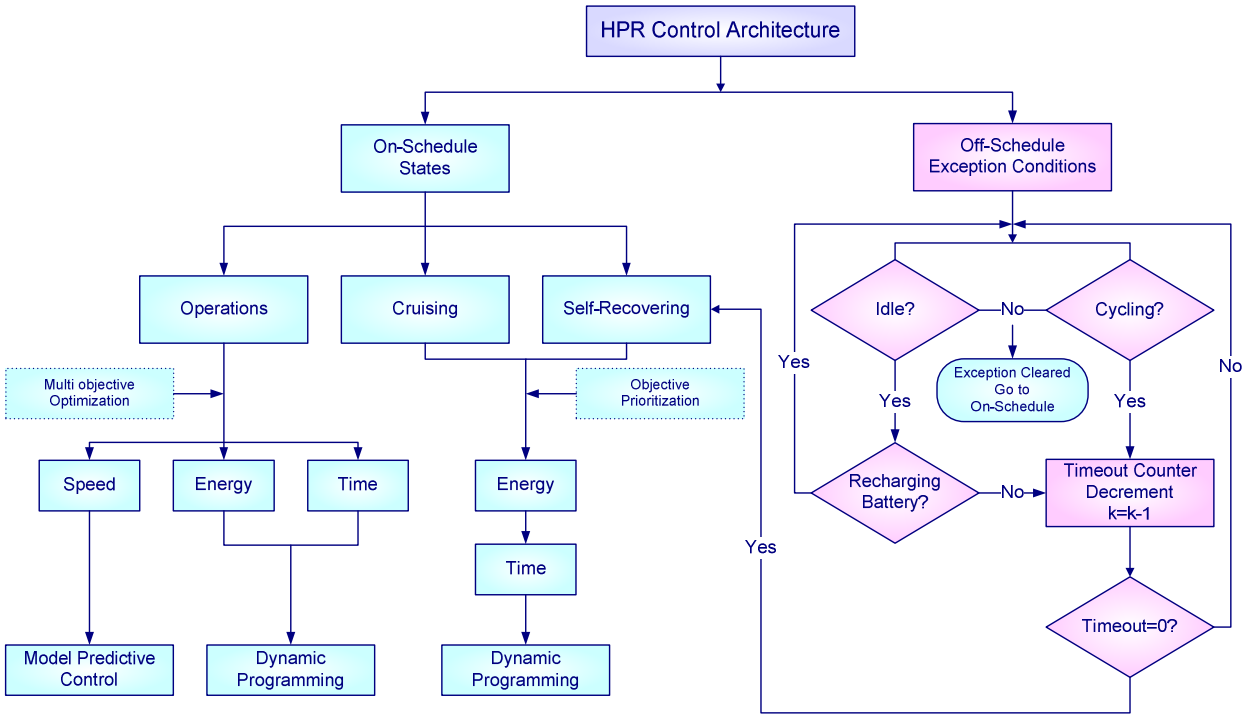

Figure 4.1-4 HPR Control Architecture

The structure shows control strategy for the on-schedule states, operating, cruising and self-recovering; and the off-schedule states idle and cycling. The control reconfiguration is denoted by the different optimization approaches of the control structures.

4.3.2. HPR Finite State Machine

The **Finite State Machine (FSM)** is an event-driven design procedure for describing a system, its states and the events that produces the transition among the states (Hatley and Pirbhai 1987). Apart from this basic description, the FSM is a complete symbolic language structure for development of the code with all the capabilities of any programming language (Harel 1987; Harel and Naamad 1996).

The HPR Finite State Machine is composed of two main states: the *HPRSupervisor* and the *HPRRegime*. The Finite State Machine for the HPR is showed in Figure 4.1-5. In this figure, the states are indicated by boxes and the transition events by arrows. The state decomposition is indicated by the frame line of the boxes: doted line means logic AND while solid line indicates logic OR. So, the state decomposition, for *HPRSupefrvisor* and the *HPRRegime,* has logic AND that means both states coexist at the same time.

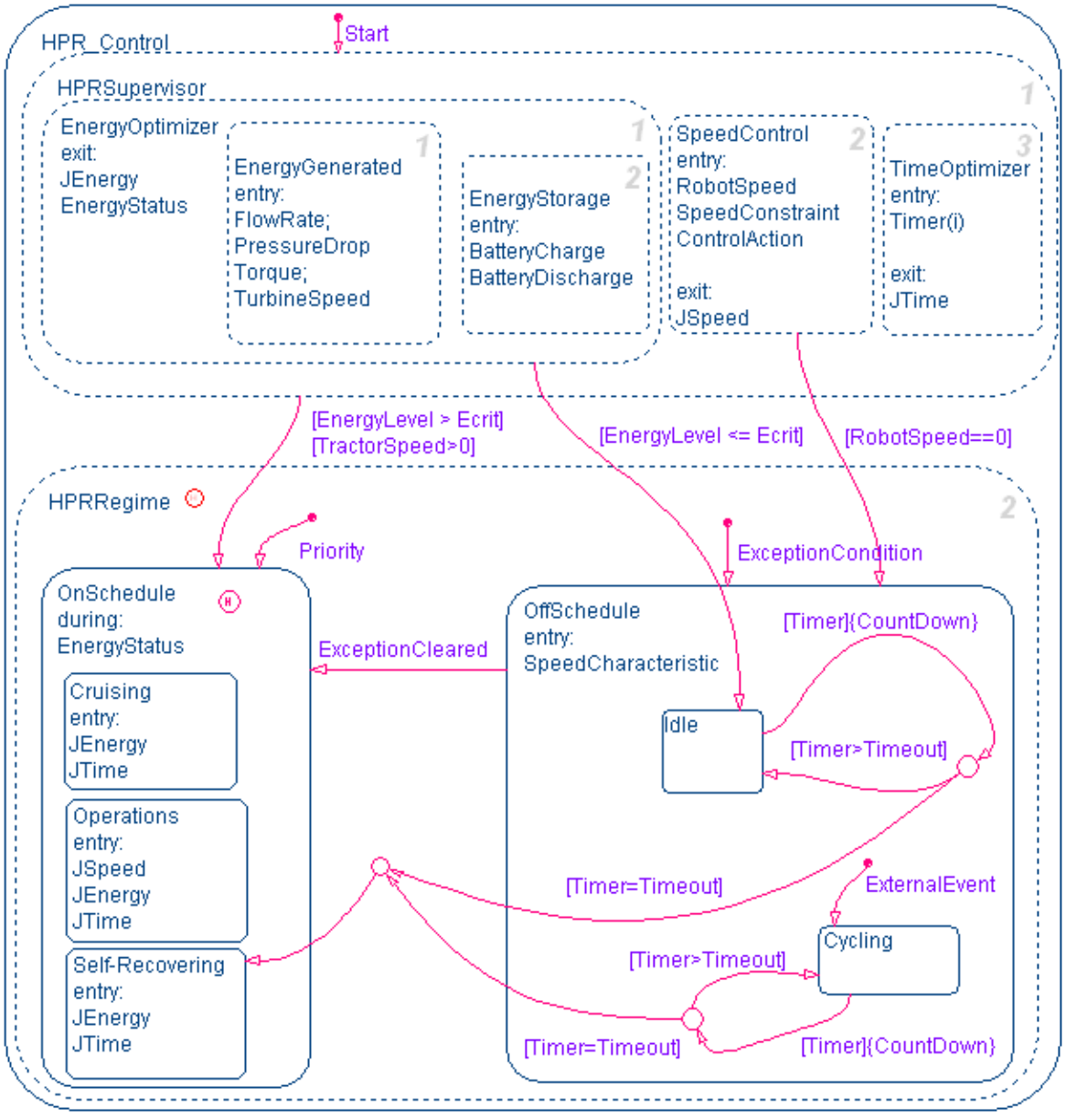

Figure 4.1-5 HPR Finite State Machine

The figure shows the control architecture with reconfiguration of the control strategy denoted as HPR Supervisor, and the transition between on and off states in the HPR Regime.

The HPR Supervisor is composed of the *EnergyOptimizer*, *SpeedControl* and the *TimeOptimizer*. These three states have logic AND as state decomposition; however,

the state priority is indicated by the position in the chart, and by the number at the top right corner. The *EnergyOptimizer* is in charge of the energy inventory upon the information from the stored energy (*EnergyStorag(e)* and generated energy (*EnergyGenerate(d)*. The variables of the system are evaluated upon the entry to the respective state for example when the *EnergyGenerated* state is activated, the variables *FlowRate*, *PressureDrop* and so forth are evaluated so as to calculate the HPR efficiency.

The dotted line of the boxes, for theses states, means that the state decomposition has logic AND that means both states are active at the same time that is reasonable because both states are evaluated simultaneously in order to get the instantaneous level of energy. The *EnergyOptimizer* state gives the cost function index *JEnergy* and the status of energy *EnergyStatus* as a result of the state evaluation, when the state is exited.

The second main state is the *HPRRegime,* which contain the *OnSchedule* and O*ffSchedule* states. Similarly to the Figure **4.1-4**, the *OnSchedule* state contains the states *Cruising*, *Operations* and *Self-recovering*. The state decomposition for these states has logic OR that means one of those states is active at the time when the parent state is activated. The solid line of the boxes indicates the logic OR among the states. Upon the activation of each of these states the objective functions are evaluated. The second state of the *HPRRegime* is the *OffSchedule* state composed of the *Cycling* and *Idle* states, both are mutually exclusively; so, the state decomposition is a logic OR. These states are originated by random conditions in the pipeline environment or mechanical characteristics of the vehicle; these conditions are considered as exceptions, *ExceptionConditions*. Each of these states is connected with a count-down timer, which is activated upon the state activation. When the timeout is reached the self-recovering phase is activated, otherwise the state remains active until the condition that originated the *Idle/Cycling* is cleared, in which case the normal regime are regained.

The uncontrolled *Idle* state is due to environmental causes, such as low pressure drop across the turbine that is insufficient for generating enough torque at the shaft. Conversely, the controlled *Idle* state is due to a low level of energy in the system, as low as it is indicated by a critical value. It is important to note that the critical value is the energy necessary for self-recovering. So, whenever a critical energy value is reached the robot is set to *Idle* so as to generate energy for battery charging. However, the criticality of the energy it is important to note that the HPR at the last stage has

enough energy for completing the self-recovering stage. That makes the HPR performance robust to failures compromising the robot self-recovering.

4.4. HPR Controller Design

As it was presented in the Literature Review, the HPR controller is based on four control approaches: Model Predictive Control, Reconfigurable Control, Hybrid Control Systems and Artificial Neural Networks for Control. The following paragraphs describe how the HPR controller is built upon these knowledge fields.

4.4.1. Model Predictive Control

The speed control for the HPR is based on the model predictive control MPC structure, composed of the model of the system and the control law. The control law is obtained by optimising the objective function, which is an efficient and flexible tool for including any control strategy of interest. The control action, or manipulated variable derived from the control law, is applied to the system in a receding horizon strategy, which is explained later in this chapter.

One of the attractiveness of the MPC is that it leads to a stable plant/process in a finite number of steps due to the receding horizon approach, which calculates the present and future sequence of control actions necessary for stabilise the plant in the desired horizon. In this way the present control action contains the information required for stabilise the plant in the predefined time span. This approach is explained in detail in section 4.4.6.

Originally, the drawback of the MPC was the computational expensive optimisation of the objective function at every control step. Thus, it was mostly applied successfully to slow petro-chemical processes. Nowadays, this is not anymore a problem considering the availability of powerful microprocessors.

The optimisation of the objective function and the receding horizon approach assure the stabilisation of a non-minimum phase plant, with zeros outside the unit circle, and with variable or unknown dead-time; recalling that zeros outside the unit circle of the open-loop transfer function, produce instability of the closed loop system, as they are shifted to the denominator of the closed-loop transfer function. The design of the HPR objective function and the system performance are analyzed in sections 4.4.8 and 4.4.12 respectively.

Another appealing feature of the MPC is the flexibility in choosing the plant model for the problem of interest. Several approaches to modelling are suggested in the literature (Camacho and Bordons 2004) For example, in petro-chemical industry, the complexity of non-linear models can be approximated by a single first order or a chain of first order model (Clarke, Mohtadi *et al.* 1987 (a); Clarke, Mohtadi *et al.* 1987 (b); Clarke and Mohtadi 1989; Gawthrop 1996 (a)).

Originally the plant model was based on the Controlled Auto-Regressive Moving Average (**CARIM(A)** model; and the modification of its structure gave rise to several subclasses of controllers from which the Generalized Predictive Controller (GP(C) contains the main features suitable for most common control problems.

The modification of the MPC structure and parameters give rise to several subclasses of controllers from which, the Generalized Predictive Controller (GP(C) contains the main features of this kind of controller (Gawthrop 1996 (a); Garcia and Morari 2002; Gawthrop, Virden *et al.* 2008). The plant model of the **GPC** proposed by Clarke (Clarke, Mohtadi *et al.* 1987 (a)) is described by the CARIMA model as follows:

4-1

$$A(q^{-1})\,y(t) = B(q^{-1})u(t-1) + C(q^{-1})\frac{\zeta(t)}{\Delta}$$

This plant model is based on the Controlled Auto-Regressive Moving Average (**CARIM(A)** model. The controlled variable is the measured output *y(t)* of the plant. The **autoregressive term (AR)** refers to the auto regression, or memory of the system output *y(t)* and input *u(t)*and it is expressed through the polynomials *A(.)* and *B(.)* respectively expressed by the backward shift operator q^{-1} , which represent the "memory" of the input and output, in other words, the extent to which the past values affect the present value of the variables of the system (Ljung 1987). The application of the backward shift operator transforms the polynomials in the following expression.

4-2

$$A(q^{-1}) = a_1 q^{-1} + \cdots + a_{na} q^{-na}$$
$$B(q^{-1}) = b_0 + b_1 q^{-1} + \cdots + b_{nb} q^{-nb}$$

The argument of *u(t-1)*, shifted in *-1* with respect to the input, is the dead time of the system, and represents a causal system, where the input is applied to the system at least one unit before the output *y(t)* takes effect (Clarke, Mohtadi *et al.* 1987 (a)).

The **moving average (M(A)** approach is the model of the **random disturbances, *ξ(t)*** represented in the equation 4-1. These disturbances affect the output *y(t)* and are not necessarily the same as the disturbances affecting the states (Ljung 1987). **Disturbances** may be stationary or variable, deterministic or stochastic.

The variations in the disturbances are represented by the backward shifted polynomial C(.),becoming a moving average approximation of the disturbance.

Some variations of the GPC model accounts for considering *C(.)* as the unit value to simplify the computations; another variation consists on truncating *C(.)*and including the resulting polynomial in the *A(.)* and *B(.),* affecting the input and output alike (Clarke, Mohtadi *et al.* 1987 (a)). The **integrating factor (I)** is represented by *1/Δ* in the disturbances term, producing the smoothness of the non-stationary disturbances.

The **predictive approach** of the GPC stands for prediction of the output and future control moves under a horizon of interest. The classical approach for solving the predictor problem is through the recursion of the Diophantine equation in order to derive the future j-step control moves (Clarke, Mohtadi *et al.* 1987 (a)).

The system identification based on neural networks, which is the model approach of this research project presented in Chapter 3, accounts for the non-steady disturbances, which is a substitute of the moving average and integrative factors of the CARIMA model. The autoregressive characteristic is performed by the tapped delay line of the neural networks, which is the state feedback of the control block. So, the neuro-system identification approach not only efficiently replaces the CARIMA attributes, but also incorporates adaptively the nonlinearities of the pipeline robot.

4.4.2. Reconfigurable Systems

System reconfiguration, in the context of the HPR, is a change in the control strategy to maintain the robot under control when unexpected events occur. Spacecraft is one of the leading fields for application of reconfigurable control (Steinberg 2005).

Examples in the literature report a reconfigurable controller for facing aircraft's actuator failure. In this case, the failure is of the sensor-saturation type and the reconfiguration is based on the actuator redundancy. The reconfigurable strategy is performed by mapping the reconfiguration matrix, containing the input-output weights, each of those related to an arrangement of actuators (Soloway, Shi *et al.* 2004 (b)).

The reconfiguration of autonomous control system can be classified in three categories: operating system regime, performance improvement, fault accommodation

(Rauch 1995). In terms of system model, the literature cites two approaches for reconfiguration: a multi-model case and a unitary model with adaptive feature to uncertainties. Rauch gives examples for fault diagnosis and isolation (FDI) combined with reconfigurable control system are given in (Rauch 1994).

Soloway presents a GPC approach as the base for a **reconfigurable controller** for handling aircraft's actuator failures (Soloway, Shi *et al.* 2004 (b)). The controller model has two different structures for reconfiguration: a SISO (Simple Input-Simple Output) for the case without reconfiguration and MIMO (Multiple Input-Multiple Output) for reconfiguration state. The aircraft model is based on the CARIMA (Controlled Auto-Regressive Integrated Moving Averag(e) model, solved by the Diophantine equations leading to a Riccati recursion over few steps in the horizon control. The model includes terminal state constraints with the aim of guaranteeing the stability of the system.

The HPR control architecture is based on the reconfiguration of the performance index and optimisation approach for each of the on-schedule states, operations, cruising and self-recovering. The architecture includes also the failure detection and reconfiguration with the capability of self-recovering feature if the journey is impeded for any environmental reasons. Therefore the HPR system belongs to the categories of reconfiguration of operating system regime, performance improvement and fault accommodation mentioned by Rauch (Rauch 1995).

4.4.3. Hybrid Control System

A hybrid control system includes signals of different nature such as switching input/outputs, logical states and constraints, heuristic decision and constraints prioritization (Bemporad and Morari 1999 (b); Bemporad, Heemels *et al.* 2001; Dechter, Cohen *et al.* 2003; Bemporad 2006). These signals may coexist in the same level of a hierarchy (**Mixed Logical Dynamical (ML(D)**) or at different hierarchical levels (Bemporad and Morari 1999 (b)). One of the hybrid control strategies suggested in the literature and intended to stabilise the system under control consists on dividing the control space in subspaces and performing the control action in a piecewise approach (Koutsoukos and Antsaklis 1999; Antsaklis 2000; Koutsoukos and Antsaklis 2001).

They HPR can be classified as a hybrid system, mainly because the reciprocating traction leads to a switching vehicle speed, which is a periodic with variable dead-time.

The HPR control architecture is also designed as multi-objective optimization for control speed and objective prioritisation for cruising and self-recovering states. Thus, the HPR control strategy is a constrained optimisation problem to be solved in the space defined by the different variables to be optimised, which is solved by considering the system as a piece-wise space. In addition, the transition between states can be treated as the transition between planes of the piece-wise space composed of the HPR states.

4.4.4. Artificial Neural Networks and Model Predictive Control

The **ANN**-based **Model Predictive Control** presents different combinations of neural networks, for example for representing the system model, for tracking system, and for optimization, just for citing the main ones (Miller III 1990; Hecht-Nielsen 1992; Kosko 1992; Willis, Montague *et al.* 1992; Cichocki and Unbehauen 1993; Quero, Camacho *et al.* 1993; Haykin 1994; Pham and Xing 1995; Gawthrop 1996 (a); Chong and Parlos 1997; Dingankar and Sandberg 1998; Haley, Soloway *et al.* 1999; Lazar and Pastravanu 2002; Soloway and Haley 2004 (a); Herrmann 2007; Ławry Nczuk 2007).

For the particular case of the HPR controller, the neural networks are used for system identification and tracking system. The artificial neural network adaptation and representation of non-linear systems is a good feature for representing the non-linear and dynamic characteristics of the HPR and the pipeline environment. The ANN-based system identification and tracking system for the HPR are presented in section 4.5.4 and 4.5.5 respectively.

4.4.5. HPR Control Design: NMPC

The block diagram of the Figure 4.1-7 represents the **Model Predictive Control (MP(C)** strategy applied to the HPR speed control. The system model and tracking system are based on ANN. The sequence of control actions is the result of solving the control law by optimising the objective function. Simultaneously, the energy and time are optimised for the scheduled operations. The system constraint is of the type of terminal-state membership where the vehicle speed is confined, assuring the stability of the system for speed control.

The HPR control strategy is designed as robust to transient changes in the regime, such as cycling or idle, in order to consider only significant changes in the robot behaviour. The HPR system is also robust to tracking errors, to consider only the actual

robot displacement instead of short displacements due to the reciprocating nature of the vehicle.

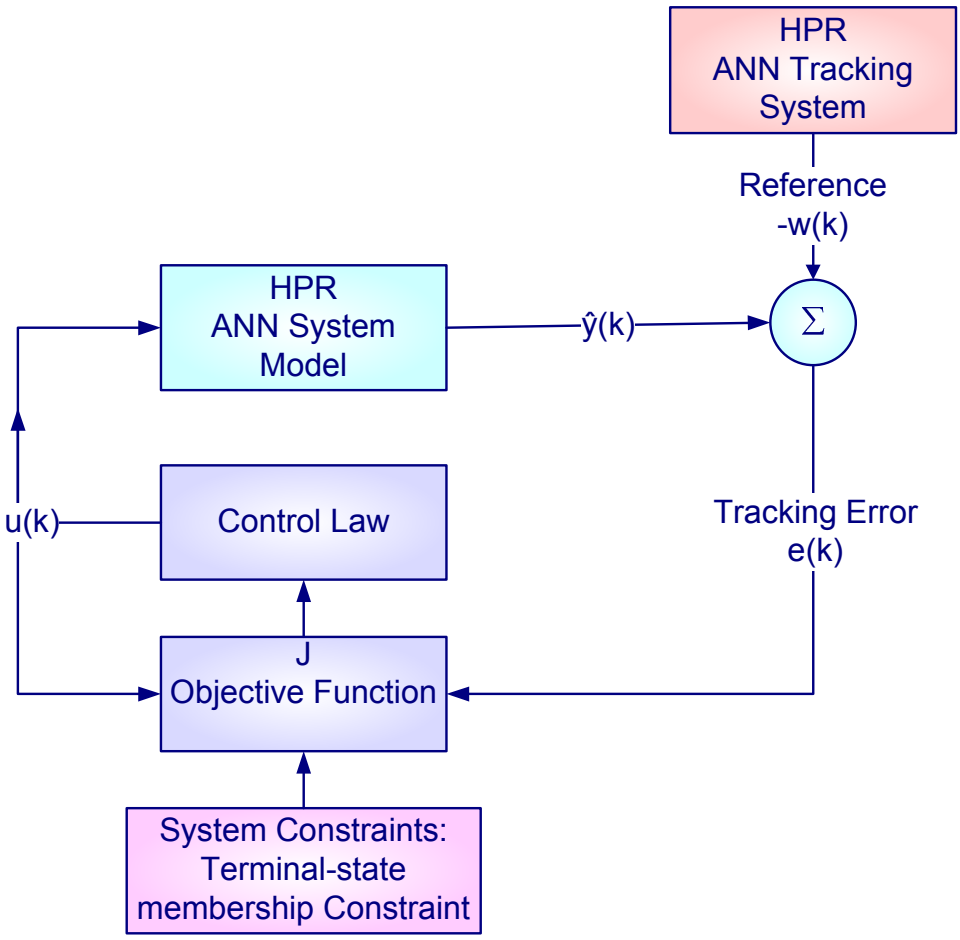

Figure 4.1-6 Block diagram for the HPR Model Predictive Control (MP(C)

The control law is the result of the optimisation of the constrained objective function. Particularly, the terminal-state membership constraint is to guaranteeing the stability of the speed control

4.4.6. Receding Horizon Strategy: Prediction and Control Horizons

The **model predictive control** (**MP(C)** is based on the **receding horizon** strategy, and consists on the computation of the present control action based on the control law. The control law includes a sequence of future control moves until a predefined control horizon; the control law also includes the tracking errors and their predicted future values for the output span horizon. Figure 4.1-7 from the literature shows the relation between the prediction and control horizon (Shreve and Bertsekas 1977; Clarke, Mohtadi *et al.* 1987 (a); Clarke, Mohtadi *et al.* 1987 (b); Alamir and Bornard 1994; De Nicolao and Scattolini 1994; Yoon and Clarke 1995; Primbs, Nevisti *et al.* 1999; Bemporad and Morari 1999 (a); Rao, Rawlings *et al.* 2001; Lee, Kouvaritakis *et al.* 2002; Torrico and Normey-Rico 2007; Grune and Rantzer 2008).

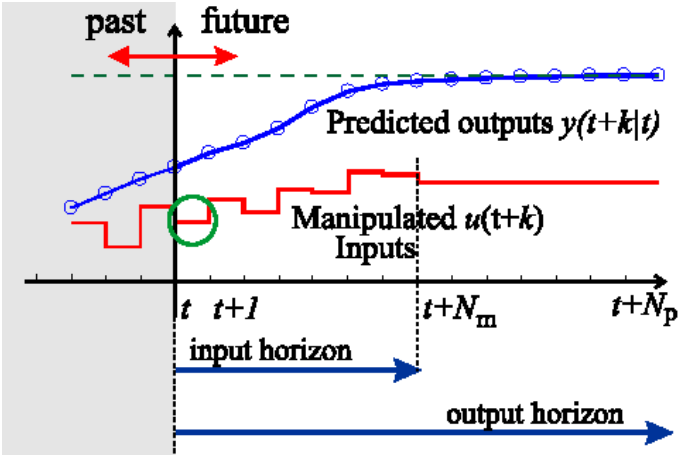

Figure 4.1-7 Model Predictive Control (MP(C): Receding Horizon approach

The green circle shows the present control action, which is the only one effectively applied to the system under control; the future control signals are only used in the calculus of the control law (Bemporad 2006).

The Figure 4.1-7 shows the two main components of the MPC objective function: predicted output value *y(t+k|t)* observed at the time *t;* and the input steps or manipulated variable *u(t+k).* The encircled step is the control signal effectively applied to the plant.

The result of the objective function optimization gives a control sequence, from which only the present control value is in effect applied to the plant, the rest of future moves are discarded, and only are considered in the optimization of the objective function. The process repeats in every sample step. Therefore, the name of receding horizon control (**RH(C)** comes from this concept of shifting the horizon towards the future at every sample interval.

HPR model (ANN System Identification)

The HPR system identification model is based on Artificial Neural Networks, the theoretical rationale is presented in Chapter 3; simulation and results are presented in section 4.5.

4.4.7. HPR Tracking System

Tracking in its simple conception means to follow a target value. The idea behind tracking systems is to reach an **offset-free** terminal state otherwise to get a bounded error for the stable dynamic system, in a Lyapunov sense (Clarke and Mohtadi 1989; Mayne, Rawlings *et al.* 2000; Lee, Kouvaritakis *et al.* 2002; Soloway and Haley 2004 (a); Bemporad 2006; Pannocchia and Bemporad 2007; Wei 2007; Maeder, Borrelli *et al.* 2009).

The HPR presents a particular displacement pattern due to the reciprocating traction, which is also affected by the conditions of the pipe wall. This is the reason for considering a tracking system rather than a target follower.

The research literature offers several approaches to solve the stability problem, for example the reference smoothing for preventing sudden control steps in the tracking procedure. A model for reference smoothing may be expressed as a linear combination of the slack variable ε as follows (Clarke and Mohtadi 1989):

4-3

$$w^*(t+j+1) = (1-\varepsilon)w^*(t+j) + \varepsilon w(t+j)$$

The auxiliary reference w^* is a transition state of the reference and it helps to smooth the transition from one state to the next one, by varying the slack variable ε and its complement $(1-\varepsilon)$. This smooth transition allows the system to gradually adapt to the new state, leading to **stable systems** and preventing the actuator saturation (Bemporad 2006).

Another tracking approach presented in the literature is based on the reconfiguration of the tracking system, applicable mainly to unmanned vehicles. A particular case consists on the reference reconfiguration to account for obstacle-free and obstacle-on-sight scenarios (Wang, Yadav *et al.* 2007). An alternative approach is presented by the multi-objective controller composed of several sub-controllers upon tracking changes (Koutsoukos and Antsaklis 1999; Koutsoukos and Antsaklis 2001).

For stability reasons, it is desirable a constant or asymptotically constant reference. The HPR case presents a combination of **constant speed reference,** for each operation regime, and a **non constant vehicle speed**, due to the reciprocating locomotion. Therefore, the HPR speed can be modelled as a reciprocating regime belonging to a set-membership in the speed space, instead of a valued function. As a consequence, the tracking error is bounded and it is a sufficient reason for the system to be considered stable. The stability performance is analyzed in section 4.4.12.

4.4.8. MPC: Objective Function J_{Speed}

The mathematical expression of the objective function for speed control is the expectation of two terms, the set of tracking or output errors, under the prediction horizon ranging from N_1 to N_2; and the set of control actions, under the control horizon ranging from the present state to N_u. Each term is squared to consider only absolute

values. The unconstrained objective function J, is expressed in the following equation (Clarke 1994):

4-4

$$J_1(N_1, N_2, N_U) = E\left\{ \sum_{j=N_1}^{N_2} \left[\hat{y}(t+j \mid t) - w(t+j \mid t)\right]^2 + \sum_{j=1}^{Nu} \lambda(j)\left[\Delta u(t+j-1 \mid t)\right]^2 \right\}$$

The output error, $\left[\hat{y}(t+j \mid t) - w(t+j \mid t)\right]$, is the difference between the estimated output and the reference. The second term of the objective function, Δu, is the sequence of control moves.

The **prediction horizon** is the period in which the tracking error is driven to a stable region or zero; and the **control horizon** is the period of future control moves required to drive the system to the stable point. The penalising factor $\lambda(j)$ reduces the weight of future control actions, after a determined horizon, in order to reduce control efforts of the actuator; this notion is expressed in equation 4-5. Therefore, the present control action accounts for future penalties (Clarke, Mohtadi *et al.* 1987 (a); Clarke, Mohtadi *et al.* 1987 (b); Clarke and Mohtadi 1989; Camacho and Bordons 1999).

4-5

$$\Delta u(t+j) = 0 = u(t+j) - u(t+j-1)$$
$$\text{for all } j > N_U \text{ , the control horizon}$$

The prediction horizon may be used to produce a smooth evolution of the error, with the purpose of stabilising the system; the smoothing strategy is expressed as follows:

4-6

$$J(N_1, N_y, N_2, N_U) = \sum_{j=N_1}^{N_y-1} \mu(j)\left[y(t+j) - w(t+j)\right]^2 +$$
$$+ \sum_{j=N_y}^{N_2} \frac{\mu(j)}{\gamma}\left[y(t+j) - w(t+j)\right]^2 + \sum_{j=1}^{N_u} \lambda(j)\left[\Delta u(t+j)\right]^2$$

Where the non-negative penalty γ ($\leqslant 1$) is applied from the horizon Ny until the end of the prediction horizon, N_2 (Yoon and Clarke 1995). The purpose of this penalty is to enhance the stabilizing effect of weighting errors of the standard Generalized Predictive Control, similarly to the reference smoothing strategy analyzed in the HPR tracking system section, page 117.

The **expectation** in the equation 4-4 indicates the probabilistic nature of the objective function, based on the prediction of future output values. The **control law** is

the result of the optimization of the objective function. The following expression shows the standard approach to derive the control signal by inversion of the transfer function *G*, which is a limitation to this method system (Camacho and Bordons 1999).

4-7

$$u(t) = (G^T G + \lambda I)^{-1} G^T (w(t) - y(t))$$

The objective function of the equation 4-4 is solved efficiently by quadratic programming. An alternative is to use the **multi-parametric programming (MP)** to solve linear and quadratic programming problems (Baotić 2005; Borrelli, Baotic *et al.* 2005; Bemporad 2006). Multi-parametric programming solves the open-loop **piecewise affine (PW(A) control law** by dividing the state space in a set of polyhedrons; the solution of the objective function consists on evaluating the reachability of the target solution in the space of polyhedrons, delimited by the horizon of interest (Bemporad and Mosca 1998 (a); Bemporad, Heemels *et al.* 2001; Munoz de la Pena, Alamo *et al.* 2004; Baotić 2005; Borrelli, Baotic *et al.* 2005; Munoz de la Pena, Alamo *et al.* 2005; Björnberg and Diehl 2006; Rakovic, Kerrigan *et al.* 2006; Baotic, Borelli *et al.* 2008). The drawback is that the number of polyhedrons increase with the number of constraints (Baotic, Borelli *et al.* 2008).

4.4.9. HPR Objective Function and Constraints

The optimisation problem can be considered as a **constrained optimization,** where the objective function is bounded by the constraints; or as **multi-objective optimization**, where the constraints are considered as additional objective functions in themselves.

The general expression of the optimization problem consists on finding the design vector $x=\{x_1,\ldots,x_n\}$ that minimizes the objective function $x = \arg\min_x f(x)$, subject to equality constraints $I_j(x) = G$ or inequality constraints $g_j(x) \leq G$ (Rao 1996). The **constraints** are also classified in behavioural or functional constraints and geometric or side constraints (Rao 1996).

An example of constrained optimization for solving a law rule of a **reconfigurable system** is presented by (Soloway and Haley 2004 (a); Soloway, Shi *et al.* 2004 (b)); where the constrained hybrid system is represented by a **piece wise affine function (PW(A),** and the constraints are expressed as polygons (Bemporad, Heemels *et al.* 2001; Rakovic, Kerrigan *et al.* 2006).

In the HPR architecture, the speed control is a **multi-objective optimization**, optimising the speed while optimising the energy and time; and it is a case also of **objective prioritization** for cruising and self-recovering states, prioritising the energy consumption. The energy and time optimization are developed in the section 4.4.11.

In the HPR case, the constraint for the operations state is the terminal state value to belong to a **set-membership speed space.** The speed constraint is to guarantee the system stability after a predefined horizon (Clarke, Mohtadi *et al.* 1987 (a); Alamir and Bornard 1994; De Nicolao and Scattolini 1994; Bemporad and Morari 1999 (a); Mayne, Rawlings *et al.* 2000; Torrico and Normey-Rico 2007). Therefore, the **HPR objective function**, J_{Speed}, is expressed as a quadratic programming problem in the following equation:

4-8

$$J_{Speed}(N_1, N_2, N_u) = \underset{Energy,Time}{\arg\min} \sum_{N_1}^{N_2} [(\hat{y} - w)]^2 + \sum_{1}^{N_u} [\Delta u]^2$$

With terminal state constraint for guaranteeing the stability

$$\left\| (y - w) \right\|^x \in \Omega$$

Ω is a Set Membership where the reciprocating strokes (driving and recovery) belong.

Summarizing, constraints can be considered either a boundary conditions of the objective function or as a separate objective function. The first case is a problem of **constrained optimization** and the second a problem of **multi-objective optimization**. Therefore, the HPR control strategy for speed control has both characteristics; it is a **multi-objective optimization,** for optimizing the performance index of the speed control, while optimizing the energy and time; while the performance index of the speed control includes constraints for guaranteeing the stability, which is a problem of constrained optimization.

4.4.10. HPR Objective Function Optimization

From the previous section, the objective function has quadratic-type structure, solved as a constrained optimization problem (Fletcher 1987; Sciomachen 1994; Rao 1996; Mayne, Rawlings *et al.* 2000; Ruzika and Wiecek 2005; Bemporad 2006; Roy, Hinduja *et al.* 2008; Utyuzhnikov, Fantini *et al.* 2009). The explicit control law is expressed in a quadratic form as follows (Bemporad 2006):

4-9

$$U^*(x(t)) = \arg\_\min_U x'_N P x_N + \sum_{k=0}^{N-1} [x'_k Q x_k + u'_k R u_k]$$

Where x(·) is the state space vector

$x_{k+1} = Ax_k + Bu_k$

$k = 0,...N-1, N$, N is the prediction horizon

Input/Output Constraints :

$u_{\min} \le u_k \le u_{\max}$

$y_{\min} \le Cx_k \le y_{\max}$

$\le$ is a component – wise inequality

4-10

Applying the horizons :

$x_k = A^k x(t) + \sum_{i=0}^{k-1} A^i B u_{k-1-i}$

The equation is the state observer as a function of the present state and future control actions for the defined receding horizon (Rao, Wright *et al.* 1998; Mayne, Rawlings *et al.* 2000; Rao, Rawlings *et al.* 2001; Alamo, de la Pena *et al.* 2005; Alamo, Ramirez *et al.* 2007).

The **multi-objective optimization** problem consists on finding the solution vectors $X\{x_1,..,x_n\}$, which minimizes simultaneously the set of functions that constitute the multi-objective problem $f_1(X)$, .., $f_n(X)$, subject to a gradient constraint $g_j(X) \le 0$ *for* $j=1,2,..m$. (Rao 1996). The multi-objective optimization, or vector minimization problem, is characterized by the absence of unique solution x_i that simultaneously satisfies all the objective functions f_i. The solution is instead a **Pareto-type optimal solution**, or vector of solutions, defined as follows:

Definition 1 ***A feasible solution X, which is a solution that satisfies the constraints, is a Pareto optimal solution if it minimizes one of the objective functions without increasing at least one of the other objective functions*** *(Rao 1996).*

Additional methods for solving the multi-objective optimisation problem are in the field of **global optimization solution**. Global optimal values are reached by applying evolutionary algorithm or methods of closest neighbour search (Rao 1984; Rao 1996; Rangan and Poolla 1997; Bhaskar, Gupta *et al.* 2001; Biegler and Grossmann 2004; Floudas, Akrotirianakis *et al.* 2005; Ng and Leng 2007; Tarafder, Rangaiah *et al.* 2007). The objective function for energy and time optimisation are analysed by applying dynamic programming and they are presented in the next section.

4.4.11. HPR Dynamic Programming model J_{Energy} and J_{Time}

In relation to the HPR energy management system, it is rather difficult to know in advance the availability and consumption of energy for the whole journey. It is far more difficult to know the energy balance at different time steps. The only certain value is the stored energy at the starting point and the expectation of the consumption and generation of energy for the trip.

In addition to the turbine efficiency, the total value of energy is severely affected by the efficiency of the vehicle, which is a mirror of the pipeline environmental conditions. Therefore, friction, drag losses and trip delays produce a deviation of the actual energy balance from the expected one.

Rationale for Dynamic programming approach

The Hybrid Pipeline Robot controllability is a problem of optimization through the time. It is required to optimize the robot speed while optimising the energy consumption and the duration of the journey. Optimization over time is therefore a problem of dynamic programming, where the whole trajectory of the HPR is divided into successive stages and the transition from one stage to the next one is produced by actions penalized by incurred costs. Therefore, the optimization takes place in the policy space of control actions, with the aim of the overall cost optimization (Bertsekas 2005 (b)).

It is therefore necessary to define the HPR as a dynamic programming problem. So, it is necessary to define the **stages** for the robot journey, the **policies and actions** that produce the change from one stage to the next one and the **cost** associated with each transition. This model is the base for the mathematical formulation of the optimization problem and is developed in the next section.

States and stages

The dynamic programming model for the HPR consists of the total journey of the robot from the launching point until the target place, where the operations are carried out; and the journey finalizes with the self-recovering state that leads the robot back to the starting point. Therefore, the total journey may be divided into the three main states of the HPR: **cruising, operations and self-recovering states**.

Note that in this research project the definition of states differs from the one of stages. **State** is defined by the desired conditions of a controlled system; and it is one of

the defined in the HPR architecture for the on-schedule conditions, cruising, operations and self-recovering states; and the off-schedule conditions, cycling and idle. Whereas **stage** is a sub class of the state defined by the subdivision of the trajectory in time units, with the purpose of categorizing the dynamic programming problem in costing units. Therefore any *stage* is defined by itself and the parent *state*. The dynamic programming model is described in **Figure** 4.1-8.

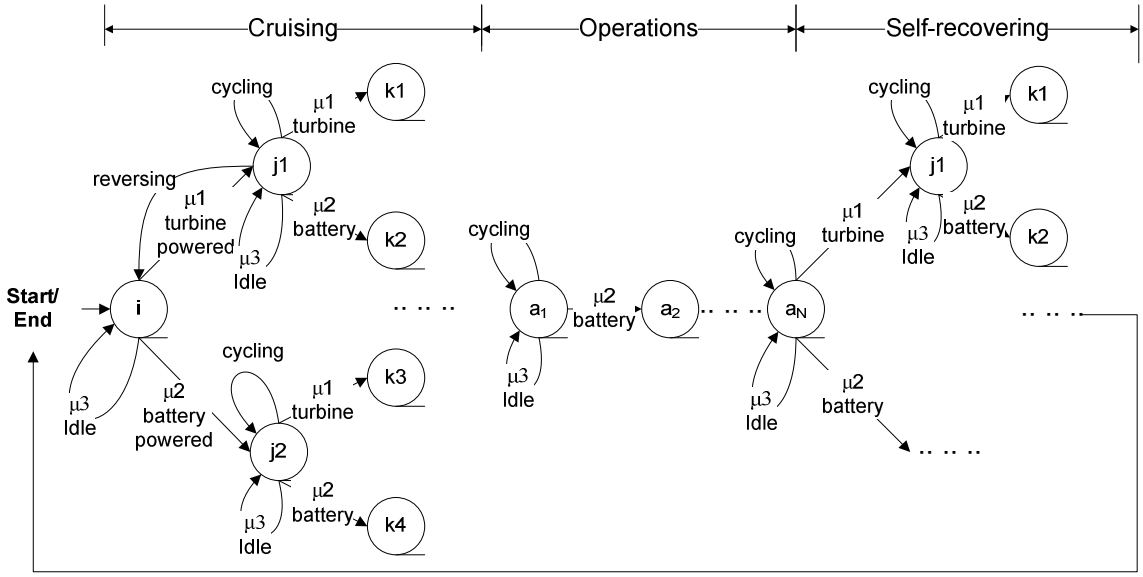

Figure 4.1-8 **HPR Dynamic Programming Model**

Stage transition for the three on-schedule states, operations, cruising and self-recovering; the transition between stages depend on the source of power, turbine or battery powered. Note that off-schedule states, idle and cycling can occur at any time within the stages and the states.

In **Figure** 4.1-8 the circles indicate stages belonging to the general class of one of the three states of cruising, operations and self-recovering. The arrows are actions that drive the HPR from one stage to the next one. The ellipses indicate the continuation of the sequence of stage-actions with unknown-finite number of steps. This unlimited yet bounded number of stages is a distinctive characteristic of the HPR that calls for a dynamic programming approach.

The long arrow connecting the self-recovering state with the start/end condition indicates that starting and ending points are the same physical point. This is because the pipeline robot is a **bidirectional** device; unlike standard PIGs, with journeys located far apart between launching and receiving point, up and down stream respectively.

The **stages** of the total HPR journey are defined as equally separated units in time so as to match the coherent sample time used for system identification and control. The **time division** approach is rather different from the classical distance division used in

many journey optimization problems. The reason for choosing the time division is because time is one of the variables to optimize; additionally, the time measurement is more consistent compared to the distance measurement, due to the reciprocating vehicle behaviour and the randomness in magnitude and direction of the robot displacements. The transition from one stage to another result in as many stages as policies applied; as a result, the distance travelled in the same unit time depends on the selected policy of turbine or battery powered or idle or cycling conditions.

The stage transition depends on the scheduled activity and the value of the variables, mainly the generated and stored energy. These variables are affected by disturbances; thus, it is rather difficult to know with precision the transition values. A solution is offered by Mini-max control for controllability of variables defined in a critical range (Bertsekas and Rhodes 1971 (d)). Therefore, the min-max control is a useful approach for defining the energy levels for the Hybrid Pipeline Robot, which may be confined to a range of feasible values instead of an actual valued function.

Policies, actions and transition cost

The Hybrid Pipeline Robot control is described as driven by three **policies** or control actions **turbine powered, battery powered** and **idle**. Policies are characterized by the Greek letter μ_i in **Figure** 4.1-8.

The actions **cycling** and **undesirable reversing** are not considered as policies in themselves because they are the result of external causes out of control; for example when the robot is driving against pipeline obstructions, it starts to cycling or prematurely reversing, depending on the severity of the obstruction. Recalling that the HPR cycling is a sequence of backward and forward movements with no actual displacement; and reversing is when the bristles change the alignment to proceed with the backward displacement. So, cycling and undesirable reversing are states under no defined control law, in the scope of this project, and produce losses of energy, time and vehicle performance.

In a dynamic programming problem, a policy is composed of a set of controlled actions. A policy may be stationary or time variant. In the particular case of the HPR, the three policies are applied at random time; so, they are considered time variant policies.

The transition cost is associated with the reward and punishment approach and, in this case, the assigned scores are weighting factors with no particular relation to

physical units. The **scoring system** is described in the following paragraphs. As an example of the scores' assignation, Figure 4.1-9, shows the costs for the cruising state. Full details of the scores for other states are in the Appendix A.

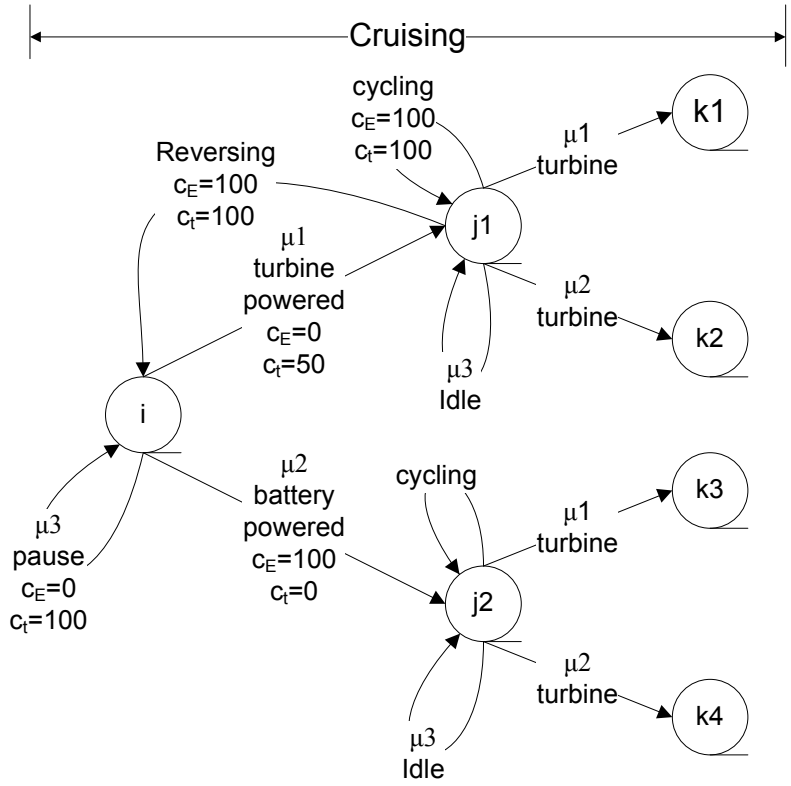

Figure 4.1-9 HPR Dynamic Programming costs model for cruising state

The energy optimization costing penalizes heavily the usage of the stored energy C_E = 100 compared with the turbine powered policy of C_E=0; however, this policy is more expensive in terms of time optimization (C_T=50).

As a multi-objective optimization, the HPR scoring system is composed of two ranges of scores or costs: energy scores and time scores. The **energy cost, c_E**, has a straightforward meaning: only the energy usage is penalized. For instance, *turbine powered* has **zero** energy cost because it is freely available, compared with *motor powered*, which is scored at **100**, because the charge/discharge cycle of the battery produces losses. *Pause* is an action of **zero** energy cost provided the battery is switched off. *Cycling* and *undesirable reversing* are scored at **100,** because they cause a waste of energy as it was mentioned before.

The **time cost, c_t**, though not so evident, is also a simple concept: if the states are uncontrolled they are penalized with 100 scores. For example the *motor powered* state is controlled through the speed control, thus scored at **0**. The exceptions for uncontrolled states are the *turbine powered* and *pause*, as long as it is a **controlled**

pause for recharging batteries; in that case the states are scored at **50**. Any other uncontrolled states, such as *stalling* and *reversing* are scored at **100**.

Summarizing, the scoring system constitutes the cost incurred in selecting a determined policy in the dynamic programming approach, which optimizes the energy and time performance at every state of the Hybrid Pipeline Robot.

Considerations about bias in the HPR Dynamic Programming model

The dynamic programming problem, in its basic conception, consists on optimizing the total cost incurred by taken step-wise decisions in a discrete observable dynamic problem (Bertsekas 2005 (a)). This concept is expressed in the equation 4-11,

4-11

$$J_k^{\pi}(x_k) = [\ \sum_{i=k}^{N} g(x_i, \mu_i(x_i), w_i) \mid x_0 = x_k\ ]$$

$J_k^{\pi}(x_k)$ is the cost-to-go at k-stage, optimized in the policy space, which is the result of the sum of all cost-per-stage *g(.),* incurred since the start of the sequence. The policy space is defined as the set of decisions or control actions $\pi\{\mu_1,\ldots\mu_k\}$. The stochastic disturbance w_k gives the characteristic of probabilistic to the objective function. The cost to go is observed from the initial stage x_0 until the final stage *N*.

The minimization of the future cost, over a set of policies π, is the optimal cost-to-go *J** at the stage *i,* and it is defined as $J^*(i) = \min_{\pi} J^{\pi}(i)$. In the final stage of the dynamic programming problem the cost-per-stage is the same as the cost-to-go at this stage $J_N(x_N) = g_N(x_N)$.

Bellman's Principle of optimality

The large number of stages and the combinatorial nature of cost-per-stage and policies produce a problem of difficult solution expressed as the curse of dimensionality of Bellman (Bellman and Dreyfus 1962; Bellman and Kalaba 1965). The solution is based on the idea of "*divide and conquer*", postulated in Bellman's principle of optimality, which states that it is always possible to reduce the dimension of the problem in order to find a policy that optimizes the sub problem (Haykin 1994).

The optimization is based upon the expected value of the objective function because of the stochastic nature of the problem. This concept has relation with the

certainty equivalence principle that states the stochastic term may be replaced by its mean value (Bertsekas 2005 (b)).

Therefore, in order to optimize the sub problem, the algorithm proceeds backwards starting with the final cost and then summing up the different stages until reach the present stage (Bertsekas 2005 (a)). The mathematical formulation of the backwards dynamic programming problem is:

4-12

$$J(x_i) = E\left\{ g_N(x_N) + \sum_{k=i}^{N-1} g_k(x_k, \mu_k(x_k), w_k) \right\}$$

Where the cost-to-go $J(.)$ is a function of $g_N(.)$, the final cost and the sum of the successive cost-per-stage g_n.

As a conclusion, modelling the dynamic programming environment means to know the number of stages of the problem, the set of feasible policies, the transition probabilities of the stochastic problem and the present cost and cost-per-stage at every stage.

Although the dynamic programming model for the HPR, presented at the beginning of this section, gives a close representation of the real HPR system, the real problem is far more complex, and the HPR model structure deviates from the Bellman's dynamic programming approach, because the locomotion irregularities, the finite but large number of stages and the unknown transition probabilities. Considerations about these differences and alternative solutions are analyzed separately in the following paragraphs.

Consideration 1: uncertainties in the policy space of the HPR dynamic programming model

The challenge of the HPR dynamic programming model is due to the non-stationary policies, the point at which the policies change and the random off-schedule cycles that break any sequence of the policy space. These random characteristics leave room for bias in the model presented before. Therefore, the uncertainties in the policy space of the HPR dynamic programming model is a bias to the standard dynamic programming approach, requiring the adaptation of the system to the uncertainties. This adaptation is performed by applying the heuristic learning approach, explained in the following section.

Heuristic learning and Reinforcement learning

Learning from experience, or heuristic learning, has two major classifications: learning with a teacher and learning without a teacher (Haykin 1994). Learning with a teacher means to count on with pairs of input output samples of the real system, not always available. An alternative is to "learn without a teacher", approach composed of two methods: self-organized structures and reinforcement learning. Particularly the second one, reinforcement learning plays a principal role in dynamic programming due to the adaptive learning characteristics.

Reinforcement learning is associated with the concept of *adaptive critic*: the critic acts as a coordinator of the activities of a dynamic programming problem based on results of the learning structure (Widrow, Gupta *et al.* 1973). The adaptive critic structure learns from the environment, heuristic learning, and adjusts the cost to go through the back-propagation of the sensibility of the objective function with respect to the control actions, $\frac{\partial J(x)}{\partial u(x)}$.

This characteristics of learning and adapting are the base of Action Dependent Heuristic Dynamic Programming (ADHDP), a class of algorithms that do not require a particular model (Lendaris and Neidhoefe 2004). Therefore, in the sense of a dynamic programming learning system, the terms Approximate Dynamic Programming (ADP), Neuro-Dynamic Programming (NDP) and Adaptive Critic (dynamic programming combined with reinforcement learning) are equivalent (Bertsekas and Tsitsiklis 1996 (a); Barto and Dietterich 2004; Lendaris and Neidhoefe 2004).

One of the outstanding meth(Lendaris and Neidhoefe 2004)ods of Action Dependent Heuristic Dynamic Programming (ADHDP) is Q-learning, which computes the optimal cost rather than performing an approximation of the cost (Watkins 1989; Lendaris and Neidhoefe 2004).

Q-learning approximates the optimal cost in the Bellman's equation, independently from the number of policies. This approach is different from other methods that approximate the transition probabilities and cost for one policy at the time. The optimal policy is associated to the respective Q-factor; therefore, if the policy is optimal, it is not required to evaluate multiple policies such is the case of policy evaluation algorithm. To conclude, Q-learning as it does not require a model, is suitable for systems that are rather difficult to model with several policies governing it.

Q-learning algorithm is based on the iteration of the Q-factors associated with each state-action pair. Q-factors are defined as the sum of the immediate cost, *c(i,(a),* plus the addition of the cost-to-go of all successive stages for a given policy. In that sense the Q-factors depend not only from the state but also from the selected policy, containing more information than the objective function, which depends only from the state. Q-factors are defined as follows:

4-13

$$Q^{\mu}(i,a) = c(i,a) + \sum_{j=1}^{n} p_{ij}(a) J^{\mu}(j)$$

The Q-factor satisfy the right hand side of Bellman's equation and it is expressed in the "Q-factor version" of the Bellman's equation (Bertsekas 2005 (a)) as follows,

4-14

$$Q^{*}(i,u) = \sum_{j=1}^{n} p_{ij}(u)[g(i,u,j) + \alpha \min_{u' \in U(j)} Q^{*}(j,u')]$$

Although Q-factors are similar to the cost-to-go expression, the order of expectation and minimization is reversed. The following equation is the cost-to-go expression where the minimization is over the expectation.

4-15

$$J^{*}(i) = \min_{u \in U(i)} \sum_{j=1}^{n} p_{ij}(u)[g(i,u,j) + \alpha J^{*}(j)]$$

Q-factors may be obtained by policy iteration and value iteration algorithms. However, the policy iteration has the drawback that the iteration is for a single policy, which is an impediment for evaluating several policies at once. The expression for Q-factors obtained by value iteration is expressed in equation 4-16. It is important to note that the minimization is over a set of policies, which solves the problem of multiple policies system.

4-16

$$Q(i,u) = \sum_{j=1}^{n} p_{ij}(u)[g(i,u,j) + \alpha \min_{u \in U(j)} Q(j,u)]$$

The damped version for Q-factors produces a smooth transition from one stage to the next one and therefore improves the algorithm convergence. The expression 4-17 shows the damped version of the Q-factors:

4-17

$$Q_{n+1}(i,u) := (1-\eta_n)Q_n(i,u) + \eta_n\left[g(i,u,j) + \alpha \min_{u' \in U(j)} Q_n(j,u') \right]$$

where

$$\eta = f(i,u)$$

Finally the iteration of Q-factors form the Q-learning algorithm is described in the following equation:

4-18

$$Q_{n+1}(i,u) = Q_n(i,u) + \Delta Q_n(i,u)$$

In the particular case of using ANN for function minimization, the error in the second term, $\Delta Qn(i,u)$, is minimized by finding the Q-factor target as a model to follow by the neural network.

4-19

$$\Delta Q_n(i,u) = \eta_n(Q_n^{target}(i,u) - Q_n(i,u))$$

One alternative method for approximate the cost-to-go is based on Monte Carlo simulation. The method starts with a stationary policy and generates a large set of pairs of state-cost-to-go that are used for a neural network adaptation. The optimized set of state-cost are used to calculate the respective Q-factor, which in turn serves to evaluate a new optimized policy of the policy improvement algorithm. The iteration repeats until no further improvement is obtained. The drawback of Monte Carlo simulation is the errors incurred in the process of the algorithm's iteration, and it is used for evaluating only one policy at the time. The simulation also needs the initial transition probability for the best initial policy for seeding the simulator (Bertsekas 2005 (b)).

As a conclusion, the HPR control strategy for energy and time optimization borrows from Q-learning approach the model-free characteristic, in the sense that the transition probabilities between stages are unknown. Therefore, the proposed solution for the optimization over time of the system energy and mission time is based on the Q-learning approach, combined with the transition cost model for the HPR, given in Figure 4.1-9, for the particular case of cruising state.

Consideration 2: large unknown number of stages for the HPR dynamic programming model

The second consideration has relation with the number of stages or the dimensionality of the dynamic programming problem. In relation to the HPR journey, it is not possible

to determine in how many steps the vehicle completes the total journey including the assigned task. Even more, the random states, cycling and idle, render the number of stages to variable. However, there exists a terminal state at the end of the journey, with a constraint of bounded for below level of energy, for completion of the self-recovering state. Summarizing, the number of stages is finite large and unknown in advance due to non stationary policies, creating a cumbersome dynamic programming approach (Bellman and Kalaba 1965).

The solution for a large unknown horizon problem consists on approximating the problem to a finite yet large number of stages and including a discount factor α. This approach is denominated discounted problem and it is a class of stochastic shortest path. Both classes of problems share the concept of bounded cost. However, the discounted approach adds a discount factor, which acts as forgetting factors for irrelevant past values of the cost, with the purpose of reinforcing recent costs, which are more influential in the present and future costing function. The Q-factors expression for the discounted problem is (Haykin 1994):

4-20

$$Q^*(i,u) = \sum_{j=1}^{n} p_{ij}(u)[g(i,u,j) + \alpha J^*(j)]$$

The selection of the discount factor has a fundamental influence in the training algorithm and its convergence (Lendaris and Neidhoefe 2004).Small values at the beginning are designed for guaranteeing the stability of the algorithm. Besides that, the discount factor bears relation with the **HPR energy costing system** and the source of energy utilized: every time a battery powered cycle starts from a fully-charged condition, the discount factor starts anew. However, this is not the case for the **HPR time costing system**, which requires a long term "memory", so as to account for totalizing time.

Consideration 3: unknown transition probabilities of the stochastic HPR problem

The transition probability characterizes the evolution from one stage to another stage upon the application of a determined policy. Therefore the transition probabilities depend on how many policies may be selected and how many stages are feasible to be visited. As a consequence, the determination of transition probabilities is rather cumbersome.

So, the solution for observable systems is to replace the expectation of the transition probabilities by a single sample, so as to seed the Q-learning iterative algorithm, making the transition probabilities unnecessary (Bertsekas 2005 (a); Bertsekas 2005 (b)). The following expression shows the Q-factors as a function of the error step between two samples of Q-factors for different policies a_n and b.

4-21

$$Q_{n+1}(i,a) := (1-\eta_n)Q_n(i_n,a_n) + \eta_n\left[g(i_n,a_n,j_n) + \alpha \min Q_n(j_n,b) - Q_n(i_n,a_n)\right]$$

wehre

$$\eta_n = f(i_n,a_n)$$

therefore

$$J_{Energy} = f(Q_{n+1}(i,a))$$

As a conclusion, and from the expression 4-21, the HPR energy optimisation is solved by applying Q-factors iteratively. As Q-factors are based on the optimal policy, they adapts to the actual system by heuristic approximation. The finite large number of stages of the HPR problem is solved by including the discounted factor in the iteration of the Q-factors; and the unknown transition probabilities are replaced by seeding the recursive algorithm with a sample of the actual system.

4.4.12. System Performance Evaluation

The performance of the HPR system is evaluated based on three concepts: stability, robustness and feasibility, which are explored briefly in the next sections.

System Stability and Constraints

The HPR system is time variant based on a-periodic reciprocating cycles of the cam shaft. So, how to analyze the stability of a system with such characteristics? Lyapunov analysis is the classical approach for analyzing the stability of dynamic systems; however, it is rather difficult to find a suitable Lyapunov candidate function. So, the next paragraphs explore some leading research studies about the stability analysis, for supporting the HPR stability approach.

The literature refers to two main classification of stability; the first approach is the stability in the Lyapunov sense, where a Lyapunov candidate function is minimized (Narendra 1989; Åström and Wittenmark 1990; Bemporad 1998 (b); Mayne, Rawlings *et al.* 2000). The difficulty in finding the Lyapunov's candidate functions is overcome

by the Hamilton-Jacobi-Bellman solution, in the field of optimal control of nonlinear systems. This approach is supported by the sufficient condition for optimality and the principle of optimality of Bellman, which allows to diminish the size of the problem in order to find a feasible solution (Bellman 1965). The proof and analysis of the stabilizing characteristic of the Constrained Receding Horizon Predictive Control combined with Dynamic Programming approach are given in (Chisci and Mosca 1994; De Nicolao and Bitmead 1997).

The second stability approach is the asymptotic stability explicitly expressed as a state contraction. The following is a list of state constraints (a class of constraints), in order to guaranteeing the system stability (Bemporad and Morari 1999 (a)). The classification is in accordance to the type of mathematical solution, quadratic programming (QP) or linear programming (LP):

1. End or terminal constraint (QP: L_2-norm) $x(t+N_p \mid t)=0$
2. Invariant Terminal Set (QP: L_2-norm) or Terminal constraint belonging to a set-membership constraint $x(t+N_p \mid t) \in \Omega$
3. Prediction Horizon. Stable System at the infinity (QP: L_2-norm) $N_p \to \infty$
4. Contraction constraint of the end state in some norm or convex constraint. If the norm is L_2-norm then the problem is solved by quadratic programming (QP) If the norm is L_1 or L_∞ then the problem is solved by linear programming (LP) $\|x(t+1)\| \le \alpha \|x(t)\|$
5. Terminal weighting Matrix constraint. P_0 is a solution of the Riccati inequality (no equality because it is a constraint in the infinity!!)

In periodic systems, the stability can be guaranteed by a periodic receding horizon strategy, where the control law is recalculated at defined periodic steps; unlike the standard receding horizon where the control law is recalculated at every sample step. This approach helps to smooth the control action improving the system stability in particular for plants with high frequency dynamics requiring high sample rate (De Nicolao and Scattolini 1994; Primbs, Nevisti *et al.* 1999). Equivalent result is given by the stability of a piecewise system, linearized at points of a seed trajectory combined with terminal inequality constraints (Lee, Kouvaritakis *et al.* 2002).

The stability of a closed-loop system by including the state observer in the feedback loop and fulfilling a Lyapunov candidate function is given in (Rao, Rawlings

et al. 2001). Examples of terminal equality constraint for assuring the stability after the reconfiguration of the control system, in case of actuator saturation, is presented by Soloway (Soloway, Shi *et al.* 2004 (b)). Although the importance of the stability, it can be relaxed in practical system with the purpose of achieving a feasible control law

The comparison of stability for receding and infinite horizon control algorithms are presented in (De Nicolao and Bitmead 1997). The study remarks the application of the truncated or Fake Riccati Equation for analysis of stability in two different modes: monotonic and cyclic-monotonic.

The stability of a multi-objective control space is presented in (Koutsoukos and Antsaklis 2001). The strategy consists on dividing the control space in multi-objective independent controllers. The optimization is performed over the set of conic partitions of the control space. The stability is guaranteed provided each conic division is stable in a piecewise Lyapunov sense (Koutsoukos and Antsaklis 2001).

HPR Stability approach

In the case of the HPR stability, and for the on-schedule state operations, the vehicle speed is enforced to belong to a certain region of invariant terminal constraint, instead of a single valued function. This is due to the reciprocating behaviour of the vehicle. The HPR stability analysis is presented in Figure 4.1-21, under variations of the forgetting factor to improve the stability of the robot, concluding that “forgetting” past values of the output error improves the stability of the system. The other states, cruising and self-recovering have a relaxed stability imposed by a soft constraint of maintaining the speed bigger than zero. The off-schedule states of cycling and idle are transient states and uncontrolled in themselves; therefore, the stability analysis is not applicable. These transient states are only constrained by a time-out algorithm.

Robustness, Uncertainty and Feasibility

Robustness is defined as the low sensibility of the system to the change in the parameters. Examples of robustness are: robust to model uncertainties, robust to noise or disturbances, robust to specific uncertainty range of the variable, robust to specific stability, robust to performance criteria and robust to constraint fulfilment, just for citing the most relevant approaches (Bemporad and Morari 1999 (a)).

Particularly, the uncertainties can be classified as uncertainties of the model's parameters, and uncertainties of the measured inputs. A combination of these uncertainties may be visualized as a convex hull or Polytopic uncertainty.

Another way of robust analysis is the **robustness of closed and open loop**. The closed-loop system is inherently robust; however, in an open-loop system the robustness is guaranteed by including the uncertainties in system model (Bemporad and Morari 1999 (a); Mayne, Rawlings *et al.* 2000). A model for robustness is proposed by Bemporad and Morari, which includes modelled disturbances in the input and output, similar to the proposed model of Ljung for system identification and expressed in equation 4-22 (Ljung 1987; Bemporad and Morari 1999 (a)).

4-22

$$\Sigma\begin{cases} x(t+1) = Ax(t) + Bu(t) + Hw(t) \\ y(t) = Cx(t) + Kv(t) \end{cases}$$

Where the vector w(t) is the disturbance in the states, and v(t) is the uncertainty in the measured output. A model for robustness **to errors of dead time** analyzed in a closed-loop with a Smith predictor is presented in (Camacho 2002; Torrico and Normey-Rico 2007),(Yoon and Clarke 1995). The model is robust to variations of dead time of the system, when it is under norm-bounded uncertainties.

Bemporad and Morari pose useful questions to be considered in the design of a robust controlled system (Bemporad and Morari 1999 (a)):

- Optimize Nominal Model Performance or Robust Model Performance? (Primbs and Nevistic 2000)
- Enforce states constraints or enforce the constraints robustly?
- Is the robustness assured by the open or closed-loop prediction?
- How to guarantee robust stability?

The robust performance is based on the concept of feasibility of the control sequences; a system is unfeasible in terms of the control actions when it is not controllable by these actions. There are two main approaches of feasibility, feasibility of a sequence of control actions and feasibility in relation to constraints (Bemporad and Morari 1999 (a)). Considering the sequence of control actions as $\{u(t+1|t),...,u(t+k|t),u(t+N_m|t),0\}$, the action at (t+1) is required to be feasible in order to consider the feasibility of the controller.

Feasibility in relation to constraints is defined as $F_1 u(t) \leq G_1$, where G is the constraint and F is a suitable transformation to accomplishing this constraint, the inequality, $\leq$ indicates hard contraint. The transformation of the hard constraint into soft constraint results in $E_2 x(t) + F_2 u(t) \leq G_2 + \varepsilon$. The constraint relaxation or soft constraint is achieved by adding the slack variable ε to ensure the feasibility of the control sequence. The approach of soft constraints on the states is a reasonable because the states may be affected by unmeasured disturbances and numerical errors. Conversely, hard constraints are preferred as bounds of the manipulated variable, because they are bounding the mathematical expression of the objective function optimization.

HPR Robustness approach

In the particular case of the **HPR**, a desirable condition is the robustness of the energy optimisation for robot operation, cruising, and self-recovering action, and robustness of the self-recovering action, in case of severe environment constraints avoiding the lost of the vehicle.

The control design is also robust to transient conditions such as idle and cycling. This kind of robustness is included in the model as conditional states, modelled by the robot speed behaviour and processed by an inference algorithm.

Robustness of the vehicle to pipeline environmental conditions, such as drag and friction, is modelled by the robot speed and included in the strategy of reconfigurable control; if the environment conditions are severe the self-recovering action is deployed.

Robustness to uncertainty in the variables is assured by the measurement system developed in Chapter 5, by means of the calibration curves of the probes and the estimation and prediction intervals. Robustness to disturbances in the variables, such as water hammer in measuring the flow rate, are identified and included in the control model.

To conclude, the HPR stability, robustness and feasibility are modelled as terminal state constraints in the measured variables, to ensure a feasible control design. Table 4-1 summarises the HPR control strategy for the on and off-scheduled states.

Table 4-1 Summary of the HPR control approach

	On-schedule		Off-schedule
	Operations	Cruising / Self-recovering	Cycling / Idle
Source of Energy	Battery	Battery/Generated	Generated
Performance Index	J_{Speed} J_{Energy} J_{Time}	J_{Energy} J_{Time}	Not applicable
Constraints	Speed belongs to a terminal invariant set-membership	Speed > 0	Timeout specified by Inference Algorithm
Stability	Asymptotic stability	Relaxed Stability by relaxed constraint, Speed > 0.	Not applicable
Robustness	Robustness of the Energy Optimization Robustness of the self-recovering action	Robustness of the Energy Optimization Robustness of the self-recovering action	Robustness of the self-recovering action
Algorithmic Theory	Multi-objective Optimization Model Predictive Control Neuro-dynamic Programming Discounted Problem, Q-learning	Constrained Optimization Objective Prioritization Neuro-dynamic Programming Discounted Problem, Q-learning,	Inference Algorithm

4.5. HPR Controller: Trial Models

The first section of the trial models relates with the raw data analysis and data conditioning. The leading idea in the raw data analysis is to gain insight about the HPR behaviour through the collected data. The insight about the system has a twofold purpose: firstly, to know what kind of data conditioning is required and to verify the coherence of the conditioning results and secondly, to corroborate the meaning of the results of the controller simulation. So, the next section relates with the HPR data analysis and data conditioning as a preliminary for the controller model simulation, in the last section.

4.5.1. HPR Data Analysis and Conditioning

The data for the trial models for the HPR are measurements from rig tests for the self-powered pipeline vehicle carried out by an undergraduate group (Durham University 2008). The raw data is listed in the Appendix A.

The tests relate to the arrangement of the self-powered vehicle with two different size of turbine: 6 inch and 10 inch of diameter. From now, the tests are mentioned as to 6 inch and 10 inch but assuming they refer to the turbine-crawler vehicle assembly. The experiments relate to the characterization of the HPR through the robot speed as a function of the flow rate. They are divided into two regimes: upstream and downstream. Although these data is a good base for developing trial models, it is

required to do more exploratory experiments so as to get information about the energy conversion from the turbine and energy dissipation by the vehicle, which characterizes the random character of the pipeline environmental constraints.

Remark about the denomination of self-powered machine and Hybrid Pipeline Robot (HPR): these terms are equivalent from the mechanical point of view; however, the HPR term is the one used in this research project to design a class of controlled self-powered machine, which is in its base conception a non-controlled unit.

Remark about the turbine efficiency: data from turbine efficiency is included in the graph for the self-drive machine in order to compare the generation and dissipation of energy in the HPR system. However, the data for the turbine belongs to a different experiment (Pulker 2005) based upon a different turbine design, size and flow density. This experiment was intended to prove the performance of the twisted blade turbine under air flow. In this particular case the mentioned turbine test does not apply to the 6 and 10 inch turbine of the self-drive machine test.

By dimensional analysis theory, the result of the twisted blade turbine is valid for all turbines of the same design characteristics. Recalling that dimensional analysis theory proves the applicability of experiments results to a wide range of parameters variations, provided the experiments are expressed as a function of dimensionless coefficients (Taylor 1974; Massey 2006; White 2008). The importance of the dimensional analysis is that a single curve for the results represents any variation of the parameters, which constitute the dimensionless coefficients; so, no further tests are required whenever new variations of the parameters need to be explored.

The only condition is to apply a scale factor to get the right dimensions of the desired variable. For example, the mentioned turbine test was performed for air flow, if it would required to know the turbine characteristics for water flow it would be required to multiply the coefficient by 1000, which is the relation of density of water to air. So, it is no need of particular test for any changes of the density or any variables included in the dimensionless coefficients. The same principle applies to turbine diameter, flow rate and pressure drop, because all of them constitute the dimensionless coefficients. However, the theory does not apply to cases of design change such as the case for the 6 inch and 10 inch turbine, due to changes in the blade design.

That is the reason for pointing out that the turbine efficiency curves of the data analysis Figure 4.1-10 and Figure 4.1-11, although from real test, bears no relation with the self-drive machine tests. The purpose of including such a curve is to give the idea of

what would be like if the measurements of the turbine of the self-drive machine were performed together with the vehicle characteristic. In the

Figure 4.1-10 and Figure 4.1-11, with the purpose of matching the different experiments for the vehicle and turbine, the flow rate of the vehicle data has been scaled.

Furthermore the tests of the twisted blade turbine were only for the turbine without the vehicle; so, the interesting characteristics of the vehicle and its relation with the environment are missed.

The **raw data** for the self-drive machine characterization is presented in the

Figure 4.1-10 and Figure 4.1-11. They refer to vehicle speed as a function of the flow rate for the 10 inch and 6 inch turbine size respectively. Each of the mentioned figures contains the two regimes up and downstream. A curve of the turbine efficiency is superposed to the HPR data in a secondary axis for comparison energy generation and dissipation. The figures show the nonlinear nature of the turbine-vehicle-environment system and the two main robot behaviours, which are crawling and driven by the flow.

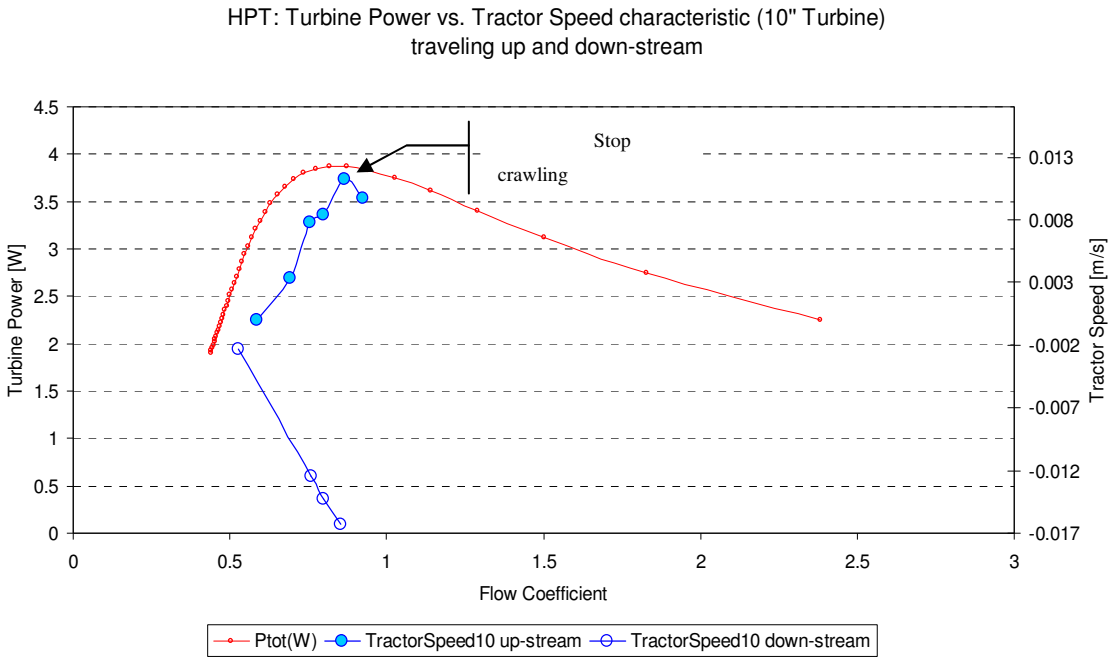

Figure 4.1-10 HPR 10'' Turbine: Tractor Speed vs. Flow Rate

The upstream robot speed (solid blue circles) reaches a maximum point of energy, where stops crawling and starts the excursion with the flow. Note that this point reaches higher values of energy due to the high power of the 10'' turbine.

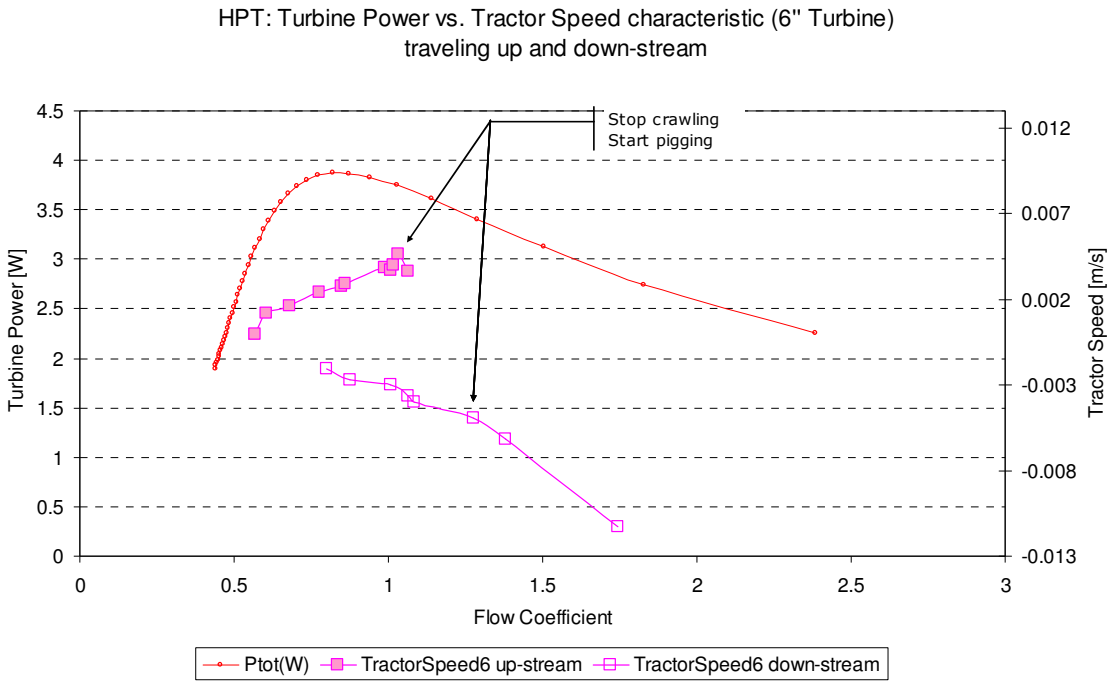

Figure 4.1-11 HPR 6" Turbine: Tractor Speed vs. Flow Rate

The upstream robot's speed (solid pink squares) reaches lower values of speed at the breaking point, where the robot stops crawling and starts the excursion with the flow.

Crawling is the desired behaviour of the HPR because the driving forces of the bristles units are in full control of the displacement of the vehicle. **Driven by the current** behaviour is the undesirable characteristics because in this situation the vehicle flows with the flow rate and the reciprocating movement of the bristles has little or no effect in the HPR displacement. It is called pigging because the HPR behaves like any standard utility pipeline inspection gauge or pig with no driving capability. There are several reasons that make a vehicle to stop crawling and start pigging.

At the core of the problem are the bristles units losing grip of the pipe wall. This may be because the high flow rate renders useless the crawling effect of the bristles. Other reasons are a mismatch of the bristle surface and the pipe diameter: an excessive wear of the wire bristles or lose of the elasticity of the wires result in a permanently deformed bristle shape. They become over adapted to the pipe wall and they yield to the pipe wall instead of gripping to it, therefore losing the contact with the pipe. Another reason for pigging may be due to mechanicals problems at shaft level that compromise the reciprocating movement. These are only few reasons for pigging instead of crawling.

In the mentioned figures, the slope corresponding to the upstream crawling phase brakes at a point indicating the onset of the pigging condition, with steep slop heading a

different direction. This point of high flow rate probably produces high turbine efficiency. Although this high efficiency value, it doesn't help to avoid the HPR from pigging. The neighbourhood of this point is critical because it has a double effect. On one side, the high turbine efficiency means high rate of the reciprocating movement therefore high vehicle's speed. On the other side, the unfavourable effect is that the high flow rate helps the HPR to start pigging. The importance of this point is in terms of energy management: in order to prevent the HPR from pigging and to keep the speed in a steady rate, it is required to add extra power from batteries.

It would be interesting to do tests around this critical point so as to determine the appropriate combination of energy sources and the mechanical reasons for the pig to lose grip around this region. From the figure, the pigging slope is the same as the downstream that corroborates the pigging behaviour where the vehicle flows at the speed of the main stream.

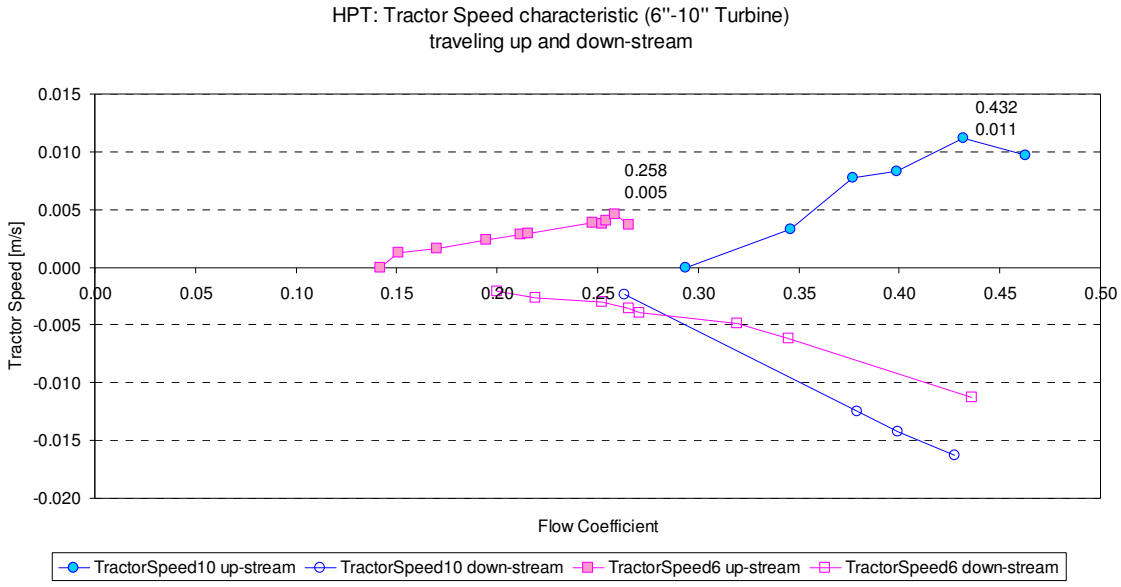

Figure 4.1-12 HPR 6" and 10" Turbine comparison

The robot with smallest turbine ϕ=6'' (pink squares) starts earlier than the one with the turbine ϕ=10'' (blue dots). This apparent contradiction can be explained by the fact that the larger mass of the 10'' turbine has higher inertia to overcome.

Comparative characteristics for the 6 and 10 inch turbine arrangements are plotted in the Figure 4.1-12:

The down stream behaviour is similar to the upstream in the sense of having the crawling and pigging condition. Although the downstream inflection point between crawling and pigging is not as noticeable as it is in the upstream regime, the change is marked by the sudden increase of the slope. The steepest slope, which apparently

indicates an increase in the HPR speed, it is unrealistic and indicates the beginning of the pigging behaviour.

The following are the main point of the self-drive machine behaviour derived from the Figure 4.1-12.

1. Upstream and downstream starting points are different for both HPR configurations; however, the small turbine arrangement shows a bigger gap between the starting point of the up and downstream regime.
2. Bigger turbine has steepest slope, higher acceleration and higher speed.
3. Small turbine starts to move before than the bigger. That may be due to the high inertia of the bigger turbine.
4. Small turbine, smaller acceleration (slope less steep) and therefore smaller maximum speed for crawling conditions, upstream and downstream as well.
5. The range of flow rate at which the vehicle crawls is: 0.14 m/s for 10 inch turbine compared with 0.12 m/s for 6 inch turbine. Therefore the 10 inch turbine arrangement has a wider range of flow rate operating conditions.
6. Maximum vehicle's speed for 10 inch arrangement is 0.011 m/s compared with 0.005 for the 6 inch; so, the bigger turbine is capable or reaching 0.007 m/s more than the smaller.
7. The starting point for downstream crawling is before the upstream crawling for the 10 inch turbine. That is reasonable because the downstream crawling has a double advantage, the flow and the robot share the same direction, and the reciprocating movement. However, this is not the case of the 6 inch turbine. It would be advisable to do some test in this working region of the crawler vehicle so as to discard possible data errors otherwise to understand the meaning of such contradiction.

To conclude, the 10 inch turbine arrangement provides widest range of operating flow rate and highest vehicle's speed compared with the 6 inch turbine. However, if the requirement is low flow rate operating points, the solution is a compromise between the two turbines.

The next paragraph relates with the data conditioning, which is a necessary step for model building and controller development

HPR Data Conditioning

The raw set of data, composed of few points and analyzed in the previous section, has been conditioned in the context of this research project, with the purpose of obtaining a meaningful set of data suitable for building the HPR model through system identification. The system model is in turn included in the controller loop for model based controllers.

The **first step** in data conditioning is to **resample** the raw data set of few points, between 4 and 11 points, so as to increase the number of data to 1101 point, with the purpose of considering the vectors in the category of large number of data. This classification of large numbers means the data has high probability of normal distribution and may be analyzed with standard statistic methods (Keller and Warrack 2000).

The **second step** in data conditioning is to **normalize** the data vectors so as to get a population of normal distribution N(0,1) with zero mean and standard deviation one. The **third step** is a **complementary normalization** so as to distribute the data between a min-max range of -1 and 1; this min-max normalization is useful for the function approximation performed by the sigmoid function, which takes values between -1,+1 when the input range from $-\infty$ to $+\infty$, in other words the sigmoid function exert a "squashing" effect of the input.

In the **fourth step**, the overall data set is processed by Principal Component Analysis (**PC(A)** in order to form the final vector with data that accounts for variations of at least 0.001 of the variance of the set; so, values with less contribution of this mark are discarded (Jolliffe 2002). In that sense, PCA works as a decimation procedure. The HPR system is a SISO (Simple Input Simple Output) plant; so, it was no need of finding the correlation of multiple input vectors, this is another approach considered by PCA analysis.

The **fifth and last step** of data conditioning relates to the **data set division** in three groups training, validation and test of 367 point each group. This division is of fundamental application in neural networks processing. The **training data** is used with the purpose of training and consequently change the network parameters. The **validation data** is used to perform an online monitoring of the training process: if the error, resulting from testing the network with the validation data, starts to increase whilst the training error decreases then the conclusion is that the network starts to over

fit to the data set. So, an early stopping procedure is recommended to maintain the adaptability of the network to any sample data from the main data set. The last group, **test data**, similarly to validation data, is used to verify the network adaptation to a different data set; however, the procedure is offline. In the HPR case the information was divided into the three mentioned groups and the criteria for the data selection was to evenly distribute the information in the three groups.

The next sections are devoted to the system identification procedure, based on the data conditioned. System identification is the method used in this research project for building the model of the HPR, which is the base for the controllers developed in the last sections of this chapter.

4.5.2. HPR Trial Models: Model Reference Control (MR(C)

Why MRC?

The strategy of the **Model Reference Controller (MR(C)** is to drive a nonlinear plant to behave in a linear way. This is produced by comparing the output of a predefined linear model with the output of a controlled nonlinear plant, provided the input reference is the same for the plant and the linear model. So, the linear model is paired to the output of the controlled plant, and the difference, the **control error**, is fed back to the controller block so as to compensate for the differences.

Considering that the HPR is nonlinear, the only way of making the set, HPR and controller, to behave as linear is through the **variation of the controller parameters**. So, the controller changes its parameters in order to produce an overall linear behaviour in the controller-plant. Figure 4.1-13 depicts the MRC scheme for the HPR, where the plant and controller are neural networks-based models. The HPR model is obtained through nonlinear system identification so as to preserve the dynamics characteristics Hybrid Pipeline Robot.

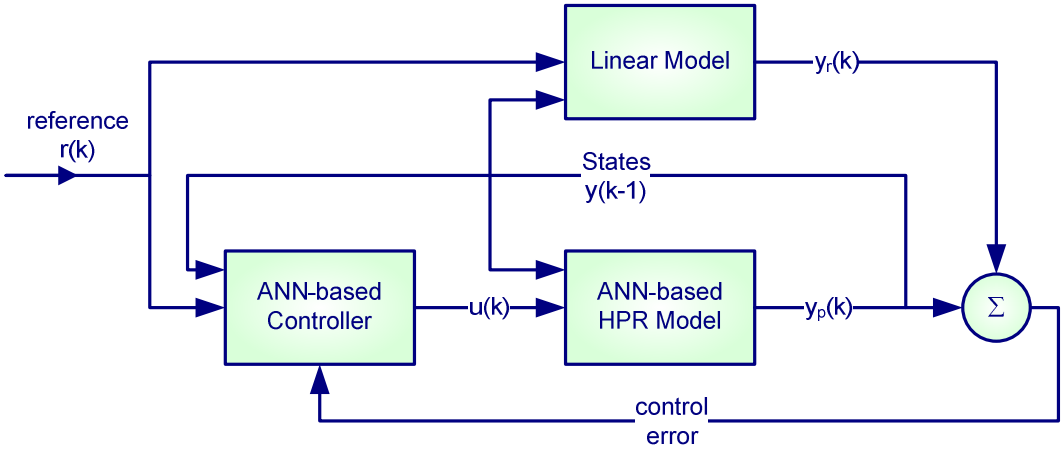

Figure 4.1-13 Model Reference Controller (MR(C) Structure

The HPR ANN model has free parameters to change in order to emulate a linear model while following the reference.

The general characterization for the control signal is described by the following discrete time equation (Narendra 1989):

4-23

$$u(k) = \sum_{l=h_3}^{q} \hat{\gamma} r(k-l) + \sum_{j=h_2}^{m-1} \hat{\beta} u(k-j) + \sum_{i=h_1}^{n} \hat{\alpha} y_p(k-i)$$

This expression shows the dependency of the controller signal, *u(k)*, from its own past values, from the output of the system, $y_p(k\text{-}i)$, and from the reference, *r(k-l)*, and their related past values (Narendra 1990 (a)). The estimated parameters, α, β and γ, represent the weight of a neural network and are calculated through the network training with a back-propagation algorithm. The controller, as a compensator for a nonlinear system, is a nonlinear system as well. Therefore, the key role of the neural networks is to perform nonlinear approximations.

The **ARMAX** structure **(Auto Regressive Moving Average with eXogenous variabl(e)** is selected to represent the linear block of the HPR system. The choice is because it gives the best fit (91.73%) among other linear structures, such as models based on the Prediction Error Method. See Figure 4.1-14 for models fit comparison. Although the HPR is a nonlinear system, the linear approximation of the ARMAX model is a close approach to the HPR behaviour.

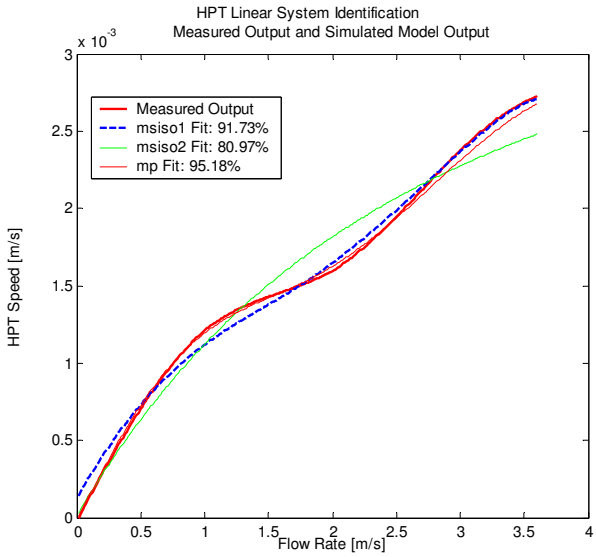

Figure 4.1-14 Linear Model: HPR linear system identification

,

The HPR model is based on the nonlinear system identification described in Figure 4.1-17. Figure 4.1-15 shows the MRC performance curves; where Figure 4.1-15 ((a) shows the HPR model output (blue dashed lin(e) following the reference (magenta solid lin(e) in a mirrored way, after a transient of nearly four time steps. The mirroring effect is due to the control compensation to produce a zero difference between the linear model and the HPR model, which is the principle of Model Reference Control: to drive a nonlinear model to behave in a similar way to a linear one. This fact is also depicted in Figure 4.1-15 ((b), where the output of the linear model (red solid lin(e) is the envelope of the HPR output; and the output of the linear model is the mirrored image of the HPR output, with the purpose of reaching a zero difference between the two models, as it was mentioned earlier.

Figure 4.1-15 ((c) shows the control signal (green dashed lin(e) as a modulated signal, where the envelope follows the nonlinearities of the HPR (red doted lin(e), and the carrier is a mirror image of the output of the linear model (blue solid lin(e). The reason of a modulated control signal is because the control strategy accounts not only for the reference and the states of the system, but also it accounts for the error in the reference and the error between the linear and HPR models. Figure 4.1-15 ((d) shows the HPR model output following the control signal with a smoothing effect of the control envelope; and therefore showing a close tracking of the reference. The mathematical proof of the modulated amplitude of the control signal is not central to this research and it is left for future development.

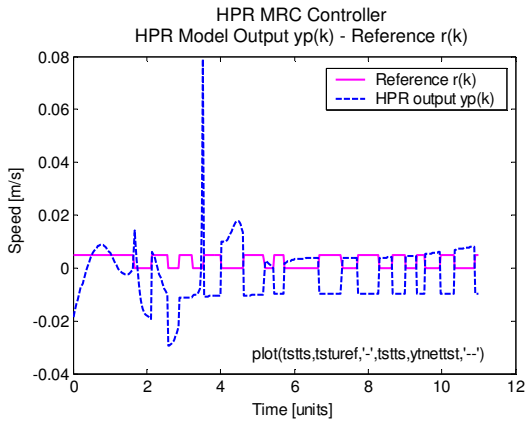

((a) HPR model output $y_p(k)$ - Reference r(k).
The mirroring effect is due to the control compensation to produce a zero difference between the linear model and the HPR model.

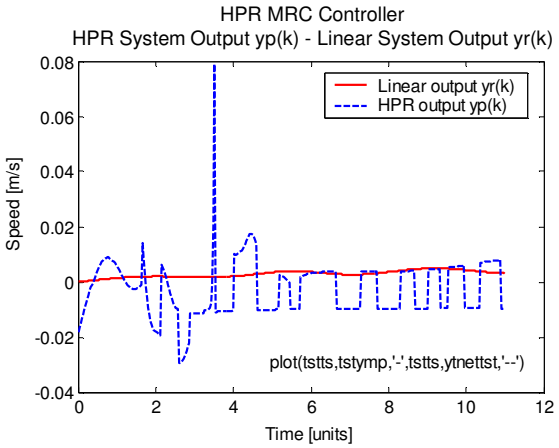

((b) HPR model output $y_p(k)$ - Linear System Output $y_r(k)$
The output of the linear model (red solid lin(e) is the envelope of the HPR output.

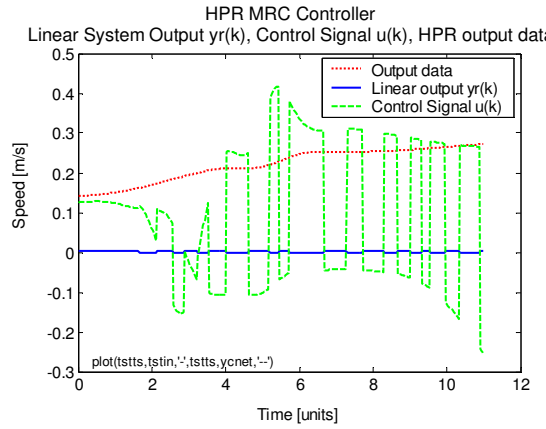

((c) Control signal u(k) – Linear System Output $y_r(k)$ - raw data of the HPR upstream regime. The control signal (green dashed lin(e) results in a modulated signal, where the envelope follows the nonlinearities of the HPR.

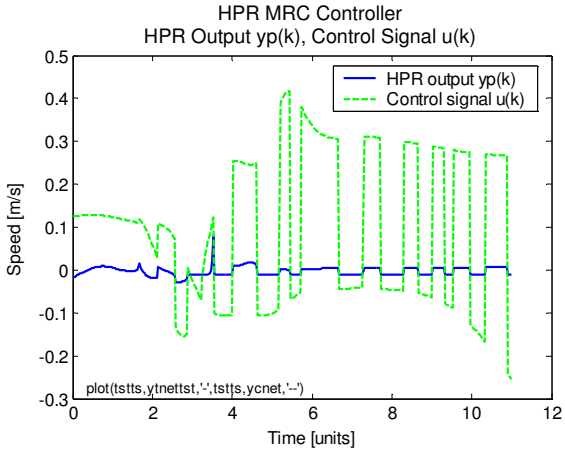

((d) Control signal u(k) - HPR model output $y_p(k)$
The HPR model output (blue solid line follows the control signal (green dashed lin(e); and therefore showing a close tracking of the reference.

Figure 4.1-15 Model Reference Controller (MR(C) responses

.

To conclude, the Model Reference Controller scheme provides the strategy for controlling the HPR in a linear way, by driving the nonlinear model to behave like a linear reference model. Although the good results of the MRC scheme as reference tracking, the controllability of the HPR toward the energy management is a constrained system far more complex, requiring a comprehensive control approach. Following this line of thought, further research has been done in the area of Neural Networks-based Model Predictive Control (MP(C) with optimization capabilities for the HPR energy and time management.

4.5.3. HPR ANN Control strategy

The HPR control strategy is based on the combination of two neural networks structures: the first performs the system identification and the second the reference tracking (Soloway 1992 (a); Beale 1993). The design of the network are developed by coding in Matlab© m-files based on modified code of Mark Beale (Beale 1993). The author decided to developing the code rather than applying the Graphical User Interface (GUI) of Matlab©, because coding allows more flexibility in terms of parameter combination, in addition to improving the understanding of the network structure, training process and optimization procedures.

Figure 4.1-16 shows the system and control network structures and the binary logic that defines the interconnection between the network layers and inputs, outputs and targets. Although a simplified diagram, because it doesn't show all the neurons in the network, it contains the basic binary structure necessary for programming the network. Detailed structure and training results are in the Appendix A.

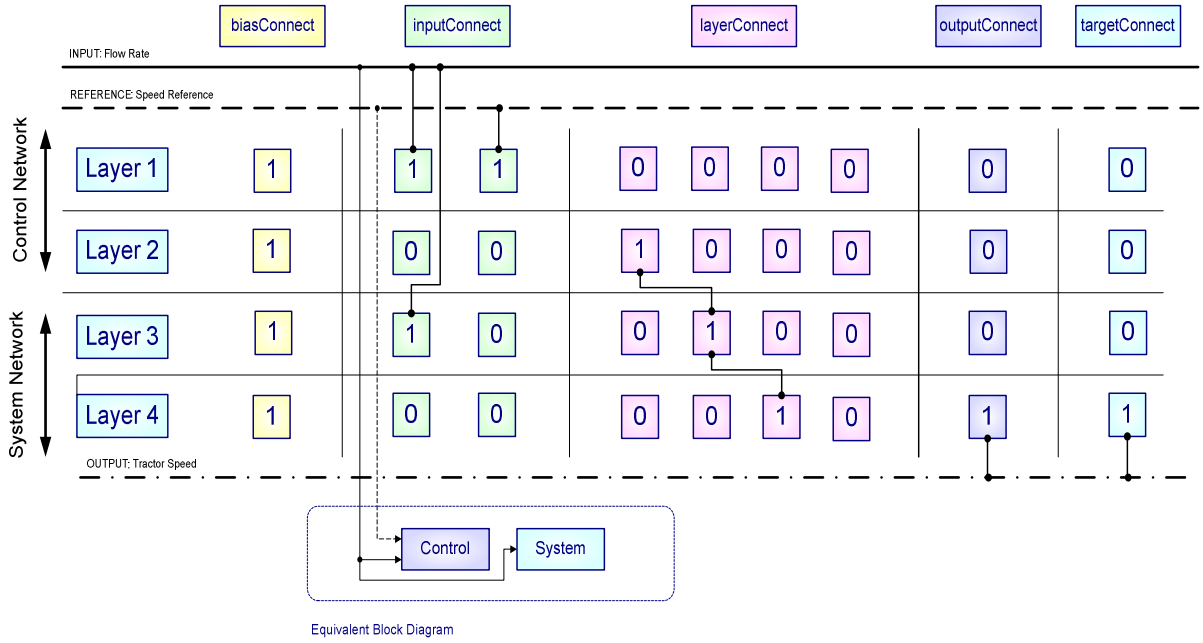

Figure 4.1-16 HPR Neural Network Structure

Layers 1 and 2 have weights free to change for tracking the reference; while the layers 3 and 4 have fixed weights after performing the network training.

4.5.4. HPR ANN System Identification

Two types of ANN strategies are selected for the HPR system identification, with the purpose of comparing the performance of the different approaches. One is the nonlinear system identification based on a static network; and the other is the adaptive

system identification based on a piecewise-linear dynamic network. The difference between static and dynamic networks is that static networks use all present values for training the network, while dynamic networks perform the system identification in an adaptive way, keeping past values of the input to be included in the network adaptation. Next paragraphs describe the static nonlinear system identification, and the dynamic network structure.

The network structure for the nonlinear system identification strategy is composed of two layers of neurons, a tan-sigmoid transfer function for the first layer, and a linear transfer function for the second layer. The tan-sigmoid transfer function performs a nonlinear approximation based on a second-order function; while the linear transfer function performs a linear transformation. Combining both networks, the first layer approximates the actual system response in a quadratic way, and the second linear layer shifts the result for offsets compensations (Hagan 1996).

During the neural network training the network changes its parameters to adapt to the robot behaviour. The static network training is of the type of off-line supervised learning, based on input-output data from measurements; the vectors are presented in a concurrent or parallel way; while the dynamic adaptive network is trained with the elements of the vectors presented sequentially, in an incremental training style. Once the static network for system identification is trained, the network parameters are kept constant during the next stage, which is the tracking process..

The training method is the Levenberg-Marquart back-propagation method, an algorithm that adjusts the step size according to the network performance, optimizing the network parameters upon the Hessian matrix calculation.

The idea behind back-propagation algorithm for training neural networks is to minimize the network error by adjusting the sensibility of the error to the change in the network parameters (Rumelhart, Hinton *et al.* 1987). So, analyzing the network from the output, the overall error is calculated applying the chain rule, as the derivative of the error with respect to the output, and then the derivative of the error with respect to the network's weights; successive calculations continue similarly for as many neurons connections are in the layers. Therefore, the network training is an optimization problem, with objective function decreasing at every step with the purpose of adapting the neural network to the problem of interest (Hinton and Sejnowski 1987).

The training data is based on data collected from the rig test, and analyzed in section 4.5.1. This data set refers to the 6 inch turbine configuration and to the robot crawling

upstream. Regardless the turbine size, the selection of the upstream data is because it conveys clearer information of the robot's crawling and pigging characteristics, which are of fundamental interest for understanding and controlling the HPR performance.

Figure 4.1-17 shows results of the network training for the nonlinear system identification, where Figure 4.1-17 ((a) shows the result of the network after training with good network adaptation to the training, validation and test data sets. Recalling that validation and test data are intended to perform an early stop of the adaptation algorithm, in case of network over fitting, for online and offline training, respectively. The Figure 4.1-17 ((b) shows the training performance asymptotic value of 0.039; though the goal zero is not attained, the performance is a very good result.

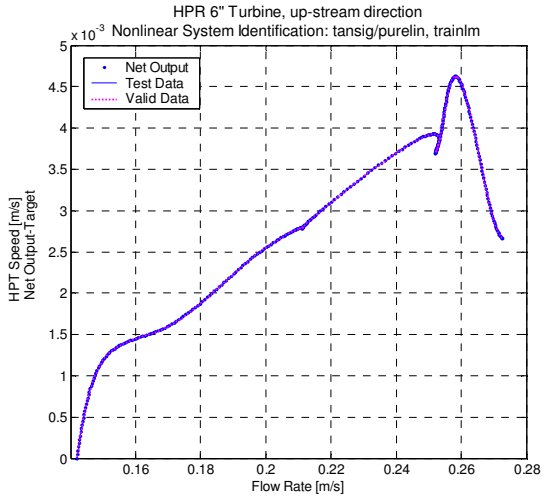

((a) HPR 6'' Turbine upstream direction
Nonlinear System Identification

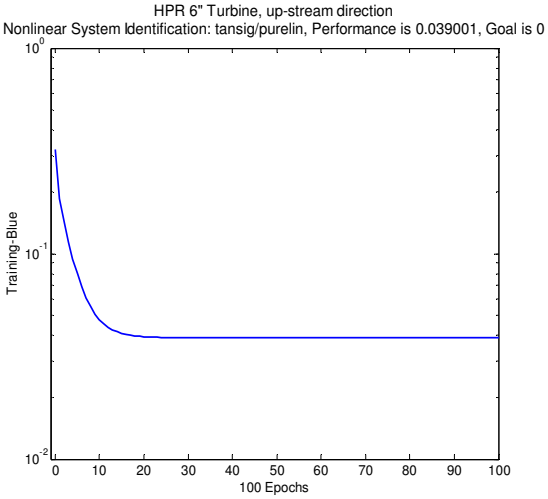

((b) HPR 6'' Turbine upstream direction
Nonlinear System Identification: Performance 0.039

Figure 4.1-17 HPR Nonlinear System Identification

The nonlinear static network is trained with a supervised learning algorithm based on the flow rate and robot speed characteristic.

The quality of the network performance is evaluated by the linear regression between the network output and the target vector. Figure 4.1-18 shows a good fit of 0.963 for the component-wise linear regression between the two un-normalized vectors.

The second ANN strategy for system identification is the **adaptive system identification**, based on a dynamic piecewise-linear network. The network used is the ADALINE (Adaptive Linear NEtwork), which includes a **tapped delay line** in the input with the purpose of incorporating past values (the states of the system) in the identification process.

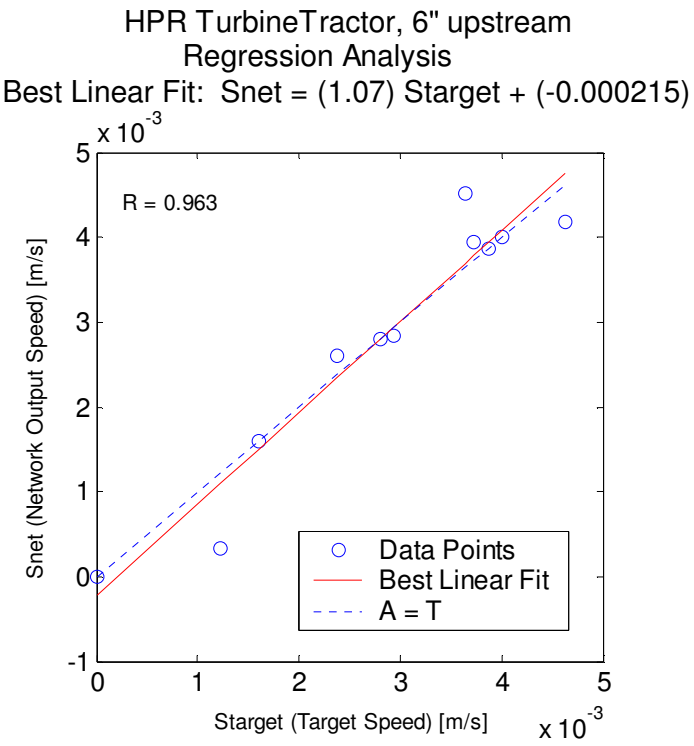

Figure 4.1-18 Regression between network output and target vector

Regression results for the HPR Nonlinear System Identification shows the data points close to the normal line, indicating a good network performance.

The network adaptation for the adaptive system identification is based on the variation of two parameters, the tapped delays (T(D) and the learning rate (LR) of the search algorithm; which is equivalent to varying the "memory" of the system and the speed of convergence in the network adaptation, respectively.

The network adaptation procedure started selecting a constant learning rate of -0.5, and changing the tapped delay in successive steps from 1 to 6; results of the network adaptation are in Figure 4.1-19 ((a) to ((d). In these figures, the network response is biased compared to the target values, for lower values of tapped delay, figures ((a) to ((c); presenting a significant improvement in adaptation for a taped delay of 6, in figure ((d). The drawback for this delay is that the system becomes unstable for small changes in learning rate, ranging from 0.5 to 0.005, where the output deviates markedly from the optimal value. As a conclusion and following the results, the best network adaptation is for a tapped delay of 6 and a learning rate of 0.5. The poor network performance for smaller values of learning rate can be explained by the fact that the search algorithm is deemed to be trapped in a local minimum when following smaller step sizes, failing to find the global minimum.

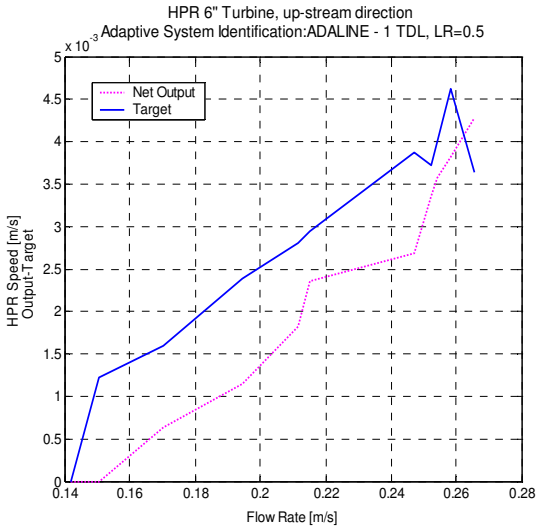

((a) HPR 6'' Turbine upstream direction
Adaptive System Identification:
TD=1, LR=0.5

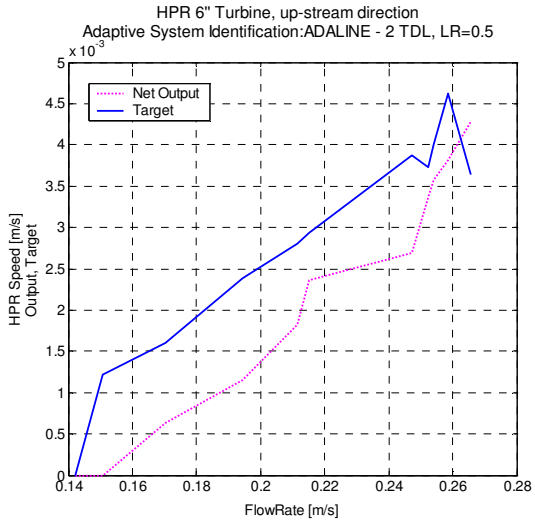

((b) HPR 6'' Turbine upstream direction
Adaptive System Identification:
TD=2, LR=0.5

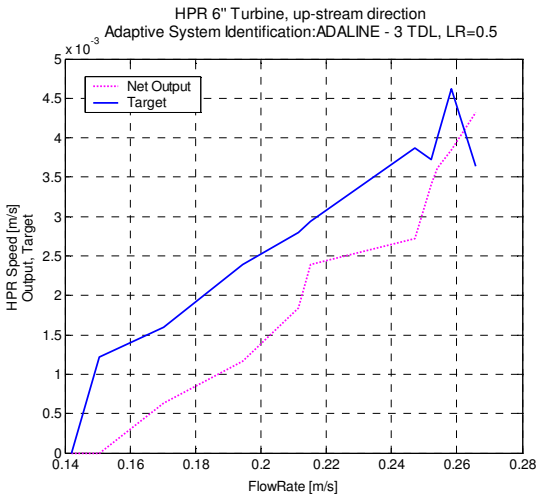

((c) HPR 6'' Turbine upstream direction
Adaptive System Identification:
TD=3, LR=0.5

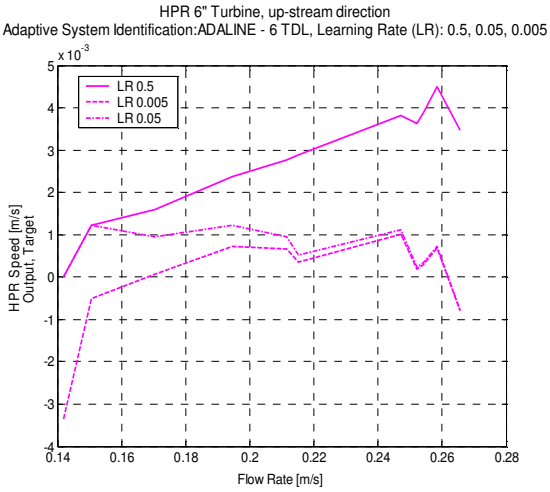

((d) HPR 6'' Turbine upstream direction
Adaptive System Identification:
TD=6, LR=0.5 - 0.05 - 0.005

Figure 4.1-19 HPR Adaptive System Identification

A dynamic piecewise-linear network is trained adaptively to compare the results with the nonlinear network presented before.

Therefore, static nonlinear network performed better than the dynamic piecewise linear network for system identification, both trained with supervised learning algorithms. Though this is a good result for trial models, it would be interesting to explore a recursive system identification approach for the onboard control strategy, to improve the adaptability of the network to the robot dynamics and the pipeline environment.

4.5.5. HPR ANN Tracking System

Once the network for system identification is trained, its weights are kept unchangeable and a second network is added with weights free to change. Both networks are presented with pairs of input-target data so as to train the second network to follow the reference. Given the good results of the nonlinear system identification, a nonlinear network has been selected for tracking purpose, with tan-sigmoid transfer function for the first network and linear transfer function for the second, to perform a nonlinear adaptation and shifting effect, for the first and second network layer, respectively; similarly to the way explained for system identification, section 4.5.4. The training style is incremental, where the components of the input vector are presented sequentially.

The network training and the results are presented in the Figure 4.1-20, where figure ((a) shows the network response to the initial conditions, before training, and the curve for the robot speed, the system output. The difference between both curves is due to the inclusion of the second network with varying parameters.

Figure 4.1-20 ((b) shows the network after training, following the reference speed. The figures show a good adaptation of the network to the first and second period in the reference. From the third period, the network output starts to deviate from the reference, resulting in a fluctuating error. The third curve in red shows this error of adaptation.

Figure 4.1-20 ((c) and ((d) show the response of the network to validation and test data. The network response is similar for the three groups, which means a good training result and no presenting an over fitting of the network parameters to the training data set.

The network training has been performed varying the initial conditions, and the number of epochs; in addition to presenting the vectors in a sequential and concurrent way. From those changes the most significant improvement is produced by the inclusion of a **time-delay** or **tapped delay network (T(D)** at the input.

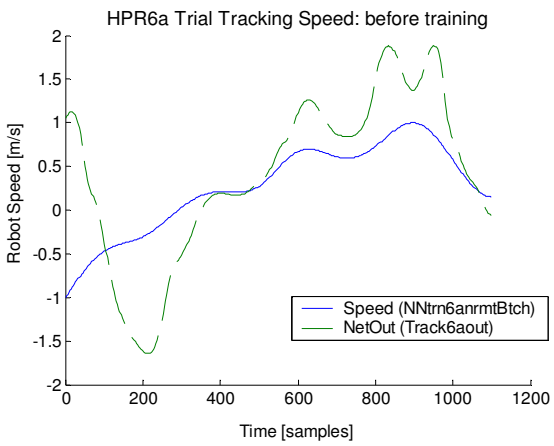

((a) Before training: Network output vs. System Output
The network output (green dashed lin(e) has the shape determined by the initial conditions of the weights.

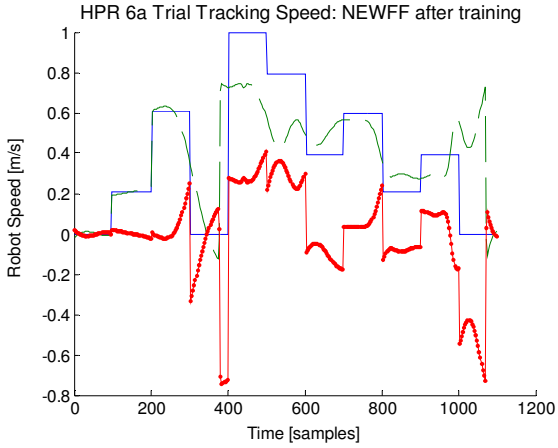

((b) Network response vs. Reference Error, after training
There is a good adaptation of the network to the first and second period in the reference, denoted by zero error. From the third period, the network output starts to deviate from the reference.

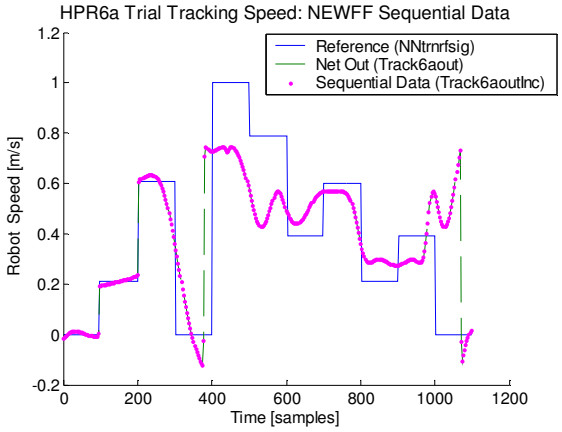

((c) Network response vs. validation data
Validation data executes an on-line verification of the algorithm and performs an early stop in case of curve over fitting.

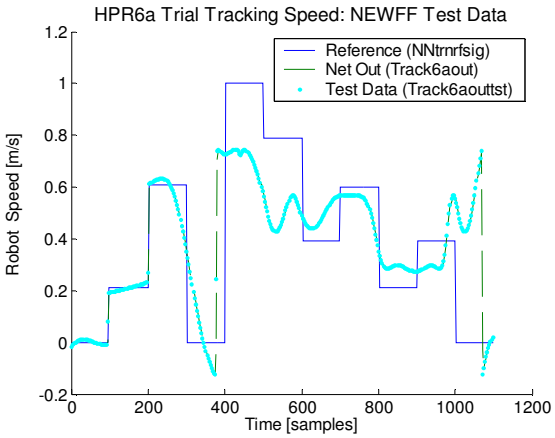

((d) Network response to test data set
Test data is the off-line verification of the capacity of the network to generalize the adaptation to a different data set.

Figure 4.1-20 HPR Tracking System: Network training and simulation

A nonlinear static network is trained adaptively to follow the reference

Figure 4.1-21 shows the progressive improvement on the network adaptation and the training performance for increasing values of TD from zero to three. Starting with zero tapped-delay TD=0 in Figure 4.1-21 ((a), the tracking network presents a good adaptation for the first three points, yet a very poor adaptation afterwards. The overall network adaptation improves markedly with the increase of tapped-delays Figure 4.1-21 ((b) and ((c). However, for TD values bigger than two, the network response presents oscillations; particularly Figure 4.1-21 ((d) shows the oscillatory effect starting at early steps of the tracking system. These oscillations in the response can produce fluttering of the control signal provided no filtering procedures are taken into account.

Recall that the effect of the **delayed input** is to incorporate the **memory** effect in the network structure, in order to smooth the network approximation and to improve the network adaptation over a long period. However, for TD bigger than zero, an interesting characteristic starts at point 400, where the network response starts to adapt in a predictive way. After that point the network shows an averaging or smoothing effect of the response rather than a close adaptation to the reference, a desirable characteristic to protect actuators from saturation.

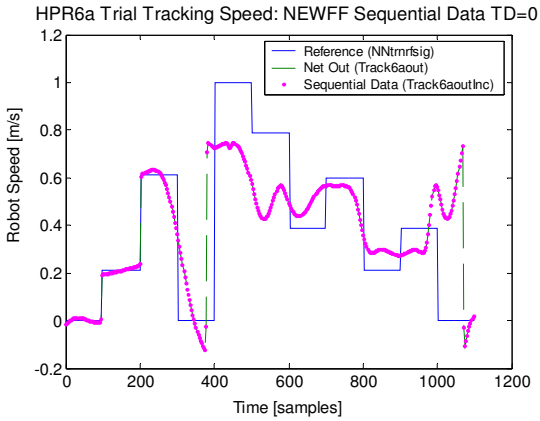

((a) Network response vs. Reference: TD=0
Good network adaptation to the first three reference changes. Performance: 0.104957 goal 0, poorest error performance, explained by the poor overall network adaptation.

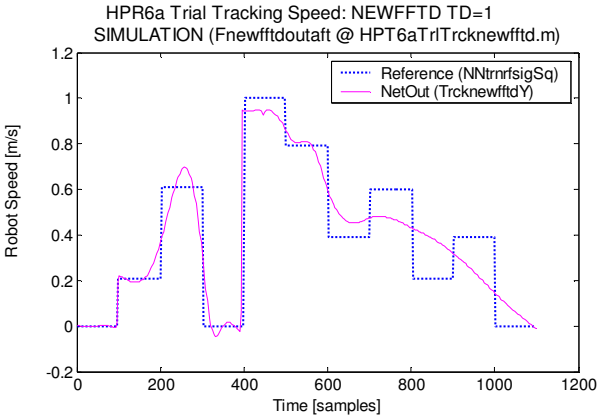

((b) Network response vs. Reference: TD=1
Overall improvement of the network adaptation to the reference. Performance: 0.0496282 goal 0, The error performance improves as the overall network adaptation improves as well

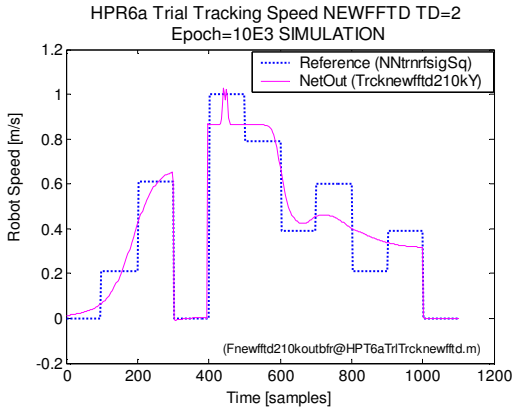

((c) Network response vs. Reference: TD=2
The network adaptation shows an integrating effect, yet poorly adaptation to the reference. Performance: 0.0134493 goal 0, the error do not change significantly.

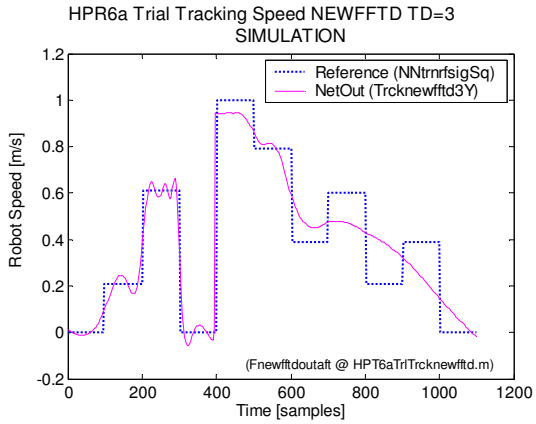

((d) Network response vs. Reference: TD=3
Markedly improvement of the network adaptation to the reference, though the network presents oscillations. Performance: 0.0151135, goal 0, the error do not change significantly, despite the increase of TD

Figure 4.1-21 HPR Tracking network response to TD variations

.

In relation to the **training error** of the network, the training of the network in Figure 4.1-21 ((a) gives a training error of 0.1, for not delayed input (TD=0). Despite

the goal of zero error is not attained, the solely addition of one tapped-delay line, TD=1, reduces the training error to 0.05 in Figure 4.1-21 ((b). The lowest error value is 0.013 for TD=2, Figure 4.1-21 ((c). However, the tendency of decreasing errors by increasing the number of delays is broken at TD bigger than two, where a slightly increase of the error to 0.015 appears, Figure 4.1-21 ((d).

To conclude, the inclusion of a tapped-delay line helps to improve the adaptation error and the smooth response with no cost of stationary-state error, as long as the tapped delays are between one and two. For higher values of the delay line the good adaptation of the response starts to fade.

4.6. CONCLUSIONS

Control Architecture and control strategy for a self-powered and bristle-based locomotion robot

The contribution of this research project for the Hybrid Pipeline Robot is the design of a **control architecture** based on the **reconfiguration of the control strategy** for each of the states. The operating state is controlled by a model predictive control MPC for speed control with energy and time optimisation, as a problem of multi-objective optimisation. Cruising and self-recovering states are controlled by a neuro-dynamic programming approach for the optimization over time of the energy and mission time, as a problem of objective prioritisation. The transient states, idle and cycling are controlled by an inference algorithm.

The control structure is presented as an event-based **Finite State Machine**, where the hierarchical structure becomes evident. The high level in the hierarchy is represented by the HPR supervisor, which performs the optimization of the performance indexes; and the low level is represented by the HPR regime constituted by the on and off scheduled states.

The HPR energy and time optimisation is a problem with unknown finite number of stages, and unknown transition probabilities between stages. Therefore, the proposed solution is based on a neuro-dynamic programming approach or reinforcement learning, based on Q-learning strategy. A **neuro-dynamic programming model of the stage transitions,** including the transition costs for energy and time, has been developed.

Due to the reciprocating behaviour of the robot's locomotion, the performance index, for speed control, includes a **terminal state constraint** for enforcing the system stability, while avoiding unnecessary control actions.

ANN System identification and tracking system for a self-powered and bristle-based vehicle

The proposed HPR system identification and tracking system strategy is composed of two neural networks structures, as it was proposed by Beale (Demuth and Beale 2000). The first performs the system identification and the second tracking of the reference. After training the network for system identification, its parameters are fixed

and the parameters of the second network are free to change in the network adaptation to the reference.

Two networks have been simulated for system identification, a static nonlinear and a dynamic linear network, from which the static nonlinear gave better results. In both cases, the networks are trained by supervised learning strategies, presenting pairs of input-output data; particularly, flow rate and robot speed respectively. The difference between static and dynamic networks is that the dynamic network is trained in an adaptive way by including the past values of the system, system states, in the input; conversely, the static network lacks of the system states in the input.

The selection of a static nonlinear network is justified by the fact that the robot and the environment are nonlinear systems. The selection of a dynamic piecewise leaner network is on the base that the robot in the pipeline environment is a dynamic system.

The best performance for system identification for the HPR system was the static nonlinear network. This result suggests that the selection of the network structure is more relevant compared with the way of training the network, for system identification of a pipeline robot.

Following the good results of ANN for system identification, a similar nonlinear network structure was used for tracking. However, the network structure was changed as a dynamic network, to be trained in an incremental way.

Variations of the delay in the input are explored in the simulation of the tracking network. The best performance was for a time delay of one in order to adapt the network to changes in the reference. From the results, it was concluded that the network performance is a trade-off between network adaptation and stability, the better adaptation the worst stability.

System identification and tracking systems are simulated with trial data from rig tests relating flow rate and vehicle's speed, which is a collaboration of a different research group. However, the two-variable data set represents limitation for testing the controller models involving energy management. Therefore, it was required the development of the necessary instrumentation to perform such tests, which is a subject of Chapter 5.

Chapter 5 HPR Instrumentation System Development

5.1. INTRODUCTION

In this chapter is described the development of the on-board instrumentation system for measuring the variables required for the Hybrid Pipeline Robot system identification. The instrumentation system consists on a set of pressure probes, torque transducer and a signal conditioning board, to be connected to a microcontroller. The objective is to determine the turbine efficiency and robot speed, which are the input and output of the HPR system.

The rationale for the development of such a measurement system is the necessity of performing on-board measurements, signal conditioning and data acquisition. The on-board characteristic is because the data transmission to an external point is rather difficult due to the constraints of the pipe wall and disturbances introduced by the fluid inside the pipeline; requiring a special development in communications. The reason for developing the set of probes is because the options available in the market are neither suitable for the HPR characteristics nor accessible at a reasonable cost.

The chapter is composed of two parts, related to the probes and embedded board development. Figure 5-1 relates the probes with the variables to be measured in order to calculate the turbine efficiency and the robot speed. The probes for determining the efficiency are the set of pressure probes: Kiel-reverse, Pitot-Gracey and Pressure Measurement Chamber (PM(C), for calculating the flow rate and pressure drop across the turbine; and the hollow universal joint, which is customized as torque transducer. Finally the output of the system, the robot speed, and speed characteristic are detected by an accelerometer. This section includes the general procedure for the probes development.

Figure 5-2 describes the procedure for the on-board signal conditioning board and it consists on the design of the general data acquisition strategy, and power architecture. Finally, the board development starting with the design criteria and components selection; followed by the simulation of the instrumentation amplifier circuits, schematic capture, board layout; and ending in the board fabrication and test.

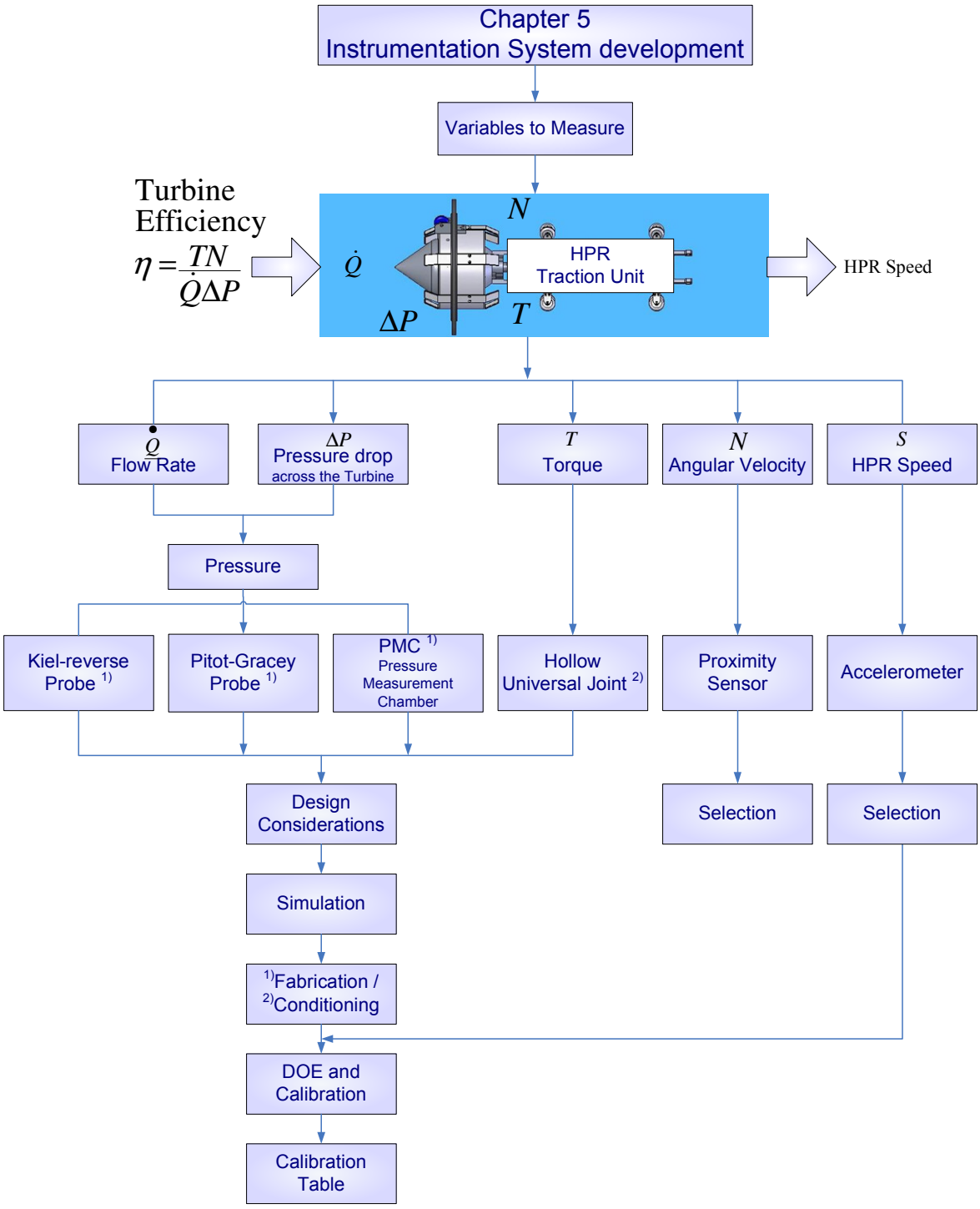

Figure 5-1 Chapter 5 contents: Instrumentation system development

Probes developed according to the respective HPR variables to be measured for system identification. Development procedures and / or sensors selection.

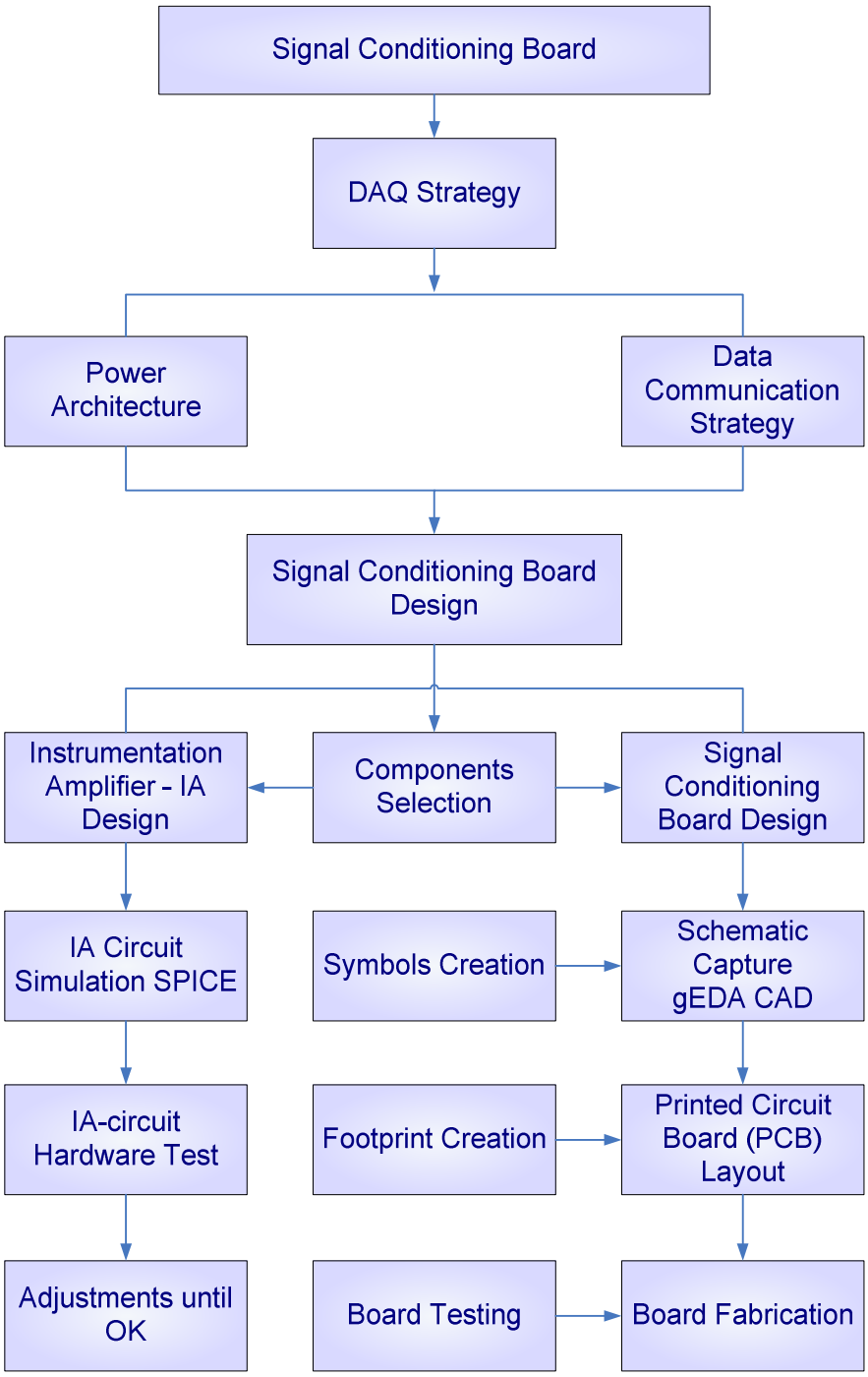

Figure 5-2 Chapter 5 contents: Signal Conditioning Board

Steps in the development of the on-board data conditioning embedded board

5.2. Determining the flow rate and pressure drop across the turbine

In previous chapters have been defined the fundamentals parameters constituting the HPR efficiency. This section relates to the determination of Flow rate (Qdot) and pressure drop across the turbine (ΔP), both of which for pressure measurement.

The pressure probes available in the market are neither suitable for the HPR dimensions and environmental conditions, nor cost effective. So, the decision was to design the probes for measure the flow rate and the drop of pressure across the turbine.

The probes are designed in a suitable size and robustness to be attached to the robot no only as measurement points for system identification, but also as a permanent on-board instrumentation, due their non-disruptive design. The probes designed are Kiel-reverse, Pitot-Gracey, and Pressure Measurement Chamber (PM(C) probes. This section relates to the design and calibration of the process.

For determining the flow rate Qdot is required to measure the stagnation and static pressure at any point inside the pipeline. Orifice plate is a standard device; however, the drawback is that the plate is constraint to the flow, which may compromise the line performance. Therefore, was necessary to design an onboard non-disruptive probe for flow rate measurement. So, it is required to analyze factors affecting the measurement of static and stagnation pressure.

Related to pressure measurement, the second parameter to determine is the pressure drop across the turbine, ΔP. Following the concept of energy transformation expressed in Chapter 3, it is required to measure the static pressure, up and downstream the turbine.

The pressure measurement involves several considerations that need a careful analysis in order to get consistent results. In order to understand the considerations needed for the pressure measurement, it is important to revise the definition of pressure: *pressure is a derived parameter; it is the relation of the force to the area over which the force is applied (White 2008).* So, the pressure can not be measured directly but through the parameters that produces the pressure, which are the force and area. So, a pressure probe is as a device intended to create the necessary conditions for the pressure to be measured, with the minimum disruption of the environment so as to do not alter the explored stream. That is a suitable instrument that relates force and area.

Therefore, in order to measure the pressure it is required to determine the place where to measure static and stagnation pressure upstream and static pressure downstream the turbine. This aspect is explored in detail in next sections.

Finally the pressure probe is connected to a pressure transducer, the device that converts the physical changes in electrical signals, and the signal is conditioning by the embedded board, explained later in this chapter.

Static Pressure

In exploring the surroundings of the HPR it is necessary to bear in mind the following definitions.

Definition 2 *In relation to static pressure, the theory recommends measuring the pressure at the boundaries of the flow, where the flow is streamlined and not curved, free from disturbances. The theory also recommends placing the tap so as to align the tap axis perpendicularly to the boundary and free from obstructions (Massey 2006).*

Definition 3 *The boundary of a flow is created by any solid object immersed in or surrounding by a fluid, for example the HPR inserted in a pipe. A boundary creates layers surrounding it of different viscosity: the closest the layer to the boundary the higher the viscosity and therefore the slower the velocity; in the closest vicinity of the object there is no relative fluid movement (Massey 2006).*

So, the presence of a boundary affects substantially the pressure measurement. As the crawling vehicle is travelling along the pipe, it has a relative movement in relation to the walls of the pipe. So, it is not possible to apply the approach of standard rigs for testing stationary devices with respect to the surroundings, where the pressure taps are also stationary. Therefore, for the HPR, the pressure probe needs to be attached to the vehicle.

By the mass conservation law, the flow rate is inversely proportional to crossing area; so, the smaller area the higher speeds. Therefore, a flow starting to curve means a change in area and therefore a change in flow rate, which renders the static pressure measurement as uncertain.

Therefore, as general recommendations for locating the static probe, it is necessary to look for flow boundary close to smooth surfaces where streamlines are created. Figure 5-3 (a) and (b) show the flow profile at the nacelle and at the wake of the turbine. The simulation was created by using finite element analysis, and shows the

turbine immersed in a simulated enclosed volume with water flow at ambient temperature. At the turbine nacelle, Figure 5-3 (a), the streamlines of the upstream flow, start to curve in the nacelle surroundings producing velocity gradients that reach highest values at the edge of the nacelle. A far more complex pattern of pressure lines is created at turbine wake, Figure 5-3 (b), where a mixture of pressure line is created by the hollow universal joint, the rotation of the turbine blades and the reciprocating motion of the tractor. Therefore, the restriction of parallel and not curved flow, leads to discard the nacelle in the front of the turbine or the gearbox cover at the back of the turbine for locating static pressure taps.

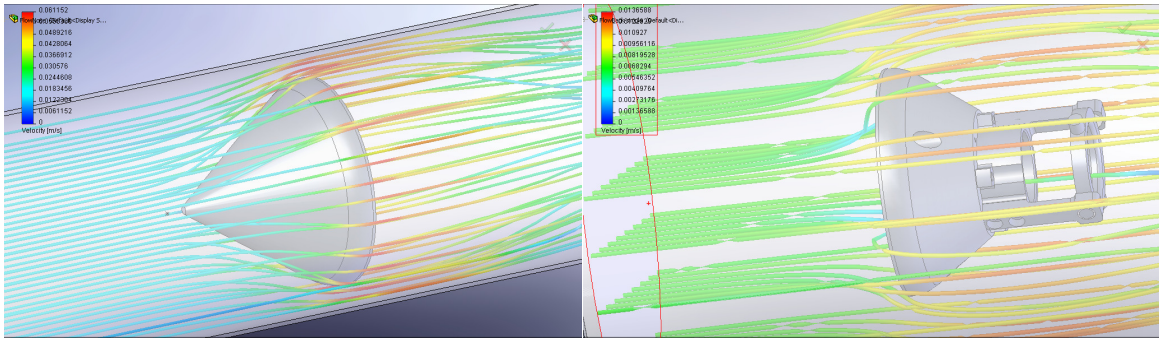

(a) Flow profile at the turbine nacelle, the gradual change of color indicates velocity gradient as the flow passes the turbine.

(b) Flow profile at the wake of the turbine. Changing line color implies turbulence at the wake of the turbine.

Figure 5-3 Flow passing the turbine

Finite element analysis performed in SolidWorks for determining the probe location for static and stagnation pressure measurement.

As a result, it is necessary to measure the static pressure up and down stream the turbine, taking into account that at the wake of the turbine is necessary to create a streamlined flow to compensate for flow disturbances.

Stagnation Pressure

In order to find the place where to measure the stagnation pressure it is necessary to consider the following definition.

Definition 4 *Stagnation pressure is the pressure at the point where the flow is brought to rest or where it has zero velocity (Massey 2006).*

Following the definition, the tip of the turbine nacelle shows clearly good conditions for zero velocity flow. The turbine nacelle is centred in the pipe by the wheels arrangement of the turbine case; so, it is a good averaging point for pressure measurement, and stable point in terms of yaw, pitch and roll angles. These symmetry

angles are a source of errors when the the flow incidence angle is not perfectly aligned; the literature reports errors of less than 1% for misalignment less than 15° respect to the horizontal (Barlow 1999).

Other important consideration is to measure the stagnation pressure far from boundary layers, formed at the turbine nacelle and at the pipe wall. The gradient of velocities of the boundary layer produces dynamic disturbances to the probe, altering the total pressure value (William 1947).

In relation to the probe for stagnation pressure measurement, the Pitot-static tube is the classical solution for measuring both, stagnation and static pressure. Stagnation pressure is measured at the tip of the probe and the static pressure at holes distributed around the probe and farther back the front of the probe (Barlow 1999; United-Sensor 2008 b)). However, the limitation for using a Pitot tube is mainly the reduced pipe section, 13inch pipe section, for standard commercialized sizes, considering the location of the tube far from boundary layers. The alternative of using a customized size was discarded for economic reasons and unfeasible manufacture in the University workshop.

As far is the author knowledge there is no standard out-of-shelf solution for measuring the flow rate and pressure drop across the turbine under the considerations mentioned before and HPR requirements. Therefore, the contribution of this research project is the design, fabrication and calibration of the Kiel-reverse probe, Pitot-Gracey probe, for flow rate measurement; and the Pressure Measurement Chamber (PM(C) for conditioning and measuring of the flow downstream the turbine. The following sections describe the design process and calibration results for the mentioned probes and a discussion about their effectiveness.

5.2.1. Kiel-reverse probe for static and stagnation pressure measurement

One alternative to Pitot-static is the Pitot-meter or Pitot-reverse probe, which has two orifices: one is facing the main stream and the other facing backwards, for measuring the stagnation and static pressure respectively. The Pitot-reverse probe requires also a correction factor because the pressure at the wake of the probe is smaller than the actual static pressure at the same point (Massey 2006). The main advantage of this probe is the simplicity of its design (United-Sensor 2008 b)).

An improvement to Pitot-tube is the Kiel probe, which combines the principle of the Pitot-tube and a Venturi-meter (Kiel 1935). It consists on a total pressure probe

inside a nozzle of the shape of a Venturi meter; a simplified version is a cylinder as the outer shell.

The Venturi-meter profile of the external nozzle of the Kiel probe has the advantage of confine the flow in the surroundings of the pressure tap, creating a streamlined control volume appropriate for the accurate measurement of total pressure, even in highly turbulent flow or higher Reynolds numbers. The advantage of the Kiel probe is its very low sensitivity to yaw angles up to 40°, for low Reynolds numbers (Kiel 1935).

One of the main findings of Kiel's study is the dependence of the total pressure error from the distance of the tip of the probe to the front section of the cylinder, *a*. The dimensionless ratio a/D, where D is the cylinder diameter, is a scaling factor. The performance curves of the Kiel probe show zero error for ratios in the surroundings of a/D ≈ 0.5, for yaw angles up to 25°. The general dimensions of the Kiel-reverse probe and performance curves are in the Appendix B.

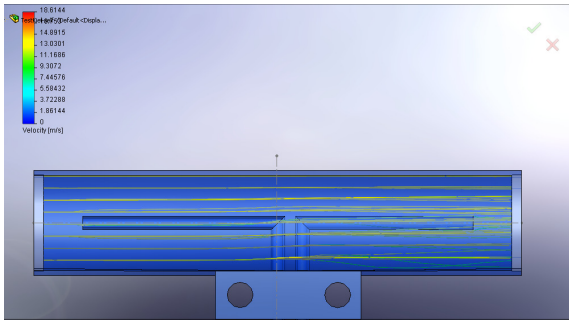

(a) Kiel-reverse probe design A, right angled pressure intake

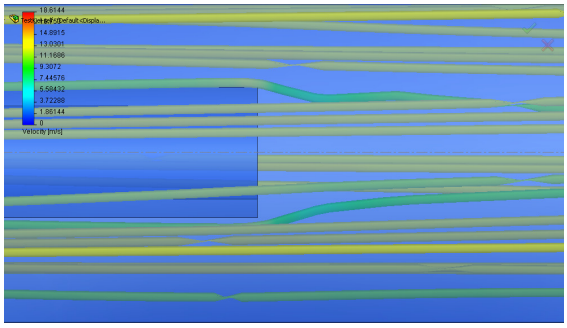

(b) Design A, wake of the pressure tap. Curved lines, adhering to the tap contour, are responsible for the lower static pressure compared with the real one

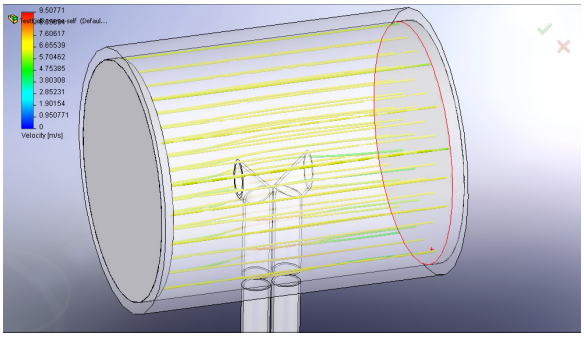

(c) Kiel-reverse probe design B. Shorter and angled pressure intake to improve time response and to avoid pressure gradients due to angled taps

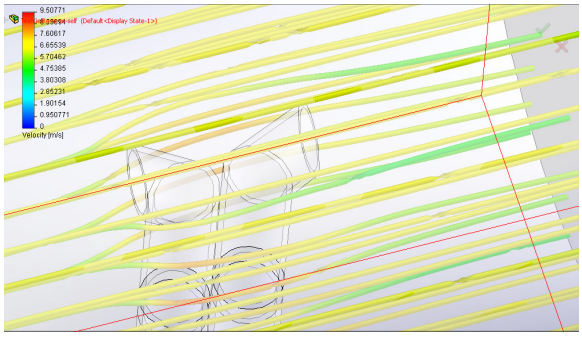

(d) Design B, wake of pressure tap. Velocity gradients show lower static pressure at the wake of the pressure intake

Figure 5-4 Kiel-reverse Probe simulation in enclosed volume

Finite element simulation in SolidWorks, for analyzing the pressure change in the probe taps, in order to evaluate the probe for static and stagnation pressure measurement.

The Kiel-reverse probe is designed by the author for solving the problem of onboard pressure measurement for the Hybrid Pipeline Robot. This probe combines the principle of two probes: the simplicity of the Pitot-reverse probe, with two tapping facing up and downstream for stagnation and static pressure respectively; and the flow-conditioning characteristic of the Kiel probe, which helps to create a streamlined flow in the surroundings of the pressure taps. This last feature is fundamental to reduce the errors due to yaw angle. Figure 5-4 (a) show Design A, one of the two models for the Kiel-reverse probe, where the relation length/diameter is fairly larger than one. The probe Design B in the Figure (c) has two improvements with respect to design A; one is the shortest inner tube to improve the time response of the probe. As a consequence, the relation length/diameter of the probe is close to one. The other improvement is the 45˚ angle of the inner tube with respect to the horizontal, for creating an even flow profile along the whole trajectory of the tube, avoiding 90˚ elbows, which create velocity gradients.

Figure 5-4, (b) and (d), show the finite element simulation for Kiel-reverse probe. In this particular case the control volume is formed by the outer cylinder of the probe, straightening the flow. It is noticeable the slightly lower pressure at the back of the probe, in the figures the green lines are indicating lower speed compared with the yellow ones. Additionally, the low pressure is denoted by the curvature of the stream lines due to the Coanda effect at the wake of the probe, with a tendency to follow the contour of the pressure tap creating a decrease in the velocity gradient; after that the stream recovers the streamlined shape. This Coanda effect is the reason for the lower pressure compared with the actual static pressure reported in the literature (Massey 2006). This difference of pressure experienced by the Kiel-reverse probe is one of the main reasons for calibrating the probe with the purpose of obtaining the correction factor. The calibration procedure is presented in the next section. Figure 5-6 shows the Kiel-reverse probe design for the HPR, compared with the commercial version of the Pitot-reverse from United Sensors (Kiel 1935; United-Sensor 2008 a); United-Sensor 2008 c); Flow-Kinetics). Figure 5-5 shows details of the Kiel-reverse probe in the open channel for calibration tests.

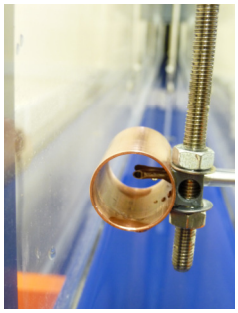

(a) Kiel-reverse probe, detail of the pressure intake and the positioning bar. Due to the pressure taps are protected by the outer cylinder, the positioning bar has little influence in the flow streams.

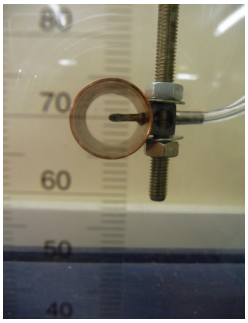

(b) Kiel-reverse probe and the tubing arrangement. Tubing layout is to avoid mixed flow densities in the tube, which may introduce hysteresis in the measurement.

Figure 5-5 Kiel-reverse probe tubing and fittings

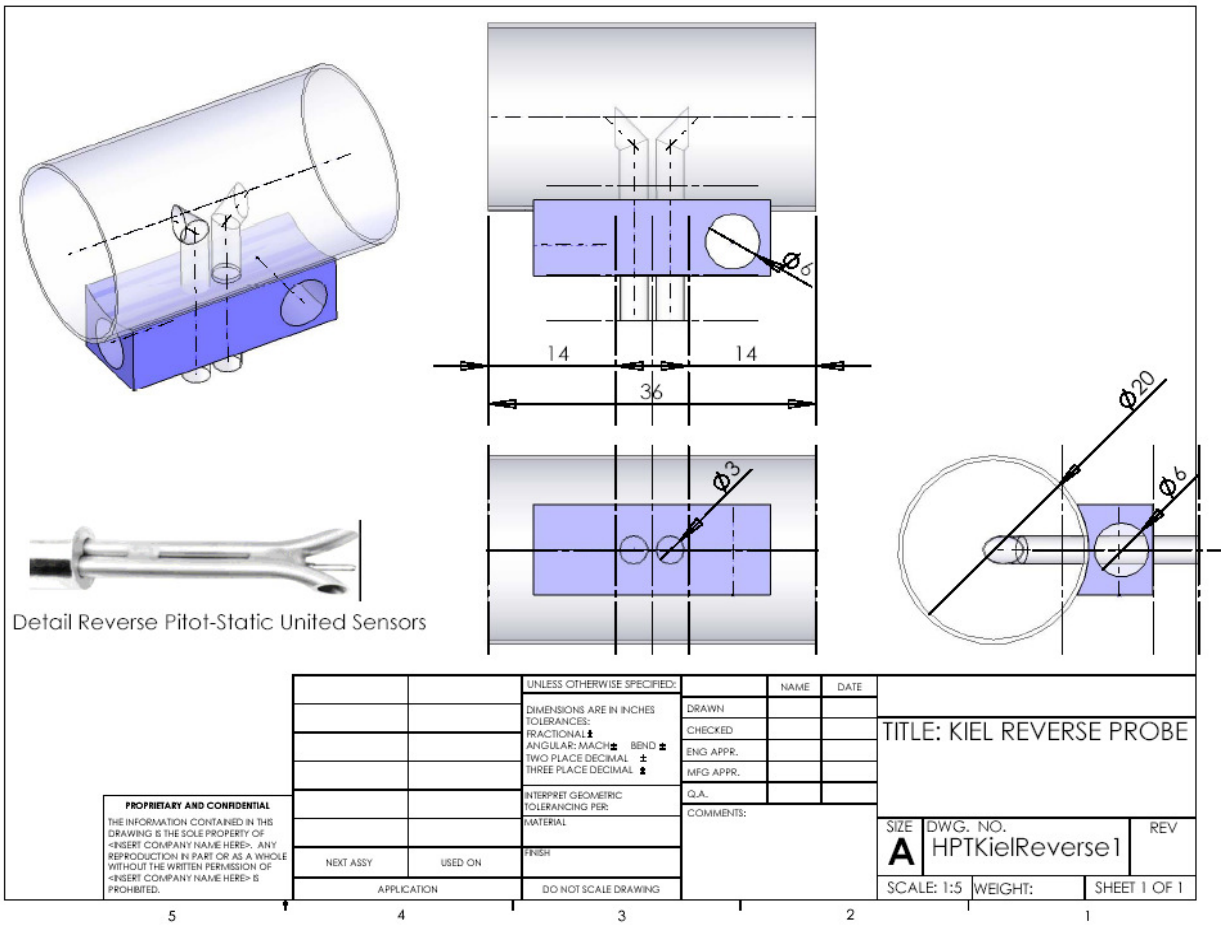

Figure 5-6 Kiel-reverse probe design

Details of the probe compared with the Pitot-reverse probe (United Sensors) (middle left)

.

Kiel-reverse Probe Calibration

Summarizing the concepts presented so far, the Kiel-reverse probe is utilized for determining the flow rate upstream the turbine, by measuring the stagnation and static pressure. Both taps are connected to one differential pressure transducer. The static

pressure of the Kiel-reverse probe is also used to determine the pressure drop across the turbine by diverting a second tube to a different transducer.

Calibration 1. Kiel-reverse probe for Flow Rate measurement: DOE

The design of experiment (DO(E) for the Kiel-reverse probe, Figure 5-7, consists on three factors referred to the flow rate measured by the Kiel-reverse probe, flow meter and calibrated tank. The DOE levels consist are intended to emulate pipeline conditions.

Pre-test trials have been performed in order to tune the micro manometer and the tubing layout of the Kiel-reverse probe. The Kiel-reverse probe test was intended to explore the flow rate over a range, starting from zero and suddenly increasing the flow to the maximum level in the scale. The sudden jump was to simulate a water hammer, which is common in pipelines and to verify the time response, saturation and hysteresis after the water hammer. Several other factors may be included in the experiment such as distances between the probes, boundary layer influence or yaw angle variation, just for cite a few; however, detailed study of the designed probes are out of the scope of this research project.

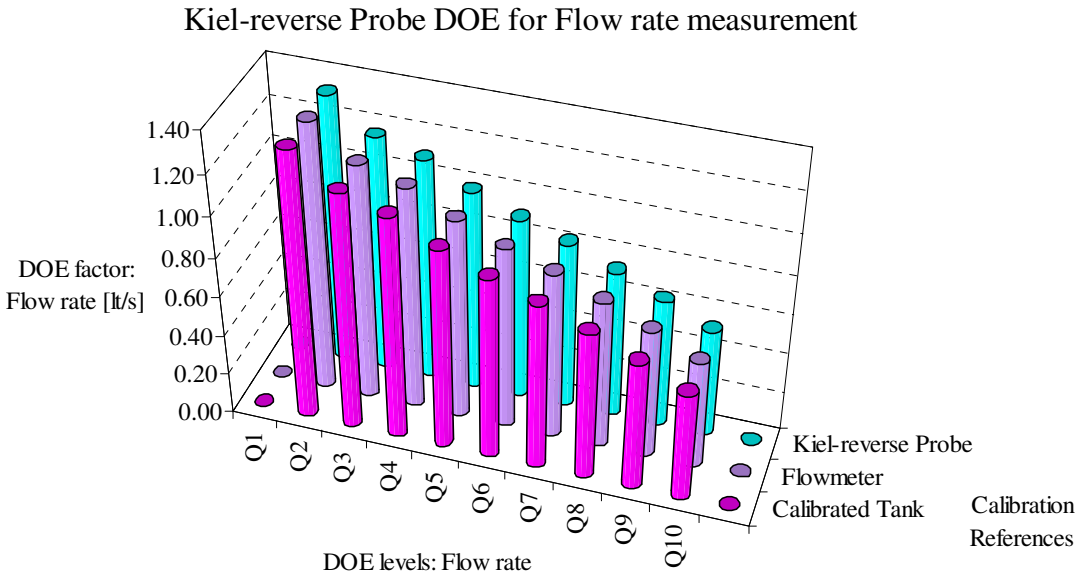

Figure 5-7 Kiel-reverse Probe for Flow Rate measurement: DOE
The Kiel-reverse probe is referenced to the flow meter and the calibrated tank.

Kiel-reverse for Flow rate measurement: Calibration Procedure

The calibration procedure, consists on comparing the flow rate obtained from the Kiel-reverse probe related to the flow rate from the calibrated tank and a rotameter. The flow

diagram Figure 5-8 (a) shows the procedure for determining the flow rate from measurements for each of the mentioned devices; the diagram helps to detect the source of errors in the flow rate determination. For instance, in the diagram of Figure 5-8 it is evident that the Kiel-reverse probe has a long chain of calculus before determining the flow rate, which means a long chain of calculus errors, such as rounded values and formulae assumptions. Therefore, the resulting regression curve from calibration compensates for instruments variability and calculation errors.

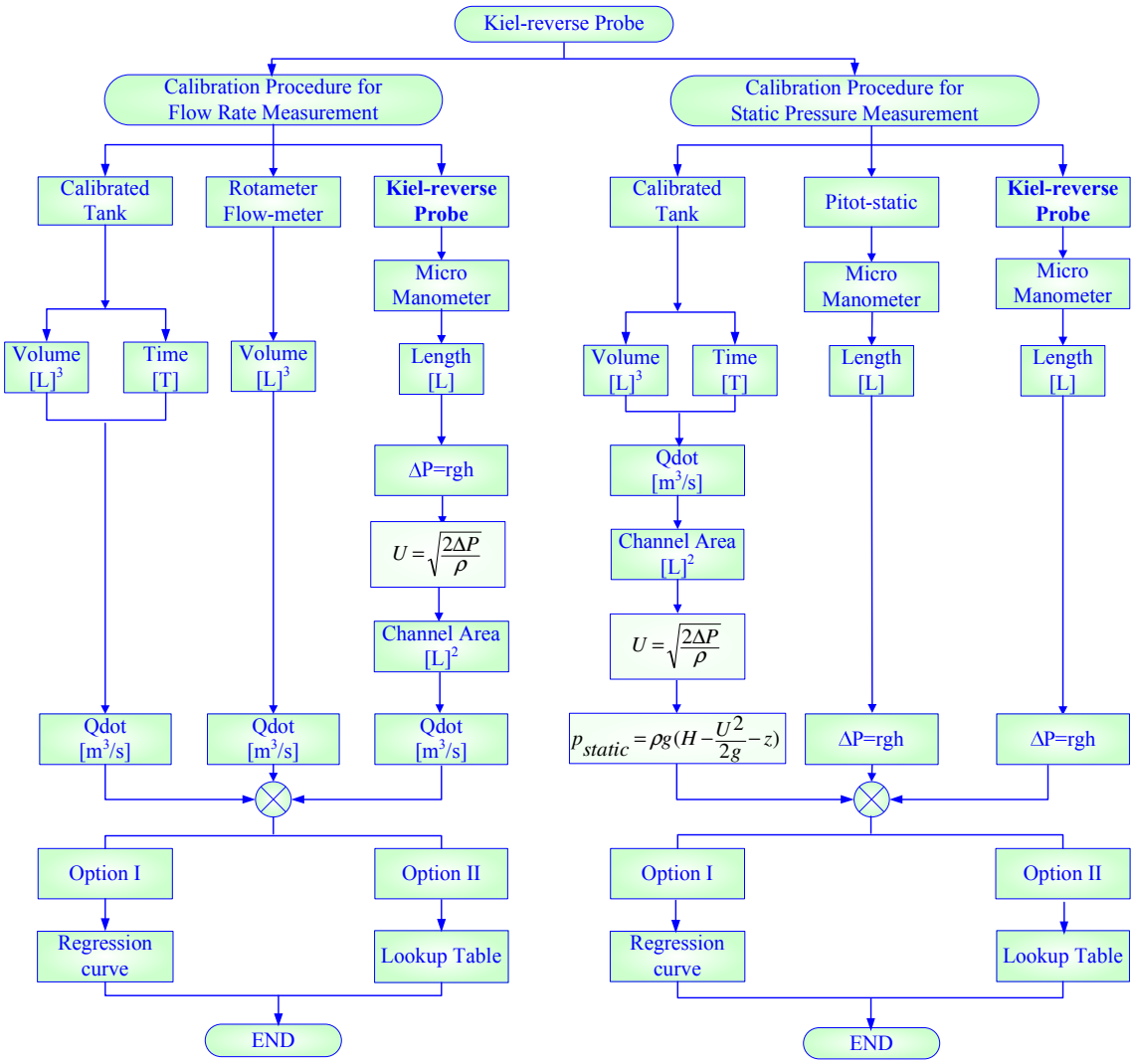

a) Flow Rate Measurement

b) Static Pressure Measurement

Figure 5-8 Kiel-reverse probe: calibration procedure

Flow diagram of the calibration procedure for determining the error in the determination. Procedure for (a) Flow Rate, and (b) Static Pressure measurement.

Kiel-reverse for Flow rate measurement: Data Analysis Procedure

The data analysis procedure for the probe calibration, schematized in the Figure 5-9, consists on data inspection for identifying outliers and to recognize the physical meaning of the plotted data, in particular saturation, offset and zero drift. As the data showed the expected behaviour, the next step is to calculate the parameters for the regression curve and the model assessment through the ANOVA test of significance.

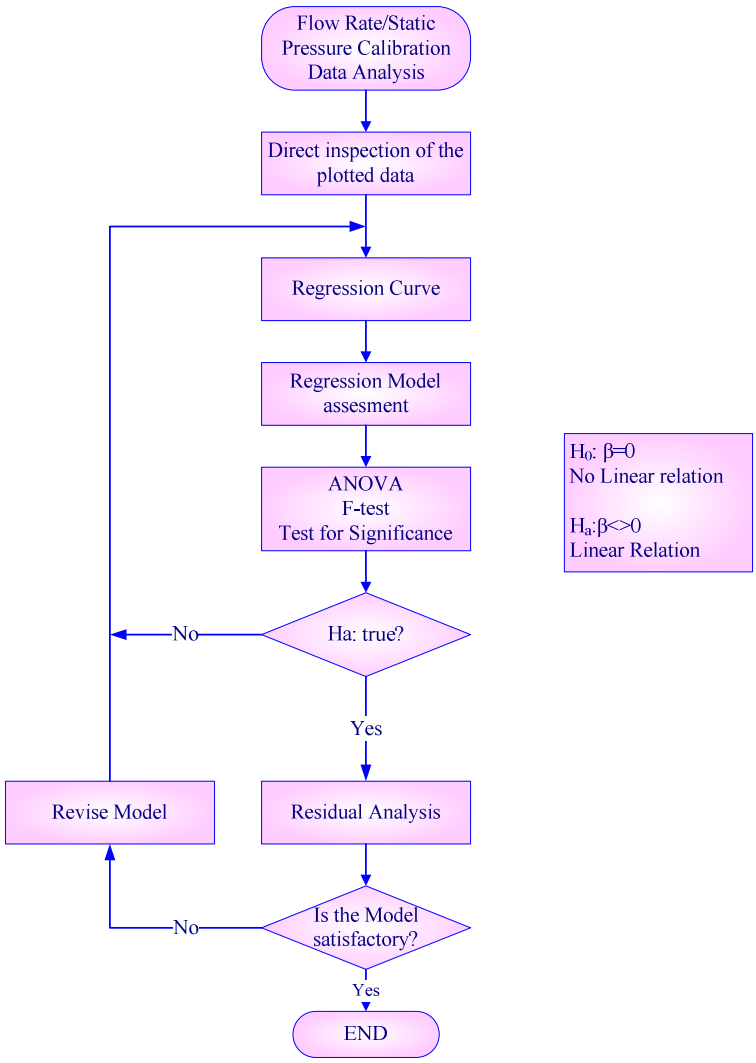

Figure 5-9 Kiel-reverse Probe: data analysis

Flow diagram of the data analysis procedure for flow rate and static pressure calibration

Kiel-reverse for Flow rate measurement: Regression model

The general linear regression model for calibrating the HPR probes, is a linear function of the coefficients z_i, expressed by $y = \beta_{0+} \beta_1 z_{1+\ldots+} \beta_n z_n$, (Keller and Warrack 2000). It is important to note that the regression do not necessarily is a linear function of the variable x, and it is expressed as a general function $z = f(x)$. The general equation for the linear regression is represented by $y=b_0+b_1 z+error$, where b_i is an unbiased

estimator of β_i. The test of significance or analysis of variance ANOVA determines the variability of the slope, parameter $b_{1;}$; slope with very low or null variability means an approximately constant slope and therefore the relationship between the variables is non-linear. Conversely, a slope with other value than zero represents a linear relationship between the variables. The hypothesis test of the ANOVA analysis, the test statistic and rejection rules are presented in Box 5-1 (a) (b), (c) and (d), according to the literature (Keller and Warrack 2000).

Box 5-1 Kiel-reverse Probe for Flow rate measurement: Regression Model

Calibration referenced to collector tank. Best fit, third order regression model

(a) Regression Statistics

Third Order Regression	
Multiple R	0.9988
R^2	**0.9975**
Adjusted R Square	0.9963
Standard Error	**0.0157**
Observations	10

(b) Regression Equation

$$y = 3.2866x^3 - 7.8069x^2 + 6.3519x + 7.3133$$

(c) ANOVA Hypothesis Test

Null hypothesis
H_0: b_1 is constant => nonlinear relationship (not enough evidence to reject H_0)
Alternative hypothesis
Ha: b_1 <> constant => linear relationship (not enough evidence to support the H_0)

(d) Test Statistic

t-test (two tails)

$$t = \frac{b_1}{s_{b_1}}$$

where b_1 is the regression slope, and s_{b1} is the estimated standard deviation of b_1

F-test (one tail)

$$F = \frac{MSR}{MSE}$$

where MSR is the Mean Square of Regression and MSE is the Mean Square of Error

Rejection Rule

Using test statistic: Reject H_0 if $t < -t_{\alpha/2}$ or if $t > t_{\alpha/2}$
Using p-value: Reject H_0 if p-value < α
in this particular case the level of significance $\alpha = 0.05$

Using test statistic: Reject H_0 if $F > F\alpha$
Using p-value: Reject H_0 if p-value < α

(e) ANOVA Test of significance results

ANOVA

	dof	*SS (between)*	*MS (within)*	*F (one tail)*	*Significance F*
Regression [1)]	p: 3	0.6037	0.2012	816.7394	**3.1857E-08 < 0.05**
Residual [2)]	n-p-1: 6	0.0015	0.0002		
Total	n-1: 9	0.6051			

[1)] Explained variations through the regression model
[2)] Unexplained variations through the regression model

(f) Regression Coefficients and test of significance

	Coefficients	*Standard Error*	*t Stat (two tails)*	*P-value*
Intercept	7.3133	0.2983	24.5145	3.0300E-07
Qdot {l/s}	6.3519	1.0248	**6.1982 > 2.447**	**0.0008 < 0.05**
Qdot-squared	-7.8069	1.1226	**-6.9543 < -2.447**	**0.0004 < 0.05**
Qdot-cubic	3.2866	0.3938	**8.3459 > 2.447**	**0.0002 < 0.05**

The regression results for the flow rate measurement using the Kiel-reverse probe are in Box 5-1 (a) and (b), showing the statistic results and the model equation respectively. The third order regression model gave good results, with a coefficient of determination, R^2 (correlation coefficient square(d), equals to 0.9976; showing a third order polynomial relationship between the flow rate measured by the Kiel-reverse probe and the calibrated tank. The model is also assessed by the Standard Error of estimates, 0.016, which is a considerable low error. The first assessment of the third order regression model gave a good estimator for the Kiel-reverse probe calibration(Keller and Warrack 2000).

The next step is a test of significance of the slope for representing the real data, by applying the analysis of variance ANOVA. Results of the test of significance are in Box 5-1 (e), where the significance F (p-valu(e) is 3.186E-08 smaller than 0.05, which is α, the value level of significance. Therefore the null hypothesis H_0 is rejected or not enough evidence to support that the slope is constant; as a result overall model is significant.

The next step consists on assess the coefficients of the regression model, by applying the test of significance, and comparing with the test statistic F-test (one tail), and t-test (two tails), as it was explained in previous paragraphs. Results of the test of significance are in Box 5-1 (f); considering the value from table for $t_{\alpha/2,n-p-1}$ is +/- 2.447, all coefficients accomplish with the rejection of the null hypothesis indicating a linear relationship of the slope of the regression model for the flow rate measured by the Kiel-reverse probe and the calibrated tank.

Kiel-reverse for Flow rate measurement: Residual analysis

As the third order regression model shows a good performance in representing the flow rate measured by the Kiel-reverse probe and the calibration tank, the next step in the calibration procedure (Figure 5-9), is to perform a residual analysis.

The “goodness” of the residuals assures the model contains all the essential features of the real system. Otherwise, if the residuals show dependency from the independent variable, thus there exists a remaining feature in the system still to be included in the model. The “goodness” of the residuals is tested by three features, normal distribution of the residuals, constant variance of the error (homoscedasticity), and independence of the residuals (Keller and Warrack 2000; Anderson, Sweeney *et al.* 2003)

The normal test of the residuals is presented in Box 5-2 (a), (b) and (c). From the direct inspection of the graphs, the residuals do not present a normal distribution. This is derived from the skewed histogram compared with the normal distribution, in Box 5-2 (a), and the quantitative analysis, Lilliefors test, in Box 5-2 (c), which gives a result of 0.096 bigger than the 0.0886, the critical value. The skewed distribution can be explained by the presence of outliers, in particular the first one, when comparing the data with the line for the normal scores, Box 5-2 (b). Although not perfectly normal, the distribution is a close approximation to the normal curve, and the three tests show that the discrepancy is not so remarkable.

The test for constant variance or homoscedasticity, Box 5-2, Figure 2, shows that the variance of the residuals is not constant. However the plots for exploring the independence of the residuals, Box 5-2 Figure 3 (a) to (c), there is no apparent pattern of the residuals in relation to the independent variable.

From these results, the residuals show a distribution close to the normal. The presence of outliers is one of the explanations for the residuals not being purely normal distributed. However, the main reason appears to be in the small sample population, which is deemed to show a non normal distribution. In order to confirm or reject the null hypothesis of normal distribution of the residuals, it would be necessary to perform further tests otherwise to apply a parametric bootstrap with the purpose of increasing the number of samples. This increase could be done in two different ways, inter sample or repetition of the experiment several times. However, given the good results for the third order regression, there is no need of re-sample the data set.

As a result, the third order regression model is good representation of the flow rate measured by the Kiel-reverse probe and the calibrated tank, assessed by the regression statistics and the test of significance of the slope and the model coefficients. However, the residuals of the model are slightly biased from the normal distribution.

Therefore, the normal tests can be regarded as weak grounds for rejecting the null hypothesis of normal distribution of the residuals, avoiding incurring in a type I error of rejecting a null hypothesis that is true. Therefore, the third order regression model is accepted for the calibration purpose of the Kiel-reverse probe as flow measurement.

Box 5-2 Kiel-reverse probe for flow rate measurement: Residual Analysis

Third Order Regression model evaluation: Normal test, Homoscedasticity and residuals Independence.

1. Normal Distribution of Residuals

(a) Histogram

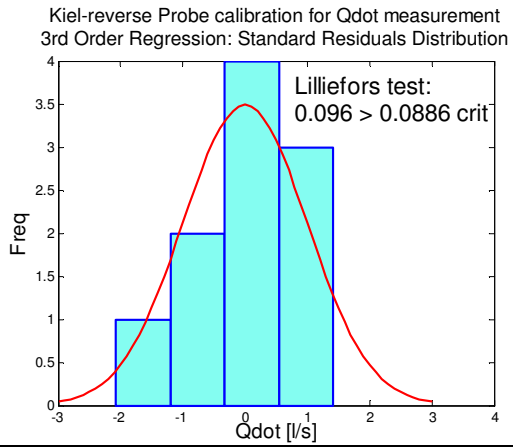

(b) Normal Probability Plot (Normal Scores)

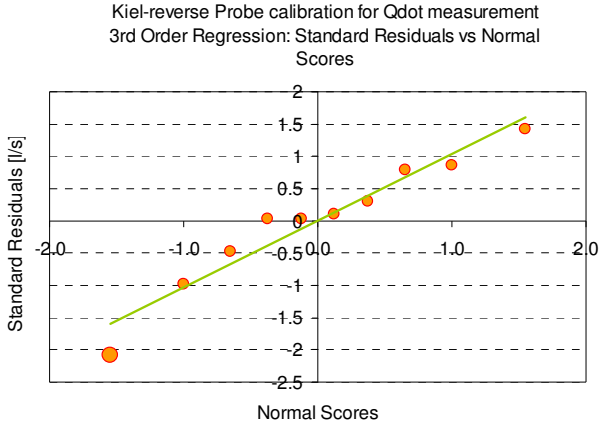

(c) Lilliefors Test of Normality

H_0: X has a Normal distribution with unspecified mean and variance
H_a: X does not have Normal distribution
Rejection rule: $D_{experiment} > 0.0886$ (D critic at 5% significance level)
=> **0.096 > 0.0886 critic**

2. Homoscedasticity (evenly distributed varianc(e)

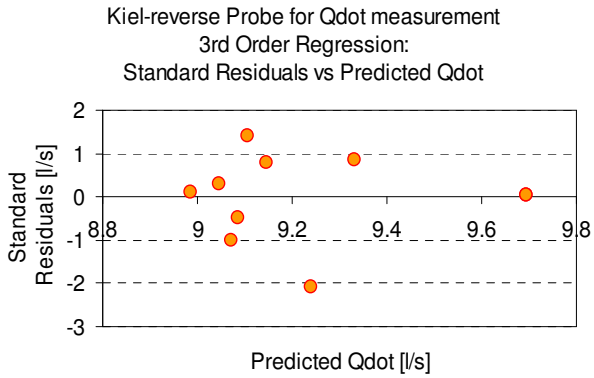

3. Independence of the Residuals:

(a) Residuals vs. Qdot

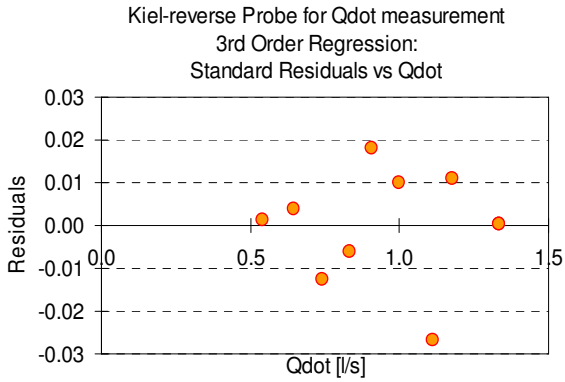

(b) Residuals vs. Qdot2

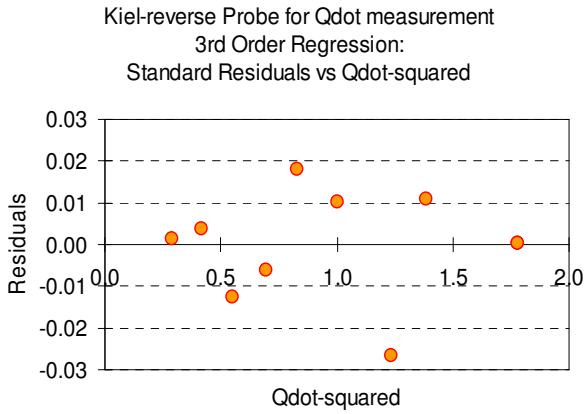

(c) Residuals vs. Qdot3

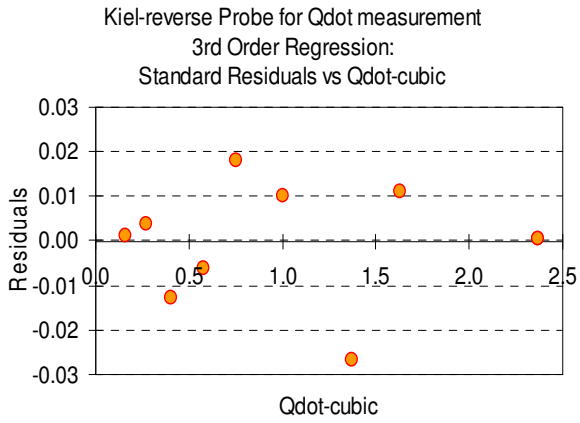

Kiel-reverse Probe for Flow rate measurement: Model for estimation and prediction

The regression results are used for determining the confidence interval for estimating values that lie in the range of the variables. Figure 5-10 shows the confidence and prediction interval. The last one is to contain the predicted values outside the range of the variables, represented by big circles in the figure; this is the reason for the prediction interval to be wider compared with the confidence interval to account for the uncertainty of the predicted values.

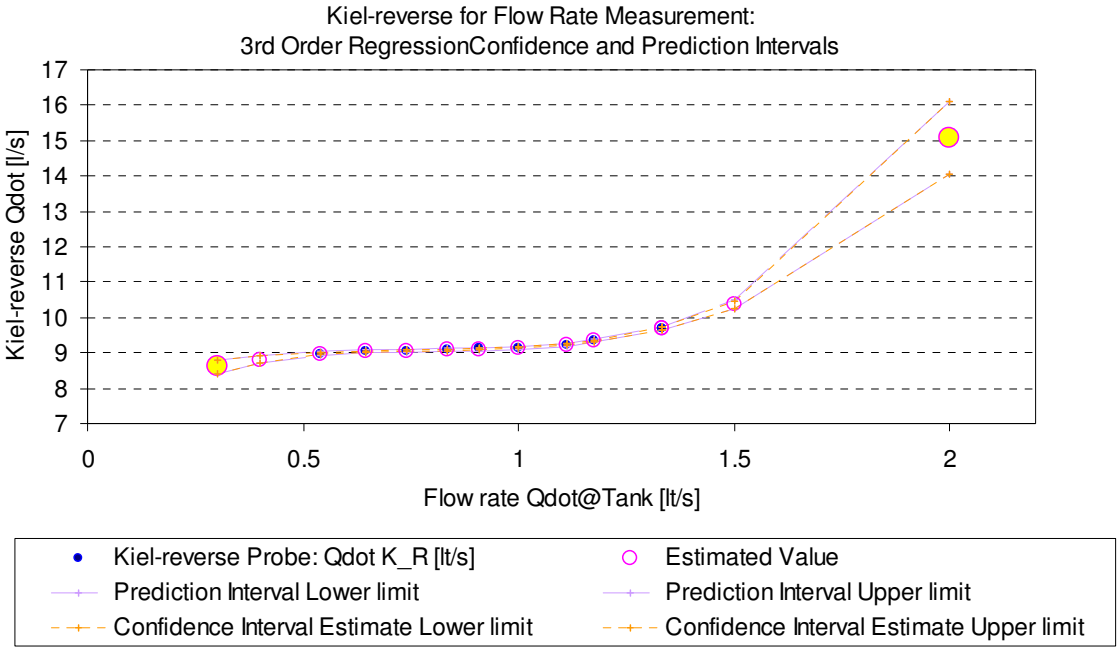

Figure 5-10 Kiel-reverse probe for Flow rate measurement: regression model

Inside the confidence interval (0.5, 1.5) {lt/s}, the estimated values are good approximated by the Third order regression curve. While outside this interval the predicted values have a slightly wide range of uncertainty in the determination of the flow rate.

Calibration 2: Kiel-reverse probe for Static Pressure measurement

The calibration procedure for the Kiel-reverse for static pressure measurement is fundamental because, as the theory reports and the simulation in Figure 5-4 confirms, the static pressure is slightly lower than the actual static pressure (Massey 2006). Therefore the calibration outcome is to determine the extent of the reported difference.

Calibration 2. Kiel-reverse for Static pressure measurement: DOE

The design of experiments DOE for the Kiel-reverse probe, Figure 5-11, for static pressure measurement is planned to explore the static pressure at different levels of flow rate, measured by the Kiel-reverse probe and the Pitot-static tube.

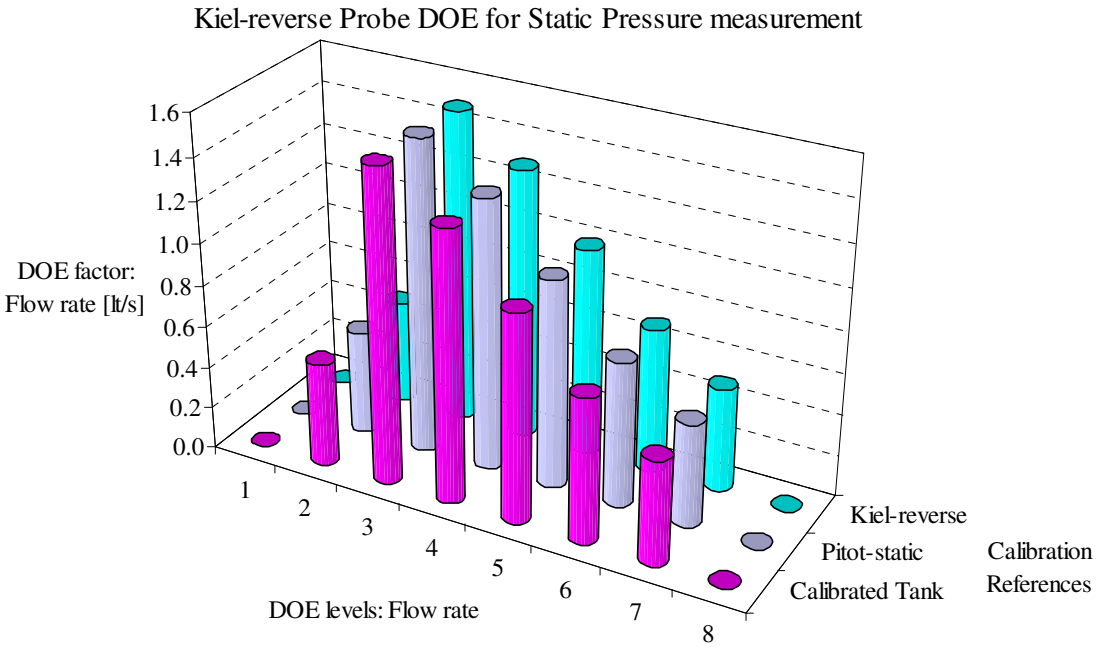

Figure 5-11 Kiel-reverse Probe for Static Pressure measurement: DOE
The probe is referenced to a Pitot-static tube and calibrated tank.

The qualitative results of the trials experiment of the Kiel-reverse probe for flow rate measurement, from previous section, are also valid for the probe measuring only static pressure. The objective of the present experiment is to explore the behaviour of the static tap, the down stream orifice so as to determine the correction factor of the Kiel-reverse probe measuring static pressure.

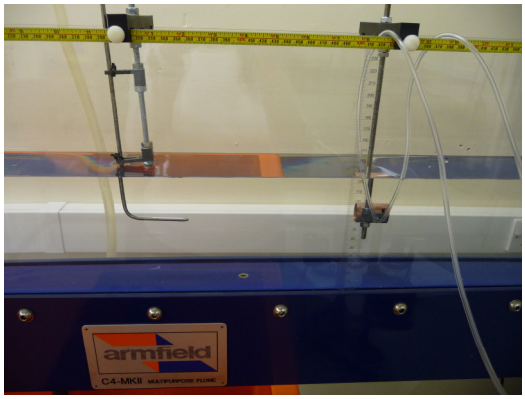

(a) Kiel-reverse and the reference Pitot-tube: setting for calibration

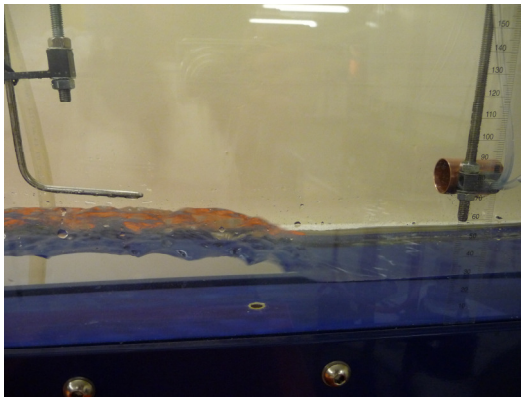

(b) Hydraulic jump for simulating surge effects of the pipeline environment.

Figure 5-12 Kiel-reverse Probe, calibration settings

.Kiel-reverse for Static pressure measurement: Calibration Procedure

The calibration procedure consists on comparing the static pressure measured by the Kiel-reverse probe, the Pitot-static tube and the calculated pressure using the

Bernoulli's equation from calibrated tank. The calibration procedure for obtaining the static pressure is depicted in Figure 5-8 (b). Figure 5-11and Figure 5-12 shows pictures of the Kiel-reverse and Pitot-static probes in the Armfield Multipurpose Flume C4-MKII. Figure (a) shows both probes aligned by the centre line in a steady stream. Figure (b) shows the hydraulic jump for testing the response of the probe to water surges (upstream at the right and the static hole of the Kiel-reverse probe is in the left side of the prob(e).

Bernoulli's equation application is for frictionless inviscid fluids, to constant density steady flow, and to any streamline sharing the same pressure, velocity and elevation conditions (Massey 2006). Despite the calibration environment for the Kiel-reverse probe is far from the ideal, Bernoulli's equation is a general frame for probe calibration.

Kiel-reverse for Static pressure measurement: Data Analysis Procedure

Figure 5-13 shows the comparison between the static pressure measured by the Kiel-reverse probe, Pitot-static tube and the calculated static pressure. The plotted data span the measured range as it was depicted in the Figure 5-11 of the design of experiment. Increasing and decreasing flow rate (filled and hollow marks respectively) indicate similar path. The last point of the descending range of the Kiel-reverse is considered an outlier because it is far not only from the full set of measurements of the Kiel-reverse probe but also it is far from the Pitot-static tube range.

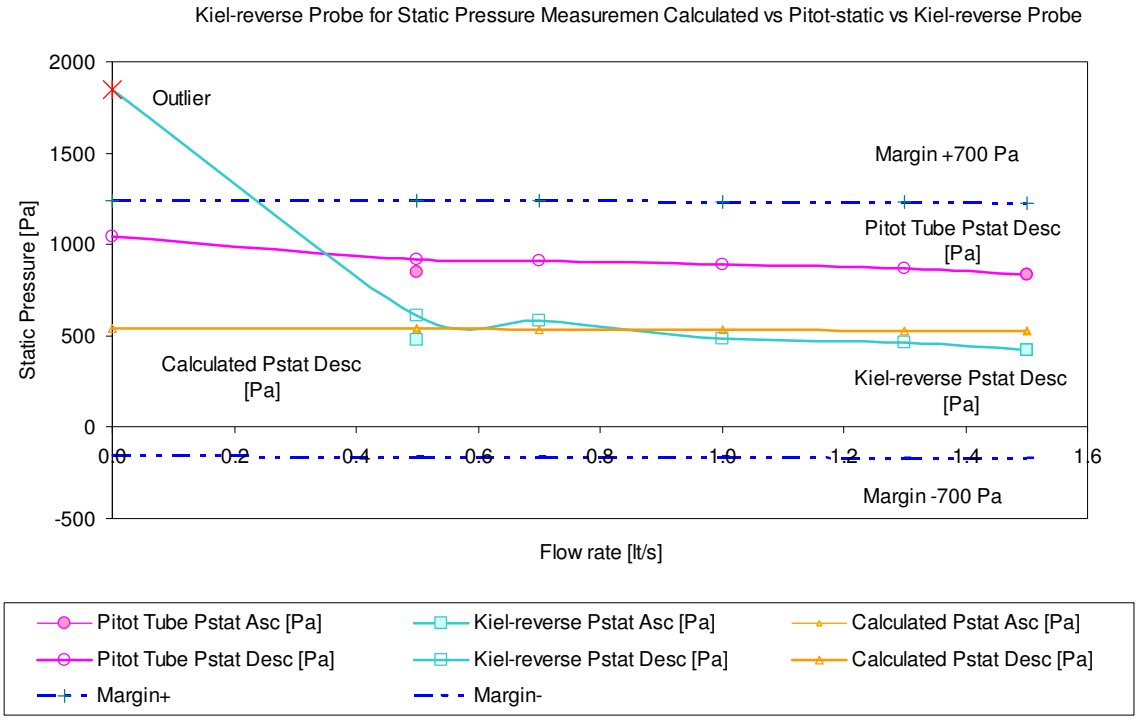

(a) Kiel-reverse static pressure of the same order as the calculated pressure, compared with the Pitot-tube, which is slightly higher. All curves fall within the range of +/- 700 Pa (All curves sharing main y-axis) compared with Pitot-static tube and the calculated static pressure.

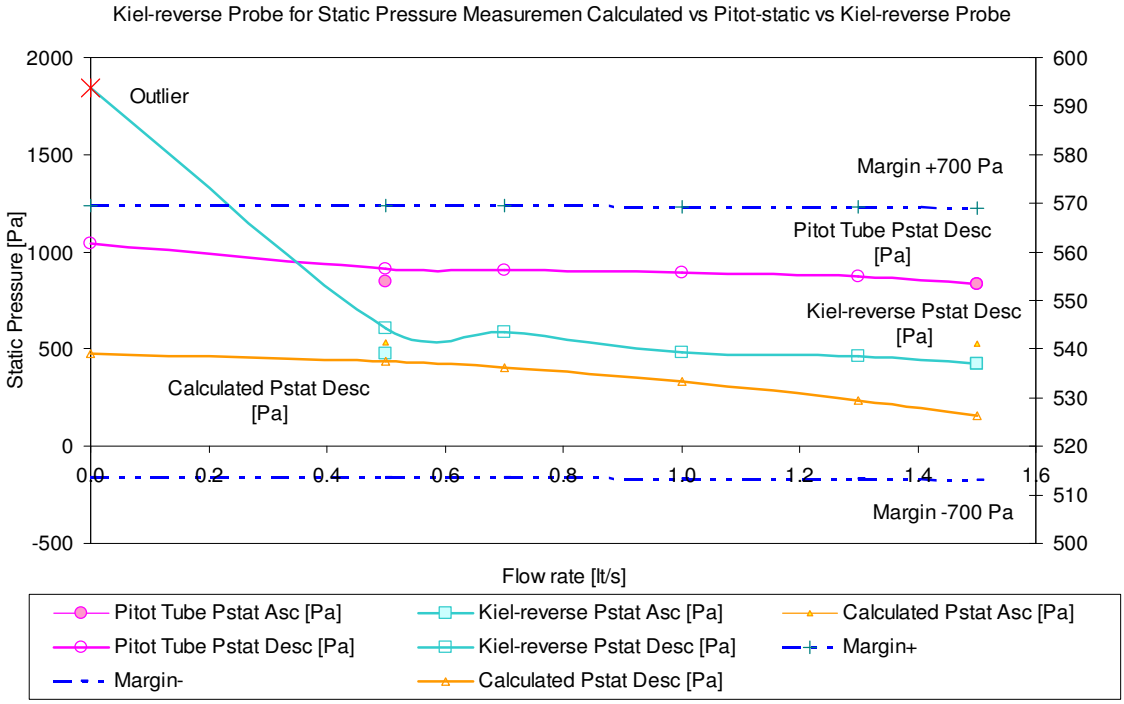

(b) Same as (a) but calculated pressure is in the secondary axis for better observation of the curves behavior

Figure 5-13 Kiel-reverse probe for Static pressure measurement: data inspection

.

Figure 5-13 shows that the calculated and measured static pressure by the Kiel-reverse probe have similar behaviour, and same order, for the flow rate range between 0.5 and 1.5 lt/s. However, the Pitot-static tube gives higher values, on average 344 Pa above the calculated static pressure. From the theory (Massey 2006), it is expected a lower static pressure for the Kiel-reverse probe than the real one; and the results are consistent with the theory and the simulation. Despite these differences, all curves fall inside the margin given in the theory for pressure measurement, which is +/- 700 Pa with respect to the calculated pressure (Japikse and Baines 1994). As a conclusion, both probes, Kiel-reverse and Pitot-static tube give consistent pressure measurement; and the Kiel-reverse probe gives closer values to the calculated one. Figure 5-13 (b) shows the calculated value in a secondary axis so it can be appreciated the decreasing trend of the calculated pressure as the flow rate increases and the measurement from the probes are all consistent with the calculated.

Kiel-reverse for Static pressure measurement: Regression model

The calibration curve is based on the second order regression model between the Kiel-reverse probe and the calculated static pressure. The results of the regression are presented in Box 5-3 (a). The coefficient of determination R squared is 0.973 and the adjusted value with respect to the degrees of freedom is 0.9465, indicate a good strength of the linear relationship between the measurements from Kiel-reverse probe and the calculated static pressure. The standard error of estimates is approximately 1.1, which indicates the model is a close approximation of the real values.

The ANOVA test of significance, Box 5-3 (c), shows that the overall relationship between the static pressure from Kiel-reverse probe and the calculated values is significant (p-value 0.03 < 0.05) therefore the second order model is a good representation for calibration purpose.

Box 5-3 Kiel-reverse Probe for Static Pressure measurement: Regression Model

Calibration referenced to Pitot-tube. Best fit, second order regression model

(a) Regression Statistics

Second Order Regression Statistics	
Multiple R	0.9865
R^2	0.9732
Adjusted R Square	0.9465
Standard Error	1.0950
Observations	5

(b) Regression Equation

$$y = -0.0003x^2 + 0.3961x + 416.95$$

(c) ANOVA Test of significance

	dof	SS	MS	F	Significance F
Regression [1)]	p 2	87.2074	43.6037	36.3679	0.0268 < 0.05
Residual [2)]	n-p-1 2	2.3979	1.1990		
Total	n-1 4	89.6054			

[1)] Explained variations through the regression model
[2)] Unexplained variations through the regression model

(d) Regression Coefficients and test of significance

	Coefficients	Standard Error	t Stat	p-value
Intercept	416.9543	43.5142	9.5820	0.0107 < 0.05
Kiel-reverse Pstatic {Pa}	0.3961	0.1702	2.3274 < 4.3	0.1454 > 0.05
Kiel-reverse $Pstatic^2$ {Pa}	-0.0003	0.0002	-1.9972 > -4.3	0.1839 > 0.05

The regression coefficients are listed in the Box 5-3 (d), although the p-values of the independent variable are not significant (0.14 and 0.18 are greater than 0.05), they have relatively low standard errors; all that means the second order regression shows an improvement to the first order regression in terms of the ability of the second order equation to represent the relationship, given through R-squared and the residuals. The first order regression is in Appendix B in order to compare.

Kiel-reverse for Static pressure measurement: Residual analysis

The goodness of a model is evaluated by residual analysis, requiring normal distribution, even error variance and independence of the residuals from the independent variable. The residual analysis is described in Box 5-4. The normal test is represented by the histogram figure (a) compared with a normal distribution, which shows a symmetrically distribution of the residuals with respect to the mean value. This effect is also reinforced by the plot of the residuals with respect of the standard scores in figure (b), which shows the residuals are generally close to the normal score line. The normal distribution of the residuals is also evaluated by the Lilliefors test of

normality that gave zero, which is lower than the critical value of the test of 0.086. The hypothesis test and the result for the Lilliefors test are in the figure (c).

Box 5-4 Kiel-reverse probe for Static Pressure measurement: Residual Analysis

Second Order Regression model evaluation: Normal test, Homoscedasticity and residuals Independence

1. Normal Distribution of Residuals

(a) Histogram

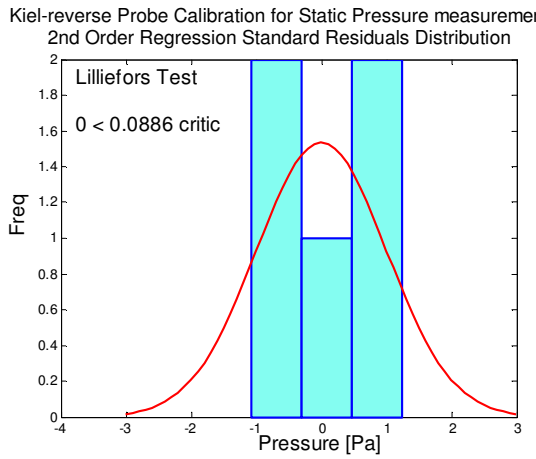

(b) Normal Probability Plot (Normal Scores)

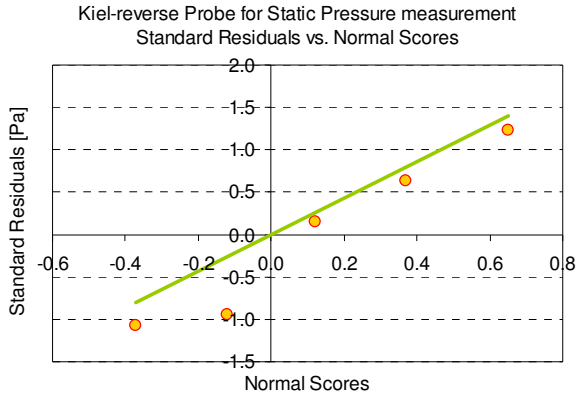

(c) Lilliefors Test of Normality

H0: X has a Normal distribution with unspecified mean and variance
Ha: X does not have Normal distribution
Rejection rule: Dexperiment > 0.0886 (D criti(c) => 0 < 0.0886 critic

2. Homoscedasticity
(evenly distributed varianc(e)

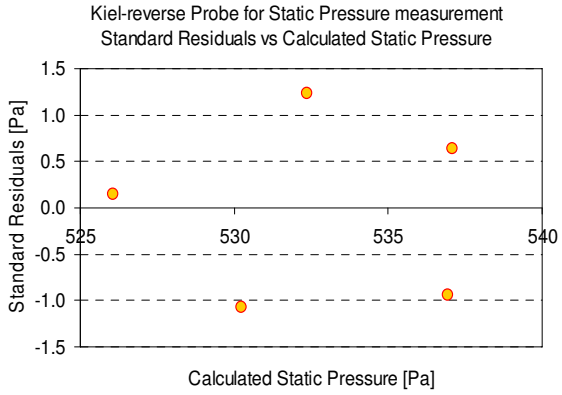

3. Independence of the Residuals:

(a) Residuals vs. Qdot

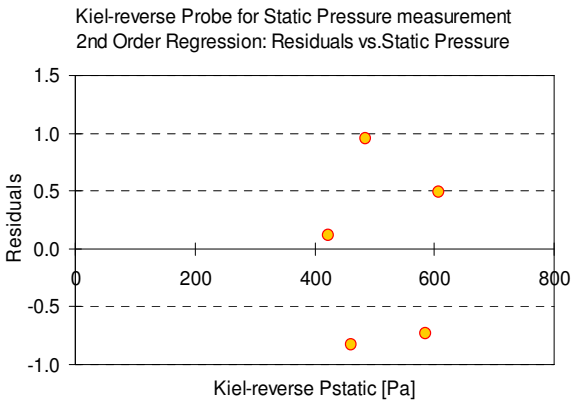

(b) Residuals vs. Qdot^2

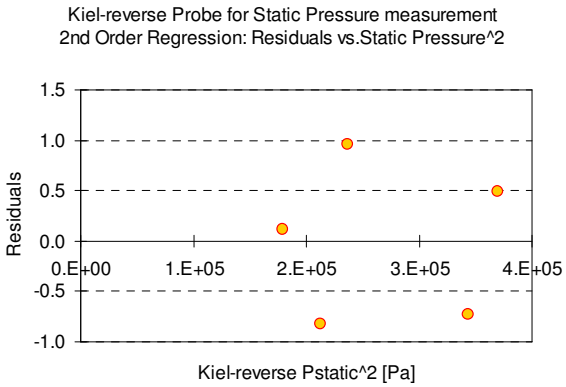

The homoscedasticity or evenly distribution of the residuals variance is plotted in figure 2 and it shows a reasonable distribution of the residuals. In relation to the independence of the residuals, no particular pattern can be described from the residual plot as a function of the independent variable and the squared value of the static pressure from the Kiel-reverse, plotted in he figure 3, (a) and (b) respectively. As a result the good distribution of the residuals reinforces the goodness of the second order regression model to describe the relationship between the static pressure measured by the Kiel-reverse probe and the calculated data.

Kiel-reverse for Flow rate measurement: Model for estimation and prediction

The second order regression model is used for determining the confidence interval for estimating values in the range of the model data, these values are plotted in the Figure 5-14 where the estimated values are compared with the calculated showing a close approximation of both sets. The model also is used for calculating the prediction interval so as to predict values outside the data range. In the figure the predicted values are bigger circles. The prediction interval broadens noticeable so as to account for an increase of the uncertainty in the prediction.

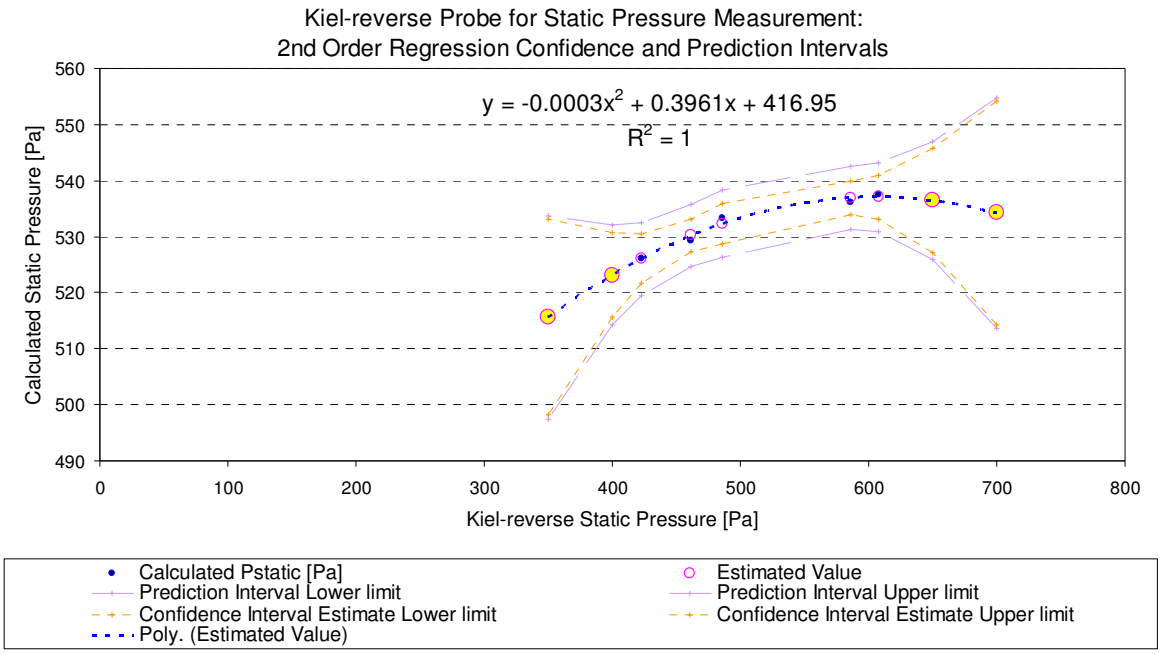

Figure 5-14 Kiel-reverse probe, static pressure measurement: regression model

Inside the confidence interval (400, 600) {Pa}, the estimated values are good approximated by the Second order regression curve. While outside this interval the predicted values have a wide range of uncertainty in the determination of the static pressure.

5.2.2. Pitot-Gracey probe for static and stagnation pressure

The Pitot-Gracey probe was the first design made by the author with the purpose of an on-board measurement of stagnation and static pressure. The Pitot-Gracey probe characteristics are based on the standard Pitot-static tube and design concepts published by William Gracey in his detailed study about on-board aircraft's pressure measurement (Gracey 1980). The probe dimensions are directly related to the pipeline diameter and the probe proximity to the HPR with the purpose of compensate for boundary layers. Figure 5-15 (b) shows the 3D concept design of the Pitot-Gracey probe.

The probe has a static pressure chamber where converge the static holes. The size of the chamber and the number and size of the static taps have been selected to produce rapid response of the probe to changes in the flow rate and the trade off of repeatability, which is compromised by potential blockages of the chamber. Figure 5-15 (a) and (b) show different views of the probe fabricated at the Mechanic workshop of Durham University; more details of the probe on Appendix B.

(a) Pitot-Gracey probe's retracted position of the front intake, for stagnation pressure measurement, lowers the sensibility to probe's misalignments.

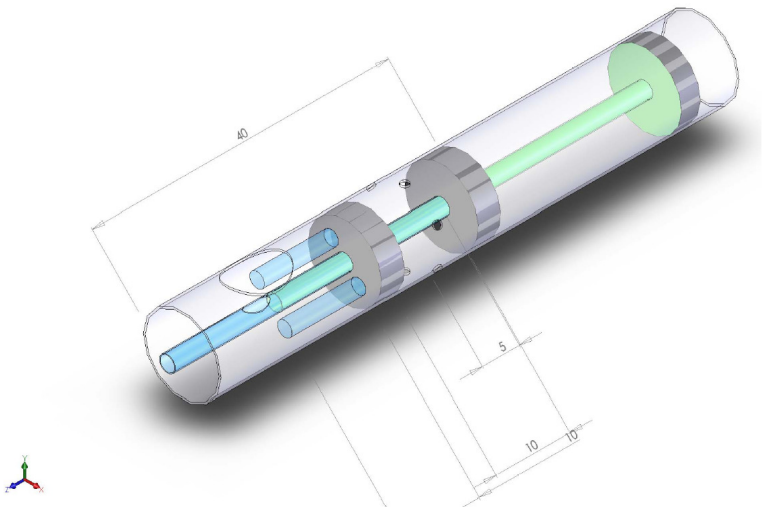

(b) Pitot-Gracey Probe design inert structure of static pressure chamber, enclosed by the two grey seals, and surrounded by the static holes. The grey seal in the front is to lower the sensibility of the probe to misalignments.

Figure 5-15 Pitot-Gracey Probe design.
Details of the probe for Static and Stagnation Pressure measurement.

Figure 5-15 (a) show details of Pitot-Gracey front pressure intake, which is the core feature of the probe and it refers to the distance of the tip of the probe to the front section of the cylinder, with the purpose of improving the probe sensibility to errors due to misalignment. This feature is the findings of Kiel for his probe and it was referred in previous paragraphs for the design of the Kiel-reverse probe. The shape of

the probe front has been selected to reduce errors and to increase the probe sensibility to pressure gradients.

The Pitot-Gracey probe was tested in the open channel Armfield as it is depicted in Figure 5-15. However, the probe showed a poor time response; saturation problems were the origin of zero drift and slow response, making the repeatability nearly impracticable. The source of the poor performance is attributed mainly to two reasons: firstly the small tubing diameter, and secondly the absence of bleeding contributed to the saturation of the static chamber. The alternatives to solve the problem were to improve the Pitot-Gracey design or to design a new concept model for the probe. The decision was to design a new probe, the Kiel-reverse probe, for efficiency of the pressure measurement.

5.2.3. Pressure Measurement Chamber: pressure at the wake of the turbine

The pressure drop across the turbine is one of the parameters required in the determination of the turbine efficiency. Therefore, the pressure drop consists on the measurement of the static pressure at the front and the wake of the turbine. The first has been analysed in 5.2.1, and this section deals with the static pressure measurement at the wake of the turbine.

As it was discussed in section 5.2, the static pressure can be measured where the stream lines are parallel and free from velocity gradients. So, the turbine wake is far from the ideal for that purpose, due to mainly three sources of turbulence, the rotation of the turbine blades, the reciprocating locomotion of the tractor and the rotation of the rotation of the turbine shaft inside the hollow universal joint.

Therefore, in order to measure the static pressure at the turbine wake it was necessary to create a streamlined flow while minimising the velocity gradients. Based on principles of wind tunnels conditioning, the author designed a customised device, which acts as flow straightener and measurement point, denominated Pressure Measurement Chamber. This is justified by the fact that, to the author's best knowledge, there is neither similar device available from the market, nor similar previous design, despite the simplicity in concept.

The Pressure Measurement Chamber (PM(C) consists on a cylindrical Perspex chamber, with static pressure taps. The PMC diameter matches the diameter of the turbine gear box cover, and the length fits exactly in the turbine wake. Therefore, the PMC creates a streamlined path for the flow concurring from the turbine and bounced

by the tractor; and creates also stream lines parallel to the pipe wall, minimising in that way the velocity gradients. Figure 5-16 shows details of the PMC design and the location of the chamber at the wake of the turbine.

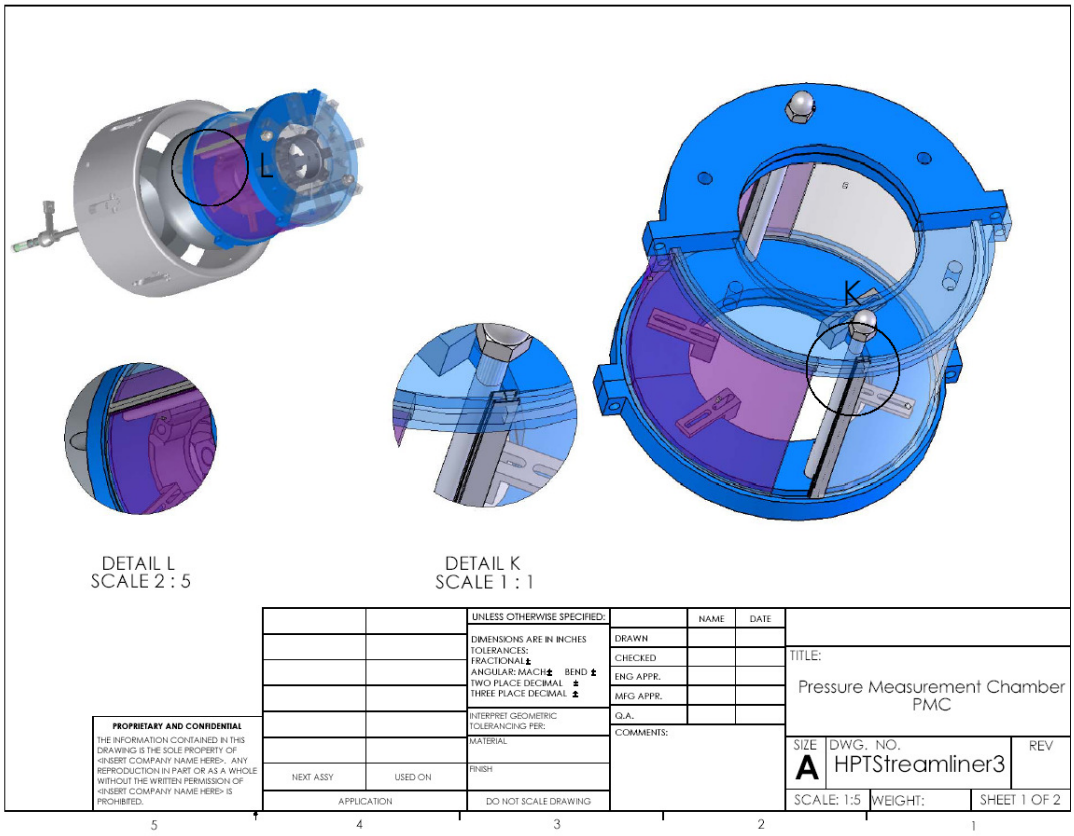

Figure 5-16 Pressure Measurement Chamber PMC design details

Design details, location of the chamber at the back of the turbine, and structure of the chamber in two halves for easy assembly enclosing the hollow universal joint.

The chamber is sealed so as to divert the total flow outside of the cylinder to improve the accuracy of the pressure reading by minimizing the flow trap in gaps. It also acts as a protection of the strain gauges of the universal joint from the pipeline environment. The pressure taps are located in the middle cross-section of the chamber with the purpose of compensating the disturbances from the turbine and the tractor.

Figure 5-17 (a) shows the finite element simulation of the flow surrounding the PMC. The simulation was performed inside an artificial control volume of dimensions big enough for housing the turbine, the universal joint and the flange where the tractor is attached. The tractor in itself is not included in the simulation so as to simplify the computational effort of all complex mechanical parts. However, for the purpose of evaluating the PMC surrounding flow, the mentioned settings are sufficient.

The simulation results are consistent with the assumption about the chamber as a suitable way of flow conditioning. This is denoted by the fairly parallel and even colour

of the flow lines, implying nearly constant flow velocity in the turbine wake. The good results of the simulation are verified by calibrating the probe in the next section.

Calibration 3. Pressure Measurement Chamber PMC: Design of Experiment DOE

Figure 5-17 (b) show the PMC in the calibration tank, with closed ends to emulate the presence of the turbine gear box in one end, and tractor flange in the other.

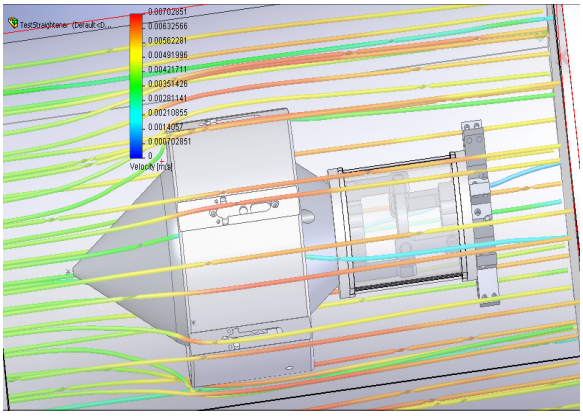

(a) PMC flow passing the turbine simulation in SolidWorks. Streamlined flow at the turbine wake

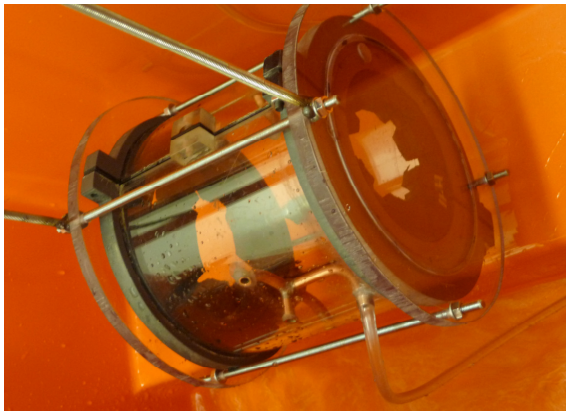

(b) PMC inner copper tubing arrangement for fluid bleeding

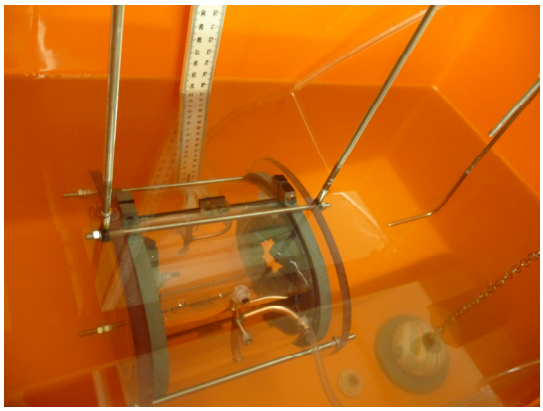

(c) PMC referenced to a Pitot-static tube (at the right), immersed in the collector tank

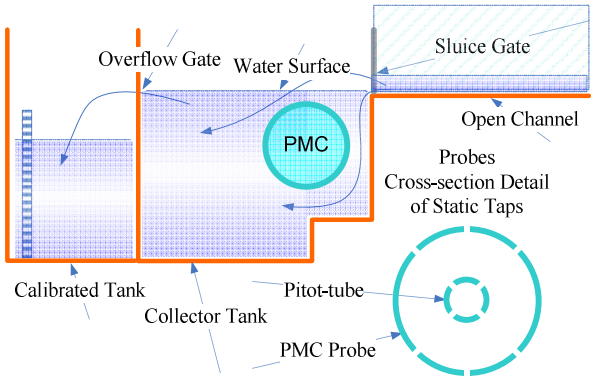

(d) PMC sketch of the calibration layout for turbulence simulation and sectional view of the static holes arrangement for the PMC and Pitot-tube

Figure 5-17 Pressure Measurement Chamber: simulation and calibration

.

Figure 5-17 (c) and (d) show the PMC and Pitot-static tube arrangement in the collector tank, and the respective sketch of the calibration layout in the Armfield Multipurpose Flume C4-MKII. The irregular contour of the tank and the discharge flow from the flume help to create turbulence, emulating the turbine wake, with complex velocity gradients surrounding the PMC.

Following the literature recommendation, the PMC static holes are arranged symmetrically distributed around the probe, so as to measure the average pressure (Logan 2003). The PMC and the Pitot-static tube are located concentrically in the collector tank of the flume, in such a way that the arrangement of static holes of each probe, gives the mean pressure at this central point, despite the differences between the probes' diameter, and number of the static holes (PMC has 6 taps and Pitot-tube 4). The static holes distribution is depicted in the sketch of the Figure 5-17 (d).

The designs of experiment DOE, for calibrating the PMC probe, consists on varying the flow rate in successive steps, and measure the static pressure from the PMC and Pitot-static tube. Figure 5-18 shows the DOE levels. The sudden increase of flow rate, between the first and second run, labelled in the Figure as Q1 and Q2, simulates a water hammer, which is of particular interest to register the probe speed response and after-shock readings.

Pre-test trials have been performed so as to calibrate the instruments and explore the PMC response. Design and calibration of the PMC's tubing are described in Appendix B.

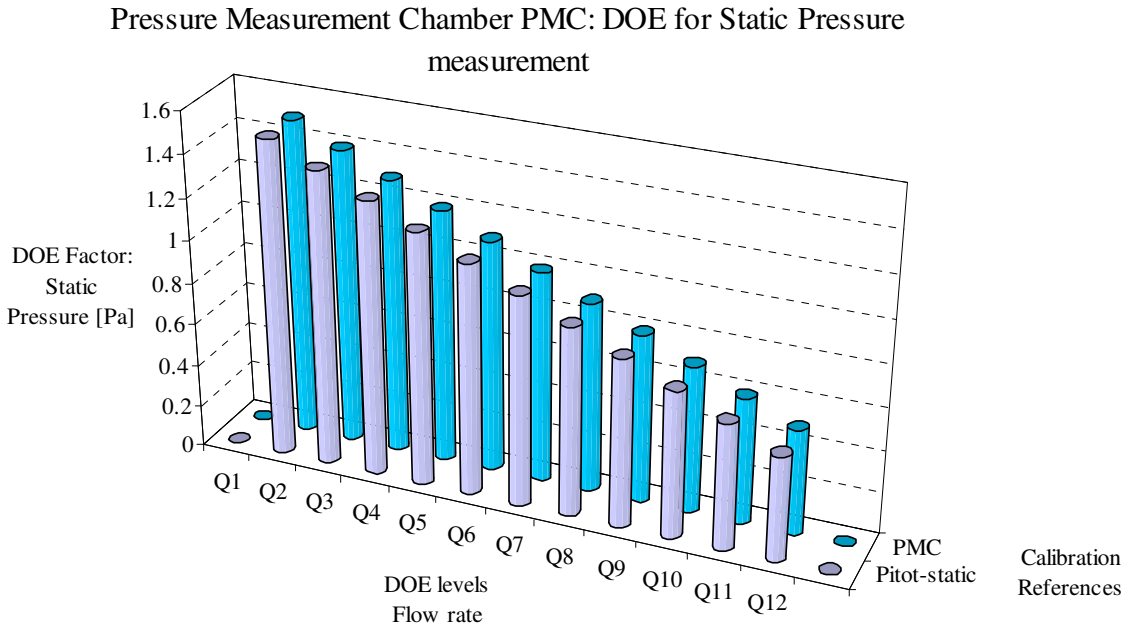

Figure 5-18 Pressure Measurement Chamber PMC: DOE
The PMC probe is referenced to a Pitot-tube.

PMC for Static pressure measurement: Calibration Procedure

The calibration procedure of the Pressure Measurement Chamber PMC consists on comparing the static pressure measured by the PMC, the Pitot-static tube and the

theoretical static pressure, which is obtained by applying Bernoulli's equation, based upon the measured flow rate in the calibrated tank. The Figure 5-19 shows the calibration procedure for determining of the static pressure and helps to visualize the source of errors incurred in the chain of calculus for the static pressure determination.

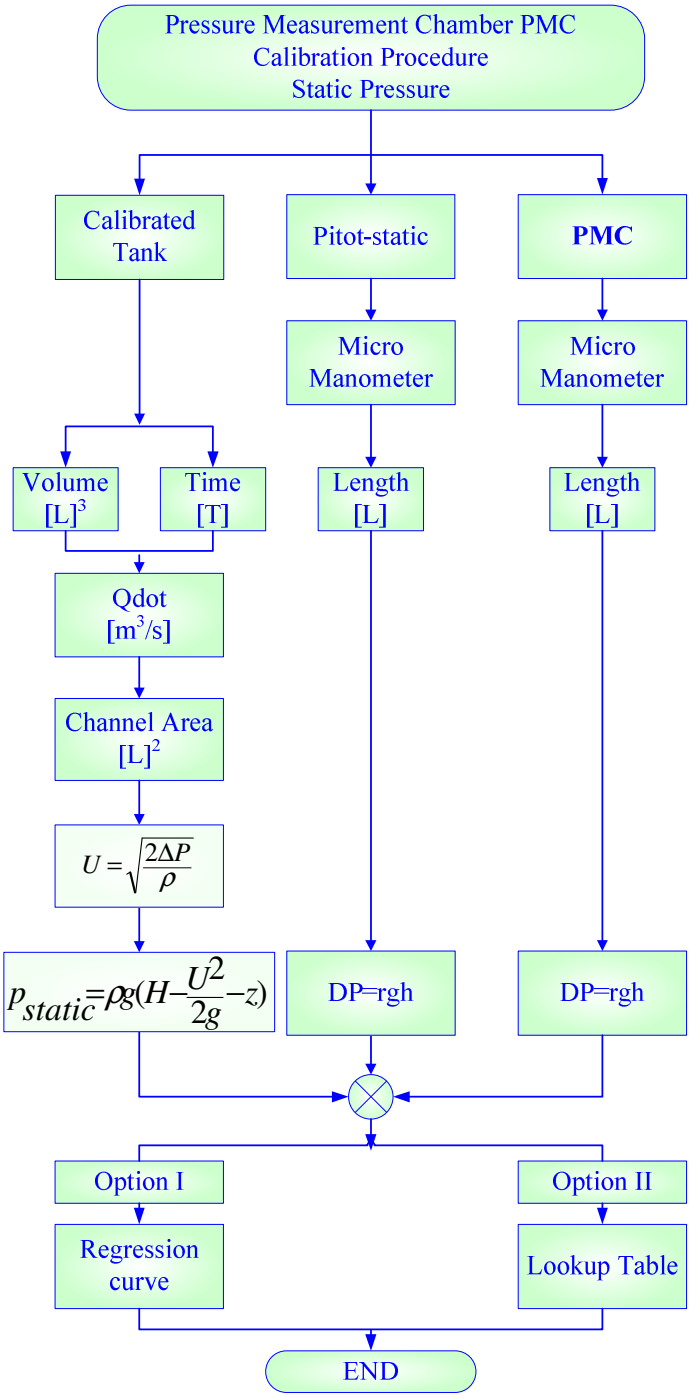

Figure 5-19 Pressure Measurement Chamber PMC: calibration procedure

Flow diagram of the calibration procedure for determining the error in the determination.

PMC for Static pressure measurement: Data Analysis Procedure

The data analysis procedure for the PMC probe is similar to the one described for the Kiel-reverse probe Figure 5-9, and it starts with a simple data inspection for identifying outliers and physical meaning of the data from calibration plotted in Figure 5-20. From this Figure, the curves of static pressure for the PMC and Pitot-static tube show similar behaviour though both are proportional. However, the two curves are inside the tolerance margin of 700 Pa for the calculated static pressure, as it is suggested in the literature as an acceptable margin for pressure measurement (Japikse and Baines 1994). It is important to note that the calculated pressure is referred to the secondary axis so as to magnify the trend of the curve.

As a conclusion from the data inspection, there is no significant difference among the static pressure measured by the PMC, Pitot-static tube and the calculated pressure, at least for the purpose of the present experiment. Therefore, the data analysis is designed to compare the data from the PMC and calculated static pressure, with the purpose of eliminating typical errors of the Pitot tube.

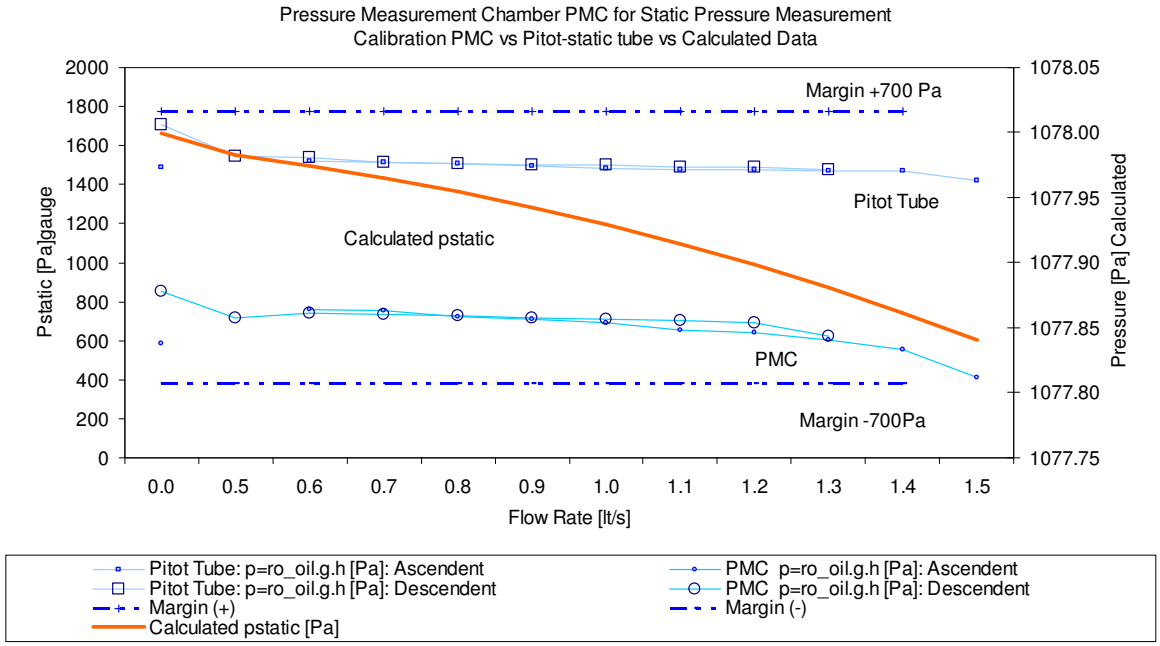

Figure 5-20 Pressure Measurement Chamber PMC: direct data inspection.

Comparison of the static pressure measured by the PMC and Pitot-static tube referenced to the calculated static pressure, the three curves fall within the recommended {+/- 700 Pa} margin for pressure measurement

PMC for Static pressure measurement: Regression model

Given the close approximation of the static pressure measured by the PMC to the calculated pressure, the regression model is designed to explore this relationship. The

first order regression gave good coefficient of determination R^2 of 0.988 and a low standard error of estimates (error in the model) of 0.004, and no higher degree models are explored for this particular case. Therefore, the first order regression is selected for the calibration of the PMC probe. The regression statistics and first order regression model are summarised in the Box 5-5 (a) and (b).

The ANOVA test of significance, Box 5-5 (c) gives strong evidence (p-value=0 < 0.05 at 95% of significanc(e), for concluding that the model is a good representation of the relationship between the pressure measured by the PMC probe and the calculated value. Regression coefficients, Box 5-5 (d), are evaluated by the test of significance (p-value 0<0.05) and the standard error (SE=0), therefore the slope of the model is significant too.

Box 5-5 Pressure Measurement Chamber: Regression Model

Calibration referenced to Pitot-tube. Best fit, first order regression model

(a) Regression Statistics

First Order Regression Statistics	
Multiple R	0.9941
R^2	0.9882
Adjusted R Square	0.9865
Standard Error	0.0045
Observations	9

(b) Regression Equation

$$y = 0.0006x + 1077.5$$

(c) ANOVA Test of significance

	dof	SS	MS	F	Significance F
Regression [1)]	p:1	0.0120	0.0120	584.5432	0.0000 < 0.005
Residual [2)]	n-p-1: 7	0.0001	0.0000		
Total	n-1: 8	0.0121			

[1)] Explained variations through the regression model
[2)] Unexplained variations through the regression model

(d) Regression Coefficients and test of significance

	Coefficients	Standard Error	t Stat	P-value
Intercept	1077.5465	0.0157	68586.3177	0.0000 < 0.005
PMC Pstat {Pa}	0.0006	0.0000	24.1773	0.0000 < 0.005

PMC for Static pressure measurement: Residual analysis

The regression model goodness is complemented by the evaluation of the residuals, and therefore they need to show a normal distribution, evenly distributed residual variance and independence of the residuals from the independent variable.

The residuals analysis for the first order regression for the PMC probe and calculated static pressure values are in the Box 5-6. Figure 1 (a), shows the normal distribution of the residuals compared to the normal (0,1) curve. The normal

distribution is verified by the plot of the standard residuals and the normal scores in the Figure 1 (b), showing the residuals are closely distributed to the line of normal scores. The normal distribution is also verified by the Lilliefors test that gives zero, which is minor than 0.0886, the critical value for the test of normality, Figure 1 (c).

Box 5-6 Pressure Measurement Chamber: Residual Analysis.

First Order Regression model evaluated by Normal distribution test, Homoscedasticity and Independence of the residuals.

1. Normal Distribution of Residuals

(a) Histogram

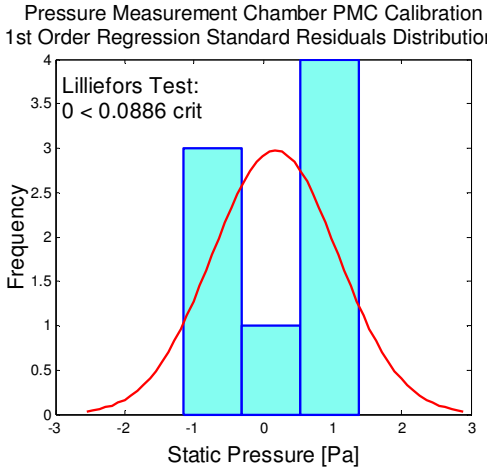

(b) Normal Probability Plot (Normal Scores)

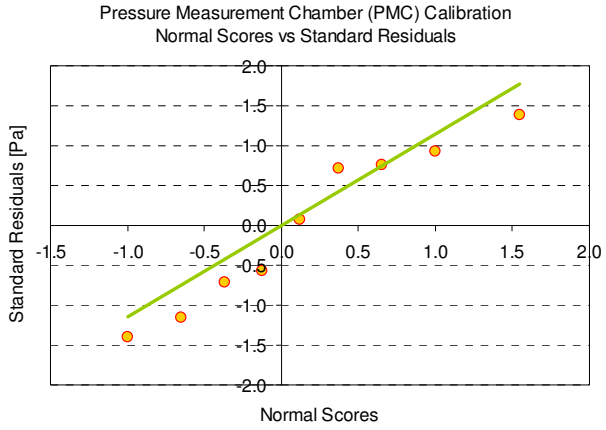

(c) Lilliefors Test of Normality

H_0: X has a Normal distribution with unspecified mean and variance

H_a: X does not have Normal distribution

Rejection rule: $D_{experiment} > 0.0886$ (D criti(c) => 0 < 0.0886 critic

2. Homoscedasticity (evenly distributed varianc(e)

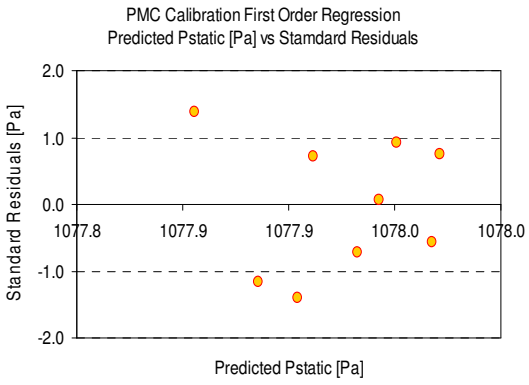

3. Independence of the Residuals: Residuals vs. Static Pressure

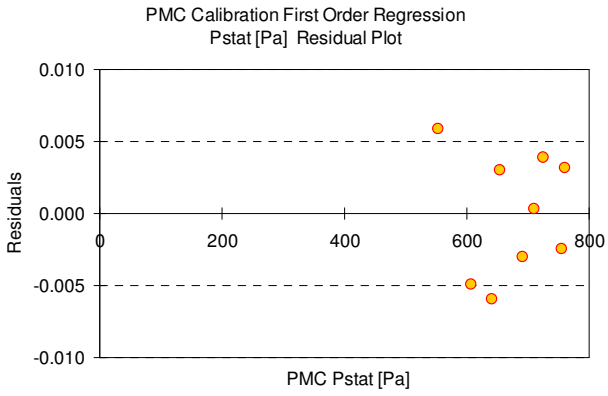

Box 5-6, Figure 2 shows an evenly distributed variance of residuals. Figure 3 shows no particular pattern of the residuals as a function of the independent variable and therefore the independence of the residuals from the model variable, which indicates the model is a good representation of linear relationship between the static pressure measured by the PMC probe and the calculated one.

PMC Probe for Static pressure measurement: Model for estimation and prediction

The regression model is useful for estimating and predicting values and for finding the boundaries inside which these values are defined. For the particular case of the PMC, both intervals fall in the same place. Figure 5-21 shows the estimation and prediction interval; big circles are indicating the predicted values. The prediction interval starts to slightly widen outside the range of data that have been used for calculating the model. However, the nearly constant interval for estimation and prediction, reaffirm the goodness of the first order regression model in representing the PMC calibration probe for static pressure measurement.

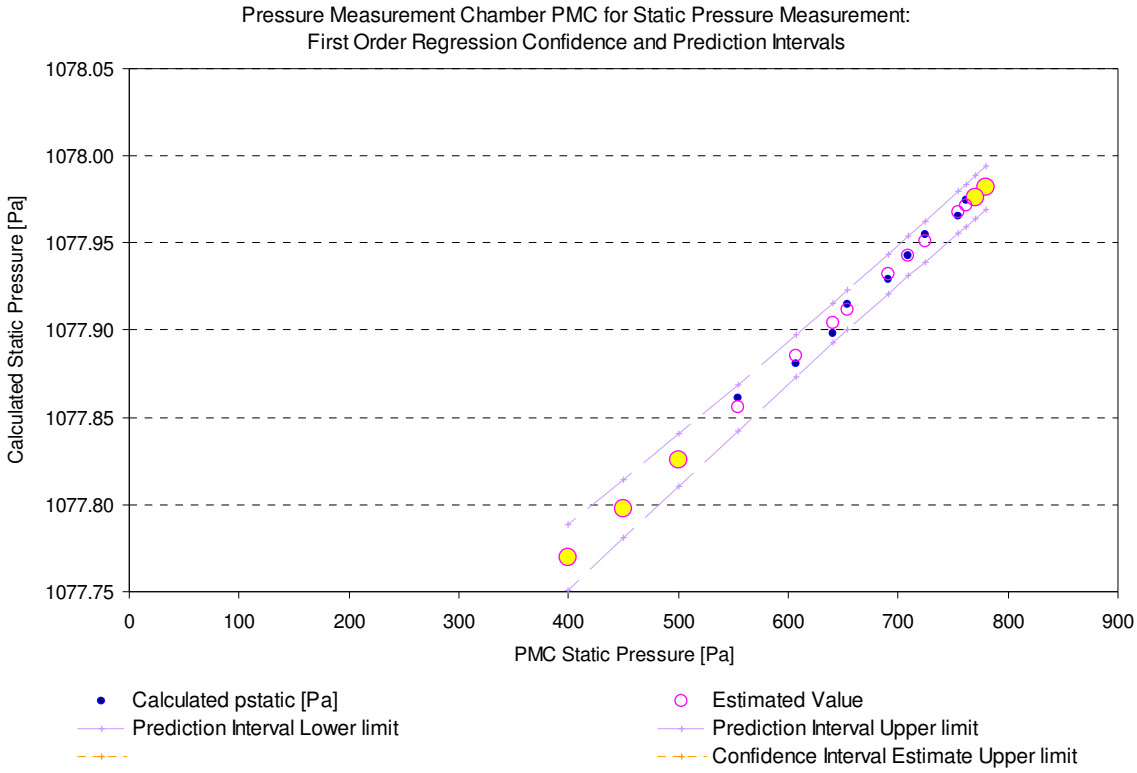

Figure 5-21 Pressure Measurement Chamber PMC: regression model

The estimation and prediction intervals are approximately of the same range inside and outside of the confidence interval (550, 760) {Pa}. Meaning that the first order regression model is as good for estimation as for prediction of the static pressure at the turbine wake.

Zero error, Saturation, Hysteresis and Repeatability

Figure 5-20 shows the curves for the repetition of the experiment, increasing and decreasing the flow rate, and they are approximately the same; in addition, the sudden increase of the flow rate for simulation of a water hammer shows no saturation and therefore an appropriate fast response. This is the result of a careful design of the pressure taps and tubing layout, as it is described in next paragraphs. The average zero

error is approximately 47 Pa for the PMC probe compared with 61 Pa for Pitot-static probe, which is a low value compared with the tolerance interval of 700 Pa given in the literature (Japikse and Baines 1994). As a result the PMC probe shows very low hysteresis, rapid response and therefore a good repeatability.

5.3. Probe: Hollow Universal Joint as Torque transducer

The torque is one of the necessary parameters to determine turbine efficiency and it represents, together with the rotational speed of the shaft, the mechanical energy given by the turbine.

A study for the twisted blade turbine presents antecedents for torque determination, by deriving the momentum of inertia from drawings instead of measuring it (Pulker 2005). This way of measuring torque is useful for turbine characterisation; however, it lacks the feedback given by the counter torque, which, in the case of the HPR, gives information about the interaction of the robot with the pipeline environment. Consequently, for the purpose of the HPR characterisation, it was preferred to perform the actual measurement of the turbine torque.

Measuring the torque at the shaft represents a potential danger due to the required leads attached to a rotational shaft. A solution is given by a wireless method based on sensing out-of-phase electromagnetic fields; this method is more accurate yet more expensive.

As a result, the torque is measured by the counter torque, of the hollow universal joint, which is stationary with respect to the turbine and tractor. The universal joint connects the turbine to the tractor and its function is to impede the rotation of the turbine by using the tractor as a pivot, recalling that the tractor is attached to the pipe wall by the bristle-based mechanism. As a result, by measuring the counter torque at the hollow universal joint, the turbine efficiency includes the effects of the tractor dynamics and the pipeline characteristics, which affect as well the tractor behaviour.

Hollow Universal Joint as Torque Transducer: Simulation for probe conditioning

In order to conditioning the hollow universal joint as torque transducer and due to the lack of antecedents in using the joint for that purpose, it was necessary to perform a finite element analysis, so as to determine the yield points. It was assumed that strain variations at yielding points are more significant and therefore they will give a more sensible reading of the counter torque.

Static displacement study, Figure 5-23 (a), fixes the vehicle side, leaving the other side free to rotate, gives the maximum joint displacement. From the Figure it can be seen that the maximum displacement is in the joint arms, more precisely where the arms are bolted to the joint base ring. The static displacement study is complemented with the nodal analysis for probe location Figure 5-23 (b), from which the point at #10494 shows a displacement of 1.3 E-05, close to the maximum displacement of 1.6 E-05 in the area where the strain gauges were effectively attached. This result shows that the region close to the joint bolts is sensible enough for placement of the strain gauges.

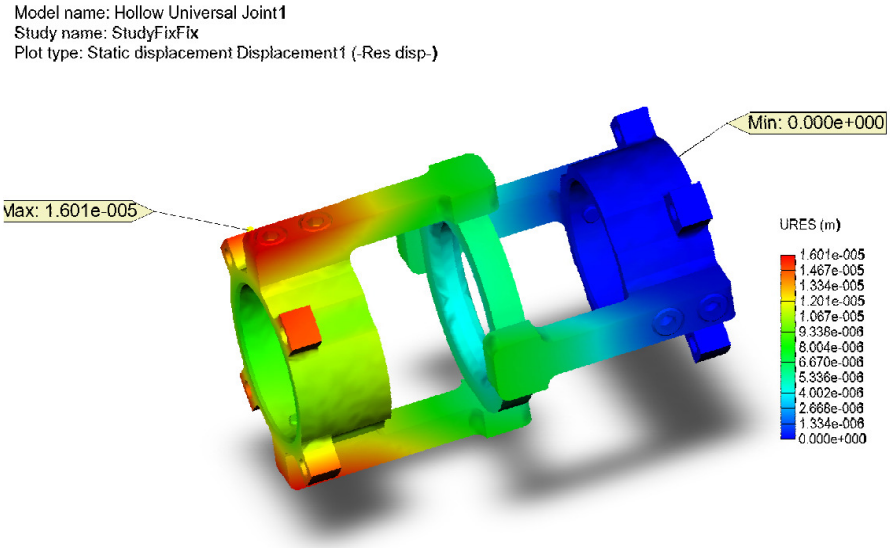

(a) Hollow Universal Joint: Static Displacement analysis. Maximum displacement supported by the joint arms, in the bolted area.

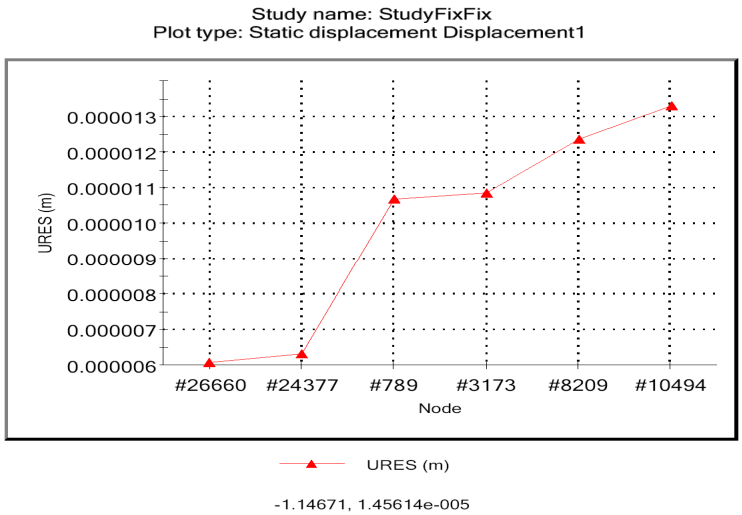

(b) Hollow Universal Joint: Static Nodal Stress Deformation scale: 878.383. Higher displacements above 1.2 E-05 {m} in the region of the joint arms.

Figure 5-22 Hollow Universal Joint as Torque Transducer: static displacement

Assessing the strain gauges location for measuring the robot counter torque. Simulation in SolidWorks..

Von Mises study for yield analysis and the static strain analysis Figure 5-23 (a) and (b) respectively, also show this region as one of the widest with high sensibility for detecting the stress of the joint. Therefore, the arm area close to the bolts is selected for placing the strain gauges. The picture in the Figure 5-24 (a) and detail in Figure 5-24 (b) shows the worn of the joint material, which can be seen in the lower right angle of the picture, confirming this sector as the most exposed to working stress.

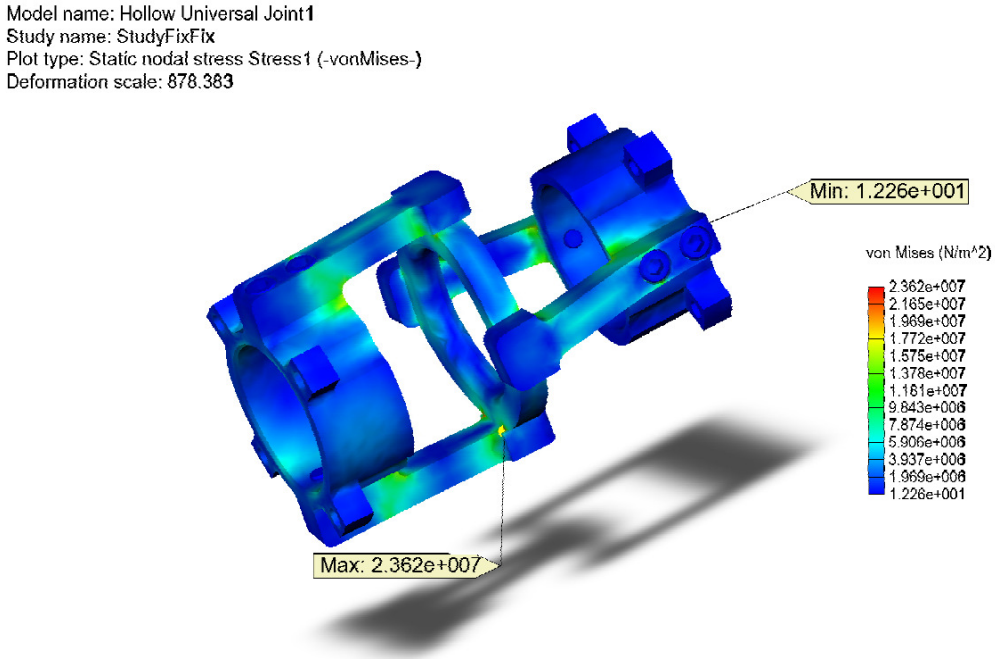

(a) Hollow Universal Joint: Static nodal stress (Von Mises) analysis to determine the yield points

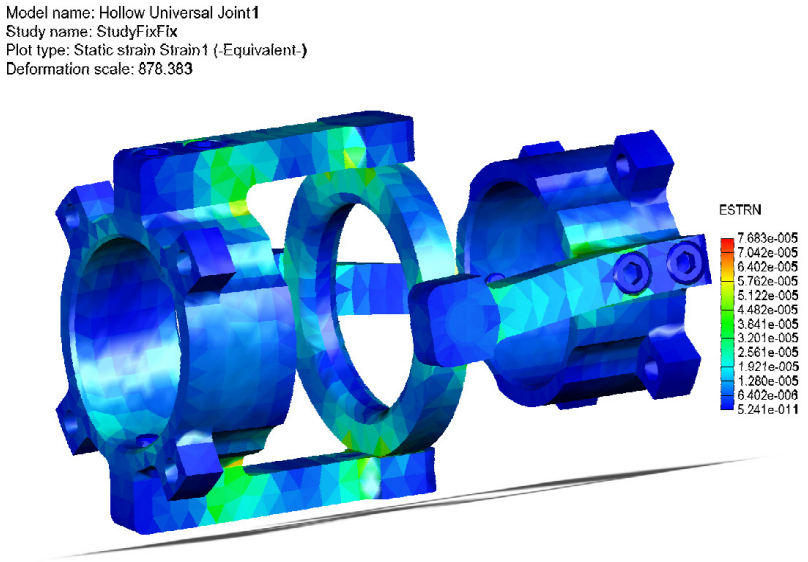

(b) Hollow Universal Joint: Static Strain analysis

Figure 5-23 Hollow Universal Joint as Torque Transducer: static stress-strain

Assessing the strain gauges location for measuring the robot counter torque (cont(d).

Hollow Universal Joint: Conditioning as Torque transducer

The strain gauge measures stress concentration by integrating the stresses under the gauge surface. The size and pattern of the gauge determine the extent and type of strain to be measured. So, the smaller the gauge (less than or equal to 2mm) the more precise is the measure of strain in a particular point yet difficult to locate the point of interest and also difficult to handle. Therefore, for conditioning the universal joint and because the interest is to measure the counter torque, it was selected larger gauges (6mm) so as to cover a broad area under stress.

The strain gauges were distributed symmetrically at either side of the arms, where the material is not weakened by the bore for bolts, and to detect torsion forces of the joint arm (Gere 2001; Hibbeler 2007). The eight gauges utilised are connected in a Wheatstone bridge arrangement in such a way that the ones under compressive and tensile stress act together, respectively. In that way the signal of the strain gauges is four times amplified and it also average the stress over the four arms.

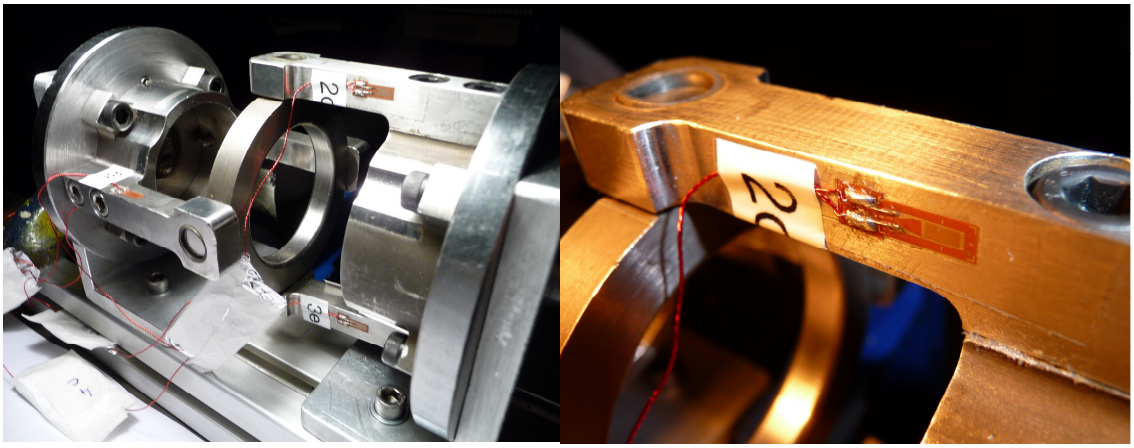

(a) Hollow Universal Joint with the arrangement of strain gauges for the Wheatstone bridge connection

(b) Detail of the strain gauge location close to the yielding point. Note the wear of the joint arm (right below) attesting the simulated yielding points.

Figure 5-24 Hollow Universal Joint as Torque Transducer: strain gauges location
Strain gauges location and orientation, following the results of the joint simulation.

Calibration 4. Hollow Universal Joint as Torque transducer: DOE

The calibration of the hollow universal joint as torque transducer was performed in blocks by loading and unloading the joint in clockwise and counter clockwise direction (Hinkelmann and Kempthorne 1994; Montgomery 2009). The experiment is a single level of successive steps of standard weights units, refer to Figure 5-25. However, the sudden increase of weight has been explored as well, so as to emulate flow surge. Note that the zero point dividing the clockwise and the counter clockwise has been

determined by levelling the joint, however in real working conditions the zero is rather a range within which the transition of rotation happens. Due to the movable parts of the universal joint it is physically of no meaning to find a fixed zero point.

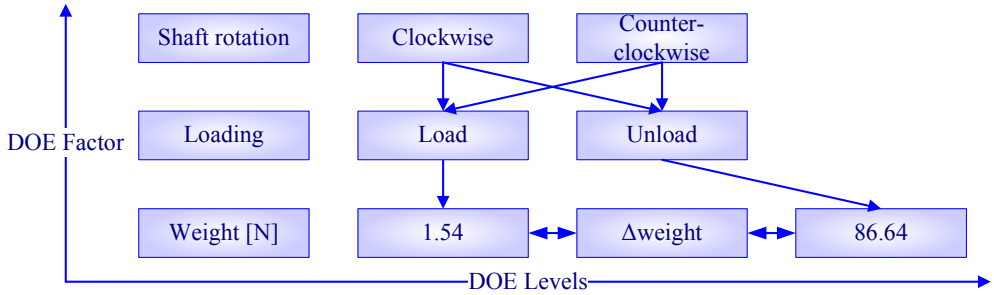

Figure 5-25 Hollow Universal Joint as Torque Transducer. DOE
Levels and factors for probe calibration referred to loading weights.

The torque calibration procedure consists on comparing the calculated torque related to teh weight units and the result from the strain indicator as micro strain {uE}. The ratiometric output of the strain indicator has been compared with the output of an instrumentation amplifier circuit designed by the author for this particular purpose. The scheme of calibration procedure is summarised in Figure 5-26. See Appendix B for data.

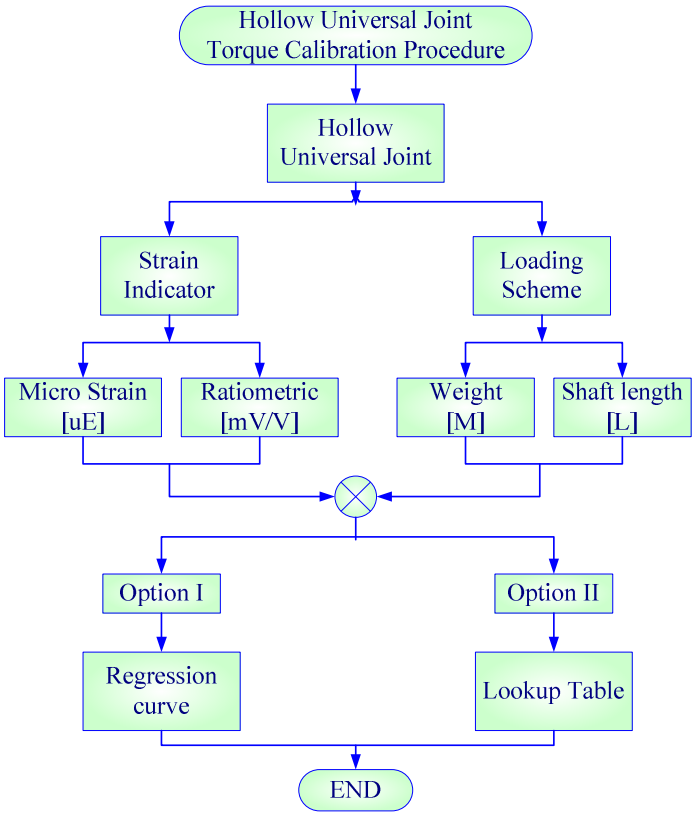

Figure 5-26 Hollow Universal Joint as torque transducer: calibration procedure
Flow diagram of the calibration procedure for determining the error in the determination.

Hollow Universal Joint: Data Analysis Procedure

The data analysis procedure is schematised in Figure 5-27.

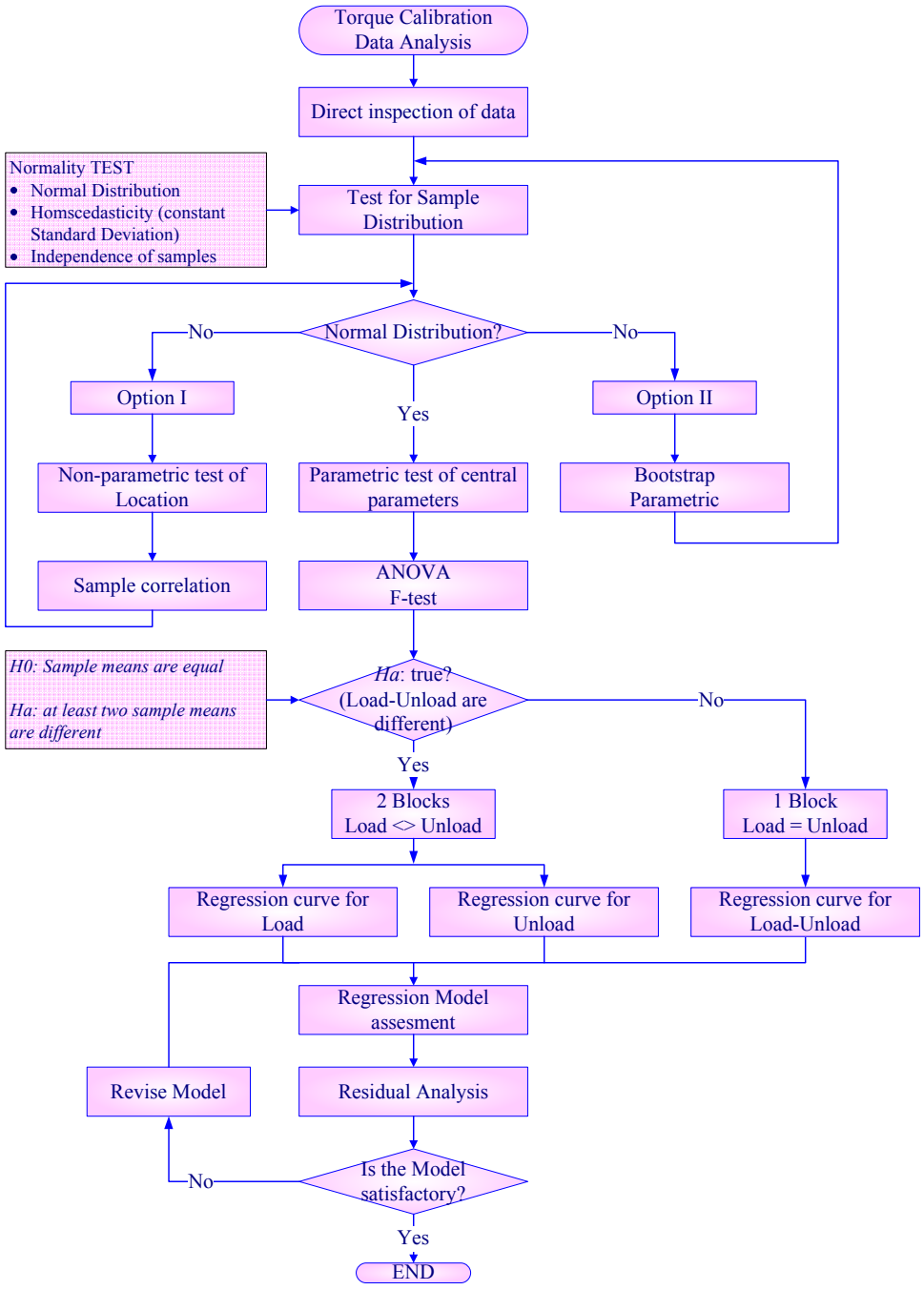

Figure 5-27 Hollow Universal Joint: data analysis for torque calibration

Flow diagram of the data analysis procedure for torque calibration

The purpose of data analysis for the calibration of the hollow universal joint as torque transducer is to determine the regression curve that represents the torque referred to the applied weights. The procedure starts performing the analysis of variance, ANOVA, so as to formally prove or not the equality four data groups, clockwise and counter clockwise performance and the loading and unloading effect.

In case of no conclusive results, a non-parametric test of location or sample correlation is performed, Option I in the diagram. If the sample distribution is not normal, due mainly to the limited number of samples, a parametric bootstrap is performed (Option II in the diagram) so as to evaluate the data on better grounds. For the particular case of the hollow universal joint, it has been proved that the clockwise behaviour equals the counter clockwise with opposed sign. However, the determination of the equality of load and unload regime was not so evident, requiring further analysis. The grounds for such conclusions are described in the following paragraphs.

From direct data inspection, Figure 5-28, clockwise and counter-clockwise curves are mirrored images, as it was expected. Though, the equality hypothesis needs a proof.

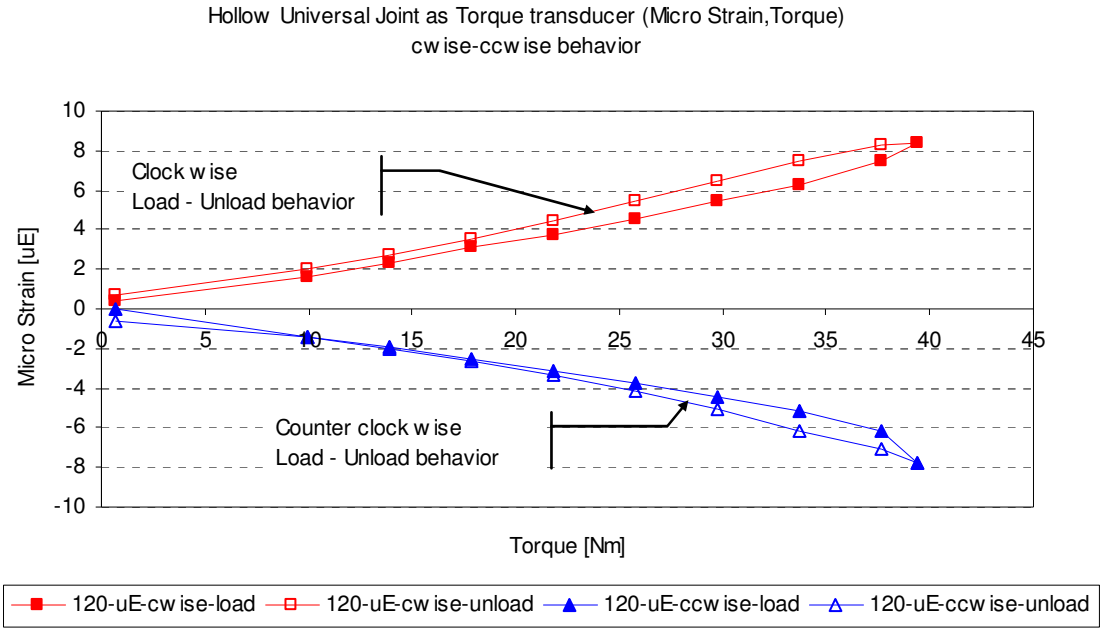

Figure 5-28 Hollow Universal Joint: direct data inspection

Loading the universal joint to determine the clockwise and counter-clockwise characteristic. Despite each curve appears to be a mirrored image of the other, they have differences. Therefore, the next step is to determine the degree of significance of such differences. Note that the zero is a zero range rather than a single point, explained by the misalignments of the movables part of the joint.

Firstly compare the four curves with the margin error. Recall that the margin error is the standard error scaled by the z-score $MrginError = z_{\alpha/2} * \frac{S}{\sqrt{n}}$; and the standard error, for small-sample case, is the sample standard deviation, s, averaged by the number of samples $StndrdErr = S = \frac{s}{\sqrt{n}}$.

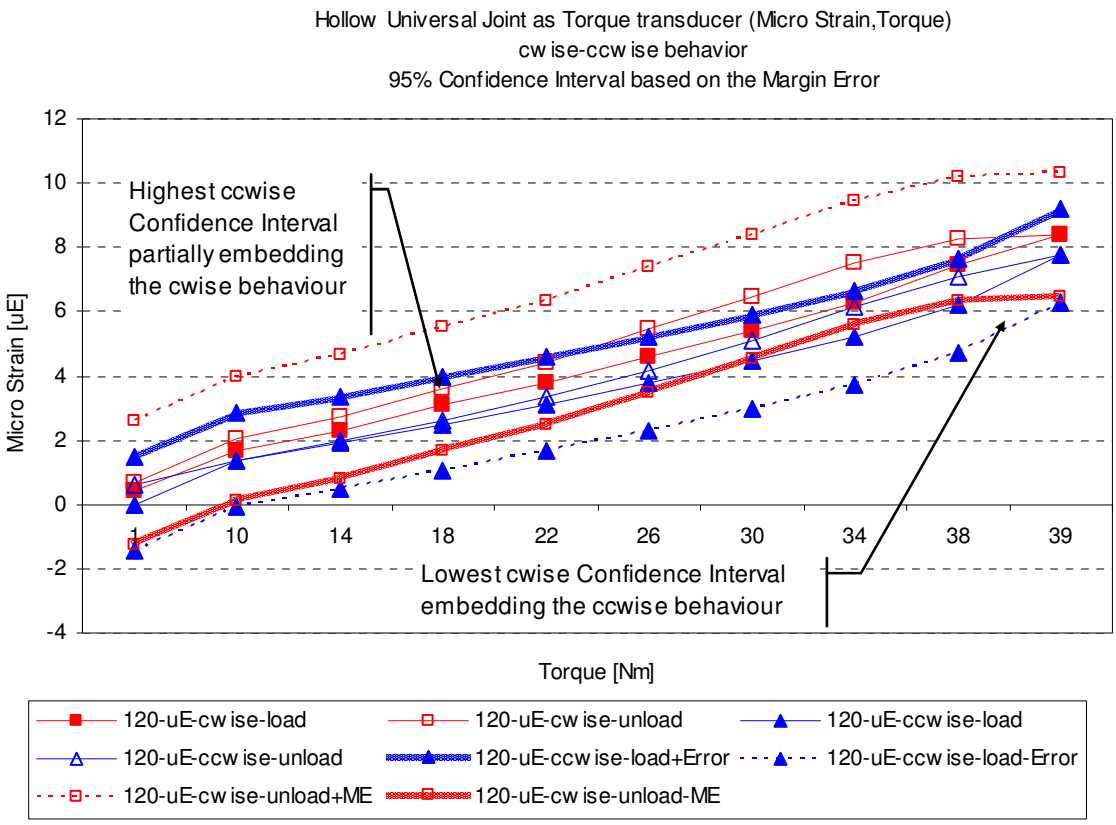

Figure 5-29 Hollow Universal Joint: confidence intervals of the measurements

The 95% confidence interval based on the margin error used as indicator of the data variability. The clock wise and counter clockwise curves appear to be embedded in the other's confidence interval; indicating the closeness of both characteristics.

Figure 5-29 shows the clockwise and counter-clockwise curves embedded in the margin error of the other curve in a fuzzy-like region for torque determination. The Margin Error considered are for the worst case, where the upper margin is the lowest bigger margin, and the lower margin is the highest lower, resulting in the narrower range for the data. To conclude, even considering the narrower range, both curves fit inside the range, which may mean sameness of the clock wise and counter clockwise behaviour. However, this assumption need to be corroborated or not by the Analysis of Variance (ANOV(A).

Note that an elastic deformation of a body, such as the universal joint under torsion forces, is characteristic of a system with memory: results are dependent on previous values. So, the strain measurement is a highly correlated process, and the theory of sample independence can not be applied. This is an important feature at the time of data analysis.

ANOVA has the particularity of distinguishing variations between groups and within groups. Figure 5-30 (a) shows a wider range due to variations within groups than

the variation between the means of the different groups. Figure 5-30 (b) show the maximum range between group's mean and the relation of the sample means and the grand mean.

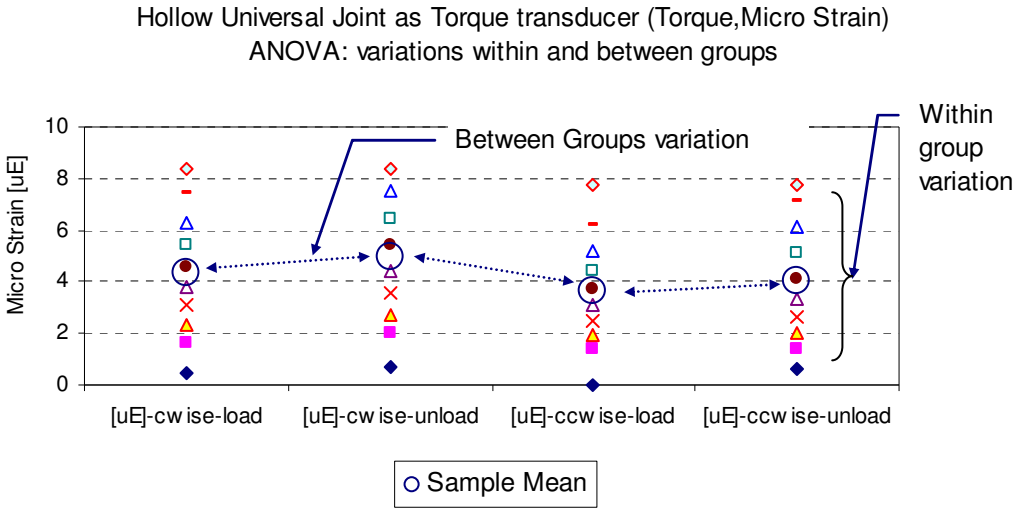

(a) Variation between and within groups

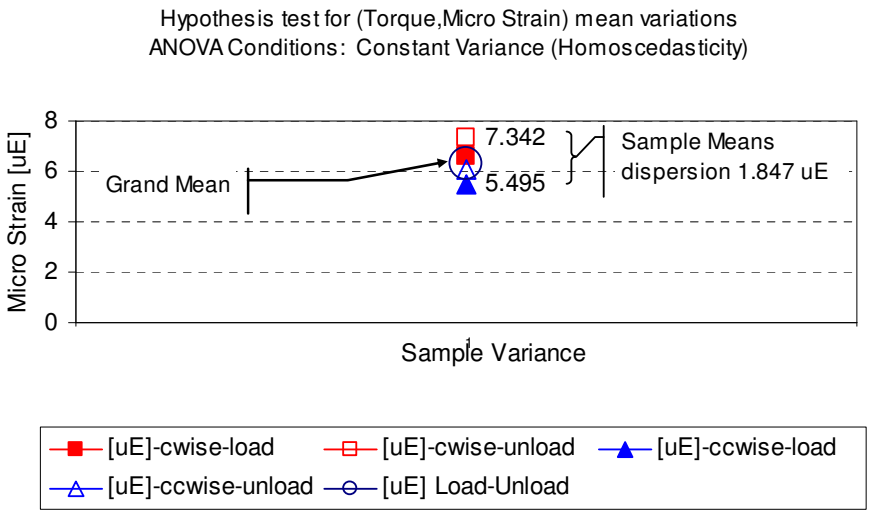

(b) Sample's mean and grand mean dispersion intervals

Figure 5-30 Hollow Universal Joint: sample variability
Data inspection for determining the variations within and between groups.

The variability analysis allows us to conclude that there is no significant variation between the clockwise and counter clockwise behaviour and the loading and unloading curves. However, in order to apply ANOVA rigorously, it is required to know if the data set meets the analysis pre requisites. The next section shows such analysis.

The first step in the ANOVA analysis is the hypothesis formulation for the four groups:

Definition 5 *H_0: the four groups, clockwise and counter-clockwise, load and unload, have a Normal distribution with unspecified mean and variance*

Definition 6 *H_a: the four groups do not have Normal distribution*

ANOVA applicability: Test for Normal Distribution

In order to apply ANOVA analysis, the data needs to meet strong conditions, namely the data presents normal distribution, constant standard deviation and independence of the sample observations. These requirements are necessarily for meaningful results of the F-test of variability; otherwise the ANOVA analysis may have misleading results.

The normality test performed for the data of the hollow universal joint are histogram plot, comparison of the data with normal scores and Lilliefors test, which is a quantitative test of normality (Keller and Warrack 2000).

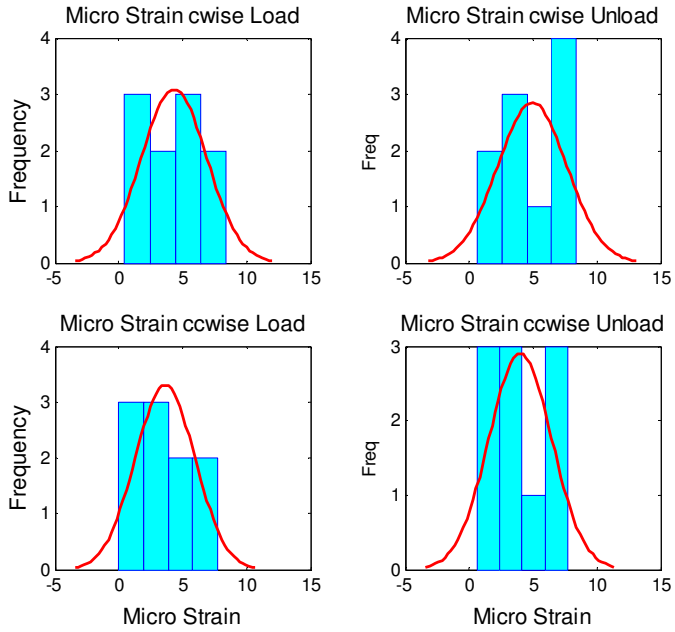

Figure 5-31 Hollow Universal Joint: Normal Test of the data histogram

Comparing the clockwise, counter-clockwise, load and unload effect against the normal distribution for determining the ANOVA test applicability: data need to be normal distributed.

The data histograms, Figure 5-31, the data plot compared to the normal scores, Figure 5-32, and the Lilliefors test, Box 5-7 all of them for the four groups, show a peculiar result, the groups for loading program, clockwise and counter-clockwise, present normal distribution, while the groups for unloading program present non-normal distribution.

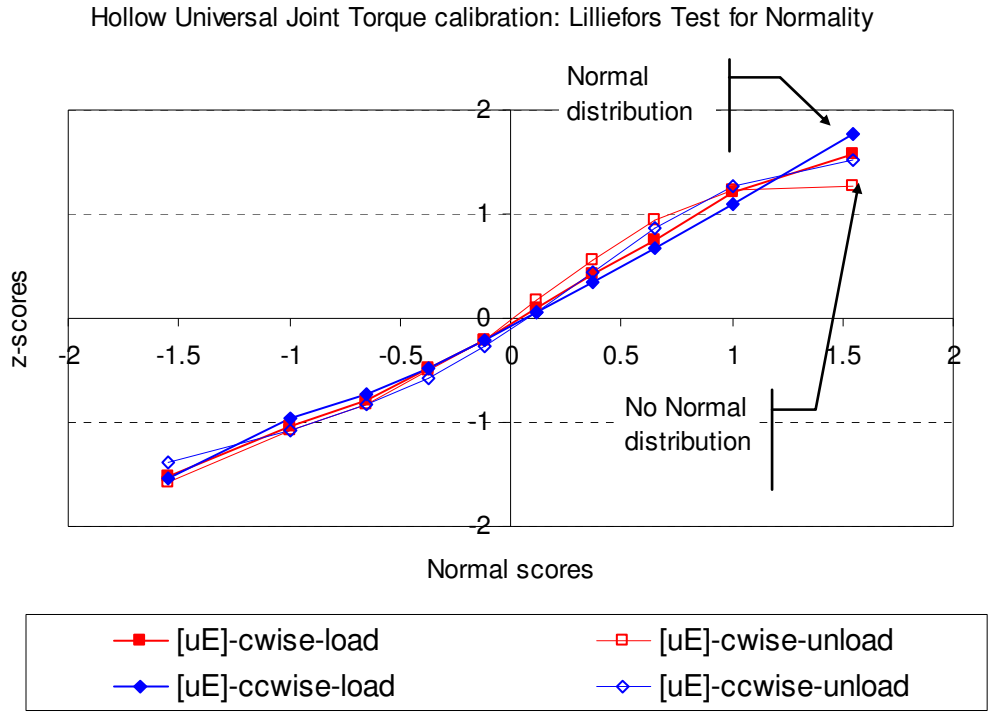

Figure 5-32 Hollow Universal Joint: Normal Test comparing with normal scores
Unload program (hollow marks) present non normal distribution, though the difference is not significant.

Apparently, there is no physical reason for such result. Despite the hysteresis of the material, the unloading program is equivalent to the loading displaced by a hysteresis factor; this fact is no enough reason for render a normal distributed sample to non normal, even more considering the experiment has been repeated eight times.

Box 5-7 Hollow Universal Joint: Lilliefors Test of normal distribution
Following these results the data from loading the universal joint can be considered as normal distributed. That is not the case for the unloading test.

Lilliefors Test of normality
Rejection rule: $D_{experiment} > 0.0886$ (D critic at 5% significance level)

	clockwise	counter clockwise
Load	D = 0.0864	D = 0.0862
Unload	D = 0.1016	D = 0.1157

The four groups may be considered to be in the boundary of a normal distribution. This result is not surprising mainly because the total levels of the loading factor are only ten, so it can be considered a small sample number however these ten values for each of the four groups has been obtained by the average of eight sets of

samples. Recalling that small set of samples convey less information than large sets; a set of at least 30 observations is considered as large set (Keller and Warrack 2000).

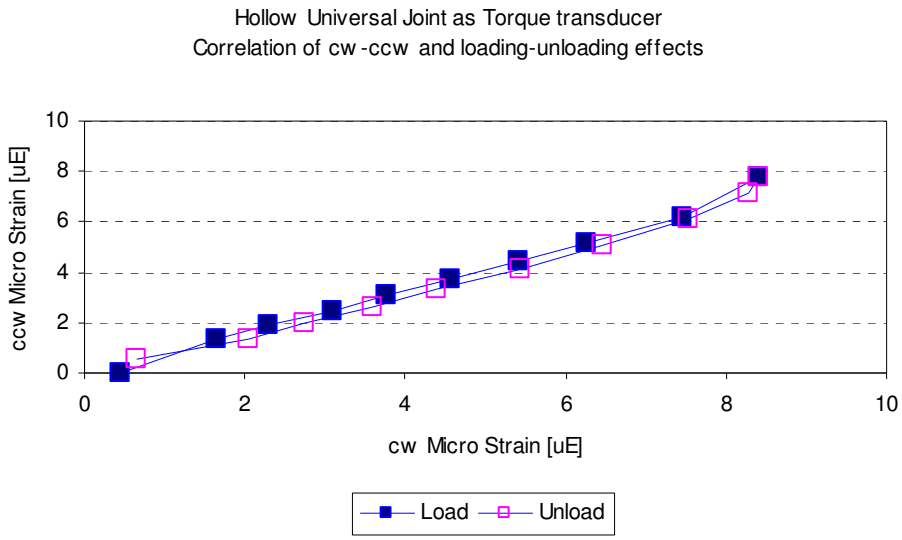

Figure 5-33 Hollow Universal Joint: Two Groups Correlation Load-Unload

The sample correlation shows a positive correlation between loading clockwise and counter-clockwise; the same for unloading. However the result is not conclusive to accept or reject the fact that both curves are the same.

So, as there is not enough evidence to reject or to prove the null hypothesis of equality of the four populations, a non-parametric test of location is performed. Following the Option I of the data analysis, Figure 5-27, the non-parametric test of location is the sample correlation plotted in Figure 5-33.

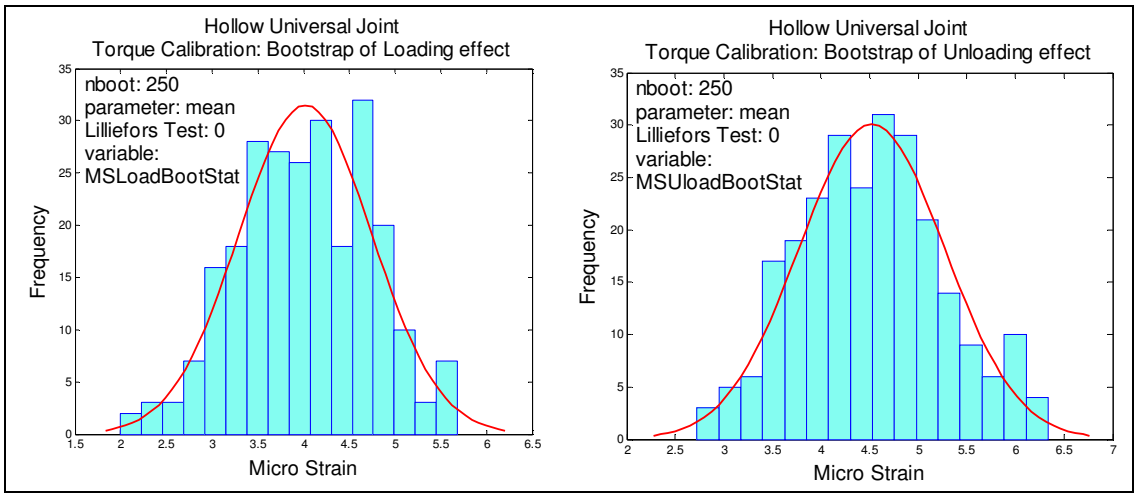

Figure 5-34 Hollow Universal Joint: Normal Test after Bootstrap

The data sets for loading and unloading characteristic show normal distribution confirmed by the Lilliefors test that gives zero lower than 0.0886 (critical valu(e).

The Option II in the data analysis procedure Figure 5-27 is to resample the data set to increase the number of observations so as to get a normal distributed population.

Thus, a parametric bootstrap was calculated for estimating the population mean. The bootstrap technique is a powerful statistics tool for randomly re-sampling a set of data and calculating the statistic of interest, in this particular case the sample mean. The Bootstrap and mean computation was calculated for 250 samples, which is the minimum recommended number of samples (Efron 1993).

Figure 5-34 shows the histogram after bootstrap, and Box 5-8 (a) presents the bootstrap results. Clearly both groups, loading and unloading, present normal distribution. This fact is reinforced by the Lilliefors test, which gives zero value. So, as both populations are normally distributed, the next step is to perform an ANOVA analysis for load and unload program, in order to accept or reject the equality between samples. The hypothesis can be described as follows (Anderson, Sweeney *et al.* 2003):

H_0: sample means are equal

H_a: at least two sample means are different

The test statistic of the relationship of the mean square for treatment to mean square of error: F=MSTR/MSE

Rejection rule using test statistic: reject H_0 if $F > F\alpha$

Rejection rule using p-value: reject H_0 if p-value $< \alpha$ (level of significanc(e), in this particular case level of significance $\alpha = 0.05$

Results from ANOVA for 250 samples, are presented in Box 5-8 (b), where the p-value equals 1.70 E-13 is smaller than the level of significance α of 0.05; and the one-tail F-test equals 57.45, which is bigger than F critic of 3.86. All that means there is enough evidence to reject the null hypothesis H_0 of equality of the sample means of load and unload data; therefore both curves can be considered different.

Box 5-8 Hollow Universal Joint: ANOVA Load-Unload characteristic

Bootstrap Summary

Groups	Count	Sum	Average	Variance
MSLoadBootStat	250	1005.0070	4.0200	0.5321
MSUloadBootStat	250	1130.2597	4.5210	0.5603

(a) Bootstrap statistics summary

ANOVA Single Factor

Source of Variation	SS	dof	MS	F	P-value	F crit
Between Groups	31.3765	1	31.3765	57.4471	1.7086E-13	3.8602
Within Groups	271.9979	498	0.5462			
Total	303.3744	499				

(b) ANOVA after bootstrap, for load-unload characteristic: reject H_0 : load and unload are similar
Rejection proof: F = 57.45 > F critic = 3.86 and p-value = 1.71 E-13 < α = 0.05

The next step in the data analysis of the Figure 5-27 is to find respective regression models for load and unload program that explains the torque-strain relation.

Hollow Universal Joint: Regression models for Load and Unload

This section shows the regression model for load and unload program. Both models present good coefficient of determination R^2 , 0.990 and 0.998 for load and unload models respectively, showed in Box 5-9. The good result is confirmed by the standard error of the models, which are 0.27 and 0.10 for load and unload respectively. These results mean the second order model is a good representation of the Torque-strain characteristic for load and unload program. Details of the ANOVA analysis for regression, residuals and the data for the estimated and predicted values and intervals are in the Appendix B.

Box 5-9 Hollow Universal Joint: Regression Model

High correlation coefficient R2 (approx 0.99) Second Order Regression for Load-Unload

Second Order Regression Statistics	Load	Unload
Multiple R	0.9953	0.9994
R^2	0.9906	0.9987
Adjusted R Square ($R^2/do(f)$	0.9879	0.9984
Standard Error	0.2697	0.1040
Observations	10	10

Figure 5-35 shows the regression curves for load and unload program, where each curve is embedded in the other's confidence interval; even more both regression curves are embedded in a fuzzy region conformed by the prediction and estimation interval, confirming the first assumption presented in Figure 5-29. Therefore, for the function of the hollow universal joint as torque transducer, both curves load and unload can be considered similar, without any loss of significant information. The next paragraphs show the regression model for one group containing the load and unload program.

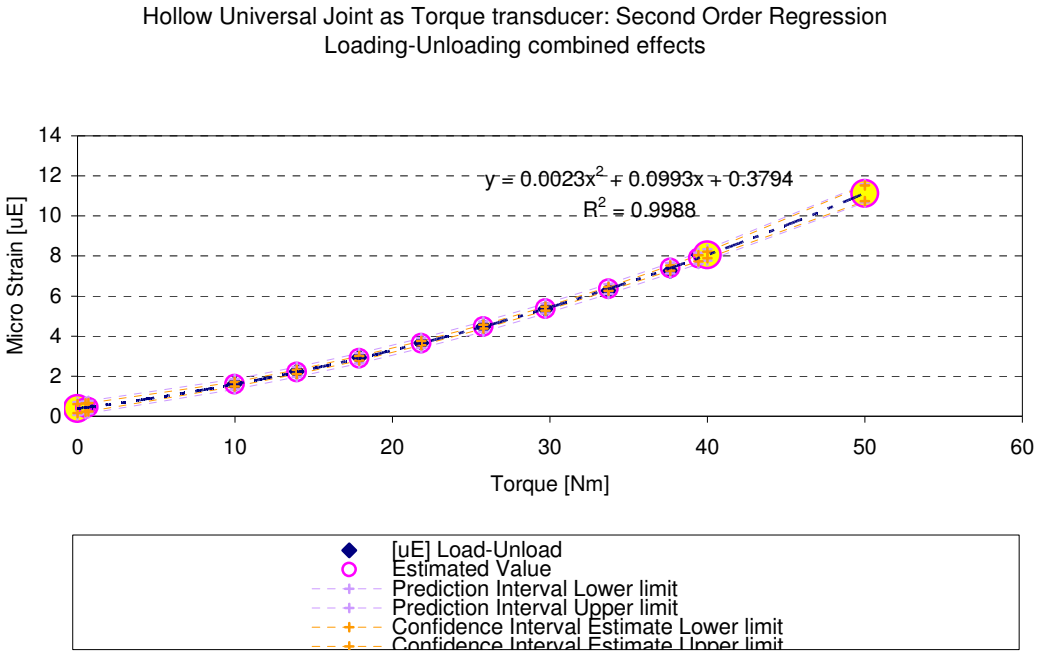

Figure 5-35 Hollow Universal Joint Load-Unload Effects: regression model

The range for estimation and prediction intervals is approximately the same, inside and outside of the confidence interval (0.7, 39.42) {Nm}. Though, a slightly wider above 39 Nm, which means the second order regression model is as good for estimation as for prediction of the torque measured by the universal joint.

Torque-strain characteristic: Regression model for Load-Unload combined effects

"First it is important to know the performance of the model and then to perform an analysis of coefficients" {Keller 681}. The regression model is evaluated by means of the coefficient of determination R^2 , which is proportional to the correlation coefficient; it shows the strength of association between the dependent and independent variables and therefore the strength of the model to explain the physical relation between the variables. The coefficient of variation R^2 shows that the 98% and 99% of the micro strain variation is due to the torque, and it is explained in the regression equation, for the first and second order model respectively.

Box 5-10 Hollow Universal Joint for Torque Measurement: Regression model

Comparison of First and Second Order models

Regression Statistics	(a) First Order Regression	(b) Second Order Regression
Multiple R	0.9902	0.9994
R Square	**0.9804**	**0.9988**
Adjusted R Square	0.9780	0.9985
Standard Error of Estimate	**0.3726**	**0.0970**
Observations	10	10

The test of significance ANOVA determines the variability of the slope, parameter b1; therefore, by hypothesis test the null hypothesis H_0 is rejected and the slope is constant, implying a nonlinear relationship. Refer to Box 5-11 for hypothesis and test statistic. Therefore, the first and second regression models show F-values bigger than F-critic and p-values smaller than the level of significance 0.05 as it is described in Box 5-11 (a) and (b).

Box 5-11 Hollow Universal Joint: ANOVA 1st and 2nd order regression

(a) First Order ANOVA for test statistic of linear relation

	dof	SS	MS	F	Significance F: p-value	F crit
Regression[1)]	1	55.6657	55.6657	400.8821	0.00	5.318
Residual[2)]	8	1.1109	0.1389			
Total	9	56.7765				

F = 400.88 > Fcrit = 5.311 and p-value = 0.00 < α = 0.05 => reject H_0

(b) Second Order ANOVA for test statistic of linear relation

	dof	SS	MS	F	Significance F	F crit
Regression[1)]	p = 2	56.7107	28.3553	3014.8026	5.3097E-11	4.737
Residual[2)]	n-p-1 = 7	0.0658	0.0094			
Total	n-1 = 9	56.7765				

F = 3014.80 > Fcrit = 4.74 and p-value = 5.31 E-11 < α = 0.05 => reject H_0

[1)] Explained variations through the regression model

[2)] Unexplained variations through the regression model

(c) Second Order Regression Coefficients

	Coefficients	Standard Error	t Stat	p-value
Intercept	0.3794	0.0942	4.0268 > 2.365	0.0050 < 0.05
Torque {Nm}	0.0992	0.0096	10.2755 > 2.365	1.7880E-05 < 0.05
Torque Squared $\{Nm\}^2$	0.0023	0.0002	10.5408 > 2.365	1.5102E-05 < 0.05

The evaluation of the coefficient by applying t-statistic and the p-values gives a linear relationship of the slope, which means the second order model is a good approximation to represent the torque-strain characteristic. The t-value from table *t(α/2 and n-p-1)* degrees of freedom, is t(0.025 and 7) = 2.365. Refer to Box 5-11 (c) for details of the regression model. The positive slope of 0.197 shows a direct relation between torque and strain that means for each additional torque unit of {Nm}, the strain increases 0.197uE.

Hollow Universal Join as Torque Transducer: Residual analysis

Following the good results of the first and second order regression models, the next step consist on evaluating the residuals. Recalling from previous section, Page 174, there are three tests indicating the goodness of residuals: normal distribution, homoscedasticity and the independence of residuals.

Box 5-12 Hollow Universal Joint for torque measurement: Residuals Analysis

First Order Regression

(a) Standard Residuals vs. Normal Scores

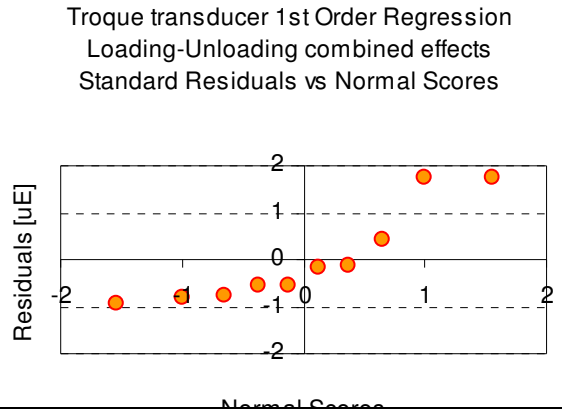

(b) Standard residuals vs. Torque

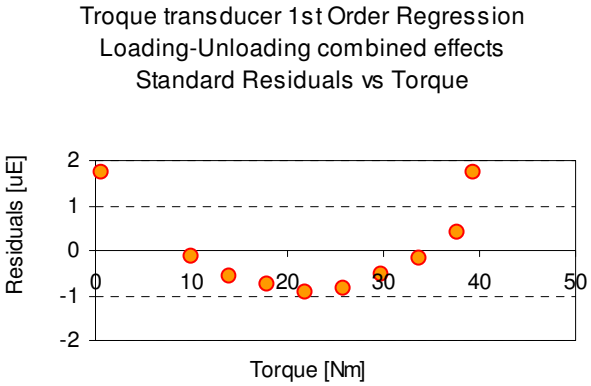

Second Order Regression

(a) Standard Residuals vs. Normal Scores

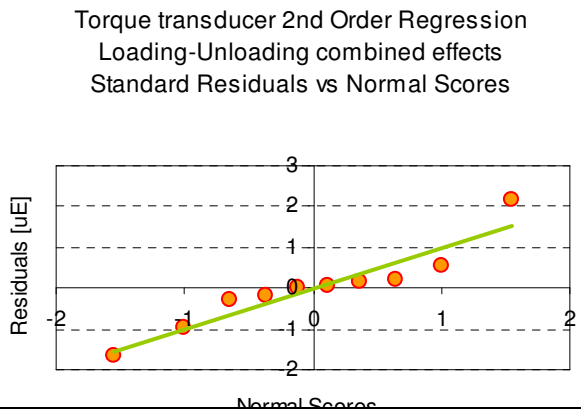

(b) Standard Residuals vs. Torque

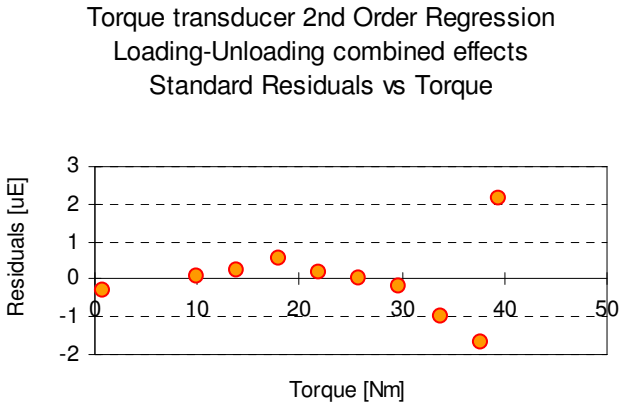

(c) Standard residuals vs. Torque^2

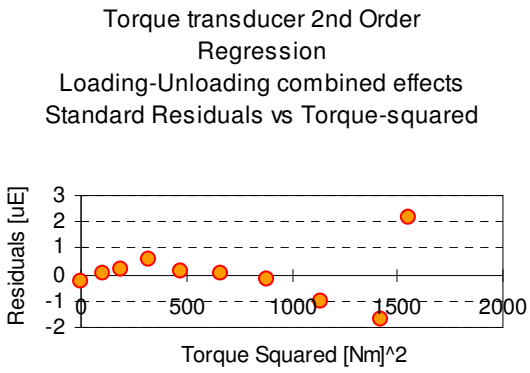

Box 5-12 (a), (b) and (c) contains the plot of the residuals as a function of normal scores and as function of the independent variable, respectively, for the first and second order regression model. It is important to note that both models present a close distribution of the residuals around the normal line, with the exception of the values in the extremes of the scale. However, it is important to understand the physical meaning

of these out-of-range residuals, which lie in the extreme of the torque scale, suggesting that the uncertainty increases close to zero and close to the higher value of the scale. This is in accordance to the "zero range" rather than a unique value, discussed in the Design of Experiment section, Page 198. Similar effect will be compromising the applicability of the homoscedasticity and the independence of residuals criteria.

As a conclusion, and due to the peculiarities of hollow universal joint, the second model is accepted as valid despite not accomplishing with the residuals conditions of acceptance of the model. Even more, the increase of order of the model do not necessarily means an improvement in the model, as it has been demonstrated by comparing the first and second order model along this section.

Hollow Universal Joint: Prediction and Estimation intervals

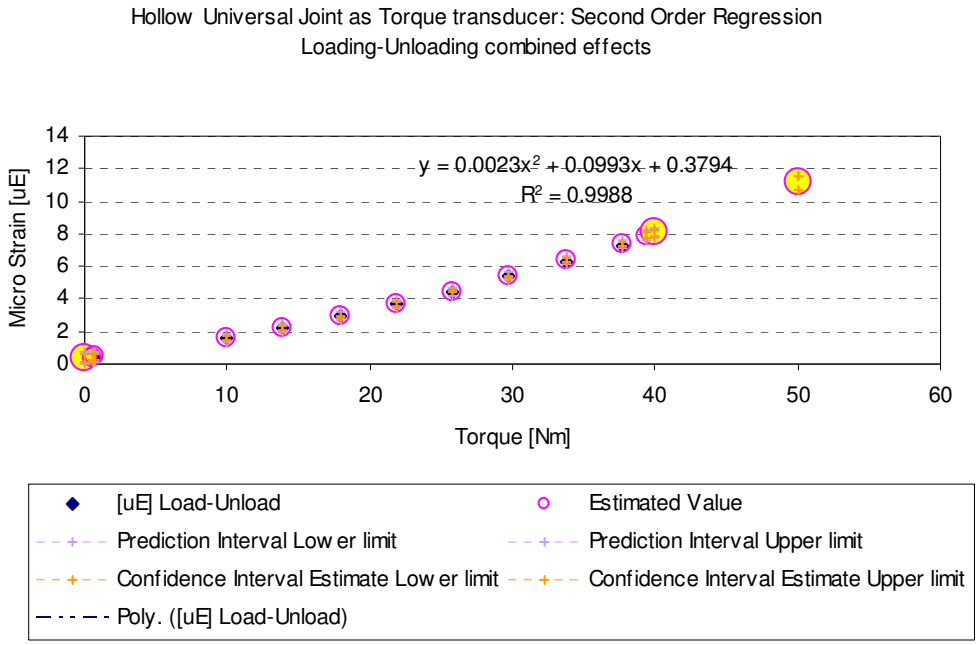

Figure 5-36 Hollow Universal Joint Loading-Unloading mode: regression model

The estimation and prediction intervals are approximately of the same range inside and outside of the confidence interval (0.7, 39.42) {Nm}, which means the second order regression model is as good for estimation as for prediction of the torque measured by the universal joint.

Figure 5-36 shows the regression curve for the relation of micro strain as a function of torque and the estimation and prediction intervals. The predicted values are shown in hollow circles at the beginning and end of the curve. Around these values the prediction interval becomes wider than anywhere else and wider than the estimation interval, this is because prediction has inherent uncertainties compared with estimation. The comparison of the first and second order regression models for estimating values are in Appendix B.

Although the second order regression shows very good explanation of the physical relation between torque and strain, note that the regression only explains the system as a function of these two variables, disregarding other factors such as uneven worn material, location of the stress nodes and the interaction of forces between the articulated parts of the joint, just for citing a few. These factors and many others contribute to characterize the universal joint in an accurate way; however for the purpose of the hollow universal joint as torque transducer, the second order regression is a very good approximation. To conclude, the second order regression is an improvement with respect to the first order, giving a good statistical ground for accepting the second order regression as the torque transducer model.

5.4. Robot's speed determination: Accelerometer calibration

The robot speed is measured by the accelerometer EK3LV02DQ. The speed of interest is in the longitudinal axis of the pipe. The other axes are used for characterising the robot behaviours, and for measuring the speed in other directions for pipe loops with different directions. The collected data is stored in the accelerometer build-in memory, at a sample rate determined by the microcontroller via the I2C/SPI serial communication bus.

The reciprocating motion of the HPR poses a challenge in measuring the vehicle speed. So, the requirement for the accelerometer is to determine the effective linear speed, while characterising the vehicle behaviour. Therefore, design of experiment is divided in behavioural and quantitative calibration. The behavioural analysis is designed to detect expected and unexpected patterns such as cycling, stalling or excursion with the flow, while detecting and isolating vibration that do not contribute to the robot characterisation. The quantitative calibration is to determine the actual speed of the vehicle.

The behavioural calibration was performed emulating the robot movements with a radio-controlled vehicle. The quantitative calibration was performed by emulating typical robot regimes in a CNC (Computer Numerical Control) machine; Settings of both calibration procedures are in Figure 5-37 (a) and (b); and details of the DOE program are in Appendix B.

The accelerometer data analysis follows the procedure in Figure 5-38, and starts with the direct inspection of the tree axis behaviour and classification of potential cycles, such as reciprocating, adverse conditions in the pipe, changes in direction, etc.

Examples of the robot pattern are in Box 5-13. Finally, the quantitative data analysis requires a data de-trend and the bias elimination. The noise reduction consists on data filtering, decimating, and processing by using principal components analysis PCA.

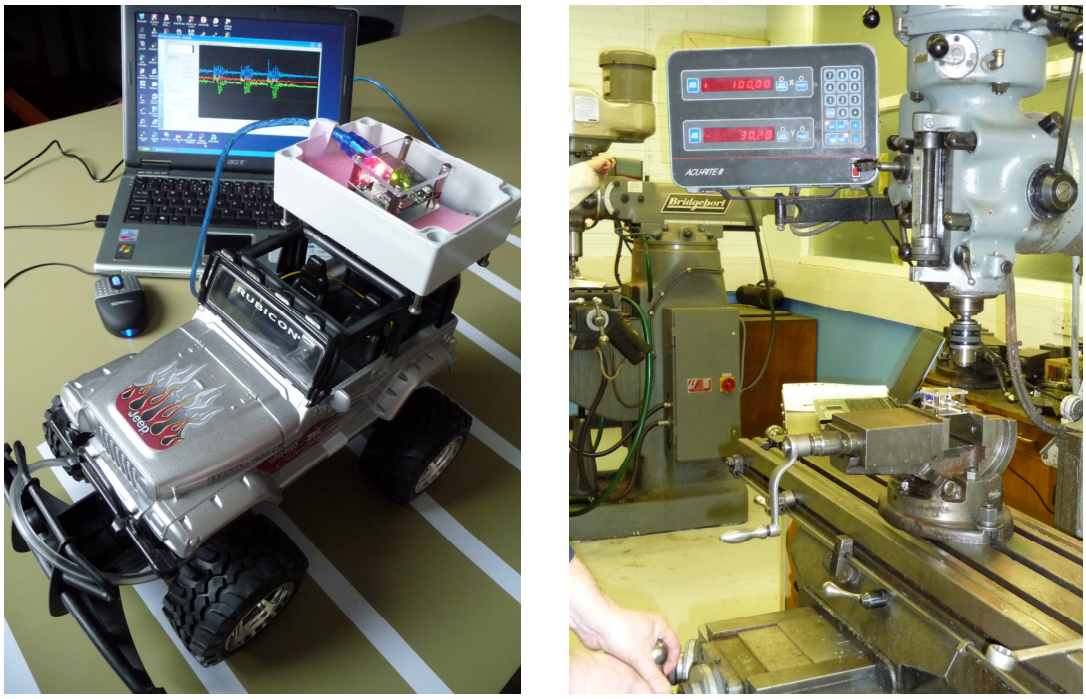

(a) A radio-controlled vehicle carrying an accelerometer is used for simulating the robot behavior inside the pipeline.

(b) The accelerometer attached to a CNC machine is used for simulating different robot speeds

Figure 5-37 Accelerometer Calibration for characterizing the robot behaviours

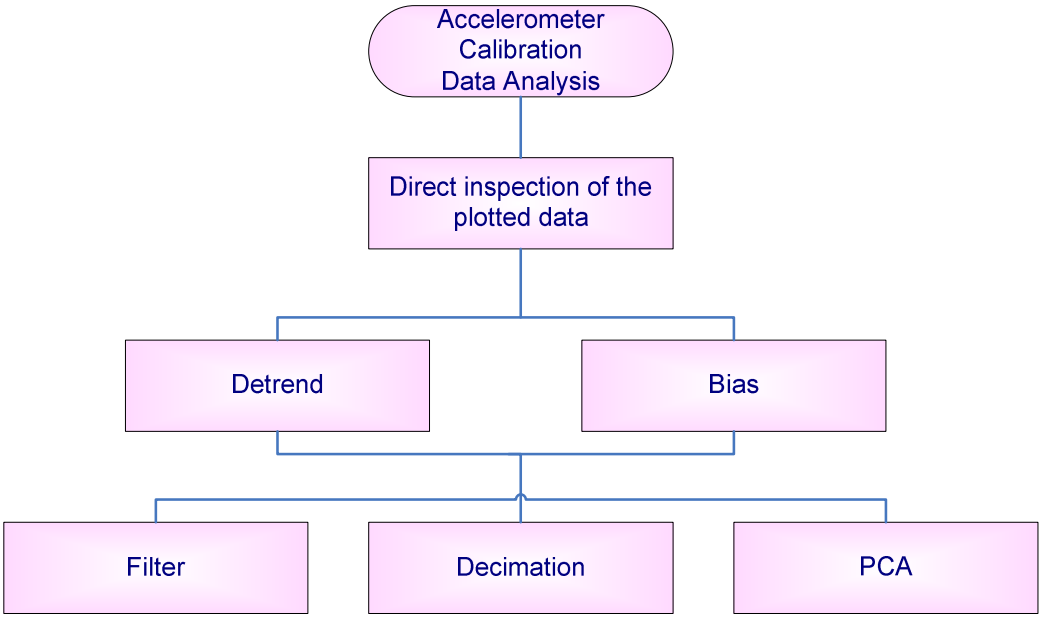

Figure 5-38 Accelerometer Calibration: flow diagram of the data analysis

Qualitative and quantitative approaches

Box 5-13 Accelerometer examples of behavioral patterns identification

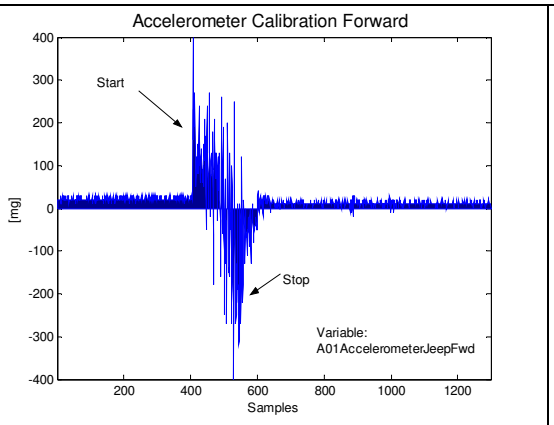

(a) Vehicle forward single start and stop

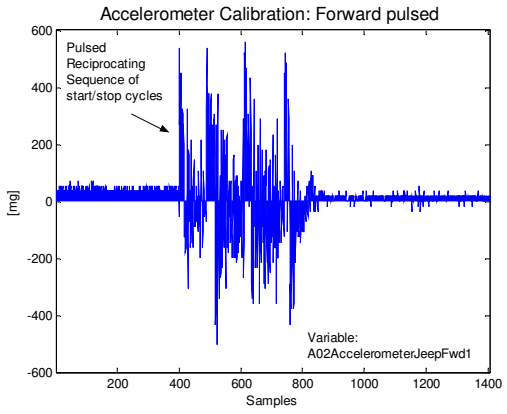

(b) Vehicle forward pulsed sequence emulating reciprocation

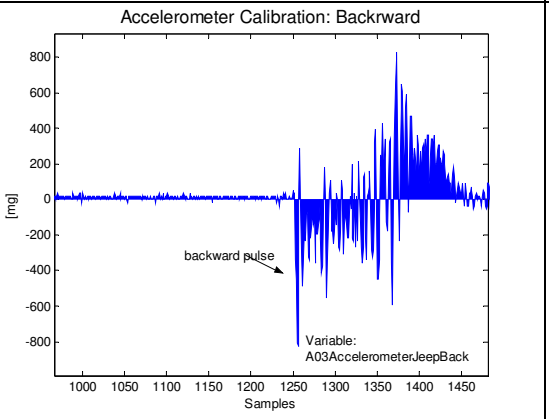

(c) Vehicle backward single start and stop

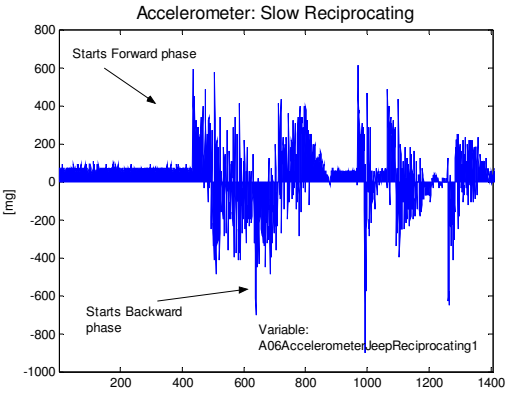

(d) Vehicle slow reciprocation

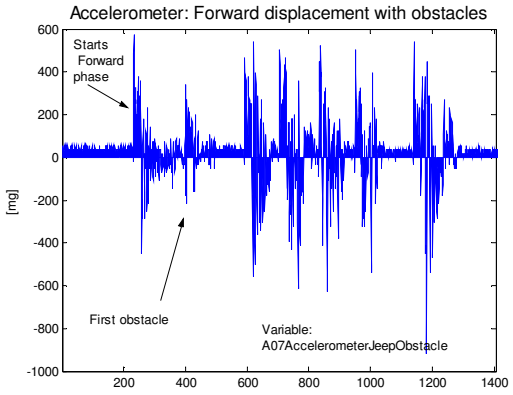

(e) Vehicle displacement with obstacles emulating pipe wall with irregularities

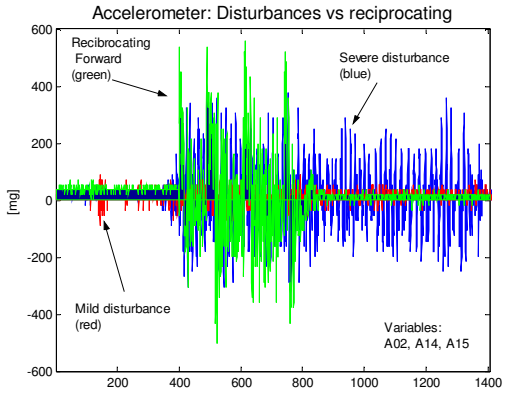

(f) Vehicle reciprocating with disturbances, small and bigger magnitude.

5.5. Hybrid Pipeline Robot: Signal Conditioning Board

The measurements for the HPR system identification need to be conditioned before processed. The author designed an embedded signal conditioning board because it was no suitable solution in the market for the on-board measurements. The on-board signal

conditioning allows also perform a recursive system identification to be included in the adaptive control loop.

The four-layer embedded board structure is in Figure 5-39, where the shaded layer relates to the physical components layout of the board and the top layer includes the functional blocks. Top and bottom layers contain low-power and power components respectively; one of the inner layers contains the power buses, and the other the ground level; refer to Appendix B for the scheme of the circuit and the pcb layout of the layers. The board consist on a section of Wheatstone bridges for sensors connection; the section of signal filtering and amplification; and the section of data conditioning for the analog to digital converter ADC (Baker 2003) (Kay, Ivanov *et al.* 2005).

The board has three working modes as indicated in Figure 5-39. Mode A consists on all the mentioned sections. Mode B includes the same features but the microcontroller can be replaced by any other data acquisition unit. Finally, mode C allows the board to be used as test bed for the microcontroller and accelerometer. The useful feature is that all modes can use the power buses of the embedded board, without the need of external power supply.

The collected data is stored in the on-board memory, and the embedded board, the microcontroller and accelerometer are placed in a water-proof box (IP67), which will be attached to the Hybrid Pipeline Robot (HPR). It is important to note that, despite the RF communication capability of the microcontroller, the data is not transferred to the outer world while the robot is in operations. The flow and the material of the pipe wall create interferences challenging the wireless communication; this matter may be a subject of research in a different area.

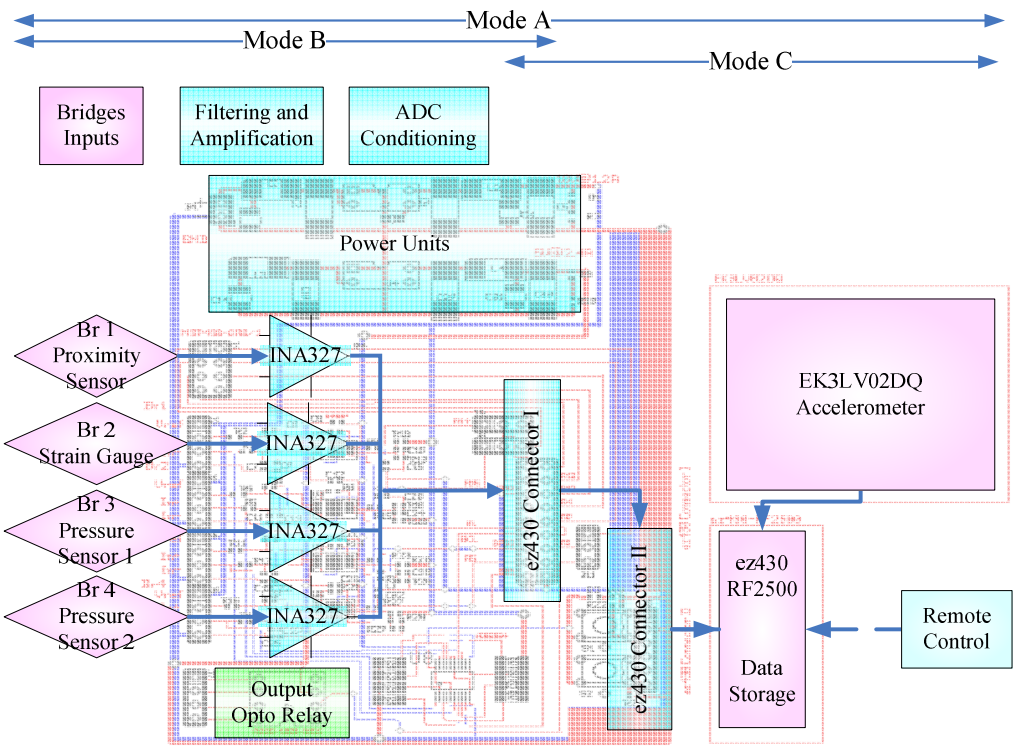

Figure 5-39 HPR Signal Conditioning Board: Functional Block Diagram

Shaded layer contains the actual layout of components, top layer contains the related functional blocks. Upper arrows show the three modes of operation. Mode A: signal conditioning and data acquisition by microcontroller ez430. Mode B: signal conditioning to be connected to any data acquisition device. Mode C: the board function as experimenter board for the microcontroller ez430.

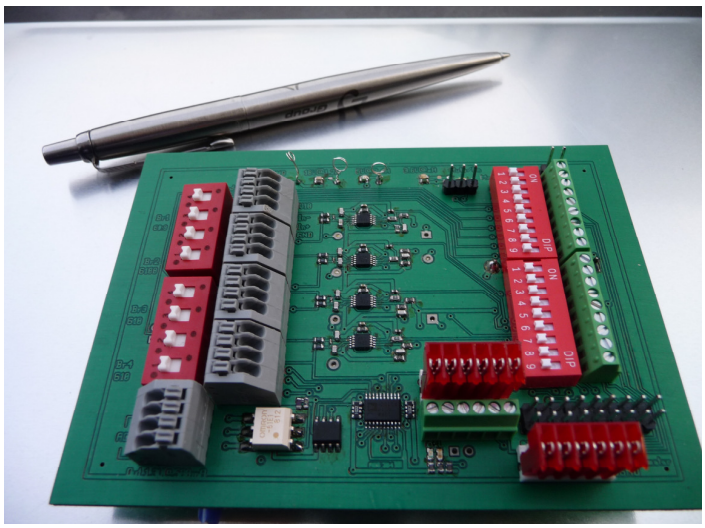

Figure 5-40 HPR Signal Conditioning Embedded Board:

Red switches for changing between modes. Grey connectors for connecting external devices. Green testing points for testing the microcontroller. Red connectors for connecting to the microcontroller and accelerometer.

The power architecture for the board has three independent power buses described in Figure 5-41. The 10V bus is the reference voltage for the Wheatstone bridges. This power bus is also the source for the Low Dropout Output (LDO) bucket converter, with

the purpose of converting the 10V to 3.3V required by the accelerometer (USB standar(d). The 5V power bus is the power supply for the integrated circuits (IC's), such as instrumentation amplifier, INA327 and the digital potentiometer (Baker 2004).

The overall system is powered by a cell battery, and the design considers aspects of power save through the enable characteristics of the IC's and the LDO, which are controlled by the microprocessor.

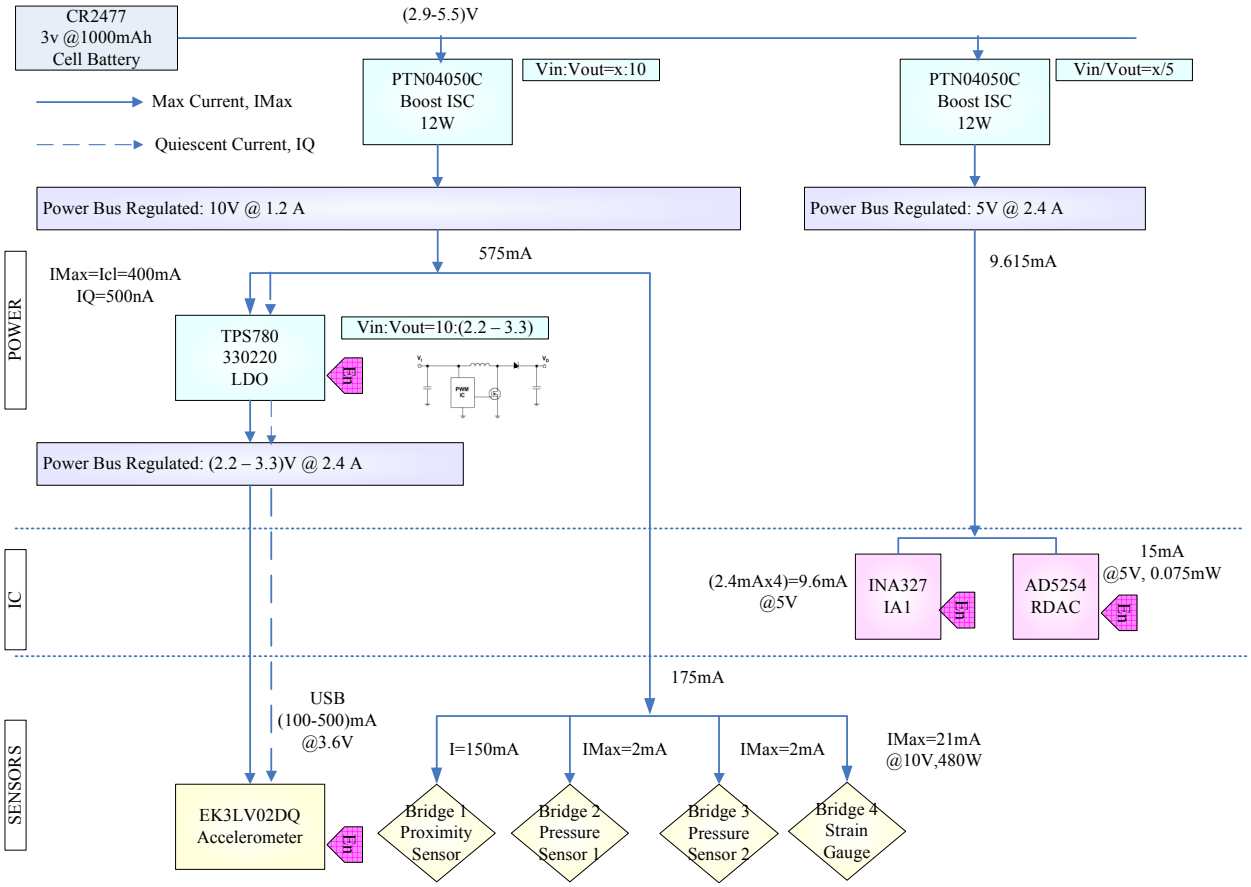

Figure 5-41 HPR Embedded System board: Power Architecture
Consists on three power buses of 10V, 5V and 3.3V (USB power) for ICs and sensors.

Instrumentation Amplifier Configuration

The Instrumentation Amplifier (I(A) has the function of filtering and amplification in successive stages. The IA's of the embedded board are configured for working as a general purpose amplifiers but they can be customised by software. This feature is due to each of the HPR sensors requires different configuration. For example, the strain gauges, for torque measurement, are thermal compensated but not calibrated. The two pressure sensors, for flow rate and pressure drop measurement, based on laser trimmed piezo-resistive bridge, are thermal compensated, calibrated and have a ratiometric

output referred to the power supply. The inductive proximity sensor does not require a particular bridge arrangement; however it can be attached to one arm of the bridge output so as to keep the standard arrangement of the bridges.

The network configuration for the instrumentation amplifier IA is described in Figure 5-42. At the input of the IA, a voltage divider acts as zero adjustment by hardware for each of the Wheatstone bridges. This hardware zeroing is complemented by software compensation (Baker 2008).

The output of the IA has an excursion out of the rails of the IA so as to keep the four bridges as standard as possible and independent of the rails of the amplifier and its margins. So, the output of the IA fluctuates at 10V reference. The same bus is the power supply of the sensor's bridges, giving the network a real span between 0-10V (Kugelstadt 2005).

The other circuits of the IA are filters; a low pass filter at the input of the IA (R9-C3 and R10-C5). C4 is to provide a separation of the inverting and non-inverting lines and a current path to ground. The output has a low impedance-low pass filter (R2-C2) to remove high frequency noise before the ADC. Additionally C6 provides a filter for the power supply and it is laid out as close as possible to the power pins of the IC to avoid current loops. The parallel circuit, C1-R3||R8 reduces the noise due to the gain configuration of the network (Texas Instruments 2004; Kay, Ivanov *et al.* 2005).

SPICE simulation results of the filters and INA327.

The instrumentation amplifier network was simulated using the programme TINA-T from Texas Instrument. The selection of the INA327 as instrumentation amplifier for this project is because it has low offset, low noise, reduced external circuitry, and therefore a reduced radiated source of noise (Texas Instruments 2004). A fundamental feature is the shutdown by software, a key feature for power saving for battery powered boards; the energy management is an important feature for autonomous systems such as the HPR, particularly because the embedded board is specified to work, in principle in the system identification stage, without any external assistance for periods at least of one hour.

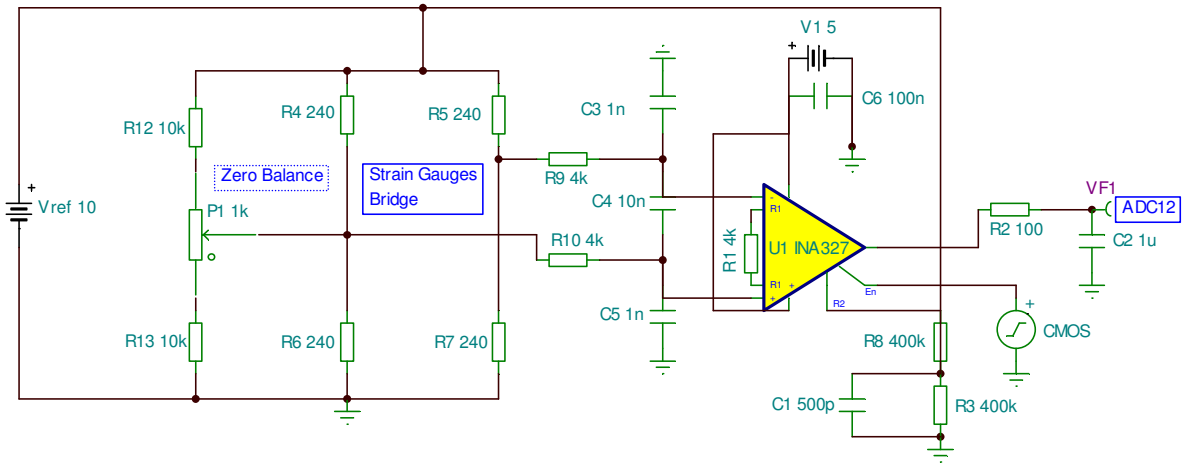

Figure 5-42 Instrumentation Amplifier: circuit simulation in SPICE

Circuit simulation for the particular case of the strain gauge bridge, including zero adjustment and bridge compensation. The simulation is to calibrate the input and output filters and the off-rail balance.

Results of the SPICE simulation are presented in Figure 5-43 (Catsoulis 2003; Heath 2003). DC operating point information, nodes and values, is in Appendix B. From simulation, the bandwidth of the amplifier stage is approximately 716 Hz; refer to Figure 5-43 (a). This bandwidth is suitable enough for sampling the HPR sensors. It is important to note that the set of variables defined in Chapter 3, are bounded by the slowest one, the flow rate, which gave a time constant of approximately 60 seconds during calibration.

The amplifier bandwidth acts also as low-pass filter, rejecting noise of high frequency. Figure 5-43 (b) shows the noise rejection of the amplifier network, rejecting noise of 148 uV at 5 kHz. The stability of the amplifier network is represented by the relative stability in Figure 5-43 (c). The Bode plot gives a gain margin Gm = -65dB, and the Phase Margins Gp = -123 degrees, which indicates a stable open loop system.

Signal conditioning supplementary design: Accelerometer stand-alone power board

By default, the accelerometer board is USB powered; so, in order to use it as stand alone device, the author developed an independent power supply board for the accelerometer. Additionally, the embedded signal conditioning board includes a USB bus for the accelerometer. Details of the circuit and power board are in Appendix B.

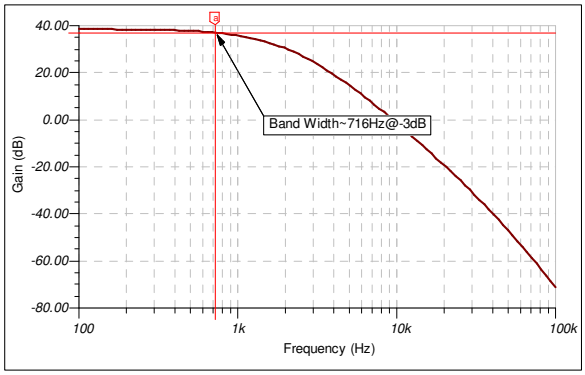

(a) Instrumentation Amplifier circuit simulation: Band Width, fc = 716Hz. Considering the HPR's sensors are of lower speed, particularly the pressure measurement, the band width is good enough.

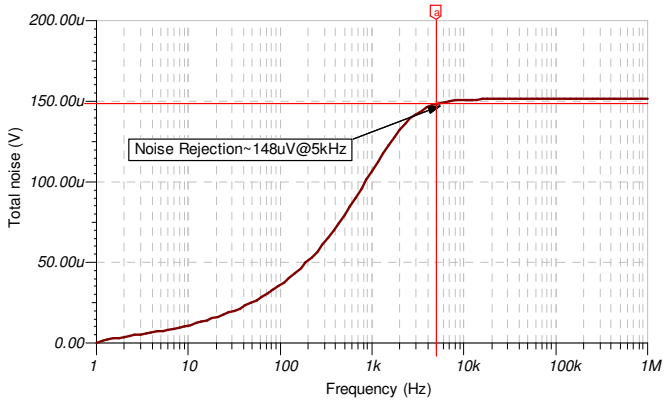

(b) Instrumentation Amplifier circuit simulation: Noise Rejection of 148 uV at 5 kHz, which is an ample range for the working region of the HPR's sensors.

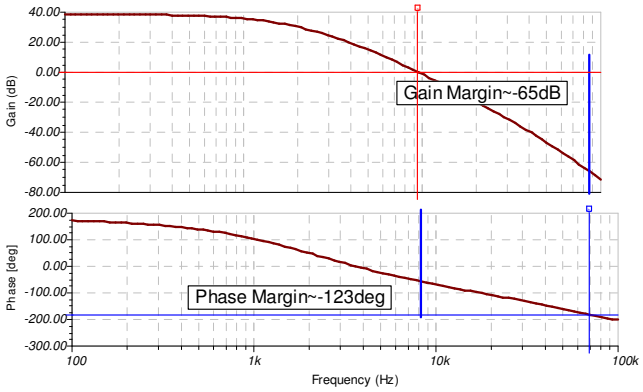

(c) Instrumentation Amplifier circuit simulation: Relative Stability, Gain and Phase Margins. Gm = -65dB and Gp = -123 degrees respectively, indicating a stable system.

Figure 5-43 Instrumentation Amplifier: SPICE simulation curves

.

5.6. CONCLUSIONS

Instrumentation System Development

Following the recommendations from the analyses in Chapter 3, the system identification of the HPR calls for the measurement of the **variables included** in the turbine efficiency, torque, rotational speed, flow rate and pressure drop across the turbine; and the robot linear speed. Therefore, it was decided to develop a set of suitable instruments called instrumentation system.

This **instrumentation system consists on** the original design, fabrication and calibration of pressure probes; conditioning of a torque transducer, calibration of the appropriate sensors; and developing a signal conditioning board for measuring the HPR's variables, contributing in this way, to the **characterization** of the robot's dynamics and nonlinearities when it is working in the pipeline environment. However, as to the best author's knowledge, there are no antecedents of the robot characterization as a whole unit, including the turbine and bristle-based vehicle, considering its interaction with the environment.

Pressure Probes for determination of the flow rate and pressure drop across the turbine

The pressure probes designed are Kiel-reverse, and Pitot-Gracey probes for static and stagnation pressure; and the pressure measurement chamber for measuring the static pressure at the wake of the turbine. As to the best author's knowledge, these probes are original in the design and implementation. However, as their names suggest, they are based on well known and proved pressure probes.

Standard rig's taps are normally for stationary measurements. Conversely, the HPR requires on-board measurement of the flow rate and pressure drop across the turbine, as it travels inside the pipeline. Alternatively, the pressure drop can be measured in stationary points, up and down stream the robot. However, the presence of the bristle-based vehicle introduces disturbances, altering the required conditions for measuring static pressure.

A common option for measuring pressure is the Pitot tube. However, the errors in the pressure measurement increase with small misalignment of the Pitot. So, the HPR's probes are designed as robust to probe misalignment.

The orifice plate is a standard option for measuring the flow rate, yet not suitable for pipelines where the flow degradation is not admissible.

The HPR's pressure probes have been designed on the base of the robot's needs, and calibrated for such purpose. Results from calibration gave good characteristics of the probes' measurements, such as repeatability and good time response, in addition to their robustness and suitable size to be mounted in a constrained space of the HPR. They can be used in different settings and in different vehicles, requiring further calibration to generalize their applicability.

The pressure measurement chamber PMC has been designed with specific dimensions to fit in the space surrounding the hollow universal joint. However, the chamber principles of functioning can be applied to any other usage of the probe for an on-board flow straightener and static pressure measurement point

The probes are designed in a suitable size and robustness to be attached to the robot no only as measurement points for system identification, but also as a permanent on-board instrumentation, due their non-disruptive design. As a conclusion, the design, fabrication and calibration of the pressure probes is a novel contribution of this research for the system identification of the HPR in its working pipeline environment.

Hollow universal joint vs. self drive and bristle-based robot

The HPR energy optimization calls for the characterization of the turbine efficiency by determining the bristle-based counter torque, while including in the characterization the dynamics of the turbine, bristle-based vehicle and the pipeline environment. Previous research determined the torque by the momentum of inertia from drawings. This method is useful for a rapid and inexpensive turbine characterisation. However, it lacks the feedback from the dynamics of the bristle-based vehicle and the pipeline environment.

A limitation of the joint as torque transducer is that it requires periodical maintenance due to the cables of the strain gauge, which may be damaged during the robot manipulation, in spite of the protection provided by the pressure measurement chamber and the waterproof neoprene coating.

Calibration results confirmed the suitability of the joint as torque transducer. As a result, only one curve, a second order regression, is necessary to represent the load-unload characteristic of the joint, in its clockwise and counter clockwise operation. All that mean, the joint measures consistently the torque in any direction of the turbine

rotation, and under changes in loading and unloading represented by different robot behaviour and pipe wall conditions.

Summarizing, the most important feature of the hollow universal joint as torque transducer is to measure the counter torque of the vehicle, which is the result of the turbine efficiency under different loading characteristics posed by the tractor nonlinearities and dynamics of the pipeline environment. This information is important for the energy optimisation and for determining ranges of operation of the robot, necessary for triggering the self-recovering state in case of potential failures due to energy availability. Therefore, the contribution of this project is the conditioning and calibration of the hollow universal joint as torque transducer for full characterization of the HPR.

Signal Conditioning Board

It was required a signal conditioning strategy for the HPR measurements. The signal conditioning options in the market are expensive and most of them dedicated for one type of sensors. Comparatively, for data acquisition, there are feasible solutions in the market at reasonable price such as the one selected for this application (ex430). However, this device still requires a signal conditioning device for protection of the microcontroller and for consistency of the acquired data.

Although the board has been designed as a general purpose for any sensor with working conditions within 0-10V as a requirement, and variable gain by hardware and software, it is advisable to do more trial tests for different sensors whether the board is required for other use rather than the specified for the HPR instrumentation system. Therefore, the signal conditioning embedded board design and development is a contribution of this research for the data acquisition of the HPR for the system characterization.

Chapter 6 Discussion, Conclusions and Future Work

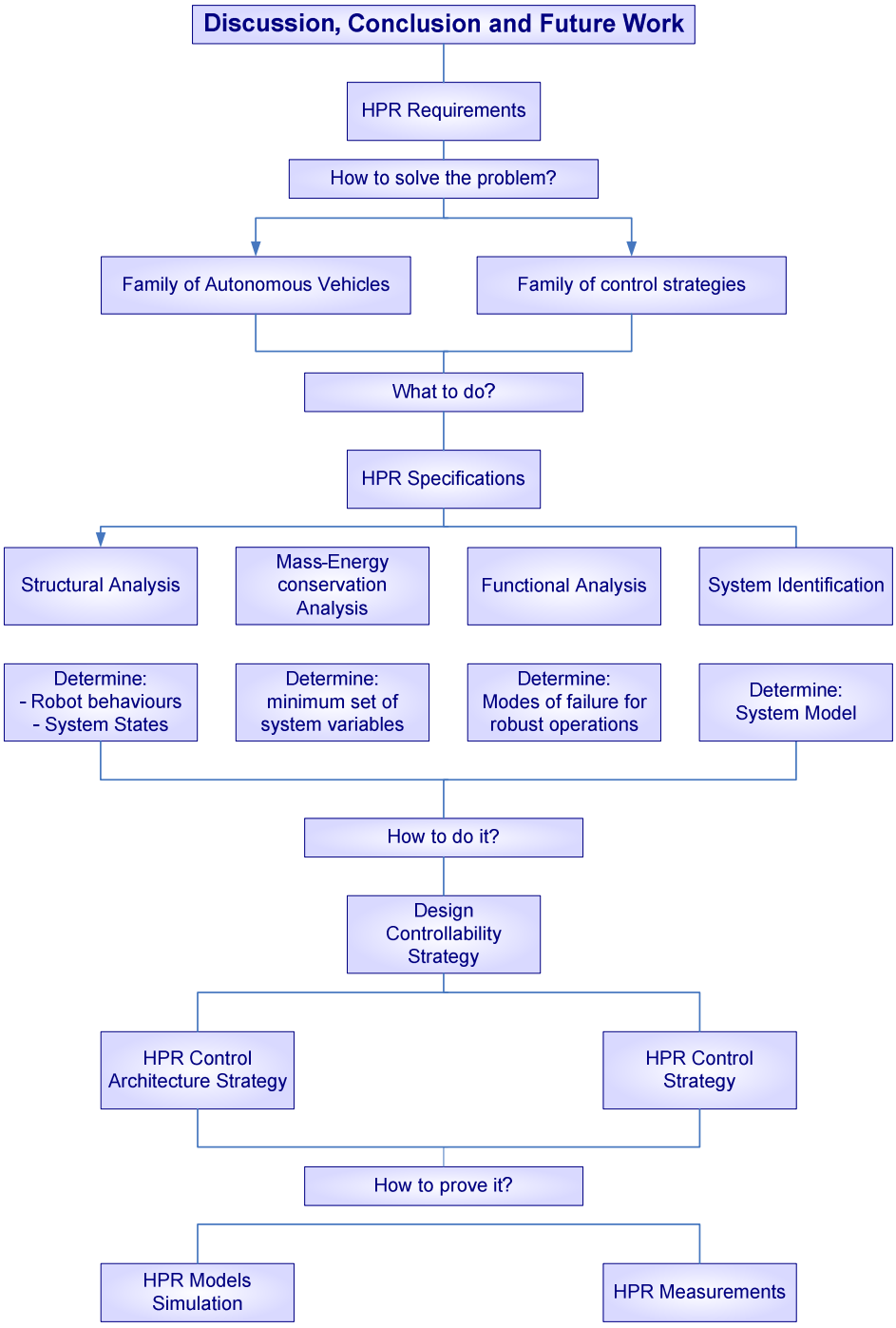

Figure 6-1 Chapter 6 contents

Flow diagram of the line of discourse for Discussion, Conclusion and Future Work

6.1. Discussion

HPR Requirements

The HPR also as a **bidirectional vehicle**, with bristle-based locomotion, calls for a **cruise control**, to accomplish with the scheduled operations at the specified location inside the pipeline, and to perform a **self-recovering** action after completion of the mission.

The hybric pipeline tractor, as **a flow-powered vehicle** calls for a **robust energy management** for coordinating the power generated, and stored in order to accomplish with the whole mission.

The whole mission of the bidirectional pipeline robot calls for a **robust operation** including a **self-recovering** state either after completion of the mission, or as a result of failures leading to the loss of the robot inside the pipeline.

How to solve the problem?

The HPT **controllability** was explored as a class of vehicle belonging to different families such as hybrid vehicles, autonomous vehicles, pipeline vehicles and self-powered, bristle-based pipeline vehicle.

The **control strategy** was explored from the stand point of model predictive control, reconfigurable systems and hybrid control, and the how these approaches are combined with neural networks to improve the results.

What to do?

HPR Specifications

Structural analysis to determine robot's behaviours and system states

A structural analysis of the forces governing the bristle-based vehicle gave the identification of the patterns of the robot interacting with the pipeline environment. As a result, the main HPR behaviours has been characterised, and these states are **crawling, reversing, cycling** and **idle** and **excursion**. Therefore, the proposed states namely, **operating, cruising** and **self recovering** for the on-schedule states; and **cycling** and **idle** for the off-schedule states, intend to capture the expected and most of the unexpected robot behaviours.

Mass-energy conservation analysis to determine the minimum set of system variables

As the controllability of the HPR is a problem of **energy generation and optimisation**, thus the energy-mass conservation analysis for the vehicle and turbine has been performed.

Similar analyses have been applied to seal pigs supported by **disc units**, including the simulation of different pipeline scenarios. However, this device lacks the self power characteristic and the bristle-based locomotion of the HPR.

Related research for a class of bristle-based pipeline vehicle, gives the characterisation of the bristle base locomotion and studies of the **buckling effect** of the bristles for the unidirectional vehicle and the reconfigurable shape vehicle. However, to the best author's knowledge, **there is no characterization** of the bristle-based pipeline vehicle and its effect over the turbine,

The energy analysis if based on a conservative system for inviscid flow and therefore without losses due to friction. However, for the purpose of determining the minimum set of variables to be observed, the energy-mass conservation analysis is good frame, and the recommendations are to measure the turbine efficiency for energy management and the vehicle speed for robot controllability and pipeline environment identification.

Functional analysis to determine modes of failure of the HPR

Fault tree analysis is an effective method in determining the probability of failure of components and the probability of a joint failure. However, determining the probability of failure of the components is rather difficult for real cases. So, results of the FMEA (Failure Mode and Effects Analysis), an heuristic approach, suggests that a robust control strategy for the HPR requires the identification of the behaviour of the bristle-based vehicle and the performance of the turbine

The FMEA results indicates also that, including an additional strategy of fault detection and isolation at component level, would contribute with less than the 25% to solve the causes of failure. Therefore, by including a **self-recovering state** either after completion of the mission, or as a result of failures leading to the loss of the robot inside the pipeline, the robust robot's operations is guaranteed. The reliable robot operation was the subject of a paper presented in the International Conference in Manufacturing Research 2010.

System Identification to determine System Model

A traditional option for system model for the MPC control is the CARIMA model. This model was successfully applied in several industrial problems where the nonlinear processes are approximated as a chain of linear systems. However, the model-based system identification becomes cumbersome for controlling nonlinear systems. Therefore, the HPR model follows data-based system identification, using ANN due to the good performance of the networks for approximating nonlinear dynamic systems.

The proposed HPR system identification and tracking system strategy is composed of two neural networks structures, trained in a supervised way (Demuth and Beale 2000). Evolutionary techniques are a rather different approach to network adaptation, with the advantage of convergence to the global minimum. However, the adaptive training search, based on variable step size, is a efficient approach to solve convergence problem.

Using a supervised learning approach is a limitation, particularly for non-observable systems, when it is not possible to count with input-output data; and for dynamic systems like the HPR, which are better identified by recursive algorithms. However, at the time of this research it was possible to count with a set of input-output data, flow rate and robot speed, which allows to train the networks in a supervised way.

How to do it?

HPR Control Architecture

The contribution of this research project is the design of a **control architecture** based on the **reconfiguration of the control strategy** for each of the states. The operating state is controlled by a model predictive control MPC for speed control with energy and time optimisation, as a problem of multi-objective optimisation. Cruising and self-recovering states are controlled by a neuro-dynamic programming approach for the optimization over time of the energy and mission time, as a problem of objective prioritisation. The transient states, idle and cycling are controlled by an inference algorithm.

The control structure is presented as an event based **Finite State Machine**, where the hierarchical structure becomes evident. The high level in the hierarchy is represented by the HPR supervisor, which performs the optimization of the

performance indexes; and the low level is represented by the HPR regime constituted by the on and off scheduled states.

The HPR control architecture with reconfiguration of the control strategy is based on Brooks' ideas of decomposing the whole system in functions and activities rather than a whole knowledge representation (Brooks 1991). Brooks' subsumption approach, where each hierarchical layer summarizes the knowledge of lower layers, is present in the HPR control architecture, in the form of optimisation strategies clustering the system states.

The **mullti-resolutional hierarchical planning MHP** approach from Meystel and Albus provides three operators in a hierarchical architecture (Meystel and Albus 2002). **Job assignment**, the first operator, is the base for the division of the HPR in operative states. F**ocus attention,** the second, is present in the HPR by changing the optimization prioritization. Finally schedule concatenation, the third operator, is performed by changing states upon the evaluation of the energy available in the system.

Meystel and Albus also propose the evaluation of the control architecture by a performance function. In the HPR case, the architecture is evaluated by state-dependent performance indexes.

The reconfigurable control approach was initially applied successfully in aircraft as fault detection and isolation, with software and hardware reconfiguration (Rauch 1994; Soloway, Shi *et al.* 2004 (b)). The reconfiguration of control strategy proposed for the HPR is the base of the robust operation of the robot, with self-recovering strategy.

HPR Control Strategy

The **robust energy management** is as the energy and time optimization. The HPR energy and time optimisation is a problem with unknown finite number of stages, and unknown transition probabilities between stages. Therefore, the proposed solution is based on a neuro-dynamic programming approach or reinforcement learning, based on Q-learning strategy. A **neuro-dynamic programming model of the stage transitions,** including the transition costs for energy and time, has been developed.

Alternative approaches to the controllability of the robot speed is the hybrid control in particular for cases with mixed signals, which perform the control of a piecewise affine function in a segmented state space. Hybrid control is at the core of commercial control units such as Honeywell Experion and HC 900 for control,

optimization, planning, scheduling and management with a knowledge base system. Applying hybrid control at this stage of the HPR was not particularly relevant. However, this approach will be fundamental at the time of closing the loop of the control system.

How to prove it?

HPR Model Simulation

System identification and tracking systems are simulated with trial data from rig tests relating flow rate and tractor speed, which is a collaboration of a different research group. However, the two variables data set represents limitation for testing the energy management strategy. Therefore, it was required the development of the necessary instrumentation to perform such tests, which is a subject of Chapter 5.

HPR Tests

HPR Instrumentation System Development

The system identification of the HPR calls for the measurement of the variables included in the turbine efficiency, torque, rotational speed, flow rate and pressure drop across the turbine; and the robot linear speed. Therefore, it was necessary to develop a set of suitable instruments called instrumentation system.

This instrumentation system consists on the original design, fabrication and calibration of pressure probes, conditioning a torque transducer, calibrating appropriate sensors and developing a signal conditioning board for measuring the HPR's variables, contributing in this way to the characterization of the robot's dynamics and nonlinearities when it is working in the pipeline environment.

6.2. Conclusions

Therefore, the contribution of this research project toward the HPR controllability is the controllability specification based on the analyses presented in Chapter 3. These specifications were the base for designing the control architecture and control strategy presented in Chapter 4. The simulation of the system and tracking models are also novel contributions, presented in Chapter 4. Finally, the instrumentation system has been designed in order to perform further tests for simulation of the energy management and as a base for control implementation.

6.3. Future work

During the development of this research project extraneous behaviours of the robot have been observed such as temporarily excursions with the flow or irregular dead time compared with the average. The control strategy has been designed as robust to such behaviours; however, these patterns have no clear explanation and may affect the overall robot performance if they persist. Therefore, these states deserve a dedicated qualitative and quantitative characterization further than direct observations reported in this project.

Thus, the instrumentation system described in Chapter 5 is designed and calibrated to measure the minimum data set, to characterize the dynamics of the robot. Additionally, this instrumentation system will allows to identify the system and to train the networks in a recursive way for better adaptation to the environment of the HPR, which is a matter of future work.

The minimum data set suggested in this thesis, will helps to simulate and test strategy time optimization under real environmental conditions. Additionally, the probes and signal-conditioning board designed and fabricated in this project, can be incorporated as permanent onboard instrumentation for future control implementation.

Appendix A

Table A-1 HPR Dynamic Programming model: Cost structure

Energy Cost $c_E(i,u)$ and Time Cost $c_t(i,u)$, for the three on-schedule states, operating, cruising and self-recovering; and for the off-schedule states cycling and idle.

Policy	Energy Cost $c_E(i,u)$	Time Cost $c_t(i,u)$	Speed Cost $c_s(i,u)$
Cruising			
μ1 Turbine powered	0	50	50
μ2 Battery powered	100	0	0
μ3 Pause (Idle state)	0	100	100
Self-recovering			
μ1 Turbine powered	0	50	50
μ2 Battery powered	100	0	0
μ3 Pause (idle state)	0	100	100
Operating			
μ1 Turbine powered	0	50	50
μ2 Battery powered	100	0	0
μ3 Pause (idle state)	0	100	50
Actions (out of control)			
Cycling	100	100	100
Undesirable Reversing	100	100	100

Table A-2 HPR flow rate-speed characteristics

Measurement from rig tests for the HPR's configurations: 6'' and 10'' turbine

HPR: Tractor Speed characteristic (10" Turbine)		
FlowRate10 up-stream {m/s}	Qcoef up-stream	TractorSpeed10 up-stream
0.293794	0.587589	0.000000
0.345987	0.691974	0.003303
0.376787	0.753574	0.007760
0.398985	0.797971	0.008356
0.431603	0.863206	0.011209
0.462831	0.925662	0.009666
FlowRate10 down-stream	Qcoef down-stream	TractorSpeed10 down-stream
0.263257	0.526513	0.002363
0.379010	0.758020	0.012491
0.399511	0.799023	0.014290
0.427447	0.854894	0.016290

HPR: Tractor Speed characteristic (6" Turbine)		
FlowRate6 up-stream	Qcoef up-stream	TractorSpeed6 up-stream
0.141990	0.283980	0.000000
0.150603	0.301206	0.001219
0.170240	0.340480	0.001600
0.194428	0.388856	0.002384
0.211501	0.423002	0.002802
0.215192	0.430385	0.002939
0.247212	0.494423	0.003870
0.252257	0.504515	0.003726
0.254124	0.508247	0.004000
0.258426	0.516852	0.004624
0.265639	0.531278	0.003641
FlowRate6 down-stream	Qcoef down-stream	TractorSpeed6 down-stream
0.200018374	0.400036748	0.002048942
0.218821417	0.437642834	0.002674941
0.252257285	0.504514569	0.002986858
0.265639125	0.53127825	0.003601551
0.270923073	0.541846145	0.003972936
0.319477691	0.638955382	0.004897639
0.345075346	0.690150691	0.006137228
0.436200843	0.872401687	0.011253657

Table A-3 HPR: Turbine Power and Efficiency vs. Flow coefficient

Values from twisted blade turbine characterization (Pulker 2005)

Qcoef	Ptot(W)	eff
2.384252	2.250903	0.383081
1.828672	2.744522	0.46709
1.502798	3.123598	0.531605
1.289068	3.406651	0.579778
1.138443	3.609708	0.614337
1.026828	3.746597	0.637634
0.941002	3.829204	0.651693
0.873105	3.867715	0.658247
0.81817	3.870819	0.658775
0.772903	3.845899	0.654534
0.735033	3.799193	0.646585
0.702944	3.735951	0.635822
0.675455	3.660556	0.62299
0.651679	3.576647	0.60871
0.630943	3.487219	0.59349
0.612721	3.394711	0.577746
0.596601	3.301091	0.561813
0.582251	3.207918	0.545956
0.569405	3.116411	0.530382
0.557846	3.027494	0.515249
0.547392	2.941848	0.500673

Qcoef	Ptot(W)	eff
0.537894	2.85995	0.486735
0.529229	2.782104	0.473486
0.521289	2.708476	0.460956
0.513987	2.639118	0.449152
0.507245	2.573989	0.438067
0.500999	2.512975	0.427683
0.495194	2.455907	0.417971
0.489781	2.40257	0.408894
0.484719	2.352722	0.40041
0.479972	2.306096	0.392475
0.475509	2.262416	0.385041
0.471303	2.221397	0.37806
0.467331	2.182757	0.371484
0.463572	2.146218	0.365265
0.460009	2.111511	0.359358
0.456626	2.078381	0.35372
0.453409	2.046586	0.348309
0.450347	2.015903	0.343087
0.44743	1.986126	0.338019
0.444648	1.957072	0.333074
0.441994	1.928576	0.328224
0.43946	1.900495	0.323445

Table A-4 Neural Network: Structure

System and Control Network Parameters

```
ctrlnet6a =     Neural NetOperating object:
   architecture:
       numInputs: 1
       numLayers: 2
     biasConnect: 2
    inputConnect: {1; 0}
    layerConnect: {0 0; 1 0}
   outputConnect: {0 1}
   targetConnect: {0 1}
      numOutputs: 1  (read-only)
      numTargets: 1  (read-only)
   numInputDelays: 0  (read-only)
   numLayerDelays: 0  (read-only)
:          inputs: {1x1 cell} of inputs
          layers: {2x1 cell} of layers
         outputs: {1x2 cell} containing 1 output
         targets: {1x2 cell} containing 1 target
          biases: {2x1 cell} containing 2 biases
inputWeights: {2x1 cell} containing 1 input weight
layerWeights: {2x2 cell} containing 1 layer weight
   functions: adaptFcn: 'trains' initFcn: 'initlay'
   weight and bias values:
IW: {2x1 cell} containing 1 input weight matrix
LW: {2x2 cell} containing 1 layer weight matrix
 b: {2x1 cell} containing 2 bias vectors
```

```
mrcnet =     Neural NetOperating object:
   architecture:
       numInputs: 2
       numLayers: 4
     biasConnect: {0; 0; 0; 0}
    inputConnect: {0 0; 0 0; 0 0; 0 0}
    layerConnect: {4x4 boolean}
   outputConnect: {0 0 0 0}
   targetConnect: {0 0 0 0}
      numOutputs: 0  (read-only)
      numTargets: 0  (read-only)
   numInputDelays: 0  (read-only)
   numLayerDelays: 0  (read-only)
          inputs: {2x1 cell} of inputs
          layers: {4x1 cell} of layers
         outputs: {1x4 cell} containing no outputs
         targets: {1x4 cell} containing no targets
          biases: {4x1 cell} containing no biases
inputWeights: {4x2 cell} containing no input weights
layerWeights: {4x4 cell} containing no layer weights
  functions: adaptFcn: (none) initFcn: (none)
weight and bias values:
 IW: {4x2 cell} containing no input weight matrices
LW: {4x4 cell} containing no layer weight matrices
b: {4x1 cell} containing no bias  vectors
```

Table A-5 Neural Network: Training Results

{terrormrcnet,terrormrcnetrcd,terrorymrcnet,terrormrcneterr} = train(mrcnet,{un4s4rnd;trnp6a},{yn4s4rnd}) TRAINBFG-srchbac, Epoch 0/600, MSE 2.33891e-005/4e-006, Gradient 1.29572e-013/1e-006 TRAINBFG, Minimum gradient reached, performance goal was not met.	{terrormrcnet,terrormrcnetrcd,terrorymrcnet,terrormrcneterr} = train(mrcnet,{trnp6a;un4s4rnd},{yn4s4rnd}) TRAINBFG-srchbac, Epoch 0/600, MSE 2.33891e-005/4e-006, Gradient 1.71828e-008/1e-006 TRAINBFG, Minimum gradient reached, goal was not met.	{terrormrcnet,terrormrcnetrcd,terrorymrcnet,terrormrcneterr} = train(mrcnet,{trnp6a;un4s4rnd},{trntref}) TRAINBFG-srchbac, Epoch 0/600, MSE 1.0301e-005/4e-006, Gradient 4.786e-008/1e-006 TRAINBFG, Minimum gradient reached, goal was not met.
terrormrcnet = Neural NetOperating object: architecture: numInputs: 2 numLayers: 4 biasConnect: 2 inputConnect: {1 1; 0 0; 1 0; 0 0} layerConnect: {4x4 boolean} outputConnect: {0 0 0 1} targetConnect: {0 0 0 1}	terrormrcnet = Neural NetOperating object: architecture: numInputs: 2 numLayers: 4 biasConnect: 2 inputConnect: {1 1; 0 0; 1 0; 0 0} layerConnect: {4x4 boolean} outputConnect: {0 0 0 1} targetConnect: {0 0 0 1}	terrormrcnet = Neural NetOperating object: architecture: numInputs: 2 numLayers: 4 biasConnect: 2 inputConnect: {1 1; 0 0; 1 0; 0 0} layerConnect: {4x4 boolean} outputConnect: {0 0 0 1} targetConnect: {0 0 0 1}
numOutputs: 1 (read-only) numTargets: 1 (read-only) numInputDelays: 0 (read-only) numLayerDelays: 0 (read-only)	numOutputs: 1 (read-only) numTargets: 1 (read-only) numInputDelays: 0 (read-only) numLayerDelays: 0 (read-only)	numOutputs: 1 (read-only) numTargets: 1 (read-only) numInputDelays: 0 (read-only) numLayerDelays: 0 (read-only)
subobject structures: inputs: {2x1 cell} of inputs layers: {4x1 cell} of layers outputs: {1x4 cell} containing 1 output targets: {1x4 cell} containing 1 target biases: {4x1 cell} containing 4 biases inputWeights: {4x2 cell} containing 3 input weights layerWeights: {4x4 cell} containing 3 layer weights	subobject structures: inputs: {2x1 cell} of inputs layers: {4x1 cell} of layers outputs: {1x4 cell} containing 1 output targets: {1x4 cell} containing 1 target biases: {4x1 cell} containing 4 biases inputWeights: {4x2 cell} containing 3 input weights layerWeights: {4x4 cell} containing 3 layer weights	subobject structures: inputs: {2x1 cell} of inputs layers: {4x1 cell} of layers outputs: {1x4 cell} containing 1 outp targets: {1x4 cell} containing 1 target biases: {4x1 cell} containing 4 biases inputWeights: {4x2 cell} containing 3 input weights layerWeights: {4x4 cell} containing 3 layer weights
functions: adaptFcn: (none) initFcn: (none) performFcn: 'mse' trainFcn: 'trainbfg'	functions: adaptFcn: (none) initFcn: (none) performFcn: 'mse' trainFcn: 'trainbfg'	functions: adaptFcn: (none) initFcn: (none) performFcn: 'mse' trainFcn: 'trainbfg'
parameters: adaptParam: (none) initParam: (none) performParam: (none) trainParam: .epochs, .show, .goal, .time, .min_grad, .max_fail, .searchFcn, .scale_tol.alpha, .beta, .delta, .gama, .low_lim, .up_lim, .maxstep, .minstep, .bmax	parameters: adaptParam: (none) initParam: (none) performParam: (none) trainParam: .epochs, .show, .goal, .time, .min_grad, .max_fail, .searchFcn, .scale_tol, .alpha, .beta, .delta, .gama, .low_lim, .up_lim, .maxstep, .minstep, .bmax	parameters: adaptParam: (none) initParam: (none) performParam: (none) trainParam: .epochs, .show, .goal, .time, .min_grad, .max_fail, .searchFcn, .scale_tol,.alpha, .beta, .delta, .gama, .low_lim, .up_lim, .maxstep, .minstep, .bmax
weight and bias values: IW: {4x2 cell} containing 3 input weight matrices LW: {4x4 cell} containing 3 layer weight matrices b: {4x1 cell} containing 4 bias vectors	weight and bias values: IW: {4x2 cell} containing 3 input weight matrices LW: {4x4 cell} containing 3 layer weight matrices b: {4x1 cell} containing 4 bias vectors	weight and bias values: IW: {4x2 cell} containing 3 input weight matrices LW: {4x4 cell} containing 3 layer weight matrices b: {4x1 cell} containing 4 bias vect

Appendix B

Table B-1 Kiel-reverse probe calibration: experiment conditions

Objective: determine the correction factor for Kiel-reverse measuring Flow rate Q		
R gas constant {J/kg.K}	287	
Gravity Force {m/s^2}	9.8	
C -> K	273.15	
pressure {N/m^2} ={Pa}	101300	
Temperature {K} {C}	299.55	26.4
air density {kg/m^3} = P/RT	1.1783	
water density @0C {kg/m3}	1000	
oil density {kg/m3}	784	
DistanceStagnation(Pitot-KIel) {mm}	230	
Channel width {m}	0.075	
H: Water height {m}	0.125	from pic
Channel Area{m^2}	0.009375	from measurement
z: Probe center line height	0.07	

Table B-2 Kiel-reverse probe: flow rate determination

time {s}	time abs {s}	litre	Flow Rate @ 20lt Tank {lt/s}	Flow Rate @ Flowmeter {lt/s}	Kiel-reverse Probe: Stag-Stat h {mm}	Kiel-reverse Probe: h {m}	Kiel-reverse Probe: Pstag-Pstat=ro_oil.g.h {Pa}	Kiel-reverse Probe: Qdot=UxA {m/s}x{m^2}	Kiel-reverse Probe: Qdot K_R {lt/s}
0	0	0	0	0.0	212.09	0.0000	0.0000	0.0000	0.0000
15	15.00	20	1.33	1.5	142.50	0.0696	534.6739	0.0097	9.6946
30	15.00	20	1.33	1.4	142.50	0.0696	534.6739	0.0097	9.6946
47	17.00	20	1.18	1.3	147.45	0.0646	496.6420	0.0093	9.3435
65	18.00	20	1.11	1.2	149.22	0.0629	483.0428	0.0092	9.2147
85	20.00	20	1.00	1.1	150.03	0.0621	476.8194	0.0092	9.1551
107	22.00	20	0.91	1.0	150.46	0.0616	473.5156	0.0091	9.1233
131	24.00	20	0.83	0.9	151.03	0.0611	469.1362	0.0091	9.0810
158	27.00	20	0.74	0.8	151.34	0.0608	466.7544	0.0091	9.0580
189	31.00	20	0.65	0.7	151.47	0.0606	465.7556	0.0090	9.0483
226	37.00	20	0.54	0.6	152.30	0.0598	459.3785	0.0090	8.9861

Table B-3 Kiel-reverse probe: static pressure determination

Flow Rate {tl/s}	Pitot Tube: p=ro_oil.g.h {Pa}	Kiel-reverse p=ro_oil.g.h {Pa}	Calculated pstatic {Pa}	delta PItot-Kiel	delta PItot-Calc
0.5	846.4581	477.8950	537.5778	368.5631	308.8804
1.5	832.5516	422.9602	526.2000	409.5914	306.3516
1.3	871.7359	461.4530	529.3858	410.2829	342.3501
1.0	891.2512	486.1161	533.3111	405.1351	357.9401
0.7	907.7701	585.6903	536.2124	322.0797	371.5576
0.5	914.5313	608.2789	537.5778	306.2524	376.9535
0.0	1046.2213	1843.9680	539.0000	-797.7467	507.2213

Pressure measurement supplementary calibration: Tubing

The rationale for tubing calibration is based on the fact that the time response, saturation and hysteresis may invalidate the pressure measurement. So, in order to design the pressure probes and the pressure measurement chamber PMC was necessary to determine the bore diameter and tubing dimensions for an appropriate response.

The time response of sensors is an important feature that affects the overall time response of the system and therefore the design of hardware and software for the data acquisition. The time response of the probes is affected mainly by the pressure taps and tubing diameter and the length of the tube from the pressure tap to the pressure transducer. The fastest the measurement stabilizes the better and easier to synchronize with the sample time of the data acquisition instruments. Recall that measurements are taken in the stationary state instead of the transient. Slow response means drift in time and slow convergence to the steady state, making difficult to determine the time at which the measurement is stable.

Saturation is produced when the measurement reaches the full scale value and remains at this point even when the excitation pressure is released. On the other hand, hysteresis relates to the memory of the system and it is produced when the measurement reading does not return to the starting point even when the excitation pressure is released. In this way, saturation is a class of hysteresis. However, from the measurement point of view they have completely different effects: saturation invalidates completely the measurement while hysteresis introduces error that can be compensated.

Although different, the time response and saturation and hysteresis are produced by the same causes: the capillary effect and the mixed density fluids. The capillary effect is affected by the fluid density and the diameter of the tubes. Whilst mixed density fluids such air and water produces air bubbles trapped between layers of water. If we add the capillary effect, as a result the fluids drip with difficulty or do not drip at all, the result is hysteresis and saturation respectively. So as to avoid the three mentioned effects was necessary to perform a tubing test.

In relation with timing, manufacturer of pressure probes gives some tube timing recommendations. The time constant is very short for any of the standard tubes down to 1/8" diameter; however, it increases rapidly for smaller diameters. For this reason 1/16" diameter is the smallest recommended size for standard use, taking 15 to 60 seconds to

reach equilibrium (Dwyer_Instruments_Inc. 2005; United-Sensor 2008 a); United-Sensor). Therefore, summarizing problems to be solved:

Problem 1 PMC tubing. Firstly, find the diameter, number and distribution of pressure taps. Secondly, find the suitable tubing layout and material so as to have fast readings, whilst minimizing saturation and hysteresis.

Problem 2 Kiel-reverse and Pitot-Gracey probes tubing. The pressure probes, Kiel-reverse and Pitot-Gracey dimensions are not specified in the literature. Find suitable hole diameter, tubes material and tube angle bent for fast and accurate readings.

Problem 3 Speed. Tubing connecting probes junctions and pressure transducers. Find tube diameter and material in addition to tubing layout for fast and accurate readings, adaptable to traversing the turbine contours.

Problem 4 Junctions. Perform a test for the junctions' material and shape (tees and crosses) and diameter to avoid pressure loss in the junctions.

Design of Experiments for Tubing and junctions

The design of Experiments DOE for tubing is not completely randomized because the pressure measurement systems, like strain measurement, has memory. So, the sequence of the flow rate increments and decrements is important. The experiment design considers the effect of the hydrostatic pressure, so all measurements have been taken at the same head level

Pressure measurement Tubing calibration

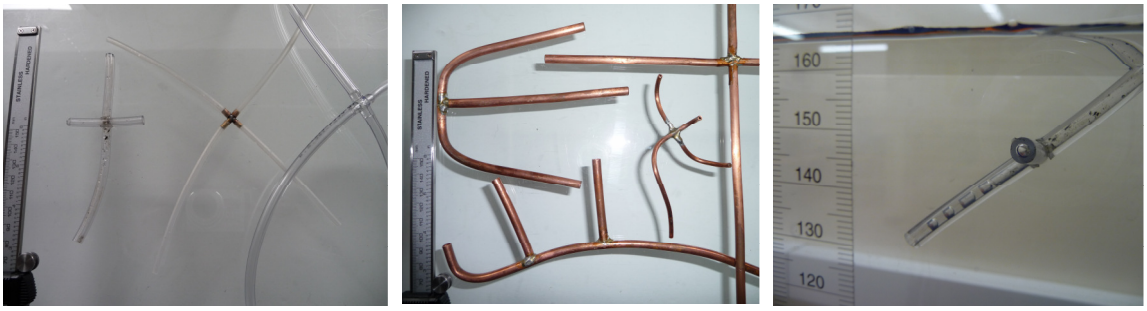

a) DOE Junctions
DOE Tubing

b) DOE Tubing
DOE Layout

c) Test: capillary effect

Figure B-1 Pressure Measurement Tubing Test

Test performed at Armfield Multipurpose Flume C4-MKII. Pressure measured with micro manometer. Material of tubes: copper, brass and plastic of different density. Material of junction: brass, embedded plastic and glass. Layout as described in Figure B3 a) and b).

Conclusion 1: plastic has higher capillary effect than copper, even for different plastic density. Therefore, copper was selected for the PMC tubing. However, plastic tubes are selected for external tubing due to the flexibility required to reach long distances from the pressure taps to the data acquisition equipment.

Conclusion 2: Higher bore present less capillary effect and propitiates the tube drain, diminishing the probability of air bubbles trapped by water. However, higher diameter is more likely to be blocked with extraneous particles. This aspect needs to be considered for probes maintenance.

Conclusion 3: the longer the tubes the higher the pressure loss; however, the HPR requires length of tube less than one meter for a low loss of pressure.

PMC tubing layout considerations

The requirements for selecting the tube layout for the PMC, was to fit the tubes inside the chamber without interfering with the universal joint and shaft, which are enclosed in the chamber. However, the pressure chamber is not all the time completely immersed in water and it is located in a region with turbulence of difficult characterization. So, considering that having immersed only few of the total holes, means a loss of pressure through the taps exposed to the atmosphere and therefore the reading may be inaccurate.

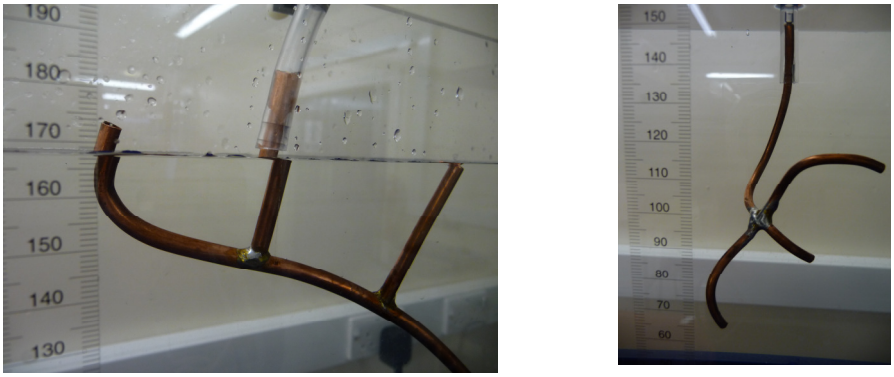

a) Layout 1 b) Layout 2 (selected)

Figure B-2 Pressure Measurement Chamber PMC: Tube Layout tests

Results: Tubing layout 2 shows fastest response even when only one stem was immersed in water, compared with layout 1, which requires three out of four stems immersed to start giving some readings. So, for the layout 2, even under higher hydrostatic pressure the readings were poorer compared with layout 1.

Conclusion Layout: The immersed length of layout 1 was higher than the immersed length of layout 2 so, the fast readings are predominantly affected by the

effective tube length immersed in water disregarding the effects of the hydrostatic pressure, which depend on the immersion depth.

Conclusion Material: Different tube materials have been tested basically copper, brass and plastic of different density. Copper gave the best result with less capillary effect therefore fast response with low or null hysteresis and null saturation.

Conclusion Bore: PMC tube effective internal diameter 2mm.

The tube length is critical even more when some taps are at atmospheric pressure. However, it is rather difficult to eliminate the air completely from tubes even when they are prefilled with water, in an evenly distributed pattern for holes, there is always some holes facing downward and therefore the liquid inside is dripping. The coexistence of mixed density flow (water and air) was assumed as default and it is corrected through the calibration procedure. As a conclusion, it was preferred a high diameter for tubes, which are in contact with water so as to diminish the capillary effect. Tubes carrying pressure from junctions to transducer are of smaller diameter with the purpose of improving the time response and including flexible tubes in the layout that traverses the turbine contour.

Recommendation: The measure point need to be as close as possible to all of the static taps, and if it is possible equidistant. The bore need to be as big as possible for the first section of tubes, which are in direct contact with the water and restrict the bore to the final collector tubes between the junctions and transducer. Metal, copper or brass tubes are better to diminish the capillary effect. Copper is better for flexibility in terms of adapting the tubes to the desired layout. Junctions of metal gave very good result in terms of fast measurement and low capillary effect. The result arrangement is in the figure. The final tube installed is depicted in Figure. It is important to note that the two sets of tube are installed in the PMC and the orientation of the probe is to assure each collector tube has always at least one tube in connection with the flow; this arrangement also is useful because the lower tube serves as bleeding pipe for the entire tubing system.

Hollow Universal Joint as Torque Transducer

Torque-strain characteristic: Regression model for Load-Unload combined program. Comparison of the first and second order regression models as predictor. Hollow marks are predicted values and dots are observed values. From the figure can

be seen that both models are good approximation to the observed values, however the second order is an improvement of the first order model.

Box B-1 Hollow Universal Joint as torque transducer: regression model

Predictor model for first and second order regression for load-unload combined program

Universal Joint First Order Regression
Observed vs. estimated values uE

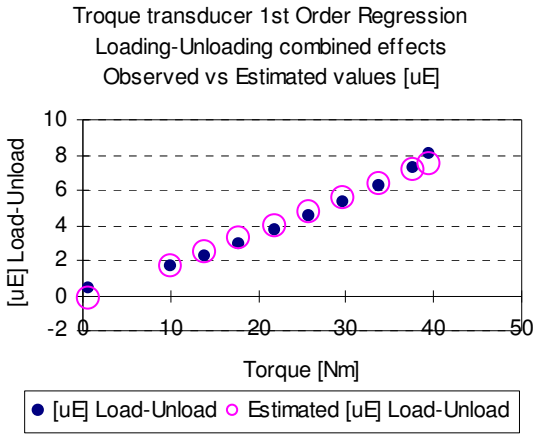

Universal Joint Second Order Regression
Observed vs predicted values uE

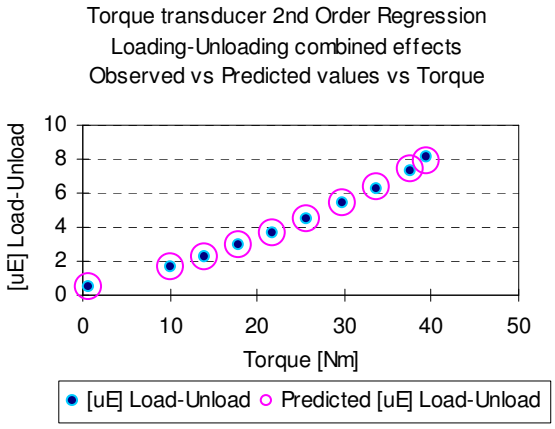

Observed vs predicted values vs Torque

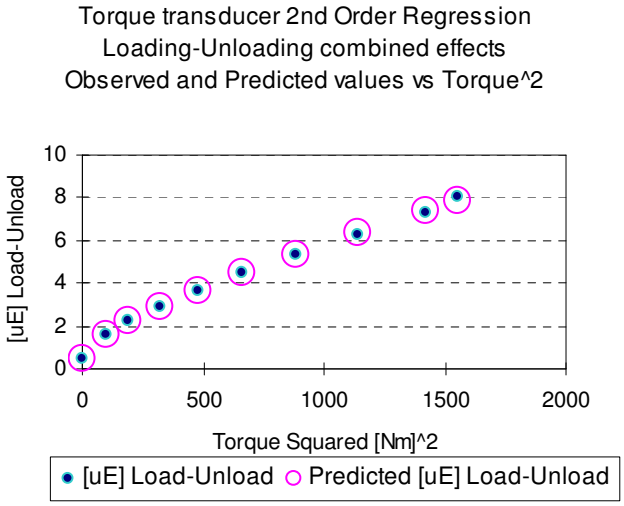

Box B-2 Pressure Measurement: Kiel-reverse probe design antecedents

a) Kiel probe curves of the error as a function of the probe dimensions. Probes profiles studied and experiment setup

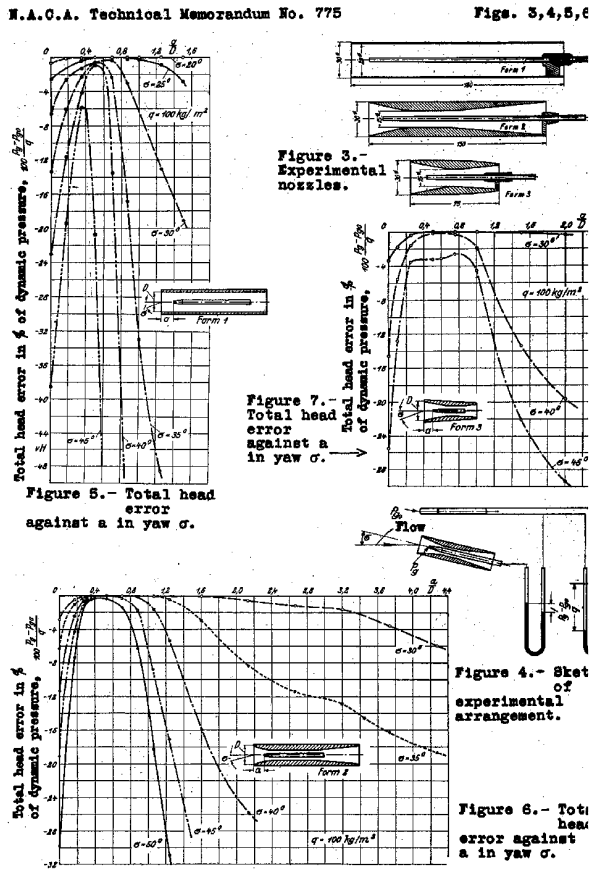

b) Error curves of the Gracey porbe as a function of the probe dimensions

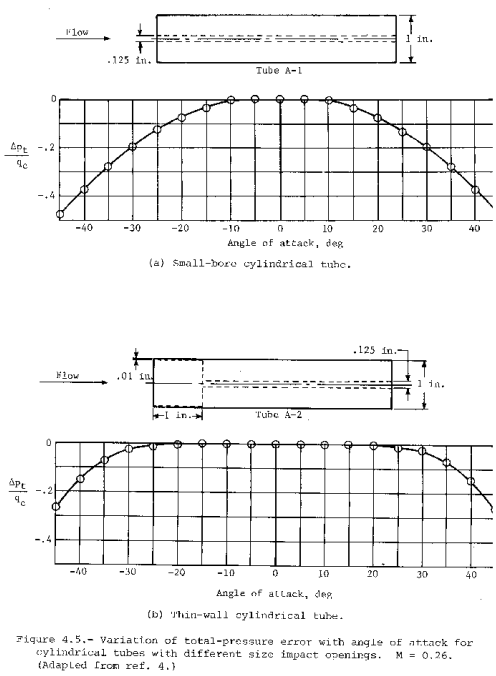

Figure 4.5.- Variation of total-pressure error with angle of attack for cylindrical tubes with different size impact openings. M = 0.26. (Adapted from ref. 4.)

c) Pitot-Gracey Probe detail of static holes

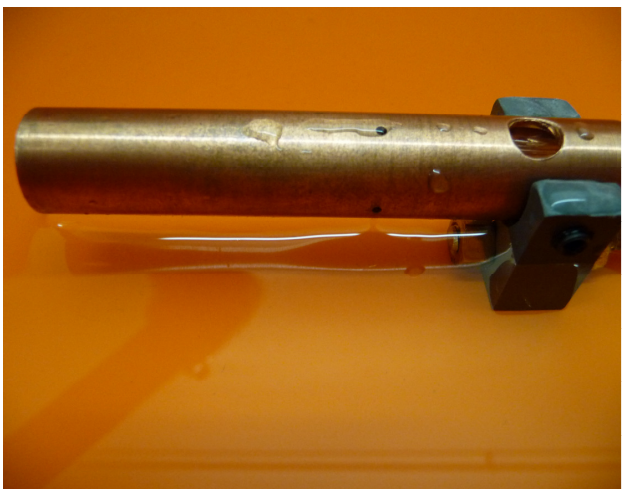

d) Design considerations of a standard Pitot-static tube

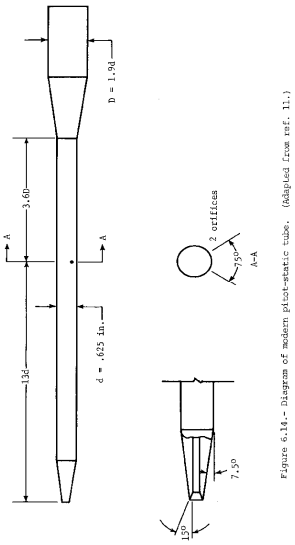

Figure 6.14.- Diagram of modern pitot-static tube. (Adapted from ref. 11.)

HPR Pressure measurement: requirements

Standard pressure taps on the wall of the pipe are discarded because the tractor displaces in both directions along the pipe. That implies the gauge pressure, or pressure measurement in relation to the atmosphere is discarded. The suitable type of pressure is the differential because it is needed to compare the stagnation and static pressure for flow rate calculation and the difference of static pressure between upstream and downstream the turbine for pressure drop. So the suitable pressure to be measured is the differential pressure. Absolute pressure, a relative pressure with respect to a vacuum, which is the one applicable when changes of atmospheric pressure need to be compensated or eliminated, is not applicable as all experiments are immersed in the laboratory atmosphere.

So, the differential pressure transducer need to be a wet/wet specification as the water is the common media. It was rather difficult or impossible to find from shelve a transducer with amplification capability. So the choice was a transducer with all that minus amplification, minus bidirectional. Differential wet/wet as no open orifice to the atmosphere,

Pressure transducer type. One of the most reliable (repetitivity, life span, drift, read specs) technology for pressure measurement is the piezo-resistive technology, which is based on the change of conductivity of particular materials when they are subject to pressure. The most common measurement element is the strain gauge, which changes its resistivity when it is pressed. The pressure transducer is based on a membrane in contact with an arrangement of strain gauges. However, the sensibility of the strain gauges to a permanent deformation is solved in part by embedding the gauges in the substrate of the transducer. So, the pressure range is a fundamental factor for selecting a proper pressure transducer. Overpressure can damage the strain gauges and produce permanent deformation of the membrane of the pressure transducer.

Type of pressure to be measured may be differential, gauge or absolute, that depends on the application. The differential and wet/wet requirement narrowed considerably the range of transducer to be selected, even without considering the economic factor. Transducer vs sensor. The transducer is a sensor with temperature compensation, calibration and amplification capabilities. However, it is difficult to find the right transducer for this particular application.

Bidirectional. Although the bidirectional capability, or the interchangeability of the pressure taps of the transducer, is a desired characteristic to avoid the risk of damage for the membrane, it was rather difficult to find

Water-hammer, do not exceed the range, no bidirectional P1>P2. The range of the transducer is of vital importance: if the range is small then the risk of saturation and permanent damage to the transducer components. Conversely, if the range is exceedingly bigger, the transducer becomes insensible and lacks of precision. The available range of pressures for the HPR from previous experiment was rather unclear, due to the transducer used and the collected data, which do not match the HPR requirements. So, the decision was to make a benchmark of the previous experiment and other similar experiments, all involving variable flow rate, performed in rigs with different flow density.

HPR Pressure measurement: Transducer Selection

Table B-4 shows the comparison of different experiments to determine a first approach of sensor selection in terms of range of flow rate. Results for different Reynolds' numbers and different density such as pressure measurement, flow around a cylinder, heat transfer and twisted blade turbine for an air rig; hydraulic pump, FAT pig and open channel for water rig and pipe flow for an oil rig. These experiments served as a guide in order to choose the appropriate sensor range and making the appropriate conversion of correction factor due to the change of density, by using dimensional analysis, when other flows rather than water have been used.

Oriffice-plate for flow rate. The idea was to use a build-in flow rate measurement, so the Boundary layer influence act as a systematic error compared with the orifice plate, which is affected in a different way upon the proximity of the tractor, therefore the error due to boundary layers is correlated with the measurement and more difficult to detect and isolate.

HPR transducer selection. As a result of the previous comparison and analysis, the requirement for the HPR pressure transducer is listed in the table Appendix for measure total and static pressure for a range of 1000 to 24000 Reynolds number and a maximum range of pressure of the order of the atmospheric pressure, 100000 Pa until 135000 Pa. The selection of the upper range was based on 2) Pressure back turbine based on Twisted blade turbine x1000 (water density) scaling factor applying dimensional analysis.

The selection of Reynolds number is done so as to cover a range from laminar to turbulent flow. However the pressure measurement for stagnation and static pressure differs being the static pressure higher than the stagnation, in general terms, the range of pressure selected was to cover both pressures in the same range. If more accuracy were required, so a smaller range for the stagnation pressure would be required.

However, it is important to remark that the difference in pressure relates to stagnation and static pressure with the same transducer, so a wide range for covering both pressures was the sensible selection for pressure transducer range. It is important to note that the ration of the stagnation to static pressure is 23%, so in using the same differential transducer for static stagnation pressure measurement the loss of sensibility for the stagnation pressure is 77%.

An alternative would be to use separate transducers for static and stagnation pressure with a common vacuum reference (recalling that the medium is water), with the inconvenience of introducing errors due to the variability of vacuum values for different transducers and the difficulty that vacuum pressures present for calibration. So the decision was to start with a reasonable cost/benefit and losing part of the dynamic range of the transducer and if the result of the stagnation pressure was not so good, change for the option of using absolute transducers.

Table B-4 Pressure measurement: transducer selection

Selection of sensor upon a benchmarking of referenced experiments

Fluid	density {kg/m3}	viscosity {Pa}	Mass Flow Rate {kg/s}	Velocity {m/s}	Flow Rate {m3/s}	Pressure delta Laminar {Pa}	Pressure delta Turbulent {Pa}	Re	Reference
air	1.18	1.80 e-05 {kg/ms}		29.11 - 11.64	-	20 - 125		9490 - 23700	Heat Transfer
air	1.2			22.3	-	40 - 200			Pressure Measurement
air	1.15			19.32	-	200 - 500		4739	Flow around cylinder
air					0.052	135			Twisted blade turbine
Oil	836	0.008		2.373	0.2079 - 0.8343	300 - 1100	1600 - 2100	1737 - 6970	TF1: Pipe Flow
water	1000		~ 5	-	0.0029 - 0.0060	31000 - 133000			TFLHydraulic Pump 2006
water	996	-			0.00011 - 0.00147	71700 - 32100			TFLHydraulic Pump 2008
water	1000	-		0.53	0.00135	-	-	-	TFL Open Channel
water	1000	-		0.46	0.1402	213			FAT PIG

Table B-5 Pressure transducer: requirements

Comparative values of pressure from similar experiments

Location	Pressure	Pa	Bar	psi	H2O	mmHg	Re	Direction	Media
Front Turbine	Ptotal	31000 (1)	0.31	4.495	124	233	6000 (3)	bi	wet
Front/Back Turbine	Pstatic	135000 (2)	1.350	20	542	1013	1000 – 24000 (4)	bi	wet
Ratio Pt/Ps		23%		23%					

Notes
(1) Pressure front turbine based on: Pipe Flow Turbulent flow (oil) Re=7000 and FAT PIG experiment
(2) Pressure back turbine based on Twisted blade turbine x1000 (water density) scaling factor applying dimensional analysis
(3) Reynolds Number for differential pressure front-back Based on Pipe Flow
(4) Based on Heat Transfer

Calibration: Tubing and PMC tubing layout

Box B-3 PMC: Tubing Layout tests

Test for selecting layout, dimensions and material for time response, repeatability and hysteresis

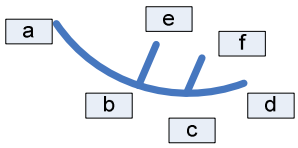

a) PMC Tubing layout 1

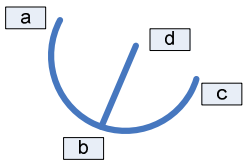

b) PMC Tubing layout 2

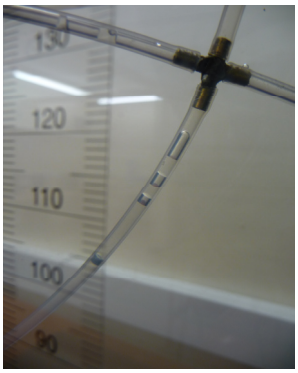

a) Test: capillary effect vs diameter, material and brass junction. Bubbles show mixed density fluids.

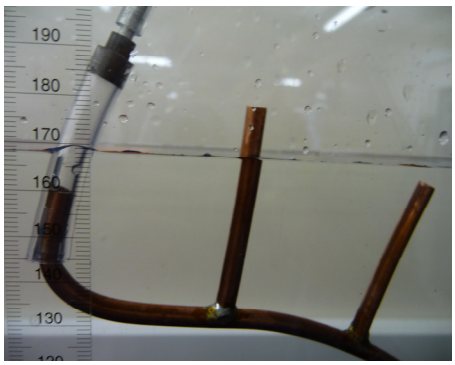

b) Variation of pressure intake Layout 1. The pressure measured at the three taps were different, suggesting a capillary effect affecting the readings

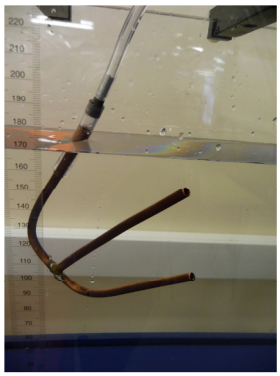

c) Layout 3. Curved layout to improve the bleeding of the fluids

Hollow Universal Joint as Torque Transducer

Table B-6 Hollow Universal Joint as Troque Transducer: Test Conditions

General laboratory conditions

Device: Strain Indicator Precission	(+/-) 0.0005	
Transducer/Strain Indicator brand	HW1-D StraiSert	
Rod length {m}	0.890	
Rod hole to end {m}	0.445	
Distance {m} (centre axel-hanging point)	0.455	
Rod weight {N}	(see Weights Table for details)	
Strain gauge characteristics:Type	FLA-3-17	
Gauge length {mm}	3	
Gauge Resistance {Ohm}	120 +/- 0.3	
Gauge Factor	2.13	(+/- 1%)
Temperature compensation Cdeg	17 E-04	
Transverse sensitivity %	0.3	

Table B-7 Hollow Universal Joint: DOE execution

Order	{g}	{Kgf}	{N}	Comments	weight	Cummulative Force {N}
Load 1	160.30	0.16	1.54	Base 1	Key	1.54
	1318.90	1.32	12.66		rod (effective length)	21.95
	305.40	0.31	2.93		hook	30.62
	501.40	0.50	4.81		Base plate	39.30
Load 2	2125.70	2.13	20.41	Base 2	rod=rod+hook+plate	47.98
Load 3	903.60	0.90	8.67	Incremental	A	56.62
Load 4	904.00	0.90	8.68		B	65.31
Load 5	903.80	0.90	8.68		C	74.10
Load 6	900.90	0.90	8.65		D	82.75
Load 7	904.40	0.90	8.68		E	86.64
Load 8	916.40	0.92	8.80		F	
Load 9	900.80	0.90	8.65		G	
Load 10	405.10	0.41	3.89	399.8	HA - HB	

RESOLUTION 120		DAY1					
Test Nr 0				Test Nr 3		Results	
Clockwise Load		(a) clock wise - FB(-)		(a) clock wise FB(-)		(a) clock wise - FB(-)	
Cumulative Force {N}	Torque {Nm}	120-uE-cwise-load	120-uE-cwise-unload	120-uE-cwise-load	120-uE-cwise-unload	120-uE-cwise-load	120-uE-cwise-unload
1.54	0.7002	1.22	NA	0.03	0.38	0.63	0.38
21.95	9.9852	2.49		2.2	1.78	2.35	1.78
30.62	13.9322	3.65		3.02	2.85	3.34	2.85
39.30	17.8808	4.47		3.76	3.96	4.12	3.96
47.98	21.8286	5.08		4.54	5.04	4.81	5.04
56.62	25.7638	5.74		5.44	6.1	5.59	6.10
65.31	29.7142	6.48		6.26	7.18	6.37	7.18
74.10	33.7170	7.02		7.07	8.13	7.05	8.13
82.75	37.6517	Saturation		7.95	8.67	7.95	8.67
86.64	39.4212			8.8	8.8	8.80	8.80

DAY 1 Counter-clockwise Load							
Test Nr 0		(b) counter clock-wise - FB(+)		Test Nr 3	(b) counter clock-wise - FB(+)		
Cumulative Force {N}	Torque {Nm}	120-uE-ccwise-load	120-uE-ccwise-unload	120-uE-ccwise-load	120-uE-ccwise-unload	120-uE-ccwise-load	120-uE-ccwise-unload
1.54	0.7002		0.15	1.02	1	1.02	0.58
21.95	9.9852	1.9	0.71	3.01	1.66	2.46	1.19
30.62	13.9322	3.21	1.48	3.58	2.24	3.40	1.86
39.30	17.8808	3.9	2.3	4.03	2.96	3.97	2.63
47.98	21.8286	4.45	3.26	4.6	3.73	4.53	3.50
56.62	25.7638	4.9	4.04	5.19	4.57	5.05	4.31
65.31	29.7142	5.59	4.97	5.85	5.5	5.72	5.24
74.10	33.7170	6.35	5.98	6.49	6.48	6.42	6.23
82.75	37.6517	6.82	7.07	7.35	7.46	7.09	7.27
86.64	39.4212	7.66	7.66	8.14	8.14	7.90	7.90

RESOLUTION 350							
Test Nr 1		(a) clock wise FB(-)		Test Nr 2	(a) clock wise FB(-)		
Cumulative Force {N}	Torque {Nm}	350-uE-cwise-load	350-uE-cwise unload	350-uE-cwise-load	350-uE-cwise unload	350-uE-cwise-load	350-uE-cwise unload
1.54	0.7002	0.10	saturate	0.01	0.48	0.06	0.48
21.95	9.9852	2.51	saturate	2.4	1.89	2.46	1.89
30.62	13.9322	3.47	saturate	3.25	2.94	3.36	2.94
39.30	17.8808	3.90	saturate	3.9	3.99	3.90	3.99
47.98	21.8286	4.65	saturate	4.6	5.07	4.63	5.07
56.62	25.7638	saturate to right	saturate	5.34	6.08	5.34	6.08
65.31	29.7142			6.17	7.08	6.17	7.08
74.10	33.7170			6.97	8.1	6.97	8.10
82.75	37.6517			7.76	8.56	7.76	8.56
86.64	39.4212			8.7	8.7	8.70	8.70

Test Nr 1		(b) counter clock-wise - FB(+)		Test Nr 2	(b) counter clock-wise - FB(+)		
Cummulative Force {N}	Torque {Nm}	350-uE-ccwise-load	350-uE-ccwise unload	350-uE-ccwise-load	350-uE-ccwise unload	350-uE-ccwise-load	350-uE-ccwise unload
1.54	0.7002	1.04	0.93	1.04	0.96	1.04	0.95
21.95	9.9852	2.72	1.59	2.78	1.53	2.75	1.56
30.62	13.9322	3.54	2.19	3.6	2.16	3.57	2.18
39.30	17.8808	4.08	2.89	4.11	2.89	4.10	2.89
47.98	21.8286	4.5	3.95	4.68	3.71	4.59	3.83
56.62	25.7638	5	4.46	5.49	4.62	5.25	4.54
65.31	29.7142	5.59	5.39	5.79	5.76	5.69	5.58
74.10	33.7170	6.4	6.09	6.52	6.67	6.46	6.38
82.75	37.6517	7.37	7.34	7.23	7.64	7.30	7.49
86.64	39.4212	7.72	7.72	8.06	8.06	7.89	7.89

Day 2		mV/V	x
Test Nr	1A	uE (micro-strain epsilon	x
Bridge Resolution	120	uEx10	
Gauge Factor	2.13	Polarity	FB(+) S+: orange, S-:blue
Options:		Load Direction	Clockwise from movable side

Test Nr	1A	(a) clock wise FB(+)				(b) counter clock-wise - FB(-)			
	weight	120-uE-cwise-load	120-mV/V-cwise-load	120-uE-cwise-unload	120-mV/V-cwise-unload	120-uE-ccwise-load	120-mV/V-ccwise-load	120-uE-ccwise-unload	120-mV/V-ccwise-unload
1	Key	0.90	0.19	1.12	0.74	0.00	0.00	1.03	0.70
2	pipe+hook	1.50	0.89	2.54	1.42	1.52	0.90	1.74	1.06
3	A	2.35	1.33	3.20	1.76	2.07	1.23	2.42	1.48
4	B	3.23	1.77	4.14	2.23	2.71	1.54	3.13	1.75
5	C	3.80	2.06	5.03	2.67	3.38	1.85	3.94	2.14
6	D	4.67	2.53	6.10	3.21	4.05	2.20	4.82	2.58
7	E	5.66	3.00	7.24	3.77	4.77	2.54	5.88	3.07
8	F	6.66	3.48	8.27	4.30	5.58	3.00	7.04	3.68
9	G	8.18	4.29	9.06	4.71	6.48	3.36	8.02	4.18
10	HA - HB	9.22	4.78	9.22	4.78	8.78	4.57	8.78	4.57

Test Nr	1B	(a) clock wise FB(+)				(b) counter clock-wise - FB(-)			
	weight	120-uE-cwise-load	120-mV/V-cwise-load	120-uE-cwise-unload	120-mV/V-cwise-unload	120-uE-ccwise-load	120-mV/V-ccwise-load	120-uE-ccwise-unload	120-mV/V-ccwise-unload
1	Key	0.00	0.00	0.20	0.29	0	0	0.15	0.25
2	pipe+hook	1.79	1.06	1.53	0.90	1.23	0.77	1.00	0.67
3	A	2.25	1.31	2.27	1.30	1.74	1.05	1.54	0.94
4	B	2.94	1.63	3.03	1.69	2.26	1.31	2.09	1.22
5	C	3.75	2.04	3.77	2.04	2.86	1.60	2.77	1.57
6	D	4.46	2.40	4.77	2.55	3.46	1.92	3.46	1.91
7	E	5.16	2.74	5.70	3.00	4.13	2.21	4.30	2.32
8	F	5.85	3.10	6.77	3.55	4.80	2.60	5.21	2.77
9	G	6.71	3.50	7.49	3.84	5.90	3.10	6.20	3.27
10	HA - HB	7.58	3.97	7.58	3.97	6.72	3.54	6.72	3.54

Test Nr	2A	mV/V	x
Bridge Resolution	350	uE (micro-strain epsilon	x
Gauge Factor	2.13	uEx10	
Options:		Polarity	

Test Nr	2A	(a) clock wise FB(+)				(b) counter clock-wise - FB(-)			
	weight	350-E-load cwise	350-mV/V load cwise	350-E-unload cwise unload	350-mV/V unload cwise	350-E-load ccwise	350-mV/V load ccwise	350-E-unload ccwise	350-mV/V unload ccwise
1	Key	0.10	0.18	-1.26	-0.82	0.00	0.00	-1.06	-0.71
2	pipe+hook	1.68	1.01	0.88	0.60	1.03	0.70	1.12	0.74
3	A	2.37	1.34	1.81	1.09	1.51	0.94	1.90	1.15
4	B	3.14	1.77	2.86	1.61	2.12	1.24	2.59	1.49
5	C	3.95	2.13	3.87	2.11	2.79	1.59	3.30	1.83
6	D	4.80	2.55	4.90	2.62	3.53	1.92	4.23	2.30
7	E	5.62	3.00	5.99	3.12	4.32	2.32	5.06	2.72
8	F	6.62	3.44	6.91	3.63	5.08	2.77	6.04	3.19
9	G	7.50	3.95	7.64	4.00	5.95	3.13	6.66	3.52
10	HA - HB	7.84	4.10	7.84	4.10	6.80	3.57	6.80	3.57

Test Nr	2B								
		(a) clock wise FB(+)				(b) counter clock-wise - FB(-)			
	weight	350-E-load cwise	350-mV/V load cwise	350-E-unload cwise unload	350-mV/V unload cwise	350-E-load ccwise	350-mV/V load ccwise	350-E-unload ccwise	350-mV/V unload ccwise
1	Key	0.00	0.00	-1.35	-1.04	0.00	0.00	-2.08	-1.20
2	pipe+hook	1.18	0.75	0.93	0.63	0.72	0.54	0.40	0.38
3	A	1.76	1.05	1.65	1.00	1.20	0.77	1.08	0.71
4	B	2.43	1.41	2.38	1.38	1.85	1.12	1.74	1.04
5	C	3.20	1.75	3.12	1.73	2.59	1.46	2.54	1.46
6	D	3.89	2.10	4.03	2.19	3.34	1.87	3.48	1.91
7	E	4.58	2.48	4.90	2.62	4.28	2.28	4.38	2.39
8	F	5.31	2.81	5.81	3.07	5.08	2.76	5.43	2.88
9	G	6.08	3.22	6.67	3.52	6.01	3.15	6.43	3.40
10	HA - HB	6.97	3.65	6.97	3.65	6.94	3.66	6.94	3.66

		(a) clock wise FB(+)				(a) clock wise FB(+)			
Cummulative Force {N}	Torque {Nm}	120-uE-cwise-load	120-mV/V-cwise-load	120-uE-cwise-unload	120-mV/V-cwise-unload	120-uE-cwise-load	120-mV/V-cwise-load	120-uE-cwise-unload	120-mV/V-cwise-unload
1.54	0.7002	0.90	0.19	1.12	0.74	0.00	0.00	0.2	0.29
21.95	9.9852	1.50	0.89	2.54	1.42	1.79	1.06	1.53	0.9
30.62	13.9322	2.35	1.33	3.2	1.76	2.25	1.31	2.27	1.3
39.30	17.8808	3.23	1.77	4.14	2.23	2.94	1.63	3.03	1.69
47.98	21.8286	3.80	2.06	5.03	2.67	3.75	2.04	3.77	2.04
56.62	25.7638	4.67	2.53	6.1	3.21	4.46	2.40	4.77	2.55
65.31	29.7142	5.66	3	7.24	3.77	5.16	2.74	5.7	3
74.10	33.7170	6.66	3.48	8.27	4.3	5.85	3.10	6.77	3.55
82.75	37.6517	8.18	4.29	9.06	4.71	6.71	3.50	7.49	3.84
86.64	39.4212	9.22	4.78	9.22	4.78	7.58	3.97	7.58	3.97

Table B-8 Hollow Universal Joint: descriptive statistics of tests

Cummulative Force {N}	Torque {Nm}	120-uE-cwise-load	120-mV/V-cwise-load	120-uE-cwise-unload	120-mV/V-cwise-unload
1.54	0.7002	0.45	0.10	0.66	0.52
21.95	9.9852	1.65	0.98	2.04	1.16
30.62	13.9322	2.30	1.32	2.74	1.53
39.30	17.8808	3.09	1.70	3.59	1.96
47.98	21.8286	3.78	2.05	4.40	2.36
56.62	25.7638	4.57	2.47	5.44	2.88
65.31	29.7142	5.41	2.87	6.47	3.39
74.10	33.7170	6.26	3.29	7.52	3.93
82.75	37.6517	7.45	3.90	8.28	4.28
86.64	39.4212	8.40	4.38	8.40	4.38
Sum		43.3300	23.0350	49.5150	26.3600
Count Nr-samples		10	10	10	10
Location Measurement/Point Statistic (a-b)					
Mean		4.3330	2.3035	4.9515	2.6360
Meadian		4.1700	2.2575	4.9175	2.6175
Mode		#N/A	#N/A	#N/A	#N/A
Percentiles					
Quartile Q0 smallest		0.45	0.10	0.66	0.52
Quartil Q1		2.30	1.32	2.74	1.53
Quartil Q2 Median		4.17	2.26	4.92	2.62
Quartil Q3		6.26	3.29	7.52	3.93
Quartile Q4 largest		8.40	4.38	8.40	4.38
IQR Inter Quartile Range		3.96	1.97	4.79	2.40
Variability Measurement {a/(a+b)}					
Maximum		8.4000	4.3750	8.4000	4.3750
Minimum		0.4500	0.0950	0.6600	0.5150
Range		7.9500	4.2800	7.7400	3.8600
Sample Variance	stdv of sample average?	6.6042	1.7980	7.3424	1.8254
Standard Deviation		2.5699	1.3409	2.7097	1.3511
Coefficient of Variation=Standard Deviation/Mean		0.593	0.582	0.547	0.513
X+s Gra		6.9029	3.6444	7.6612	3.9871
X-s Gra		1.7631	0.9626	2.2418	1.2849
Kurtosis		-0.9289	-0.7034	-1.2966	-1.3175
Skewness		0.1414	-0.0137	-0.1338	-0.1241
Relative					

Cummulative Force {N}	Torque {Nm}	120-uE-cwise-load	120-mV/V-cwise-load	120-uE-cwise-unload	120-mV/V-cwise-unload
Location Measurement					
z-score standardized value		0.3805	-5.4324	-0.3609	-6.1697
Interval Estimation of a population: Large-sample Case					
Sample Size		10	10	10	10
Mean		4.33	2.30	4.95	2.64
Standard Deviation		2.57	1.34	2.71	1.35
Confidence Coefficient		0.95	0.95	0.95	0.95
Level of Significance Alpha		0.05	0.05	0.05	0.05
z-value NORMSINV(1-Alpha/2)		1.96	1.96	1.96	1.96
Standard Error		0.81	0.42	0.86	0.43
Margin Error		1.59	0.83	1.68	0.84
Point Estimate		4.33	2.30	4.95	2.64
Lower Limit		2.74	1.47	3.27	1.80
Upper LImit		5.93	3.13	6.63	3.47
Interval Estimation of a population: Small-sample Case, Sigma estimated by s					
Confidence Coefficient		0.95	0.95	0.95	0.95
Level of Significance Alpha		0.05	0.05	0.05	0.05
Degree of Freedom		9	9	9	9
t-value TINV()		2.26	2.26	2.26	2.26
Standard Error		0.81	0.42	0.86	0.43
Margin Error		1.84	0.96	1.94	0.97
Point Estimate		4.33	2.30	4.95	2.64
Lower Limit		2.49	1.34	3.01	1.67
Upper LImit		6.17	3.26	6.89	3.60
Hypothesis Testing					
Level of significance Alpha		0.0500	0.0500	0.0500	0.0500
Hypothesized Value		4.64		4.64	
z-value Test Statistic		-0.381		0.361	

Cummulative Force {N}	Torque {Nm}	120-uE-cwise-load	120-mV/V-cwise-load	120-uE-cwise-unload	120-mV/V-cwise-unload
y esto que es? NORMSINV		1.9600	1.9600	1.9600	1.9600
Large-sample case: NORMSDIST					
p-value: Lower Tail Rejection Region		3.52E-01		6.41E-01	
p-value: Upper Tail Rejection Region		6.48E-01		3.59E-01	
p-value two tail		7.04E-01		7.18E-01	

Box B-4 Hollow Universal Joint: ANOVA 2Groups Load, unload programs

ANOVA Load and unload program to determine the variability within and between groups

Anova: Single Factor
H0: mu1=mu2 …
Ha: at least two mu are different
SUMMARY

Groups	Count	Sum	Average	Variance
{uE} Load	10	39.7750	3.9775	6.0255
{uE} Unload	10	44.8175	4.4818	6.6523

ANOVA						
Source of Variation	SS	df	MS	F	P-value	F crit
Between Groups	1.2713	1	1.2713	0.2006	0.6596	4.4139
Within Groups	114.1000	18	6.3389			
Total	115.3713	19				
66% => No Evidence to infer Ha (at least two means are different is true						
Confidence Coefficient	0.95					
Level of Significance Alpha	0.05					

Box B-5 Hollow Universal Joint: Regression for Load program

B: ANOVA for test statistic of linear relation
ANOVA
H0: beta is explained in regression curve

ANOVA: Load

	df	SS	MS	F	Significance F
Regression	2	53.7199	26.8599	369.2457	8.0222E-08
Residual	7	0.5092	0.0727		
Total	9	54.2291			

	Coefficients	Standard Error	t Stat	P-value	Lower 95%	Upper 95%	Lower 95.0%	Upper 95.0%
Intercept	0.2903	0.2620	1.1080	0.3045	-0.3293	0.9100	-0.3293	0.9100
Torque {Nm}	0.0888	0.0269	3.3073	0.0130	0.0253	0.1524	0.0253	0.1524
Torque^2 {Nm}^{2}	0.0024	0.0006	3.9772	0.0053	0.1000	0.0039	0.1000	0.0039

Table B-9 Hollow Universal Joint: residuals analysis for Load program

RESIDUAL OUTPUT				PROBABILITY OUTPUT	
Observation	Predicted {uE} Load	Residuals	Standard Residuals	Percentile	{uE} Load
1	0.3537	-0.1287	-0.5413	5	0.225
2	1.4196	0.0903	0.3799	15	1.51
3	1.9996	0.1029	0.4326	25	2.1025
4	2.6555	0.1295	0.5443	35	2.785
5	3.3870	0.0605	0.2542	45	3.4475
6	4.19152	-0.0315	-0.1325	55	4.16
7	5.0748	-0.1448	-0.6088	65	4.93
8	6.0471	-0.3246	-1.3648	75	5.7225
9	7.0788	-0.2613	-1.0984	85	6.8175
10	7.5672	0.5078	2.1348	95	8.075

Box B-6 Regression for unload program

ANOVA: Unload

	df	SS	MS	F	Significance F
Regression	2	59.7951	29.8976	2764.3292	7.1903E-11
Residual	7	0.0757	0.0108		
Total	9	59.8709			

	Coefficients	Standard Error	t Stat	P-value	Lower 95%	Upper 95%	Lower 95.0%	Upper 95.0%
Intercept	0.4685	0.1010	4.6367	0.0023	0.2296	0.7074	0.2295	0.7074
Torque {Nm}	0.1095	0.0103	10.5873	1.466E-05	0.0852	0.1341	0.0851	0.1341
Torque^2 {Nm}^{2}	0.0022	0.0002	9.3448	3.3381E-05	0.0016	0.0027	0.0016	0.0027

Box B-7 Hollow Universal Joint: residuals analysis for unload program

RESIDUAL OUTPUT				PROBABILITY OUTPUT	
Observation	Predicted {uE} Unload	Residuals	Standard Residuals	Percentile	{uE} Unload
1	0.54635	0.0786	0.8574	5	0.625
2	1.7829	-0.0804	-0.8770	15	1.7025
3	2.4235	-0.0660	-0.7197	25	2.3575
4	3.13297	-0.0354	-0.3867	35	3.0975
5	3.9108	-0.0333	-0.3639	45	3.8775
6	4.7545	0.0329	0.3593	55	4.7875
7	5.67004	0.1099	1.1988	65	5.78
8	6.6677	0.1547	1.6873	75	6.8225
9	7.7171	-0.0246	-0.2690	85	7.6925
10	8.2113	-0.1363	-1.4864	95	8.075

Table B-10 Hollow Universal Joint: prediction and estimation intervals 2 Groups

Load-Unload individual effects

Scatter Plot: Torque vs Residuals							
				0.95 Prediction Interval		0.95 Confidence Interval Estimate	
Torque {Nm}	Torque^2 {Nm}^{2}	{uE} Load	Estimated Value	Prediction Interval Lower limit	Prediction Interval Upper limit	Confidence Interval Estimate Lower limit	Confidence Interval Estimate Upper limit
0.0000	0.0000		0.2903	-0.5989	1.1795	-0.3293	0.9100
0.5000	0.2500		0.3354	-0.5356	1.2063	-0.2578	0.9285
0.7002	0.4903	0.2250	0.3537	-0.5102	1.2177	-0.2291	0.9366
9.9852	99.7052	1.5100	1.4196	0.7147	2.1246	1.1193	1.7200
13.9322	194.1054	2.1025	1.9996	1.3001	2.6991	1.7122	2.2870
17.8808	319.7246	2.7850	2.6555	1.9533	3.3578	2.3615	2.9495
21.8286	476.4897	3.4475	3.3870	2.6854	4.0886	3.0946	3.6794
25.7638	663.7721	4.1600	4.1915	3.4970	4.8860	3.9166	4.4665
29.7142	882.9333	4.9300	5.0748	4.3882	5.7614	4.8205	5.3291
33.7170	1136.8380	5.7225	6.0471	5.3543	6.7399	5.7765	6.3178
37.6517	1417.6523	6.8175	7.0788	6.3438	7.8138	6.7134	7.4442
39.4212	1554.0310	8.0750	7.5672	6.7956	8.3389	7.1328	8.0017
40.0000	1600.0000		7.7303	6.9438	8.5168	7.2701	8.1905
50.0000	2500.0000		10.8047	9.5293	12.0802	9.7002	11.9093
60.0000	3600.0000		14.3649	12.2000	16.5298	12.2961	16.4337
100.000	10000.0000		33.4634	24.5876	42.3393	24.6106	42.3163

				0.95 Prediction Interval		0.95 Confidence Interval Estimate	
Torque {Nm}	Torque^2 {Nm}^{2}	{uE} Unload	Estimated Value	Prediction Interval Lower limit	Prediction Interval Upper limit	Confidence Interval Estimate Lower limit	Confidence Interval Estimate Upper limit
0.0000	0.0000		0.4685	0.1256	0.8114	0.2296	0.7074
0.5000	0.2500		0.5239	0.1880	0.8597	0.2952	0.7526
0.7002	0.4903	0.6250	0.5464	0.2132	0.8795	0.3216	0.7711
9.9852	99.7052	1.7025	1.7829	1.5111	2.0548	1.6671	1.8988
13.9322	194.1054	2.3575	2.4235	2.1538	2.6932	2.3127	2.5343
17.8808	319.7246	3.0975	3.1330	2.8622	3.4038	3.0196	3.2463
21.8286	476.4897	3.8775	3.9109	3.6403	4.1814	3.7981	4.0236
25.7638	663.7721	4.7875	4.7545	4.4868	5.0223	4.6485	4.8606
29.7142	882.9333	5.7800	5.6700	5.4053	5.9348	5.5720	5.7681
33.7170	1136.8380	6.8225	6.6677	6.4006	6.9349	6.5634	6.7721
37.6517	1417.6523	7.6925	7.7172	7.4338	8.0006	7.5763	7.8581
39.4212	1554.0310	8.0750	8.2113	7.9138	8.5089	8.0438	8.3789
40.0000	1600.0000		8.3760	8.0727	8.6792	8.1985	8.5534
50.0000	2500.0000		11.4531	10.9613	11.9449	11.0272	11.8790
60.0000	3600.0000		14.9703	14.1356	15.8051	14.1726	15.7681

Box B-8 Hollow Universal Joint: 1 Group First order Regression

Single Block, Load-Unload combined effects

B: First Order ANOVA for test statistic of linear relation								
ANOVA H0: beta is explained in regression curve								
	df	SS	MS	F	Significance F: p-value	F crit		
Regression	1	55.6657	55.6657	400.8821	0.00	5.318		
Residual	8	1.1109	0.1389					
Total	9	56.7765						
Confidence Coefficient	0.95							
Level of Significance Alpha	0.05							
C- Regression Coefficients								
	Coefficients	Standard Error	t Stat	P-value	Lower 95%	Upper 95%	Lower 95.0%	Upper 95.0%
Intercept Beta0	-0.3226	0.2561	-1.2599	0.2432	-0.9132	0.2679	-0.9132	0.2679
Torque {Nm} Slope b1 (estimate of Beta1)	0.1974	0.0099	20.022	0.0000	0.1747	0.2202	0.1747	0.2202

Box B-9 Hollow Universal Joint: 1 Group Second order Regression

Single Block, Load-Unload combined effects

B: Second Order ANOVA for test statistic of linear relation								
ANOVA								
	df	SS	MS	F	Significance F	F crit		
Regression	2	56.710	28.355	3014.8	5.3096E-11	4.737		
Residual	7	0.0658	0.0094					
Total	9	56.776						
	Coefficients	Standard Error	t Stat	P-value	Lower 95%	Upper 95%	Lower 95.0%	Upper 95.0%
Intercept	0.3794	0.0942	4.0267	0.005	0.1566	0.6022	0.1566	0.6022
Torque {Nm}	0.0992	0.0096	10.275	1.7879E-05	0.0764	0.1220	0.0764	0.1220
Torque Squared {Nm}2	0.00231	0.000219	10.540	1.5102E-05	0.0017	0.0028	0.0017	0.0028

Table B-11 Hollow Universal Joint: 1 Group Prediction and Estimation intervals

Regression for Estimation and Prediction				0.95 Prediction Interval		0.95 Confidence Interval Estimate	
Torque {Nm}	Torque^2 {Nm}^{2}	{uE} Load-Unload	Estimated Value	Prediction Interval Lower limit	Prediction Interval Upper limit	Confidence Interval Estimate Lower limit	Confidence Interval Estimate Upper limit
0.0000	0.0000		0.3794	0.0597	0.6992	0.1566	0.6022
0.5000	0.2500		0.4296	0.1164	0.7428	0.2163	0.6429
0.7002	0.4903	0.4250	0.4501	0.1394	0.7607	0.2405	0.6596
9.9852	99.7052	1.6063	1.6013	1.3478	1.8548	1.4933	1.7093
13.9322	194.1054	2.2300	2.2116	1.9600	2.4631	2.1082	2.3149
17.8808	319.7246	2.9413	2.8942	2.6417	3.1468	2.7885	3.0000
21.8286	476.4897	3.6625	3.6490	3.3967	3.9012	3.5438	3.7541
25.7638	663.7721	4.4738	4.4730	4.2233	4.7228	4.3742	4.5719
29.7142	882.9333	5.3550	5.3724	5.1255	5.6193	5.2810	5.4639
33.7170	1136.8380	6.2725	6.3574	6.1083	6.6066	6.2601	6.4547
37.6517	1417.6523	7.2550	7.3980	7.1337	7.6623	7.2666	7.5294
39.4212	1554.0310	8.0750	7.8893	7.6118	8.1668	7.7331	8.0455
40.0000	1600.0000		8.0531	7.7703	8.3359	7.8877	8.2186
50.0000	2500.0000		11.128	10.6703	11.5875	10.7317	11.5261

Table B-12 Hollow Universal Joint: 1 Group Residuals analysis

Lilliefors Test						
Data	Ordered	S(x)	Z	F(x)	|S(x)-F(x)|	
-1.6717	-1.6717	0.1	-1.6716	0.0472	0.0527	Lilliefors Test Statistic
-0.9931	-0.9931	0.2	-0.9930	0.1603	0.039	D = 0.2146
-0.2929	-0.2929	0.3	-0.2929	0.3847	0.0847	
-0.2037	-0.2037	0.4	-0.20373	0.41928	0.0192	
0.0084	0.0084	0.5	0.00837	0.5033	0.0033	
0.0580	0.0580	0.6	0.0579	0.5231	0.0768	
0.1584	0.1584	0.7	0.1584	0.5629	0.1370	
0.2157	0.2157	0.8	0.2156	0.5853	0.2146	
0.5495	0.5495	0.9	0.5495	0.7086	0.1913	
2.1714	2.1714	1	2.1714	0.9850	0.0149	

Box B-10 Hollow Universal Joint: 1 Group Residuals analysis tests

Load, unload combined program

Observation	Torque {Nm}	{uE} Load-Unload	Predicted {uE} Load-Unload	Residuals	Standard Residuals
1	0.7002	0.4250	0.4501	-0.0251	-0.2929
2	9.9852	1.6063	1.6013	0.0050	0.0580
3	13.9322	2.2300	2.2116	0.0184	0.2157
4	17.8808	2.9413	2.8942	0.0470	0.5495
5	21.8286	3.6625	3.6490	0.0135	0.1584
6	25.7638	4.4738	4.4730	0.0007	0.0084
7	29.7142	5.3550	5.3724	-0.0174	-0.2037
8	33.7170	6.2725	6.3574	-0.0849	-0.9931
9	37.6517	7.2550	7.3980	-0.1430	-1.6717
10	39.4212	8.0750	7.8893	0.1857	2.1714

Table B-13 Hollow Universal Joint: test statistic Durbin Watson

3- Sample independence Durbin-Watson Statistic
-0.025053016
0.004957001
0.018447277
0.047001773
0.013549659
0.000716357
-0.017424212
-0.084938047
-0.142975948
0.185719157

Table B-14 Hollow Universal Joint: 4 Groups Residual Analysis

Load, unload, clockwise and counter clockwise program

Lilliefors Test of Normality
H0: X has a Normal distribution with unspecidfied mean and variance
Ha: X does not have Normal distribution
Critical value (at 5% significance level) D=0.0886
Rejection Rule: D> 0.0886

{uE}-cwise-load					
Data	Ordered	S(x)	Z	F(x)	|S(x)-F(x)|
0.4500	0.4500	0.1	-1.5109	0.0653	0.0346
1.6450	1.6450	0.2	-1.0459	0.1477	0.0522
2.3000	2.3000	0.3	-0.7910	0.2144	0.0855
3.0850	3.0850	0.4	-0.4856	0.3136	0.0863
3.7750	3.7750	0.5	-0.2171	0.4140	0.0859
4.5650	4.5650	0.6	0.0902	0.5359	0.0640
5.4100	5.4100	0.7	0.4190	0.6624	0.0375
6.2550	6.2550	0.8	0.7478	0.7727	0.0272
7.4450	7.4450	0.9	1.2109	0.8870	0.0129
8.4000	8.4000	1	1.5825	0.9432	0.0567
	D		Dcrit		
	0.0864	<	0.0886		

{uE}-cwise-unload					
Data	Ordered	S(x)	Z	F(x)	|S(x)-F(x)|
0.6600	0.6600	0.1	-1.5837	0.0566	0.0433
2.0350	2.0350	0.2	-1.0763	0.1408	0.0591
2.7350	2.7350	0.3	-0.8179	0.2066	0.0933
3.5850	3.5850	0.4	-0.5043	0.3070	0.0929
4.4000	4.4000	0.5	-0.2035	0.4193	0.0806
5.4350	5.4350	0.6	0.1784	0.5708	0.0291
6.4700	6.4700	0.7	0.5603	0.7123	0.0123
7.5200	7.5200	0.8	0.9478	0.8284	0.0284
8.2750	8.2750	0.9	1.2265	0.8899	0.0100
8.4000	8.4000	1	1.2726	0.8984	0.1015
	D		Dcrit		
	0.1016	>	0.0886		

{uE}-ccwise-load					
Data	Ordered	S(x)	Z	F(x)	|S(x)-F(x)|
0.0000	0.0000	0.1	-1.5450	0.0611	0.0388
1.3750	1.3750	0.2	-0.9585	0.1688	0.0311
1.9050	1.9050	0.3	-0.7324	0.2319	0.0680
2.4850	2.4850	0.4	-0.4850	0.3138	0.0861
3.1200	3.1200	0.5	-0.2141	0.4152	0.0847
3.7550	3.7550	0.6	0.0567	0.5226	0.0773
4.4500	4.4500	0.7	0.3532	0.6380	0.0619
5.1900	5.1900	0.8	0.6688	0.7482	0.0517
6.1900	6.1900	0.9	1.0954	0.8633	0.0366
7.7500	7.7500	1	1.7609	0.9608	0.0391
	D		Dcrit		
	0.0862	<	0.0886		

{uE}-ccwise-unload					
Data	Ordered	S(x)	Z	F(x)	|S(x)-F(x)|
0.5900	0.5900	0.1	-1.3914	0.0820	0.0179
1.3700	1.3700	0.2	-1.0743	0.1413	0.0586
1.9800	1.9800	0.3	-0.8262	0.2043	0.0956
2.6100	2.6100	0.4	-0.5700	0.2843	0.1156
3.3550	3.3550	0.5	-0.2671	0.3946	0.1053
4.1400	4.1400	0.6	0.05204	0.5207	0.0792
5.0900	5.0900	0.7	0.4383	0.6694	0.0305
6.1250	6.1250	0.8	0.8592	0.8048	0.0048
7.1100	7.1100	0.9	1.2597	0.8961	0.0038
7.7500	7.7500	1	1.5199	0.9357	0.0642
	D		Dcrit		
	0.1157	>	0.0886		

Box B-11 Hollow Universal Joint: ANOVA for group variations

Anova: Single Factor

SUMMARY

Groups	Count	Sum	Average	Variance		
MSLoadBootStat	250	1005.007	4.0200	0.5321		
MSUloadBootStat	250	1130.2597	4.5210	0.5603		
ANOVA						
Source of Variation	SS	df	MS	F	P-value	F crit
Between Groups	31.3765	1	31.3764	57.4471	1.7086E-13	3.8602
Within Groups	271.9979	498	0.5462			
Total	303.3744	499				

Anova: Single Factor

H0: mu1=mu2 …

F		Fcrit	
57.4471	>	3.8602	Fall in rejection region
p-value		Alpha	
1.7086E-13	<	0.05	

Overwhelming evidence to reject the null hypothesis, the mean of the populations are equal, in favour of the alternative one. The test is highly significant.

Accelerometer for Linear Speed Determination

Box B-12 Accelerometer Calibration: DOE sequence

Sequences from 1 to 10

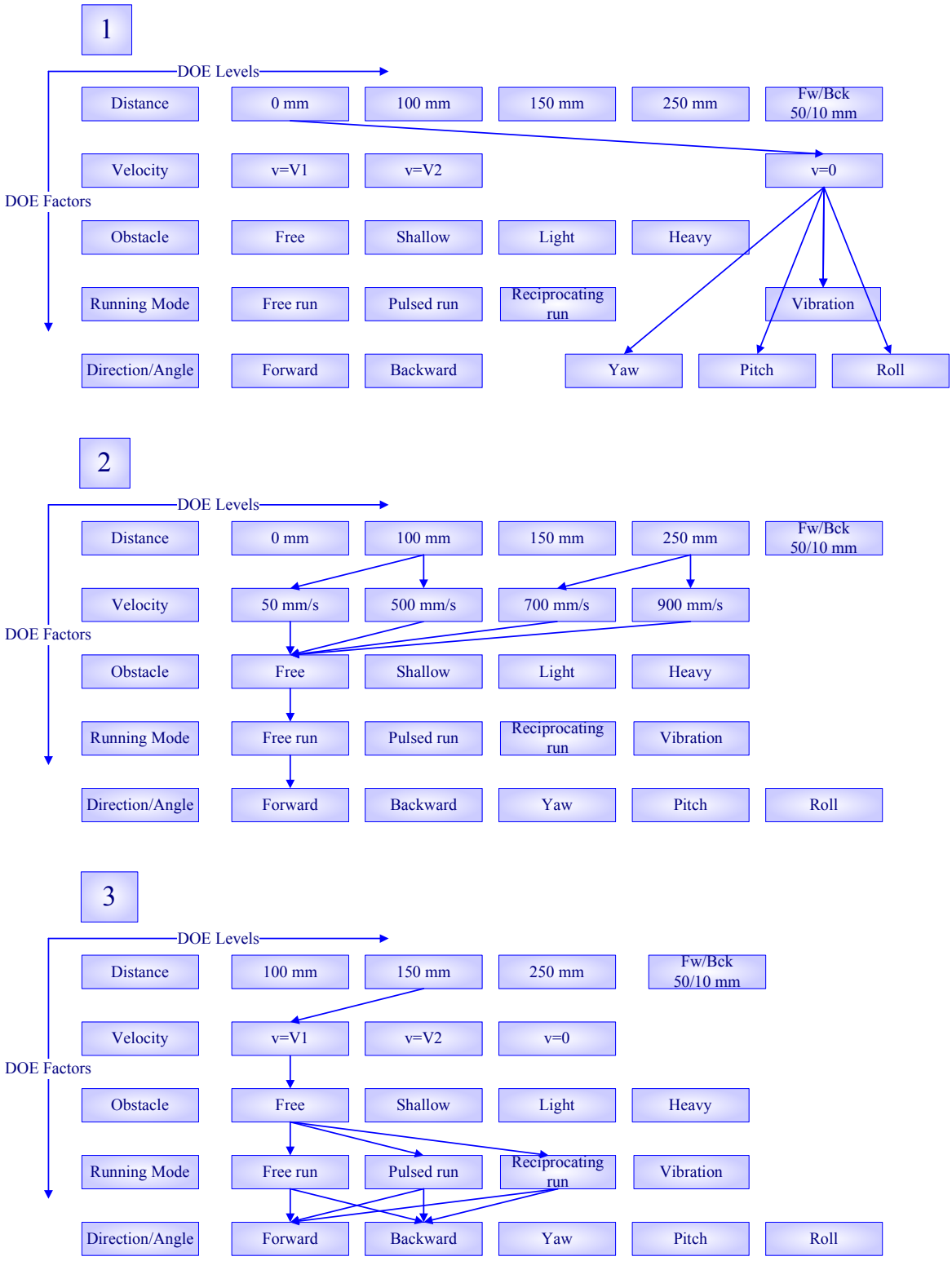

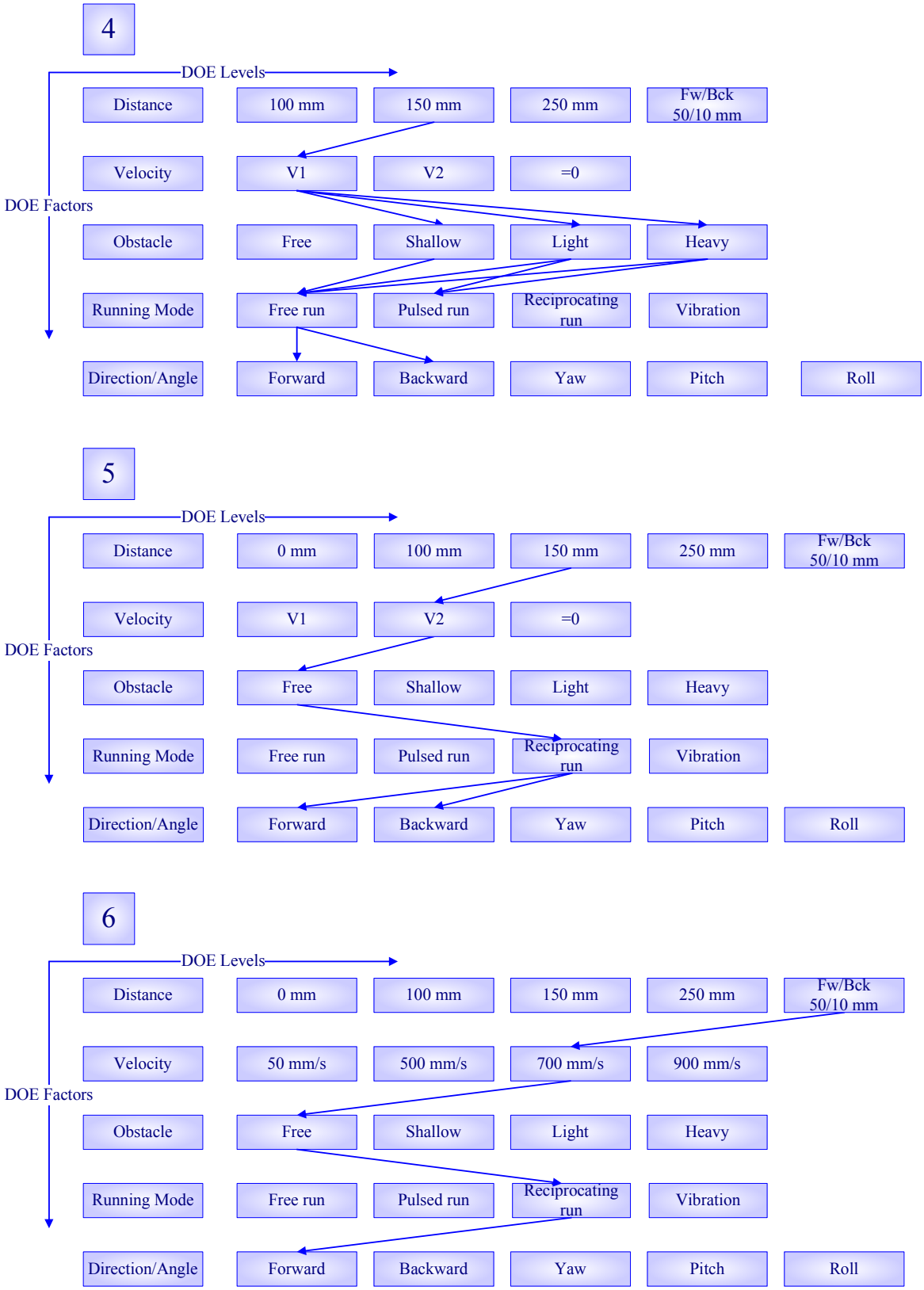
4
DOE Levels
DOE Factors
Distance
100 mm
150 mm
250 mm
Fw/Bck 50/10 mm
Velocity
V1
V2
=0
Obstacle
Free
Shallow
Light
Heavy
Running Mode
Free run
Pulsed run
Reciprocating run
Vibration
Direction/Angle
Forward
Backward
Yaw
Pitch
Roll
5
DOE Levels
DOE Factors
Distance
0 mm
100 mm
150 mm
250 mm
Fw/Bck 50/10 mm
Velocity
V1
V2
=0
Obstacle
Free
Shallow
Light
Heavy
Running Mode
Free run
Pulsed run
Reciprocating run
Vibration
Direction/Angle
Forward
Backward
Yaw
Pitch
Roll
6
DOE Levels
DOE Factors
Distance
0 mm
100 mm
150 mm
250 mm
Fw/Bck 50/10 mm
Velocity
50 mm/s
500 mm/s
700 mm/s
900 mm/s
Obstacle
Free
Shallow
Light
Heavy
Running Mode
Free run
Pulsed run
Reciprocating run
Vibration
Direction/Angle
Forward
Backward
Yaw
Pitch
Roll

Hybrid Pipeline Robot: Signal Conditioning Board

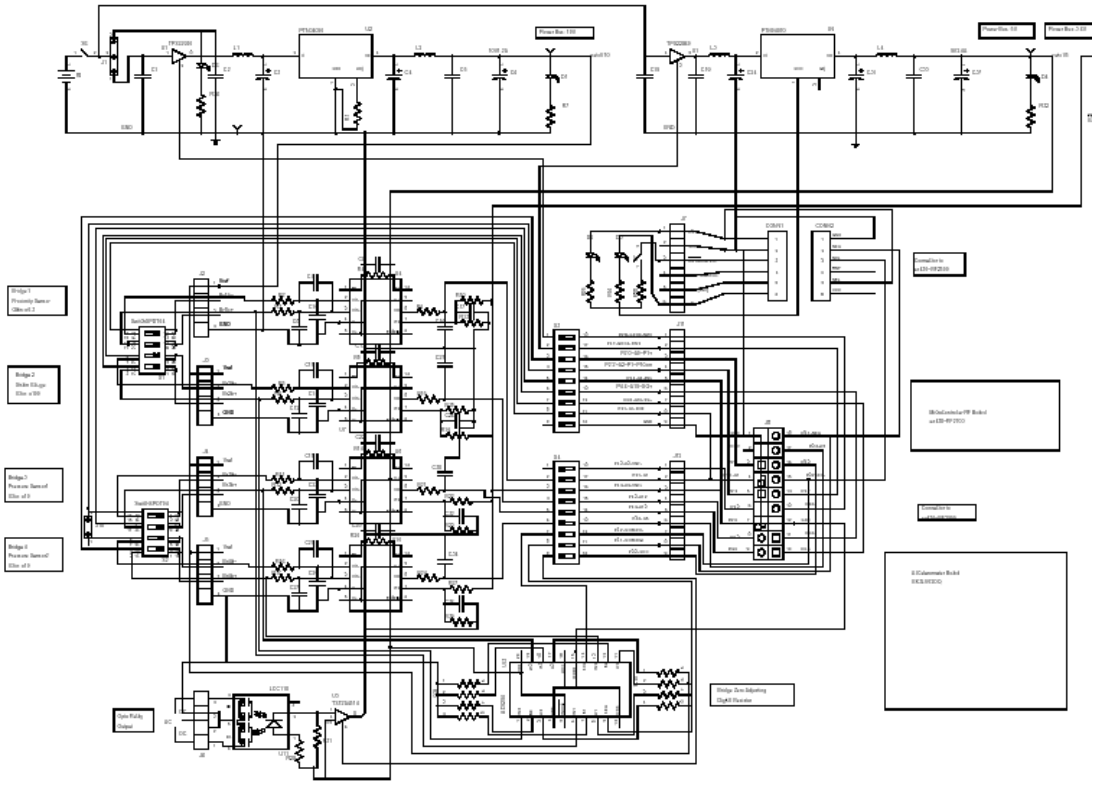

Figure B-3 HPR Embedded signal conditioning Board: circuit scheme

Scheme capture and board layout.

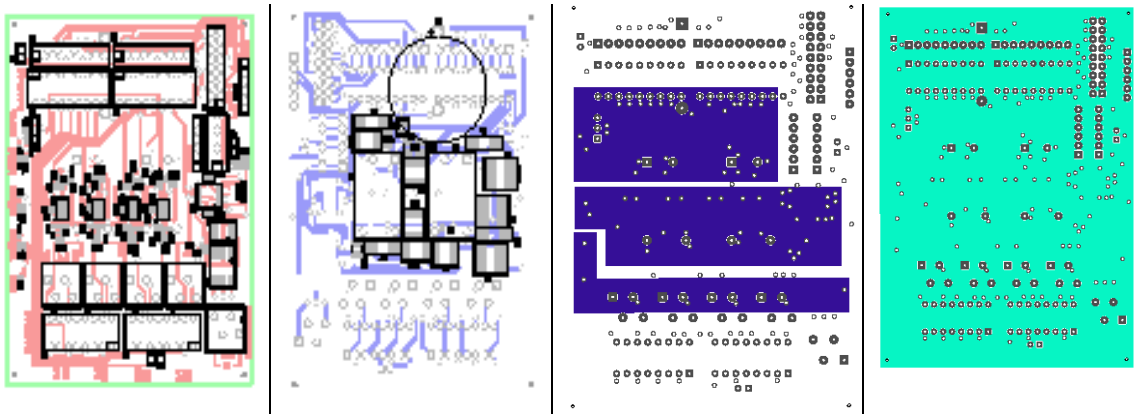

a) Layer 1: Top Layer Mixed-signals

b) Layer 4: Bottom Layer Power components

c) Layer 2: Power buses (3)

d) Layer 3: Ground

Figure B-4 HPR Embedded signal conditioning: board layout

4-Layer PCB Layout

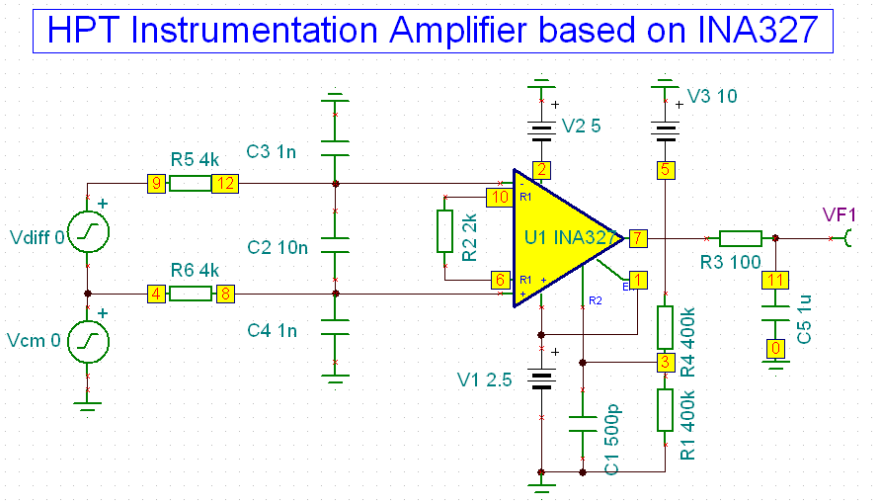

Figure B-5 Signal Conditioning: Instrumentation Amplifier circuit

IA and filters simulation in SPICE @ TINA-T

Table B-15 Signal Conditioning: Instrumentation Amplifier Nodal values

From SPICE simulation @ TINA-T

Nodes	Current	Nodes	Voltages
I_R12	-12.41uA	VF1	-4.97V
I_R2{10,6}	8.71E-17A	VP_1	2.5V
I_R3{11,7}	0A	VP_10	1V
I_R4{5,3}	-12.59uA	VP_11	-4.97V
I_R5{9,12}	-196.56pA	VP_12	1V
I_R6{4,8}	-196.56pA	VP_2	-5V
I_Vcm{4,0}	393.11pA	VP_3	-4.96V
I_Vdiff{9,4}	196.56pA	VP_4	1V
		VP_5	-10V
		VP_6	1V
		VP_7	-4.97V
		VP_9	1V

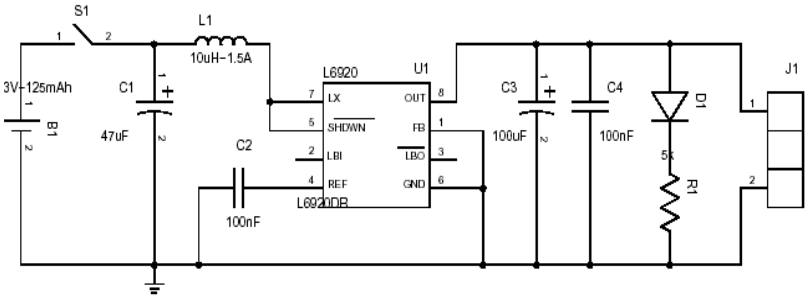

a) Accelerometer on-board power schematic

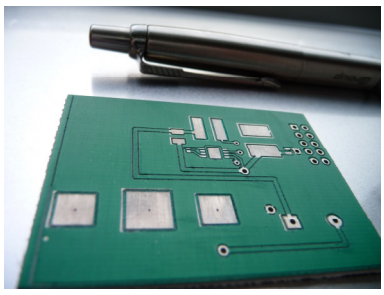

b) Power board before populating components

Figure B-6 Accelerometer stand-alone power board

Alternative to the wired USB power

Bibliography

Ahmad, S., A. Chipperfield and M. Tokhi (2001). Parametric modeling and dynamic characterization of a two-degree-of-freedom twin-rotor multi-input multi-output system. *Proceedings of the Institution of Mechanical Engineers, Part G: Journal of Aerospace Engineering*. 215**:** 63.

Alamir, M. and G. Bornard (1994). 21. New Sufficient Conditions for Global Stability of Receding Horizon Control for Discrete-time Nonlinear Systems. *Advances in Model-Based Predictive Control*. D. W. Clarke. Oxford New York, Oxford New York: Oxford University Press, 1994.**:** xii, 535 p. ill. 26 cm.

Alamo, T., D. M. de la Pena, D. Limon and E. F. Camacho (2005). Constrained min-max predictive control: modifications of the objective function leading to polynomial complexity. *Automatic Control, IEEE Transactions on*. 50**:** 710.

Alamo, T., D. R. Ramirez, D. Muñoz de la Peña and E. F. Camacho (2007). Min-max MPC using a tractable QP problem. *Automatica*. 43**:** 693.

Anderson, D. R., D. J. Sweeney and T. A. Williams (2003). *Modern business statistics with Microsoft Excel*. Cincinnati, Ohio, South-Western College Pub.

Antsaklis, P. J. (2000). Special issue on hybrid systems: theory and applications a brief introduction to the theory and applications of hybrid systems. *Proceedings of the IEEE*. 88**:** 879 - 887.

Appleton, E. (2003) "Bi-directional conduit traversing vehicle" US Patent 7398736

Appleton, E. and N. W. Stutchbury (2000). Novel brush drive robotic tractor for sewer and water main inspection and maintenance. *Industrial Robot: An International Journal*. 27**:** 370-377.

Appleton, E. and N. W. Stutchbury (2004) "Surface-traversing vehicle" US Patent 6775872 - Surface-traversing vehicle

Appleton, E. D., GB) and N. W. T. W. Stutchbury, GB) (2002) "Conduit traversing vehicle" United States Patent 6769321

Åström, K. J. and B. Wittenmark (1990). *Computer-controlled systems: theory and design*. Englewood Cliffs, N.J., Prentice-Hall International.

Åström, K. J. and B. Wittenmark (1995). *Adaptive control*. Reading, Mass., Addison-Wesley.

Azevedo, L., A. M. Braga, A. O. Nieckele and P. R. Souza Mendes (2007). Simulating pipeline pigging operations – PUC-Rio, Brazil. *Pipeline Pigging & Integrity Technology*. J. Tiratsoo, Clarion Technical Pub.

Baker, B. (2003). Matching the AMP to the ADC. EDN. *EDN*.

Baker, B. (2004). Design Effective Power Management Circuits in Battery Operated Environments. E. S. Valley, ESC Silicon Valley.

Baker, B. (2008). A Glossary of Analog-to-Digital Specifications and Performance Characteristics. Data Acquisition Products. T. Instrument, Texas Instrument**:** 32.

Baotić, M. "Optimal control of piecewise affine systems - a multi-parametric approach." Doctoral and Habilitation Theses thesis, Swiss Federal Institute Of Technology Zurich, Zürich 2005

Baotic, M., F. Borelli, A. Bemporad and M. Morari (2008). Efficient On-line Computation of Constrained Optimal Control. *Society for Industrial and Applied Mathematics, SIAM J. CONTROL OPTIM*. 47**:** 2470–2489.

Barlow, J. B. (1999). *Low speed wind tunnel testing*. New York, Wiley.
Barto, A. G. and T. G. Dietterich (2004). 2. Reinforcement learning and its relationship to supervised learning. *Handbook of learning and approximate dynamic programming*. J. Si. New York, Chichester, Wiley**:** xxi, 644 p.: ill., 25 cm.
Beale, M. (1993). Artificial Nural Networks. I. The MathWorks, The MathWorks, Inc.
Beller, M. and K. Reber (2007). Tools, vendors, and services: a review of current in-line inspection technologies – NDT Systems & Services AG, Germany. *Pipeline Pigging & Integrity Technology*. J. Tiratsoo, Clarion Technical Pub.
Bellman, R. E. (1965). *Dynamic programming and modern control theory*. New York; London, Academic Press.
Bellman, R. E. and S. E. Dreyfus (1962). *Applied dynamic programming*. Princeton, Princeton University Press.
Bellman, R. E. and R. Kalaba (1965). *Dynamic programming and modern control theory*. New York; London, Academic Press.
Bemporad, A. (1998 (b)). A Predictive Controller with Artificial Lyapunov Function for Linear Systems with Input/State Constraints. *Automatica*. 34**:** 1255.
Bemporad, A. (2006). Model Predictive Control Design: New Trends and Tools. *Decision and Control, 2006 45th IEEE Conference on*.
Bemporad, A. and A. Garulli (2000). Output-feedback predictive control of constrained linear systems via set-membership state estimation. Taylor & Francis. *International Journal of Control*. 73**:** 655 - 665.
Bemporad, A., W. P. M. H. Heemels and B. De Schutter (2001). On hybrid systems and closed-loop MPC systems. Decision and Control, 2001. Proceedings of the 40th IEEE Conference on Parallel and Distributed Systems, IEEE Transactions on, Location: Orlando, FL, USA.
Bemporad, A. and M. Morari (1999 (a)). Robust model predictive control: A survey. *Robustness in identification and control***:** 207.
Bemporad, A. and M. Morari (1999 (b)). Control of systems integrating logic, dynamics, and constraints. *Automatica*. 35**:** 407.
Bemporad, A. and E. Mosca (1998 (a)). Fulfilling Hard Constraints in Uncertain Linear Systems by Refernce Managing. *Automatica*. 34**:** 451-461.
Bernd, T., M. Kleutges and A. Kroll (1999). Nonlinear Black Box Modelling – Fuzzy Networks versus Neural Networks. *Neural Computing & Applications*. 8**:** 151.
Bertsekas, D. (1972). Infinite time reachability of state-space regions by using feedback control. *Automatic Control, IEEE Transactions on*. 17**:** 604.
Bertsekas, D. P. (2005 (a)). *Dynamic programming and optimal control*. Belmont, Mass., Athena Scientific.
Bertsekas, D. P. (2005 (b)). *Dynamic programming and optimal control*. Belmont, Mass., Athena Scientific.
Bertsekas, D. P. (2007). Separable Dynamic Programming and Approximate Decomposition Methods. *Automatic Control, IEEE Transactions on*. 52**:** 911.
Bertsekas, D. P. and I. B. Rhodes (1971 (d)). On the minimax feedback control of uncertain dynamic systems. Decision and Control, 1971 IEEE Conference on.
Bertsekas, D. P. and J. N. Tsitsiklis (1996 (a)). *Neuro-dynamic programming*. Belmont, Mass., Athena Scientific.
Bhaskar, V., S. K. Gupta and A. K. Ray (2001). Multiobjective optimization of an industrial wiped film poly(ethylene terephthalate) reactor: some further insights. *Computers & Chemical Engineering*. 25**:** 391.
Biegler, L. T. and I. E. Grossmann (2004). Retrospective on optimization. *Computers & Chemical Engineering*. 28**:** 1169.

Björnberg, J. and M. Diehl (2006). Approximate robust dynamic programming and robustly stable MPC. *Automatica*. 42**:** 777.

Bolkvadze, G. R. (2002). Identification of Hammerstein Nonlinear Stochastic Systems. *Automation and Remote Control*. 63**:** 601.

Borrelli, F., M. Baotic, A. Bemporad and M. Morari (2005). Dynamic programming for constrained optimal control of discrete-time linear hybrid systems. *Automatica*. 41**:** 1709.

Brooks, R., A. (1991). Intelligence without representation. Elsevier Science Publishers Ltd. *Artif. Intell.* 47**:** 139-159.

Brooks, R. A. (1987). Planning is Just a Way of Avoiding Figuring Out What To Do Next. Computer Science and Artificial Intelligence Lab (CSAIL). M. A. I. Laboratory. Massachussets, MIT Artificial Intelligence Laboratory**:** 7.

Brunete, A. G., E. Torres, J.E. Hernando, M. (2006). A 2 DoF Servomotor-based Module for Pipe Inspection Modular Micro-robots. *Intelligent Robots and Systems, 2006 IEEE/RSJ International Conference on***:** 1329-1334.

Bygate, C. (2005). Evaluation of DPT Pipeline Tractor. Durham, Durham University.

Camacho, E. F. and C. Bordons (1999). *Model predictive control*. London, Springer.

Camacho, E. F. and C. Bordons (2004). *Model predictive control*. London, Springer.

Camacho, E. F., Normey-Rico, J.E. (2002). A Unified Approach to Design Dead-Time Compensators for Stable and Integrative Processes With Dead-Time. *IEEE TRANSACTIONS ON AUTOMATIC CONTROL*. VOL. 47**:** 299-305.

Cambridge Dictionary. (2009). "Cambridge Dictionaries Online." Dictionaries Online, from www.dictionary.cambridge.org.

Cameron, G. R. (2007). Pigging 'unpiggable' pipelines: a guide for maintenance pigging and preparation for smart pig inspection – Exxon Co, USA. *Pipeline Pigging & Integrity Technology*. J. Tiratsoo, Clarion Technical Pub.

Catsoulis, J. (2003). *Designing embedded hardware*. Sebastopol, Calif., O'Reilly.

Chadeev, V. M. (2004). Digital Identification of Nonlinear Dynamic Systems. *Automation and Remote Control*. 65**:** 1938.

Chashchukhin, V. (2008). Simulation of dynamics and determination of control parameters of inpipe minirobot. *Journal of Computer and Systems Sciences International*. 47**:** 806.

Chen, Q., L. Gao, R. A. Dougal and S. Quan (2009). Multiple model predictive control for a hybrid proton exchange membrane fuel cell system. *Journal of Power Sources*. 191**:** 473.

Chisci, L. and E. Mosca (1994). Stabilizing Predictive Control: The Singular Transition-matrix Case. *Advances in Model-Based Predictive Control*. D. W. Clarke. Oxford New York, Oxford New York: Oxford University Press, 1994. Oxford science publications**:** xii, 535 p. ill. 26 cm.

Chong, K. and A. Parlos (1997). Comparison of traditional and neural network approaches to stochastic nonlinear system identification. *Journal of Mechanical Science and Technology*. 11**:** 267.

Cichocki, A. and R. Unbehauen (1993). *Neural networks for optimization and signal processing*. Stuttgart: Chichester, B.G. Teubner; Wiley.

Clarke, D. W., Ed. (1994). Advances in Model-Based Predictive Control. Oxford science publications. Oxford New York, Oxford New York: Oxford University Press, 1994.

Clarke, D. W. (1999 (a)). Sensor, actuator and loop validation. Advances in Control Technology (Ref. No. 1999/142), IEE Colloquium on.

Clarke, D. W. (1999 (b)). Sensor, actuator and plant validation. Intelligent and Self-Validating Sensors (Ref. No. 1999/160), IEE Colloquium on.

Clarke, D. W., Alamir M., Bornard G., Ed. (1994). New Sufficient Conditions for Global Stability of Receding Horizon Control for Discrete-time Nonlinear Systems, M. Alamir and G. Bornard. Advances in Model-Based Predictive Control. Oxford New York, Oxford New York: Oxford University Press, 1994.

Clarke, D. W. and C. Mohtadi (1989). Properties of generalized predictive control. Pergamon Press, Inc. *Automatica*. 25**:** 859-875.

Clarke, D. W., C. Mohtadi and P. S. Tuffs (1987 (a)). Generalized predictive control. Part I: The basic algorithm. Pergamon Press, Inc. *Automatica*. 23**:** 137-148.

Clarke, D. W., C. Mohtadi and P. S. Tuffs (1987 (b)). Generalized predictive control. Part II. Extensions and interpretations. Pergamon Press, Inc. *Automatica*. 23**:** 149-160.

Conover, W. J. (1999). *Practical nonparametric statistics*. New York, Wiley.

Cordell, J. (2007). To pig or not to pig: that is the question - On-Stream Systems, UK. *Pipeline Pigging & Integrity Technology*. J. Tiratsoo, Clarion Technical Pub.

Date, H., Y. Hoshi, M. Sampei and H. Ishii (2000). Dynamic Manipulability of a Snake-Like Robot with Consideration of Side Force and its Locomotin Control. *Nippon Kikai Gakkai Robotikusu, Mekatoronikusu Koenkai Koen Ronbunshu*. L0318A, VOL.2000**:** PAGE.2P1.84.129(1)-2P1.84.129(2).

Davison, A. C. and D. V. Hinkley (1997). *Bootstrap methods and their application*. Cambridge, Cambridge University Press.

De Nicolao, G. and R. R. Bitmead (1997). Fake Riccati equations for stable receding–horizon control. *European Control Conference '97, Bruxelles*.

De Nicolao, G. and R. Scattolini (1994). Stability and Output Terminal Constraints in Predictive Control. *Advances in Model-Based Predictive Control*. D. W. Clarke. Oxford New York, Oxford New York: Oxford University Press, 1994. Oxford science publications**:** xii, 535 p. ill. 26 cm.

Dechter, R., D. Cohen, P. Jeavons, F. Rossi and ScienceDirect (2003). *Constraint processing*. San Francisco, Morgan Kaufmann Publishers.

Demircioglu, H. (1994). Continuous-time Generalised Predictive Control (CGPC): Implementation Issues. *Advances in Model-Based Predictive Control*. D. W. Clarke. Oxford New York, Oxford New York: Oxford University Press, 1994. Oxford science publications**:** xii, 535 p. ill. 26 cm.

Demuth, H. B. and M. Beale (2000). *Neural network toolbox: for use with MATLAB*. Natick, Mathworks.

Dingankar, A. T. and I. W. Sandberg (1998). A note on error bounds for function approximation using nonlinear networks. *Circuits, Systems, and Signal Processing*. 17**:** 449.

Dixon, S. L. and Knovel (1998). *Fluid mechanics and thermodynamics of turbomachinery*. Boston; Oxford, Butterworth-Heinemann.

Durham University, S. o. E., Undergraduate Project (2008). Data for the Self Powered tractor.

Dwyer_Instruments_Inc. (2005). "Air Veloicity Introduction."

E. Appleton, N. W. S. (2000). Novel brush drive robotic tractor for sewer and water main inspection and maintenance. *Industrial Robot: An International Journal*. 27**:** 370-377.

Efron, B. (1993). *An introduction to the bootstrap*. New York; London, Chapman & Hall.

Eykhoff, P. (1974). *System identification: parameter and state estimation*. Chichester, Wiley.
Feroldi, D., M. Serra and J. Riera (2009). Energy Management Strategies based on efficiency map for Fuel Cell Hybrid Vehicles. *Journal of Power Sources*. 190**:** 387.
Fletcher, R. (1987). *Practical methods of optimization*. Chichester, Wiley.
Floudas, C. A., I. G. Akrotirianakis, S. Caratzoulas, C. A. Meyer and J. Kallrath (2005). Global optimization in the 21st century: Advances and challenges. *Computers & Chemical Engineering*. 29**:** 1185.
Flow-Kinetics. (2009). "Kiel Probe." from www.flowkinetics.com.
Garcia, C. E. and M. Morari (2002). Internal model control. A unifying review and some new results. American Chemical Society. *Industrial & Engineering Chemistry Process Design and Development*. 21**:** 308.
Gawthrop, P. J. (1996 (a)). Self-tuning PID control structures. *Getting the Best Our of PID in Machine Control (Digest No.: 1996/287), IEE Colloquium on***:** 4/1-4/4.
Gawthrop, P. J., R. Jones, W. and D. Sbarbaro (1996). Emulator-based control and internal model control: complementary approaches to robust control design. Pergamon Press, Inc. *Automatica*. 32**:** 1223-1227.
Gawthrop, P. J., D. W. Virden, S. A. Neild and D. J. Wagg (2008). Emulator-based control for actuator-based hardware-in-the-loop testing. *Control Engineering Practice*. 16**:** 897.
Gere, J. M. (2001). *Mechanics of materials*. Pacific Grove, CA, Brooks/Cole.
Girault, A. (2004). A hybrid controller for autonomous vehicles driving on automated highways. *Transportation Research Part C: Emerging Technologies*. 12**:** 421.
Gracey, W. (1980). Measurement of Aircraft Speed and Altitude. NASA, NASA**:** 316.
Gray, J. F. (2007). Developing a maintenance-pigging program - Pipeguard of Texas, USA. *Pipeline Pigging & Integrity Technology*. J. Tiratsoo, Clarion Technical Pub.
Grune, L. and A. Rantzer (2008). On the Infinite Horizon Performance of Receding Horizon Controllers. *Automatic Control, IEEE Transactions on*. 53**:** 2100.
Guzzella, Q. T. (2009). Quasi Static Simulation. Zurich, ETH, Zurich**:** Simulation for Hybrid electric vehicles.
Hagan, M. T. (1996). *Neural network design*. Boston, PWS.
Hagan, M. T., H. Demuth and M. Beale (1996). *Neural network design*. Boston, PWS.
Haley, P., D. Soloway and B. Gold (1999). Real-time Adaptive Control Using Neural Generalized Predictive Control, NASA Center: Ames Research Center; Langley Research Center**:** 5.
Han, C. "The experimental investigation of a pipe robot." [Durham] 1999
Harel, D. (1987). Statecharts: A visual formalism for complex systems. Elsevier North-Holland, Inc. *Sci. Comput. Program.* 8**:** 231-274.
Harel, D. and A. Naamad (1996). The STATEMATE semantics of statecharts. ACM. *ACM Trans. Softw. Eng. Methodol.* 5**:** 293-333.
Hatley, D. J. and I. A. Pirbhai (1987). *Strategies for real-time system specification*. New York, Chichester: Dorset House; Distributed by Wiley.
Haykin, S. S. (1994). *Neural networks: a comprehensive foundation*. New York; Toronto, Macmillan.
Heath, S. (2003). *Embedded systems design*. Oxford, Newnes.
Hecht-Nielsen, R. (1990). *Neurocomputing*. Reading, Mass., Addison-Wesley.
Hecht-Nielsen, R. (1992). *Neural networks for control and systems / edited by K. Warwick, G.W. Irwin, and K.J. Hunt*

Neurocomputing / Robert Hecht-Nielsen. London:
Reading, Mass., P. Peregrinus on behalf of the Institution of Electrical Engineers
Addison-Wesley.
Herrmann, G. L., F.L.; Ge, S.S.; Zhang, J. (2007). Discrete adaptive neural network disturbance feedforward compensation for nonlinear disturbances in servo-control applications. *Decision and Control, 2007 46th IEEE Conference on*. Volume, Issue, 12-14 Dec. 2007 Page(s):5965 - 5972.
Hibbeler, R. C. (2007). *Engineering mechanics: statics and dynamics*. Upper Saddle River, N.J. London, Pearson/Prentice-Hall;Pearson Education Ltd.
Hinkelmann, K. and O. Kempthorne (1994). *Design and analysis of experiments*. New York, Wiley.
Hinton, G. E. and T. J. Sejnowski (1987). Learning and Relearning in Holtzmann Machines. *Parallel distributed processing: explorations in the microstructure of cognition*. D. E. Rumelhart and J. L. McClelland. Cambridge, Mass., CogNet.
Holman, J. P. (1968). *Experimental methods for engineers*.
Hui, S. and J. Junqing Research on the system configuration and energy control strategy for parallel hydraulic hybrid loader. *Automation in Construction*. In Press, Corrected Proof.
Hunt, K. J., D. Sbarbaro, Bikowski and P. J. Gawthrop (1992). Neural networks for control systems: a survey. Pergamon Press, Inc. *Automatica*. 28**:** 1083-1112.
Huzmezan, M. and J. M. Maciejowski (1996). Constrained Predictive Control Methods A State Space Formulation. *Revue Roumaine de Science et Technique*. 41.
Israeli, N. and N. Goldenfeld (2006). Coarse-graining of cellular automata, emergence, and the predictability of complex systems. APS. *Physical Review E (Statistical, Nonlinear, and Soft Matter Physics)*. 73**:** 026203.
Japikse, D. and N. Baines (1994). *Introduction to turbomachinery*. Norwich, Vt.: Oxford, Concepts ETI; Oxford University Press.
Johannesson, L., S. Pettersson and B. Egardt (2009). Predictive energy management of a 4QT series-parallel hybrid electric bus. *Control Engineering Practice*. 17**:** 1440.
Jolliffe, I. T. (2002). *Principal component analysis [electronic resource]*. New York, Springer.
Kay, A., M. Ivanov and V. Schaeffer (2005). A Practical Technique for Minimizing the Number of Measurements in Sensor Signal Conditioning Calibration. High-Performance Linear Products. T. Instruments. Texas, Texas Instrument**:** 9.
Keller, G. and B. Warrack (2000). *Statistics for management and economics*. Pacific Grove; London, Duxbury.
Kiel, G. (1935). Total-Head Meter with small sensitivity to Yaw. *National Advisory Committee for Aeronautics*. XII**:** 10.
Kim, T. W. and J. Yuh (2004). Development of a real-time control architecture for a semi-autonomous underwater vehicle for intervention missions. *Control Engineering Practice*. 12**:** 1521.
Klebert, P. and O. J. Nydal. (2003). "Object Oriented Simulation of Multiphase Flow." Norwegian University of Science and Technology (NTNU), 7491 Trondheim Norway.
Kline, S. J. (1965). *Similitude and approximation theory*. New York, McGraw-Hill.
Kosko, B. (1992). *Neural networks and fuzzy systems: a dynamical systems approach to machine intelligence / Bart Kosko*. Englewood Ciffs, NJ, Prentice Hall.

Koutsoukos, X. and P. Antsaklis (1999). Hybrid Control Systems Using Timed Petri Nets: Supervisory Control Design Based on Invariant Properties. *Hybrid Systems V***:** 67.

Koutsoukos, X. and P. Antsaklis (2001). Characterization of Stabilizing Switching Sequences in Switched Linear Systems Using Piecewise Linear Lyapunov Functions. *Hybrid Systems: Computation and Control***:** 347.

Kugelstadt, T. (2005). Getting the most out of your instrumentation amplifier design. Texas Instrument. *Analog Applications Journal*. 4Q 2005**:** 6.

Kurowicka, D. and R. Cooke (2006). *Uncertainty analysis: mathematical foundations and applications*. Chichester, Wiley.

Lau, H. Y. K., V. W. K. Wong and I. S. K. Lee (2007). Immunity-based autonomous guided vehicles control. *Applied Soft Computing*. 7**:** 41.

Ławry Nczuk, M. (2007). A Family Of Model Predictive Ccontrol Algorithm With Artificial Neural Networks. *Int. J. Appl. Math. Comput. Science*. 17**:** 217-232.

Lazar, M. and O. Pastravanu (2002). A neural predictive controller for non-linear systems. *Mathematics and Computers in Simulation*. 60**:** 315.

Lee, Y. I., B. Kouvaritakis and M. Cannon (2002). Constrained receding horizon predictive control for nonlinear systems. *Automatica*. 38**:** 2093.

Lendaris, G. G. and J. C. Neidhoefe (2004). Guidance in the use of adaptive critics for control. *Handbook of learning and approximate dynamic programming*. J. Si. New York;

Chichester, Wiley**:** xxi, 644 p.: ill.; 25 cm.

Ljung, L. (1987). *System identification: theory for the user*. Englewood Cliffs, Prentice-Hall.

Loenhout, S. A. K. v. (2007). Real-time control for a Fuel Cell Hybrid Vehicle with the Equivalent Consumption Minimization Strategy. Department of Mechanical Engineering, Section Automotive Engineering Science, Power Trains. Eindhoven, December 2007, Technische Universiteit Eindhoven (TU/e), The Netherlands**:** 62.

Logan, E., Jr., Roy, Ramendra (2003). *Handbook of turbomachinery*. New York, Marcel Dekker.

Long, D. and R. Garigliano (1994). *Reasoning by analogy and causality: a model and application*, Ellis Horwood.

Lyons, G. (2000). Offshore technology—advances at the dawn of the new millennium reviewed from a UK perspective. *Proceedings of the Institution of Mechanical Engineers, Part E: Journal of Process Mechanical Engineering*. 214**:** 1.

Lyshevski, S. E. (2000). Energy conversion and optimal energy management in diesel-electric drivetrains of hybrid-electric vehicles. *Energy Conversion and Management*. 41**:** 13.

M'Sahli, F. and R. Matlaya (2005). A neural network model based predictive control approach: application to a semi-batch reactor. *The International Journal of Advanced Manufacturing Technology*. 26**:** 161.

Maeder, U., F. Borrelli and M. Morari (2009). Linear offset-free Model Predictive Control. *Automatica*. 45**:** 2214.

Massey, B. S. (2006). *Mechanics of fluids*. London; New York, Taylor & Francis.

Matthews, L., M. Kennard and A. O'Donoghue (2007). Velocity control of pigs in gas pipelines – Caltec, UK. *Pipeline Pigging & Integrity Technology*. J. Tiratsoo, Clarion Technical Pub.

Maxwell, R. L. (1960). *Kinematics and dynamics of machinery*. London.

Mayne, D. Q., J. B. Rawlings, C. V. Rao and P. O. M. Scokaert (2000). Constrained model predictive control: Stability and optimality. *Automatica*. 36**:** 789.

Meystel, A. and J. S. Albus (2002). *Intelligent systems: architecture, design, and control*. New York;
[England], Wiley.

Meystel, A., M. and J. S. Albus (2000). *Intelligent Systems: Architecture, Design, and Control*, John Wiley \& Sons, Inc.

Miller III, W. T., Sutton,R.S., Werbos,P.J., Ed. (1990). Neural networks for control, MIT Press.

Montgomery, D. C. (2009). *Design and analysis of experiments*. Hoboken, N.J., John Wiley & Sons.

Montgomery, D. C., G. C. Runger and N. F. Hubele (2004). *Engineering statistics*. New York, Wiley.

Munoz de la Pena, D., T. Alamo, A. Bemporad and E. F. Camacho (2004). A dynamic programming approach for determining the explicit solution of linear MPC controllers. *Decision and Control, 2004. CDC. 43rd IEEE Conference on***:** 2479- 2484.

Munoz de la Pena, D. M., T. Alamo and A. Bemporad (2005). A Decomposition Algorithm for Feedback Min-Max Model Predictive Control. *Decision and Control, 2005 and 2005 European Control Conference. CDC-ECC '05. 44th IEEE Conference on***:** 5126- 5131.

Narendra, K. S. (1989). *Stable adaptive systems / Kumpati S. Narendra, Anuradha M. Annaswamy*. Englewood Cliffs, N.J, Prentice Hall.

Narendra, K. S. (1990 (a)). Adaptive Control using Neural Networks. *Neural Networks for Control*. W. T. Miller III, R. S. Sutton and P. J. Werbos. Massachusetts, The MIT Press. I**:** 524.

Narendra, K. S. a. P., Kannan (1990 (b)). Identification and Control of Dynamical Systems Using Neural Networks. *IEEE Transactions on Neural Networks*. 1**:** 4027.

Nelles, O. (2001). *Nonlinear System Identification*. Berlin.

Ng, T. and G. Leng (2007). Design of small-scale quadrotor unmanned air vehicles using genetic algorithms. *Proceedings of the Institution of Mechanical Engineers, Part G: Journal of Aerospace Engineering*. 221**:** 893.

Núñez-Reyes, A., J. E. Normey-Rico, C. Bordons and E. F. Camacho (2005). A Smith predictive based MPC in a solar air conditioning plant. *Journal of Process Control*. 15**:** 1.

O'Donoghue, A. F. "On the Steady State Motion of Conventional Pipeline Pigs using Incompressible Drive Media." PhD thesis, Cranfield University, United Kingdom 1996

O'Donoghue, A. (2007). Why pigs get stuck and how to avoid it – Pipeline Research Ltd, UK. *Pipeline Pigging & Integrity Technology*. J. Tiratsoo, Clarion Technical Pub.

Ogata, K. (1970). *Modern control engineering / Katsuhiko Ogata*. Englewood Cliffs, Prentice-Hall.

Ong, J., D. Kerr and K. Bouazza-Marouf (2003). Design of a semi-autonomous modular robotic vehicle for gas pipeline inspection. *Proceedings of the Institution of Mechanical Engineers, Part I: Journal of Systems and Control Engineering*. 217**:** 109.

Palmer, A. C. (2008). *Dimensional analysis and intelligent experimentation*. Singapore Hackensack, NJ, World Scientific.

Pannocchia, G. and A. Bemporad (2007). Combined Design of Disturbance Model and Observer for Offset-Free Model Predictive Control. *Automatic Control, IEEE Transactions on*. 52**:** 1048.

Pebody, M. (2008). Autonomous underwater vehicle collision avoidance for under-ice exploration. *Proceedings of the Institution of Mechanical Engineers, Part M: Journal of Engineering for the Maritime Environment*. 222**:** 53.

Pérez, L. V., G. R. Bossio, D. Moitre and G. O. García (2006). Optimization of power management in an hybrid electric vehicle using dynamic programming. *Mathematics and Computers in Simulation*. 73**:** 244.

Pérez, L. V. and E. A. Pilotta (2009). Optimal power split in a hybrid electric vehicle using direct transcription of an optimal control problem. *Mathematics and Computers in Simulation*. 79**:** 1959.

Perrin, D. P., A. Kwon and R. D. Howe (2004). A novel actuated tether design for rescue robots using hydraulic transients. *Robotics and Automation. Proceedings. 1987 IEEE International Conference on 2004. Proceedings. ICRA apos;04. 2004 IEEE International Conference on*. 4**:** Page(s): 3482 - 3487.

Pham, D. T. and L. Xing (1995). *Neural networks for identification, prediction and control*. London, Springer-Verlag.

Primbs, J. A., V. Nevisti and J. C. Doyle (1999). Nonlinear Optimal Control: a Control Lyapunov Function And Receding Horizon Perspective. *Asian Journal of Control*. 1**:** 14-24.

Primbs, J. A. and V. Nevistic (2000). A framework for robustness analysis of constrained finite receding horizon control. *Automatic Control, IEEE Transactions on*. 45**:** 1828.

Pulker, S. "Development and Testing of a Pipeline PIG Turbine." thesis, Durham University, Durham 2005

Quarini, J. and S. Shire (2007). A Review of Fluid-Driven Pipeline Pigs and their Applications. *Proceedings of the Institution of Mechanical Engineers, Part E: Journal of Process Mechanical Engineering*. 221**:** 1.

Quero, J. M., E. F. Camacho and L. G. Franquelo (1993). Neural network for constrained predictive control. *Circuits and Systems I: Fundamental Theory and Applications, IEEE Transactions*. 40**:** 621-626.

Quigley, C., R. Ball and R. Jones (2000). Fuzzy modelling approach to the prediction of journey parameters for hybrid electric vehicle control. *Proceedings of the Institution of Mechanical Engineers, Part D: Journal of Automobile Engineering*. 214**:** 875.

Rakovic, S. V., E. C. Kerrigan, D. Q. Mayne and J. Lygeros (2006). Reachability analysis of discrete-time systems with disturbances. *Automatic Control, IEEE Transactions on*. 51**:** 546.

Rangan, S. and K. Poolla (1997). Weighted optimization for multiobjective full-information control problems. *Systems & Control Letters*. 31**:** 207.

Rao, C. V., J. B. Rawlings and J. H. Lee (2001). Constrained linear state estimation: a moving horizon approach. *Automatica*. 37**:** 1619.

Rao, C. V., S. J. Wright and J. B. Rawlings (1998). Application of interior-point methods to model predictive control. Plenum Press. *J. Optim. Theory Appl.* 99**:** 723-757.

Rao, S. S. (1984). *Optimization: theory and applications*. New Delhi, Wiley Eastern.

Rao, S. S. (1996). *Engineering optimization: theory and practice*. New York; Chichester, Wiley.

Rao, S. S. (1996). *Engineering optimization: theory and practice / Singiresu S. Rao*. New York; Chichester, Wiley.

Rauch, H. E. (1994). Intelligent fault diagnosis and control reconfiguration. *Control Systems Magazine, IEEE*. 14**:** 6-12.

Rauch, H. E. (1995). Autonomous control reconfiguration. *Control Systems Magazine, IEEE*. 15**:** 37-48.

Rodatz, P., G. Paganelli, A. Sciarretta and L. Guzzella (2005). Optimal power management of an experimental fuel cell/supercapacitor-powered hybrid vehicle. *Control Engineering Practice*. 13**:** 41.

Roh, S.-g., D. Kim, J.-S. Lee, H. Moon and H. Choi (2009). In-pipe robot based on selective drive mechanism. *International Journal of Control, Automation and Systems*. 7**:** 105.

Roshanian, J., A. Saleh and M. Jahed-Motlagh (2007). On the design of adaptive autopilots for a launch vehicle. *Proceedings of the Institution of Mechanical Engineers, Part I: Journal of Systems and Control Engineering*. 221**:** 27.

Roy, R., S. Hinduja and R. Teti (2008). Recent advances in engineering design optimisation: Challenges and future trends. *CIRP Annals - Manufacturing Technology*. 57**:** 697.

Rumelhart, D. E., G. E. Hinton and R. J. Williams (1987). Learning Internal Representations by Error Propagation. *Parallel distributed processing: explorations in the microstructure of cognition*. D. E. Rumelhart, J. L. McClelland and S. D. P. D. P. R. G. University of California. Cambridge, Mass., CogNet.

Ruzika, S. and M. M. Wiecek (2005). Approximation Methods in Multiobjective Programming. *Journal of Optimization Theory and Applications*. 126**:** 473.

Sciarretta, A. and L. Guzzella (2007). Control of hybrid electric vehicles. *Control Systems Magazine, IEEE*. 27**:** 60.

Sciomachen, A. (1994). Project Scheduling with parallel activities time -window and precedence constraints. *Optimization in industry 2: mathematical programming and modeling techniques in practice*. T. A. Ciriani and R. C. Leachman. Chichester, Wiley**:** xvi,214p.; 26cm.

Shreve, S., E. and D. Bertsekas, P. (1977). Alternative theoretical frameworks for finite horizon discrete-time stochastic optimal control. Decision and Control including the 16th Symposium on Adaptive Processes and A Special Symposium on Fuzzy Set Theory and Applications, 1977 IEEE Conference on.

Söderström, T. and P. Stoica (1989). *System identification*. New York, Prentice Hall.

Soloway, D. (1992 (a)). Neural networks modeling and control of dynamical systems, NASA Center: Langley Research Center**:** 18.

Soloway, D. and P. Haley (2004 (a)). Pilots Rate Augmented Generalized Predictive Control for Reconfiguration. 6th IASTED International Conference on Intelligent Systems and Control (ISC 2004), 23-25 Aug. 2004, Honolulu, HI, United States, NASA Center: Ames Research Center; Langley Research Center**:** 6.

Soloway, D., J.-J. Shi and A. Kelkar (2004 (b)). GPC-Based Stable Reconfigurable Control, NASA Center: Ames Research Center**:** 42.

Soloway, D. I. and J. T. Bialasiewicz (1992 (b)). Neural network modeling of nonlinear systems based on Volterra series extension of a linear model, NASA Center: Langley Research Center**:** 13.

Southgate, J. "Wax removal using pipeline pigs." PhD thesis, University of Durham, United Kingdom 2004

Steinberg, M. (2005). Historical Overview of Research in Reconfigurable Flight Control. *Proceedings of the Institution of Mechanical Engineers, Part G: Journal of Aerospace Engineering*. 219**:** 263.

Stutchbury, N. W. "Design characteristics of a pipe crawling robot." PhD thesis, Durham University, United KIngdom 1999

Sundström, O., D. Ambühl and L. Guzzella (2009). On Implementation of Dynamic Programming for Optimal Control Problems with Final State Constraints. *Oil & Gas Science and Technology*.

Tarafder, A., G. P. Rangaiah and A. K. Ray (2007). A study of finding many desirable solutions in multiobjective optimization of chemical processes. *Computers & Chemical Engineering*. 31**:** 1257.

Taylor, E. (1974). *Dimensional analysis for engineers*. Oxford, Clarendon Press.

Texas Instruments (2004). Precision, Rail-toRail I/O Instrumentation Amplifier: INA 326-327. Instrumentation Amplifier. T. Instrument**:** 23.

Torrico, B. C. and J. E. Normey-Rico (2007). Robust constrained horizon predictive controller for dead time systems. *World Congress, Czech Republic*. 16.

Transeth, A. A., K. Ytterstad Pettersen and P. Liljebäck (2009). A survey on snake robot modeling and locomotion. 27**:** 999-1015.

United-Sensor (2008 a)). Kiel Probe, General Information.

United-Sensor. (2008 b)). "Pitot-Static Pressure Probes."

United-Sensor (2008 c)) "Kiel Temperature Probes." DOI:

Utyuzhnikov, S. V., P. Fantini and M. D. Guenov (2009). A method for generating a well-distributed Pareto set in nonlinear multiobjective optimization. *Journal of Computational and Applied Mathematics*. 223**:** 820.

van Agthoven, R. (2007). Inspection of unpiggable pipelines: experience, history, and the future of cable-operated ultrasonic pigging - RTD BV, Netherlands. *Pipeline Pigging & Integrity Technology*. J. Tiratsoo, Clarion Technical Pub.

Wang, X., V. Yadav and S. N. Balakrishnan (2007). Cooperative UAV Formation Flying With Obstacle/Collision Avoidance. *Control Systems Technology, IEEE Transactions on*. 15**:** 672-679.

Wang, Z. (2003 (a)). Bristle mechanism study of a shape reconfigurable brush robot. *Journal:Industrial Robot: An International Journal*. 30**:** 543 - 551.

Wang, Z. and E. Appleton (2003 (b)). The bristle theory and traction experiment of a brush based rescue robot. *Robotica*. 21**:** 453.

Wang, Z. and E. Appleton (2003 (c)). A void shape detecting sensor for pipeline inspection. *Journal:Industrial Robot: An International Journal*. 30**:** 459 - 462.

Wang, Z. and E. Appleton (2003 (d)). The concept and research of a pipe crawling rescue robot. *Advanced Robotics*. 17**:** 339.

Wang, Z. and G. Hong (2008). A Bristle-Based Pipeline Robot for Ill-Constraint Pipes. *Mechatronics, IEEE/ASME Transactions on*. 13**:** 383.

Warwick, K., G. W. a. Irwin and K. J. Hunt, Eds. (1992). Neural networks for control and systems. London, P. Peregrinus on behalf of the Institution of Electrical Engineers.

Watkins, C. "Learning from Delayed Rewards." PhD thesis, University of Cambridge, United Kingdom 1989

Wei, R. (2007). On Constrained Nonlinear Tracking Control of a Small Fixed-wing UAV. Kluwer Academic Publishers. *J. Intell. Robotics Syst.* 48**:** 525-537.

White, F. M. (2008). *Fluid mechanics*. Boston, MA, McGraw-Hill Higher Education.

White, F. M. (2008). *Fluid mechanics / Frank M. White*. Boston, MA, McGraw-Hill Higher Education.

Widrow, B., N. K. Gupta and S. Maitra (1973). Punish/Reward: Learning with a Critic in Adaptive Threshold Systems. *Systems, Man and Cybernetics, IEEE Transactions on*. 3**:** 455-465.

Wikipedia. (2009, 23 December 2009 13:47 UTC). "Orders of magnitude (speed)." Wikipedia, The Free Encyclopedia. Retrieved 26 December 2009 17:24 UTC, 2009, from http://en.wikipedia.org/w/index.php?title=Orders_of_magnitude_(speed)&oldid=333553602.

William, L. (1947). Investigation of the fuselage interference on a Pitot-static tube extending forward from the nose of the fuselage. N. A. C. f. A. NACA, Langley Memorial Aeronautical Labortory, Langley Field, Va**:** 19.

Willis, M. J., G. A. Montague, C. Di Massimo, M. T. Tham and A. J. Morris (1992). Artificial neural networks in process estimation and control. Pergamon Press, Inc. *Automatica*. 28**:** 1181-1187.

Xu, L., J. Li, J. Hua, X. Li and M. Ouyang (2009). Optimal vehicle control strategy of a fuel cell/battery hybrid city bus. *International Journal of Hydrogen Energy*. 34**:** 7323.

Yoon, T.-w. and D. W. Clarke (1995). A Reformulation of Receding-Horizon Predictive Control. *International journal of systems science ISSN 0020-7721 CODEN IJSYA9*. 26**:** 1383-1400.

Zheng, H. and E. Appleton (2005). Dynamic characteristics of a novel self-drive pipeline pig. *Robotics, IEEE Transactions on*. 21**:** 781.

Zweiri, Y., L. Seneviratne and K. Althoefer (2003). Modelling and control of an unmanned excavator vehicle. *Proceedings of the Institution of Mechanical Engineers, Part I: Journal of Systems and Control Engineering*. 217**:** 259.